Metal Complexes Stabilized by Nucleobases and Their Analogues: Synthesis and Applications

GIULIA FRANCESCATO

SUPERVISOR: DR ANA RITA GUERREIRO DE BRITO PETRONILHO

Dissertation submitted in fulfilment of the requirements for PhD degree in Sustainable Chemistry

Instituto de Tecnologia Química e Biológica | Universidade Nova de Lisboa

Oeiras,

Financial support by FCT through the doctoral program in sustainable chemistry: SFRH/BD/144441/2019

Acknowledgements

Firstly, I would like to thank my supervisor, Doctor Ana Petronilho, who accepted me as a research fellow in her Erasmus trainee program and encouraged me to start a Ph.D. Your support and guidance were fundamental to my academic path and undoubtedly allowed me to learn and grow as a scientist.

I wish to acknowledge the members of the Admission Committee of the FCT for granting me the Ph.D. fellowship that allowed me to conclude this project.

I would like to thank all my colleagues who were, or still are, part of Ana Petronilho's Lab. A special thanks goes to Giulia Orsini, who was always there to support me and for all the valuable scientific discussions that certainly contributed to the success of this project. I wish to thank my colleagues from the Beatriz Royo Lab, both current and former, who are always available to help.

I am grateful to Prof Carlos Romão for sharing with our group the materials and reagents from his lab, and especially for the several teaching moments.

I want to thank Dr Clara Gomes from the Single Crystal X-ray Crystallography Service (FCT NOVA) for her dedication and amazing work in resolving the solid-state structure of some of the complexes included in this thesis. I am thankful to Helena Matias and Pedro Lamosa from CERMAX for their valuable help with the NMR, and to Conceição Almeida from the Mass Spectrometry Unity (iBET/ITQB NOVA) for her dedication and helpful insights

regarding the MS results. A general thank you to all the staff from the administrative services of ITQB, especially those from the economato who were always available to help.

I would also like to thank Prof Chiara Gabbiani from the Dipartimento di chimica e chimica industriale, Università di Pisa, for accepting me in her lab as a visiting intern for 4 months. Although the work that I had the opportunity to develop in her lab did not produce publishable results, I learned new valuable techniques. I wish to thank also all the students I met there, especially Valentina Ceccherini, for her valuable advice.

Furthermore, I would like to thank all the people who support me outside the ITQB's walls, from my Portuguese "family" to my Italian one living in Lisbon.

My deepest gratitude goes to my family and to my partner, Leonardo, for the support he gives me every day.

Lastly, a special mention in this section goes to my father, Pierangelo; this thesis is for You, wherever you are.

Abstract

This thesis work is structured into four main sections. The first chapter is a general introduction, initiated with a discussion of the structure and the electronic properties of N-heterocyclic carbenes (NHCs). Furthermore, it focuses on the importance of NHCs in organometallic chemistry and the use of NHCs as ligands for metal complexes with potential biological applications. The introductory chapter also contains a review of key examples of metal complexes containing nucleobases and their analogues. This synopsis explores both the synthesis and the biological application of these complexes. Finally, the aim of this thesis work is outlined: synthesize new metal complexes containing nucleobases or analogues as NHCs and study their biological applications.

The second chapter concerns the synthesis of nickel complexes containing xanthine derivatives bound as NHCs. A library of ligand precursors based on caffeine or theophylline were synthesized, each containing a different alkyl moiety as substituent at N7: a methyl group (methylcaffeine), an octyl group, an isopropyl group, an allyl group and a methyl pyridine group. In addition, attempts to synthesize a ligand precursor consisting of two theophyllines linked by a CH_2 bridge were performed and three ligand precursors based on guanine were synthesize: dimethyl guanine, N7-methyl guanosine and methyl acyclovir. The allyl and the pyrimidine xanthine derivatives did not lead to any identifiable product when reacting with nickelocene, and this was also the case for the guanine derivatives. In the case of ligand precursors

bearing a methyl group (methylcaffeine), an octyl group and an isopropyl group, the reaction of the ligand precursors with nickelocene afforded monocarbenes. In the case of methyl caffeine, a biscarbene was also obtained. Depending on the side chain present at N7 of the xanthine and the conditions used for the reactions with nickelocene led to the formation of a mono-or bis-carbene.

The four nickel complexes successfully synthesized were tested on two strains of Candida, *C. albicans* and *C. glabrata*, the latter of which is resistant to the most currently used antifungal agent (fluconazole). All the monocarbene complexes exhibited similar antifungal effects on both fungal strains, while the biscarbene (containing two methyl caffeine NHCs) had preferential activity on *C. glabrata*. The four compounds were tested together with two other nickel monocarbenes containing dimethyl-benzimidazole or dimethyl-imidazole as ligands, for comparative purposes. The use of these two compounds showed that the presence of a xanthine ring is not essential for the antifungal activity.

The third chapter describes the synthesis of gold complexes containing N7-methyl guanosine, mRNA cap0, as NHC ligand. Thus N7-methyl guanosine was protected at the ribose ring with acetate groups, to avoid side reactions involving the free -OH. The ligand precursor thus obtained was reacted with gold(I), $Au(SMe_2)Cl$, in the presence of K_2CO_3, leading to a high insoluble mixture of two products. Analysis of the mixture by NMR showed the presence of two NHCs. Further analysis of the mixture allowed for the identification of the two carbenes as a monocarbene (major product) and a biscarbene (minor product). By changing the stoichiometry by modifying the

ratio between the ligand precursor and the metal, enabled the selective synthesis of the compounds. The reactivity of unprotected methyl guanosine was also examined and, also in this case, the reaction led to a mixture of a mono- and a bis-carbene, which can be selectively synthesized by changing the stoichiometry of the reaction.

The last chapter concerns the synthesis of Iridium, ruthenium and gold complexes, containing uracil derivatives bearing an imidazole ring as a pendant group, and their catalytic activity on NAD^+ to NADH reduction. This imidazole ring was derivatized with methyl, isopropyl and anisole groups. The ligand precursors thus synthesized were reacted with ruthenium or iridium precursors, namely, $[Ru(p\text{-cymene})Cl_2]_2$ and $[Ir(Cp^*)Cl_2]_2$ in the presence of a base. The imidazole ring binds to the metal via C5 instead of C2, leading to the formation of an abnormal carbene with both metals. The ligand precursors can be converted into their betaine form by reaction with sodium acetate. Once converted into the betaine form, the ligand precursor bearing a methyl imidazole ring was reacted with $Au(SMe_2)Cl$. In this case the imidazole ring binds to the metal via C2, forming a normal carbene. This latter experiment suggested that the normal NHCs of iridium and ruthenium could be obtained by transmetalation. Reaction of the ligand precursor with silver(I), in the presence of $[Ru(p\text{-cymene})Cl_2]_2$ and $[Ir(Cp^*)Cl_2]_2$ lead to the formation of the corresponding normal NHC compounds.

The compounds were evaluated on the reduction of NAD^+ to NADH. Catalytic tests revealed a dependence between the metal and the catalytic performance. Iridium catalysts are more efficient than ruthenium catalysts, which revealed to be very poorly active. The connectivity to the metal, influences the catalytic activity. Normal carbenes perform better than their

abnormal counterparts. The substituents at the imidazole ring show some degree of influence and isopropyl substituents provide higher catalytic activity. Overall, the iridium normal carbene bearing an isopropyl substituent proved to be the best catalyst.

In conclusion, this thesis work presents three new classes of compounds with promising pharmaceutical activities, one of which has already been patented, paving the way for subsequent studies to improve their pharmacological activity.

List of Publications

The results obtained from this research project were published in the following peer-reviewed papers:

1. Francescato, G.; da Silva, S.M.; Leitão, M.I.P.S.; Gaspar-Cordeiro, A.; Giannopoulos, N.; Gomes, C.S.B.; Pimentel, C.; Petronilho, A.; Nickel N-heterocyclic carbene complexes based on xanthines: Synthesis and antifungal activity on Candida sp. *Appl. Organomet. Chem.* 2022, e6687. https://doi.org/10.1002/aoc.6687
2. Francescato, G.; Leitão, M.I.P.S.; Orsini, G.; Petronilho, A.; Synthesis and Medicinal Applications of N-Heterocyclic Carbene Complexes Based on Caffeine and Other Xanthine (accepted). *ChemMedChem* 2024, e202400118. https://doi.org/10.1002/cmdc.202400118

Preprint articles part of this thesis:

1. Francescato, G.; Orsini, G.; Petronilho, A.; Gold Mono and Bis N-Heterocyclic Carbenes based on mRNA cap0. Doi: 10.26434/chemrxiv - 2024-bt0dw-v2

Other related publications not part of this thesis:

1. Leitão, M.I.P.S.; Gonzalez, C.; Francescato, G.; Filipiak, Z.; Petronilho, A. On the reactivity of mRNA Cap0: C–H oxidative addition of 7-methylguanosine to Pt^0 and base-pairing studies. *Chem. Commun.* 2020, *56*, 13365–13368. https://doi.org/10.1039/D0CC06075E

2. Leitão, M.I.P.S.; Francescato, G.; Gomes, C.S.B.; Petronilho, A. Synthesis of Platinum(II) N-Heterocyclic Carbenes Based on Adenosine. *Molecules* 2021, *26*, 5384–5395. https://doi.org/10.3390/molecules26175384

3. de Alencar, D.M.; Gonçalves, J.; Vieira, A.; Cerqueira, S.A.; Sebastião, C.; Leitão, M.I.P.S.; Francescato, G.; Antenori, P.; Soares, H.; Petronilho, A. Development of Triazoles and Triazolium Salts Based on AZT and Their Anti-Viral Activity against HIV-1. Molecules 2021, *26*, 6720–6732. https://doi.org/10.3390/molecules26216720

Abbreviations and symbols

A2780	Ovarian carcinoma cell line
bs	broad singlet
ca.	*circa* (from Latin, meaning “approximately”)
$CDCl_3$	deuterated chloroform
CD_3OD	deuterated methanol
d	doublet
dd	doublet of doublet
dt	doublet of triplet
DCM	dichloromethane
DMF	dimethylformamide
DMF-d_7	deuterated dimethylformamide
DMSO	dimethylsulfoxide
DMSO-d_6	hexadeuterated dimethylsulfoxide
DNA	deoxyribonucleic acid
EA	elemental analysis
EMA	European Medicines Agency
ESI	electrospray ionization
et al.	*et alia* (from Latin, meaning “and others”)
EtOH	ethanol
Et_2O	diethyl ether
HEK-293	Human Embryonic Kidney cell line
HeLa	Human cervical carcinoma cell line

HIV	human immunodeficiency virus
HMBC	heteronuclear multiple bond coherence
HRMS	high-resolution mass spectrometry
HSQC	heteronuclear single quantum coherence
Hz	hertz
ICD	immunogenic cell death
IC_{50}	Half maximal inhibitory concentration
J	coupling constant (hertz, Hz; NMR)
M	molar, denoting a concentration equivalent to mol/dm^3
m	multiplet
M^+	molecular ion
m/z	mass-to-charge ratio (mass spectrometry)
7-MeG	7-methylguanosine
MeOH	methanol
mRNA	messenger RNA
MTT	3-(4,5-dimethylthiazol-2-yl)-2,5-diphenyl-2H-tetrazolium bromide
NMR	nuclear magnetic resonance
NHC	N-heterocyclic carbene
nm	nanometre
q	quartet
RNA	ribonucleic acid
s	singlet
S.I.	safety index
SKOV-3	cis-platin resistant ovarian cancer cell line
t	triplet

td	triplet of doublets
TfO^-	Triflate ion
THF-d_8	deuterated tetrahydrofuran
Tht	tetrahydrothiophene
TLC	thin layer chromatography
W-C	Watson–Crick
U251	glioblastoma cell line
δ	Chemical shift
µm	micrometres
µM	micromolar, denoting a concentration equivalent to 10^{-6} M

CHAPTER 1

INTRODUCTION

1.1. N-heterocyclic carbenes

Modern organometallic chemistry methods can be used to synthesize a large variety of complexes via the introduction of ligands such as carbenes, which are among the most widely used ligands to stabilize metal centre[1,2]. Carbenes are distinguished by having a carbon atom possessing six electrons in its valence shell and therefore an incomplete octet. Carbenes can assume different hybridizations and thus different geometries. The carbenic carbon can be linear with sp hybridization, or bent, with sp^2 hybridization, with the latter being the most common[3]. Nevertheless, even sp^2 carbenes are not easily isolable due to their lack of stability, in fact, they were initially recognized solely as intermediates in organic reactions[4]. In 1980, L. Pauling stated that the stability of a free sp^2 carbene may be dependent on the substitution of the carbenic carbon. In particular, it would be necessary to have two π-donor σ-acceptor substituents to ensure electroneutrality at the carbenic center.[5] In addition to the electronic properties of the substituent, steric effects should also be taken into account when considering the stability of a carbene. In fact, bulky groups are able to provide stabilization due to steric protection.[3] All these theoretical considerations led Arduengo and his collaborators, in 1991, to successfully isolate and crystallize an NHC, where two nitrogen atoms are bound to the carbenic carbon and substituted by a

hindering group (adamantyl group), which serves to sterically “protect” the reactive site of the carbenic carbon[6].

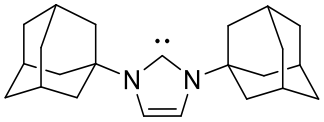

Figure 1.1 - *N-Heterocyclic carbene described by Arduengo.*

This milestone opened the gates of organometallic chemistry for the development of complexes bearing N-heterocyclic carbenes (NHCs). NHCs feature carbenes enclosed within a N-heterocycle, wherein the carbenic carbon is stabilized by at least one nitrogen atom. Once bound to a metal, NHCs generally behave like σ-donor ligands but can also have a weak π-acceptor effect on the *-d* electrons of the metal due to the empty p-orbital of the carbene[7]. The strong σ-donor component results from the displacement of the nitrogen atom’s lone pair of electrons, which increases the energy of the highest occupied molecular orbital (HOMO). This mesomeric effect increases the σ-donor component of the ligand and thus creates a very stable bond between the metal and the carbon[2,7,8]. The very nature of the heterocycle and/or the substitution present on the nitrogen atoms can easily modify the electronic and steric properties of NHCs. Substituents particularly electron-rich participate in electronic donation to the p-orbital of the carbon[8]. Because of all these properties, N-heterocyclic carbenes are excellent ligands for transition metals and are appealing ligands for various applications. This has led to their prominence in the synthesis of organometallic compounds containing NHCs, gradually replacing the previously prevalent phosphines. In comparison to phosphines, NHCs

complexes exhibit greater stability against moisture and air and demonstrate reduced susceptibility to oxidation[3].

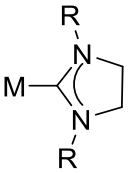

Figure 1.2 - *General structure and bonding of a typical N-heterocyclic carbene.*

The ability to create a diverse library of organometallic compounds opened the way for novel applications of these complexes, particularly in catalysis but also in pharmaceutical sector. Notably, the use of such complexes for medicinal chemistry has gained relevance in recent years. In line with this, the development of NHCs based on bioactive ligands is particularly promising[9]. The synthesis of complexes utilizing biologically relevant ligands has emerged as a valuable approach for developing more selective compounds[10] and opens the possibility of enhancing both the therapeutic efficacy and the biocompatibility of a particular drug[11].

The work described in this thesis focuses on the formation of organometallic complexes incorporating DNA or RNA bases or analogous compounds such as xanthine, bound to a metal as NHCs. This dual focus aims to understand the reactivity of nucleobases while also exploring the development of novel therapeutics employing metallonucleobases.

1.2. Metal complexes bearing NHCs based on nucleobases, nucleosides and their analogues

Methylation (or alkylation) of nucleic acids is a critical modification of the genome[12,13] and is involved in the regulation of a wide array of cellular processes[14–16]. Methylation can occur at several sites on DNA and RNA nucleobases (Figure 1.3)[16] and leads to the formation of so-called DNA and RNA adducts[17]. DNA adducts show enhanced reactivity and are responsible for a wide range of cytotoxic and mutagenic lesions[18].

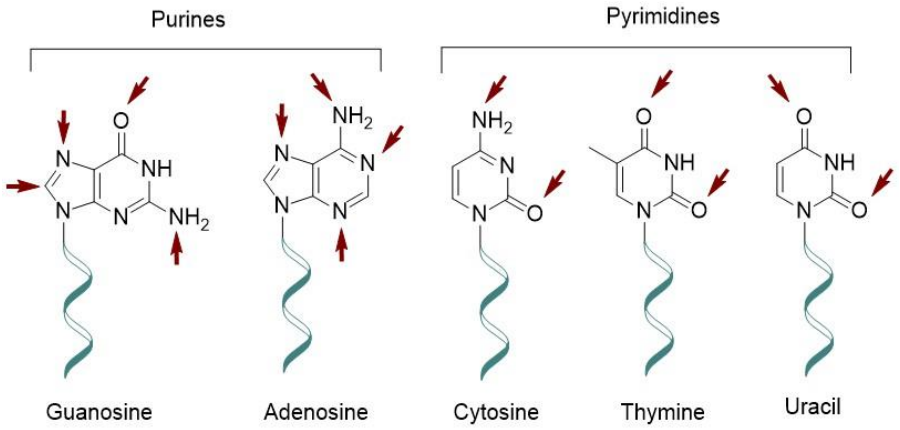

Figure 1.3 - *Most likely alkylated positions to form DNA or RNA adducts*[19,20].

Some DNA adducts are NHC precursors, as most of them are azolium or pyrimidinium cations, which can further react upon proton loss[21]. Not surprisingly, DNA adducts typically exhibit similar reactivity patterns to those of azolium salts, which is particularly evident for purines[14,22]. Early reports have focused on this latent reactivity, pointing to the formation of NHCs as intermediates, for instance, in nucleic acid damage[14]. This opens the

possibility of exploring the reactivity of nucleic acids and their derivatives in the formation of NHCs and with a metal center.

1.2.1. Pyrimidines

Although pyrimidines bind to metals mostly by coordination to the heteroatoms, the formation of M-C bonds is possible. The most common strategy for forming C-M bonds with pyrimidine rings involves C-X oxidative addition, affording the formation of the corresponding organometallic compound. Despite extensive studies on the reactivity of pyrimidine derivatives in forming organometallic compounds[23,24], only one of these comprises the formation of an NHC[25]. For example Santacroce and co-workers, in 1987, reported the oxidative addition of platinum(0) to 4-chlorothymidine, affording the formation of the corresponding metal complex with a M–C bond (Scheme 1.1)[26].

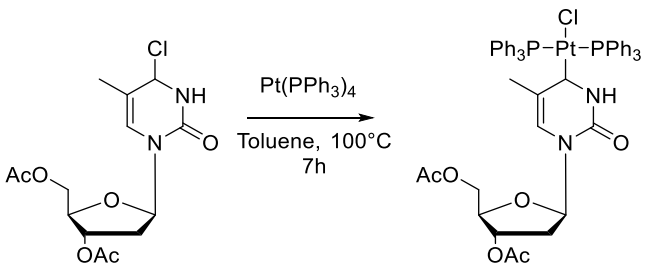

Scheme 1.1 - *Formation of a C-M bond by oxidative addition.*

Following on this earlier work, Messere and coworkers reported the first NHC derived from a pyrimidine nucleobase. Their efforts focused on the reactivity of modified thymine with palladium(0), which undergoes metalation at N3 when the natural nucleobase is used. However, when 4-chloro-thymidine is employed instead, the metalation occurs at C4 (Scheme

1.2), as observed earlier for platinum. In an acidic environment, this metalated compound can rearrange into an NHC through the formation of an enolate involving the oxygen atom at position 2, which is subsequently protonated[25].

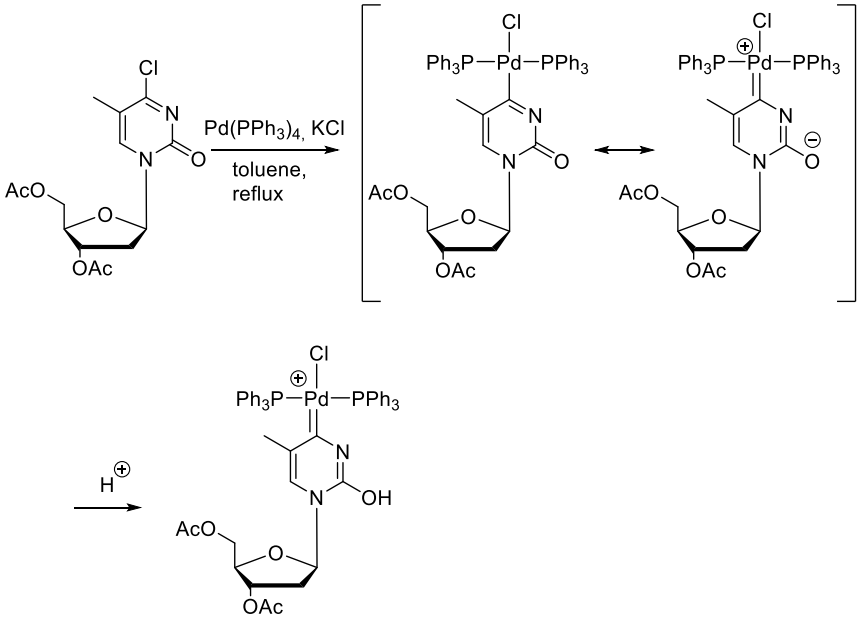

Scheme 1.2 - *Palladium NHC based on thymine described by Messere.*

However, in this case, the nucleobase was modified by replacing oxygen with chloride, which is needed for C-X oxidative addition, to form a metal-C bond at C4. Nonetheless, while the formation of the NHC is observed, the Watson–Crick or Hoogsteen base pairing sites are not preserved; therefore, the hydrogen bonding ability of the metalated nucleobase is strongly affected.

When the metalation is performed at C5 or C6, it does not preclude the potential for base pairing for cytidine and uridine or for thymidine (if metalated at C6).

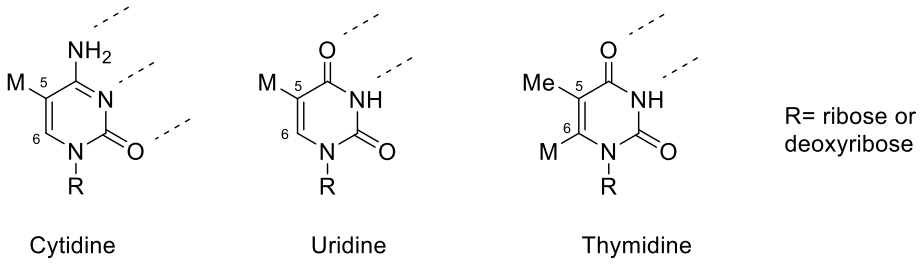

Figure 1.4 - *Metalation of the pyrimidine ring does not preclude base pairing.*

Along these lines, within our laboratory, a series of organometallic complexes have been developed that incorporate uracil, where the metal ion specifically binds at the C5 position of this pyrimidine base (Scheme 1.3). Our approach involved the derivatization of uridine and deoxyuridine at the C5 position using a halogen, specifically iodine, followed by the subsequent oxidative addition to Pt(0), affording the desired organometallic complexes[27].

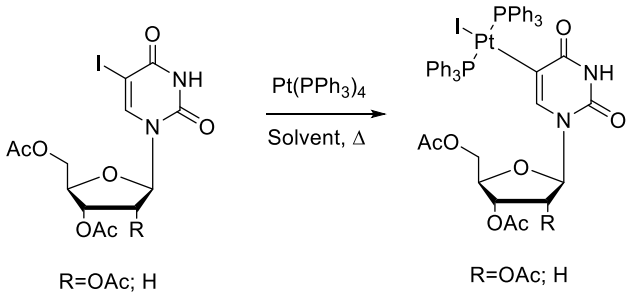

Scheme 1.3 - *Oxidative addition of platinum(0) to uridine.*

Carbenes are formally 2 electron neutral donors[28]. In some cases, it is possible to observe a resonance structure where no charges are displayed in the carbene, which is the case for normal carbenes. When a neutral resonance structure is not available the carbene constitute the so-called abnormal carbenes[28].

In the context of pyrimidines, achieving the formation of an NHC is feasible primarily due to the nucleophilic nature of the oxygen at C2 or at C4, as in the case of uracil and thymine, which can be protonated under acidic conditions. Thus, an acidic environment further promotes the formation of an NHC, when the C-M bond involves position C6 of the aromatic ring.

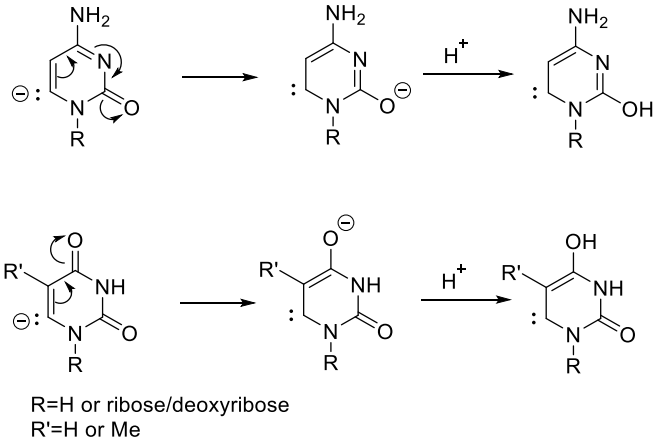

Scheme 1.4 - *Formation of a pyrimidine NHC.*

Metalation at C5 could also lead to the formation of an NHC; upon appropriate modification and subsequent protonation (Scheme 1.5).

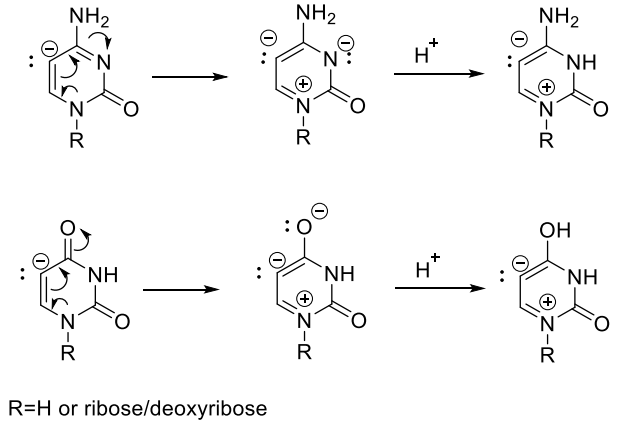

Scheme 1.5 - *Formation of a pyrimidine abnormal NHC.*

Nevertheless, also in this case the formation of an NHC leads to the modification of essential sites for Watson–Crick base pairing contrary to what is found for purines. Yet, one of the very few examples of carbene formation in nature for pyrimidine bases involves a similar situation and is a key step in nucleic acid biosynthesis. The decarboxylation of orotidine monophosphate to form uridine monophosphate involves the formation of an ylide, considerably stabilized by the corresponding neutral carbene structure.

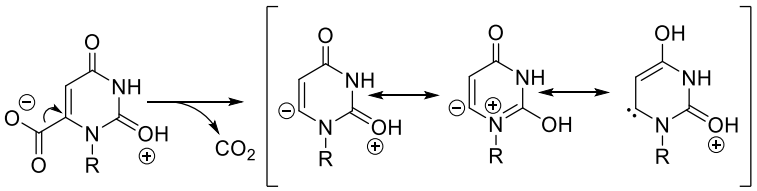

R= Ribose

Scheme 1. 6 - *Formation of the decarboxylated orotidine.*

Thus, not only the formation of NHCs is relevant in the case of DNA adducts, but NHCs are also key intermediates in nucleic acid synthesis. For these reasons, the study and the formation of metal complexes based on these ligands is key to further understand the reactivity of these species and their impact in nucleic acid chemistry and biochemistry.

1.2.2. Purines

In the case of purines, the possibility of the formation of NHCs after derivatization is more evident. The N7 position of the guanine residue, for example, is the most nucleophilic site of all nucleobases[14]. One of most notable characteristics of N7-methylated guanine adducts is the increased

acidity of the C8-H bond, which is attributed to the formation of an NHC intermediate[15].

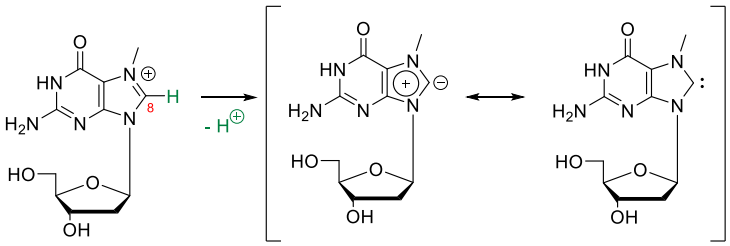

Scheme 1.7 - *Acidity of the C8-H bond.*

Several examples of metal complexes bearing purine-based NHCs have been reported in the literature[23]. The synthetic approaches involve base-assisted deprotonation, cyclometallation, transmetalation or oxidative addition. Among these methods, oxidative addition is the most recent. Hahn's group reported in 2014 the oxidative addition of 8-bromo-9-methyladenine to platinum(0), followed by treatment with NH_4BF_4 (Scheme 1.8). Ammonium tetrafluoroborate (NH_4BF_4), as a proton source, can protonate the nitrogen at position 7 of the 9-methyladenine bound to the metal center via C8, affording the corresponding NHC[29].

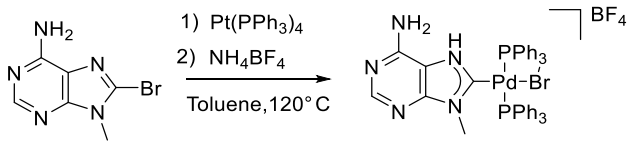

Scheme 1.8 - *Synthesis of an adenine NHC by C-X oxidative addition described by Hahn's group.*

Following earlier work from Santacroce and Messere for pyrimidines, and considering these results by Hahn, our group described the reaction of

acetate-protected bromoguanosine with $M(PPh_3)_4$ (M = Pd, Pt) in toluene or DMF, affording the corresponding guanosine complexes (Scheme 1.9). Once the nucleobase is bound to the metal center via C8, it can be protonated under acidic conditions to yield the corresponding protic NHCs[11].

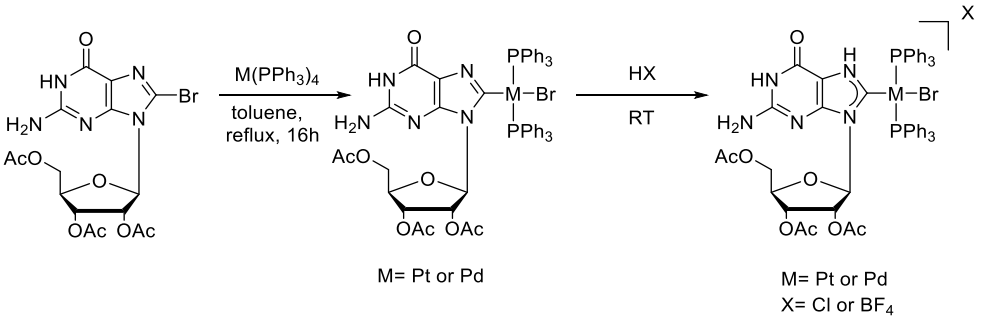

Scheme 1.9 - *Formation of NHC by oxidative addition of guanosine to platinum or palladium.*

Hahn's group also explored the oxidative addition of purines to platinum(0) by reaction with 8-bromoadenine or 8-chlorotheophilline (Scheme 1.10). The authors were able to synthesize NHCs in one step from both ligand precursors by adding a source of protons to the reaction mixture[30,29].

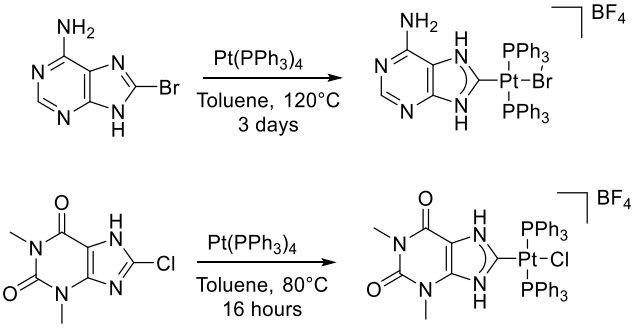

Scheme 1.10 - *Oxidative addition of bromo adenine and chlorocaffeine to platinum.*

More recently, C-H oxidative addition of purinium salts to a metal center has been explored by our group[31]. This approach follows a similar methodology to that of C-X activation. Prior studies from Cavell showed that this procedure is not effective to form NHCs from their corresponding imidazolium salts due to competitive reductive elimination[32].

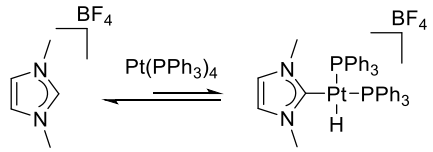

Scheme 1.11 - *C-H oxidative addition/reductive elimination of imidazolium salts to Pt(0).*

This seems not to be the case for nucleobases and xanthines. An example of this reactivity is the direct metalation of N7-methyl guanosine, or caffeine to $Pt(PPh_3)_4$, as shown in Scheme 1.12. Accordingly, N7-methyl guanosine reacted with Pt(0) in DMF at 100°C for the guanosine derivative and at 60°C for methyl caffeine[31,33].

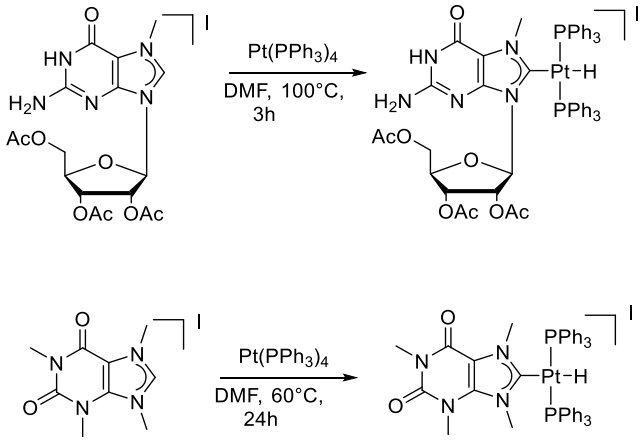

Scheme 1.12 - *Formation of NHC by direct metalation of N7-methyl guanosine.*

The same procedure cannot be used for adenosine, as the most nucleophilic site of the latter is N1; thus, treatment of adenosine with methyliodide leads to the formation of N1-methyladenosine, which when reacted with platinum under the same conditions does not lead to the formation of a M-C bond.

An alternative route was used to obtain analogous adenosine NHCs. Thus, 8-bromoadenosine was reacted with $Pt(PPh_3)_4$ to yield the corresponding neutral complex, which was subsequently methylated at N7 (Scheme 1.13). Upon metalation, N7 becomes the most nucleophilic position and ensures selective methylation to yield the corresponding NHC[34].

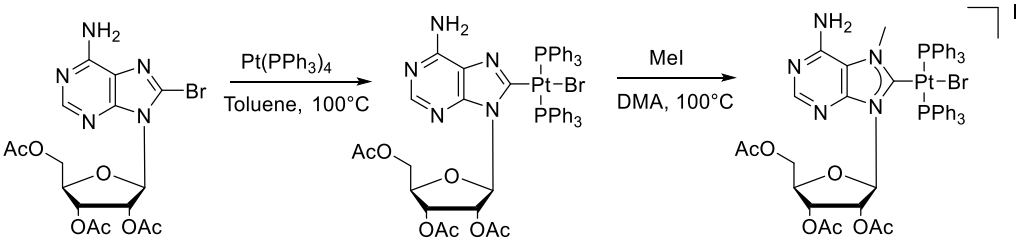

Scheme 1.13 - *Metalation and methylation of adenosine afforded the corresponding NHC.*

A different approach to obtain an NHC containing adenine was reported by Houlton's group[35] in 1997, where the authors described the synthesis of a cyclometallated adenine complex (Scheme 1.14). Adenine was derivatized at N9 with ethylenediamine, resulting in a bidentate ligand precursor capable of coordinating with the metal center. When the ligand precursor was reacted with $[(DMSO)_2H][RuCl_4(DMSO)_2]$, an intermediate was formed, corresponding to the chelate complex involving the two amine residues (Scheme 1.14). Following this, cyclometallation allows regioselective C8-H activation, leading to the formation of a C8-Ru bond.

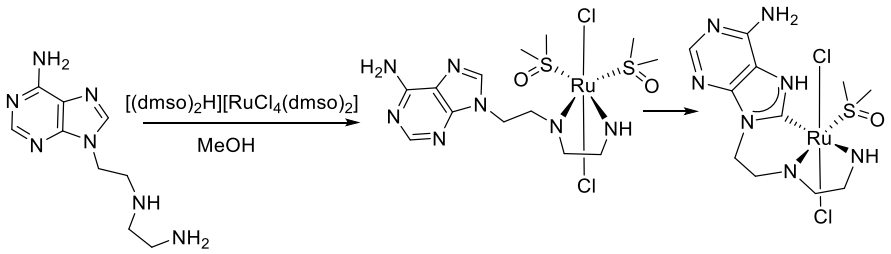

Scheme 1.14 - *Synthesis of a ruthenium NHC based on adenosine by cyclometallation.*

The same approach was recently reported by Hahn's group. The adenine was derivatized at N9 with an ethyl diphenyl phosphine group. The ligand precursor was reacted with $[IrCl_2Cp^*]_2$ (Cp*=pentamethylcyclopentadiene) in toluene at room temperature, leading to the coordination of the phosphine to the metal center (Scheme 1.15). By heating the obtained complex in acetonitrile at 100°C, the adenine pending group undergoes cyclometalation and binds to the metal regioselectively at C8[36].

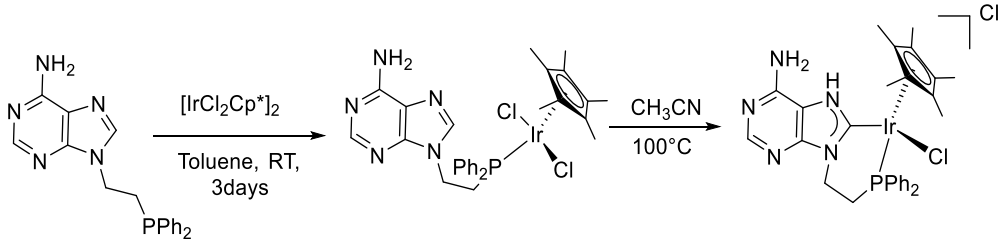

Scheme 1.15 - *Synthesis of a iridium complex featuring a phosphine tethered adenine based NHC.*

Another class of natural purines that, although not incorporated into DNA or RNA, is relevant for the metabolic route leading to the formation of nucleobases[37] is xanthines. The natural xanthines are caffeine, theophylline,

and theobromine, which are purine bases that are methylated at different nitrogen atoms.

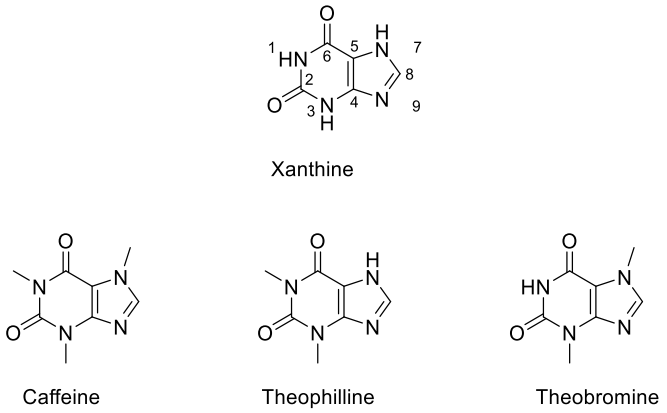

Figure 1.5 - *Natural xanthines.*

Similarly, for xanthines there is a propensity for NHC formation. In particular, in the case of caffeine or theobromine, it is possible to methylate N9, but modifications beyond methylation and benzylation are difficult to achieve. Contrastingly, theophylline can first be derivatized with different groups at N7 and then quaternized at N9 to form the corresponding xanthinium salts. Given their simple derivatization, there are many examples of metal complexes bearing NHCs based on this class of compounds. For example, metalation at C8 of caffeine was achieved by the C-X oxidative addition by Hahn's group, as discussed above[29,30]. In 2021, the same group reported the oxidative addition of a theobromine derivative (8-bromo-9-ethyl-theobromine) to palladium or platinum, followed by treatment of the metal complex with HBF_4 to obtain the corresponding NHC[38].

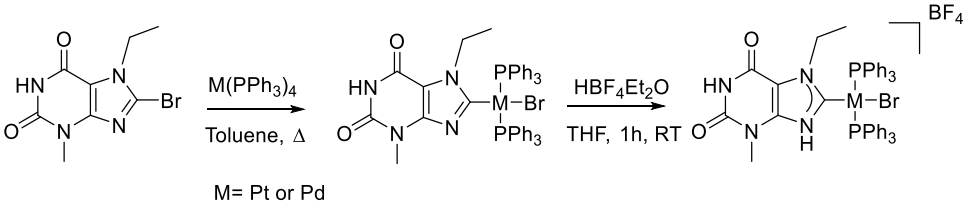

Scheme 1.16 - *Oxidative addition of theobromine to palladium or platinum.*

Taube reported the first NHC based on purines in 1975, exploring C-H activation catalysed by acid to synthetize xanthine based NHCs. Caffeine, theobromine and theophylline were reacted with chloropentaammine-ruthenium(III) trifluoroacetate under acidic conditions (Scheme 1.17). In the case of caffeine and theobromine (with N7 occupied by a methyl group), ruthenium binds the ligand only via C8, while for theophylline, both C and N complexes are formed[39,40].

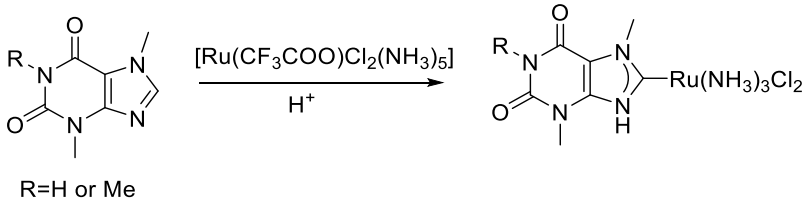

Scheme 1.17 - *Formation of ruthenium NHC based on xanthine by acid catalysed tautomerization.*

In 1976, Beck's group utilized based assisted deprotonation to synthesize the first purine-based biscarbene. Methylcaffeine was reacted with mercury acetate affording the corresponding biscarbene upon deprotonation of methyl caffeine; in this reaction, the acetate groups coordinated to mercury act as an internal base [41].

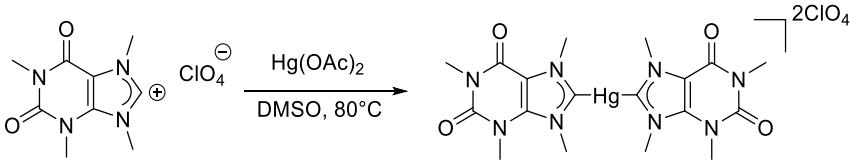

Scheme 1.18 - *Formation of a Hg biscarbene based on caffeine.*

Base-assisted metalation is also frequently employed when theophylline is used as the ligand precursor. Theophylline is mostly used when it is necessary to derivatize N7 with substituents other than methyl; this preference is due to the difficulty of N9-derivatization of caffeine with substituents other than methyl or benzyl groups due to the reduced nucleophilicity of N7[42–44]. For example, in 2016, the Movassagh group derivatized theophylline N7 with polystyrene (Scheme 1.19). The resulting derivative was then reacted with ethyl iodide to obtain the corresponding azolium salt. The obtained ligand precursor was reacted with palladium acetate, leading to the formation of a carbene supported on a solid matrix, with the final aim of creating a heterogeneous catalyst[45].

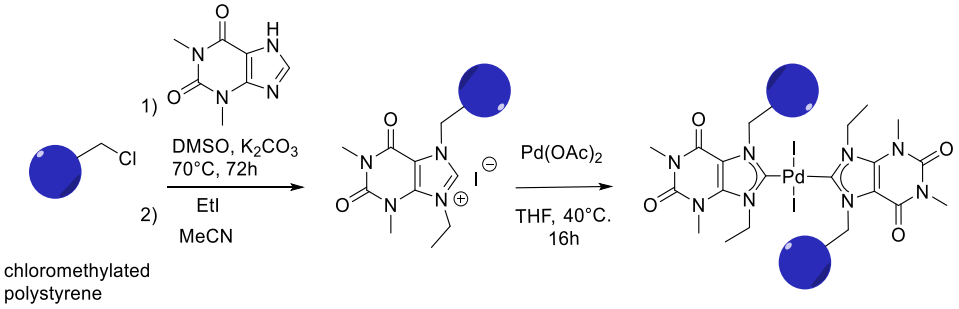

Scheme 1.19 - *Synthesis of a xanthine NHC anchored to a polystyrene polymer.*

With xanthines, the most common route for NHC synthesis is transmetalation from silver NHCs. Access to silver complexes is usually not

difficult. For example, Young's group reacted methyl caffeine and methyltheobromine with Ag_2O, resulting in the formation of the respective biscarbene complexes[42].

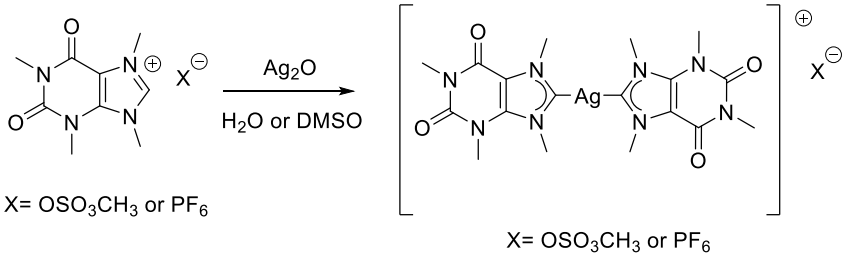

Scheme 1.20 - *Formation of a silver biscarbene complex based on caffeine.*

Later, Visentin's group synthesized a series of silver biscarbene bearing xanthine derivatives, using Young's procedure (Scheme 1.20). The compounds were subsequently used to synthesize the corresponding palladium complexes through transmetalation[46].

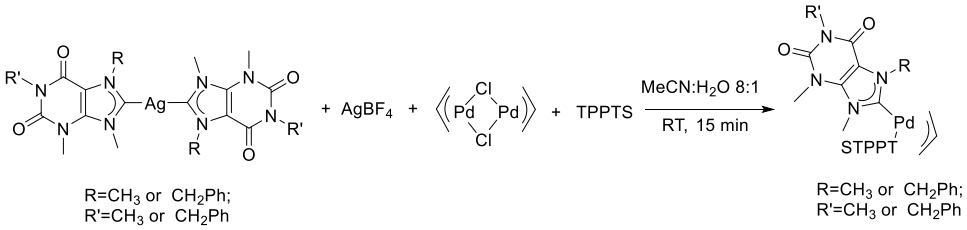

Scheme 1.21 - *Transmetalation route for the synthesis of palladium carbenes containing caffeine.*

In conclusion, many routes have been used for the synthesis of metal complexes containing nucleobases and their analogues as NHCs, despite this, there are still many avenues to be explored and studied in greater depth.

1.3. Medicinal Applications of Metal Complexes based on Purine and Pyrimidine NHCs.

Metals have been widely used in medicine[47]. Silver compounds have been employed for centuries for microbial infections[48] and the discovery and subsequent use of auranofin for rheumatism[49] and of cisplatin for cancer treatment[50] were a landmark for modern bioorganometallic chemistry[47].

Due to the high stability of their carbon-metal bond, NHCs are excellent ligands for metallodrugs. In this regard, the utilization of biologically relevant NHC precursors such as purines or pyrimidines nucleobases and xanthine is very appealing. Xanthines have been recognized as therapeutically potent compounds for the treatment of various conditions [51] and are effective in the treatment of neurodegenerative and respiratory diseases, diabetes and cancer[52,53].

Youngs's group combined the antimicrobial activity of caffeine with the antimicrobial activity of silver[54,55]. Indeed, silver has established antimicrobial activity and is often used in nanoparticles for this purpose[56,57]. Youngs and collaborators synthesized an NHC incorporating methylated caffeine, which was subsequently tested on various species representing both gram-positive and gram-negative bacteria, as well as fungi.

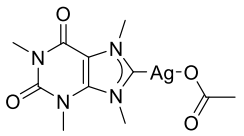

Figure 1.6 - *Silver NHC studied by Young's group with antimicrobial activity.*

In all three cases, the complex exhibited activity in the microgram range, whereas the activity of the ligand precursor alone was in the milligram range, revealing the essential role of silver. Furthermore, in vivo tests revealed low toxicity levels for both complex and methylated caffeine[54].

Silver carbenes containing xanthines may also have anticancer activity [58–60]. For example, the Willans group reported a set of silver NHCs containing xanthines and examined their anticancer activity. In both cases, the xanthine was derivatized with different substituents at N1 or N7 (Fig 1.7). The authors found that there is a direct correlation between the steric hindrance and the cytotoxicity of the complexes[58] and determined that derivatization with carborane at N1 renders the complex very active against colon cancer cell lines[59].

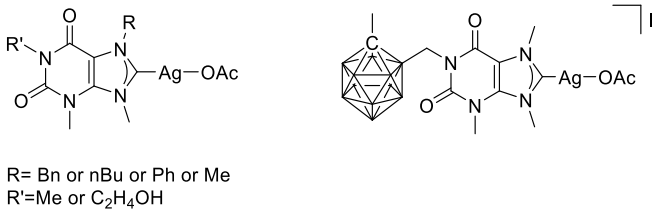

Figure 1.7 - *Compounds tested for their anticancer activity by Willans's group.*

Casini's group[61–66] reported a series of gold NHCs based on caffeine and theophylline (Fig 1.8)[65]. Among these compounds, the methylcaffeine biscarbene was found to be particularly active in two ovarian cancer cell lines (A2780 and the doxorubicin-resistant cell line A2780/R). Interestingly, this complex is selective for ovarian cancer and almost nontoxic to a noncancerous cell line, as shown by *ex vivo* studies.

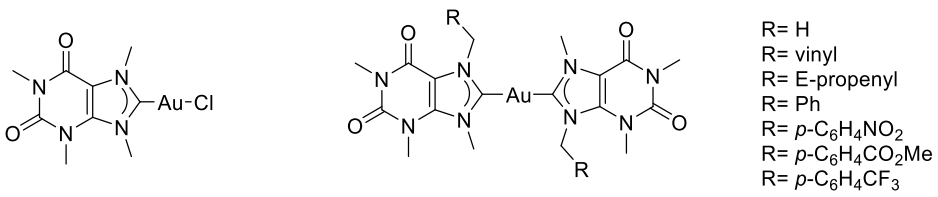

Figure 1.8 - *Gold compounds tested for their anticancer activity by Casini's group.*

Other examples of anticancer compounds based on a caffeine NHCs were reported by Ott's group, who developed platinum, ruthenium and rhodium carbenes based on this compound.

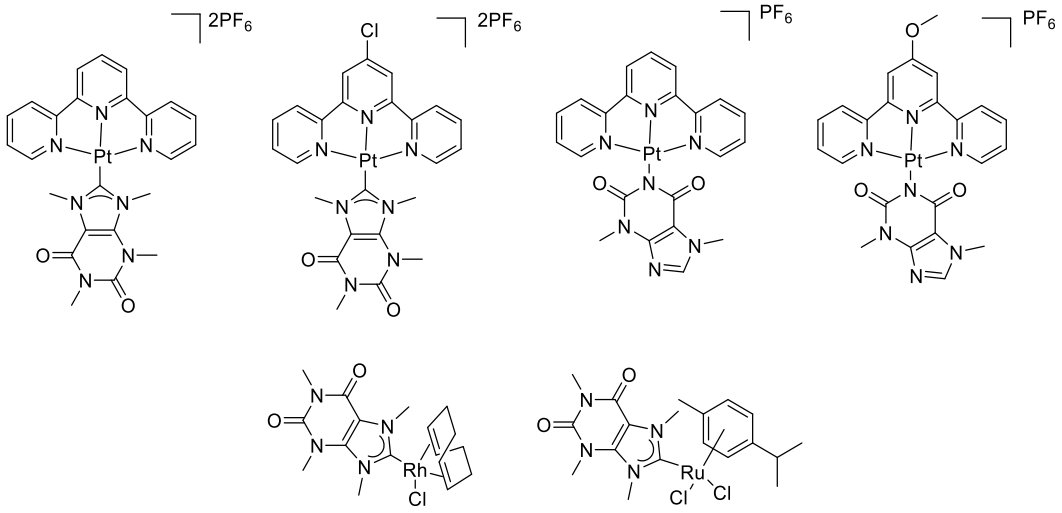

Figure 1.9 - *Complexes tested by Ott's group for their anticancer activity.*

Regarding the platinum complexes, the authors compared the activities of four different complexes, two of which were coordinated via C8 of methyl caffeine and two of which were coordinated via N1 of theobromine (Fig 1.9). This study revealed that coordination via C8 increased the cytotoxic activity against breast cancer cell lines (MCF-7 and MDA-MB-231) and against a colon adenocarcinoma cell line (HT-29 colon). The rhodium and ruthenium

complexes were tested on human neuroblastoma (IMR-32), human hepatoma (HepG2), human breast cancer (MCF-7 and MDA-MB-231), human colon carcinoma (HCT-116), human pancreatic cancer (Panc-1), and human prostate adenocarcinoma (LNCaP) cell lines. The rhodium complex shows promising activity, yet the IC_{50} is not higher than that of cisplatin[67,68].

Finally, palladium complexes bearing NHCs based on xanthines were studied by Visentin's group, who tested these complexes (Fig 1.10) on two ovarian cancer cell lines (A2780 and the cisplatin resistant SKOV-3). The study demonstrated that all the complexes displayed good activity on the cisplatinum-sensitive cell line, but the monocarbenes exhibited greater cytotoxicity on the cisplatinum-resistant cell line. The toxicity of the complexes was also tested using normal human fibroblasts, and the resulting compounds were found to be poorly toxic[46].

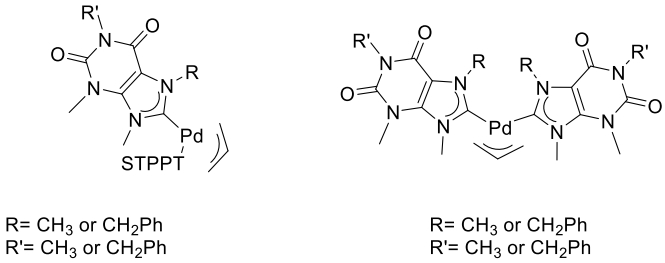

Figure 1.10 - *Compounds tested for their anticancer activity by Visentin's group.*

Regarding nucleobases and the medicinal applications of their corresponding NHCs there are much less reported examples as compared to xanthines. In this regard, our group was among the first to explore the antitumour activity of guanosine-based NHC carbenes containing platinum and palladium (Fig 1.11)[11,33]. This work demonstrated that guanosine

derivatives with palladium or platinum as the metal center are active in glioblastoma cell lines U251 but nontoxic to healthy cells[11]. Other guanosine complexes bearing an hydride were also tested (Figure 1.11). An examination of the relationship between the structural activity and the antiproliferative activity showed a hindering side chain at N7, and the presence of a hydride trans to the NHC led to enhanced cytotoxicity. Furthermore, mechanistic studies have shown that these complexes foster the induction of reductive stress[33], thus operate through a mechanism that is different from that of cis-platin.

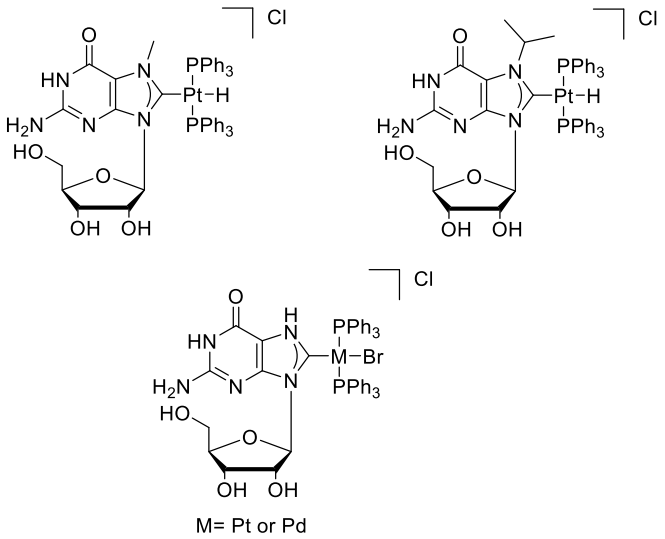

Figure 1.11 - Platinum complexes bearing *guanosine NHCs.*

Finally, concerning pyrimidines, the uridine compounds described earlier (Fig 1.2), even if are not NHCs, have been evaluated for their antitumour activity[27]. Both complexes of uridine and deoxyuridine were tested in glioblastoma cell lines and found to be highly toxic, but their safety profile is not ideal since they show a high degree of toxicity toward non tumorous cells.

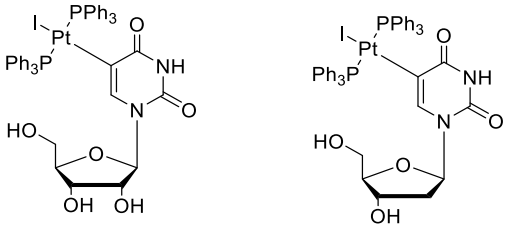

Figure 1.12 - *Platinum complexes based on uridine.*

Given the critical need to develop new compounds that are pharmacologically active both as antimicrobial agents and as anticancer agents and considering the importance of organometallic chemistry in this discovery, this thesis focuses on the synthesis of new organometallic compounds containing carbenes derived from nucleobases or nucleobase analogues (xanthines) and the assessment of their pharmacological activity.

CHAPTER 2

NICKEL N-HETEROCYCLIC CARBENE COMPLEXES BASED ON XANTHINES: SYNTHESIS AND ANTIFUNGAL ACTIVITY ON CANDIDA SP.

Introductory notes

Figure numbering

The numbering of the figures, schemes and tables shown here in Chapter 3 is independent of the use of the other chapters.

Published paper

The majority of the content of this chapter is summarized in the following paper: Francescato, G.; da Silva, S.M.; and Leitão, M.I.P.S.; Gaspar-Cordeiro, A.; Giannopoulos, N.; Gomes, C.S.B.; Pimentel, C.; Petronilho, A. Nickel N-heterocyclic carbene complexes based on xanthines: Synthesis and antifungal activity on Candida sp. Appl. Organomet. Chem. 2022, e6687.

Author contributions

The author of this thesis performed all the experiments reported in this chapter. The in vitro experiments were conducted with the laboratory of Dr. Catarina Pimentel from ITQB NOVA, under the guidance of Dr. Sofia Silva. X-ray diffraction data acquisition and analysis were performed by Dr. Clara Gomes from NOVA FCT, Portugal.

2.1. Introduction

In recent decades, a drastic increase in invasive fungal infections (FIs) has been observed, and these infections represent a global health threat[69–72]. There are three main reasons for this FI intensification[73]. First, fungi, like mammals, are eukaryotes, and many of their proteins acknowledged as targets for antifungal therapy are also found in humans, considerably decreasing selectivity[73]. Second, even drugs with better specificity for pathogens have become less efficient in recent years due to extended use and the consequent selection of highly tolerant fungi[74]. Third, while the vast majority of fungal pathogens are opportunistic pathogens, they can be life-threatening pathogens in immunocompromised patients; as such, the increased use of immunosuppressive therapies for cancer and organ transplants strongly correlates with the increasing incidence of FIs[75]. Candida sp., an opportunistic fungal pathogen, causes more than 70% of all nosocomial FIs. Among these, infections caused by *C. albicans* remain the most common, but the incidence of *C. glabrata* infections is increasing due to its reduced response to azole-based antifungals[76–78].

Azole-based antifungals are a class of antifungal agents containing an aromatic heterocycle that includes at least one nitrogen atom (the simplest heterocycle being pyrrole) and typically an additional heteroatom (nitrogen, sulfur, oxygen)[79]. The first azole-based antifungal drug introduced in the market was chlormidazole, which was initially used to treat superficial mycosis.[80] In 1989, the first oral azole-based medication, ketoconazole, was released[79,80].

However, despite being recognized as the pioneer of second-generation azoles, ketoconazole has several side effects, low selectivity, and was not consistently effective[81]. This led to the search for new azoles as antifungal agents and to the discovery of one of the most common antifungal agent used today, fluconazole[79]. Fluconazole differs from previous antifungal agents by incorporating a triazole ring instead of an imidazole[79,80,82–84].

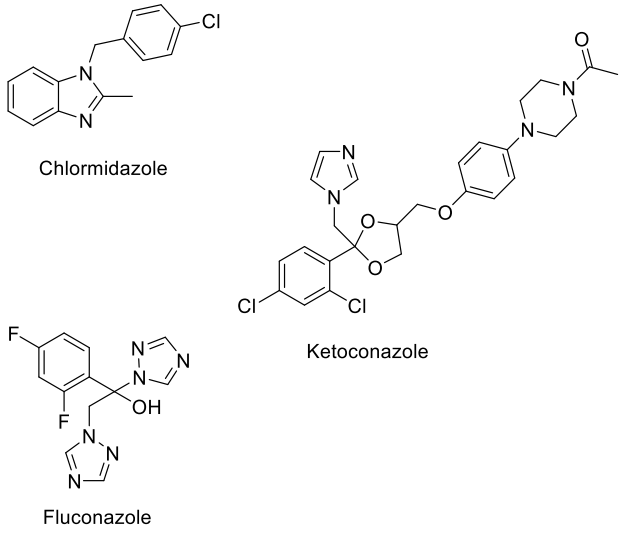

Figure 2.1 - *Relevant azole-based drugs.*

Azole-based antifungals act by interfering with ergosterol synthesis, namely, by blocking the enzyme responsible for the conversion of lanosterol and thus disrupting the composition of the cell membrane, which results in the inhibition of cell growth and replication[85,86]. However, fungi possess mechanisms to counteract the action of azoles, leading to resistance. Resistance to azoles can manifest in various ways, such as increasing the activity of efflux pumps that expel the drug and reducing its intracellular concentration. Additionally, resistance can arise from an increase in the

metabolic synthesis of the targeted enzyme or from morphological modification of the enzyme structure to reduce its affinity for the drug[87,88].

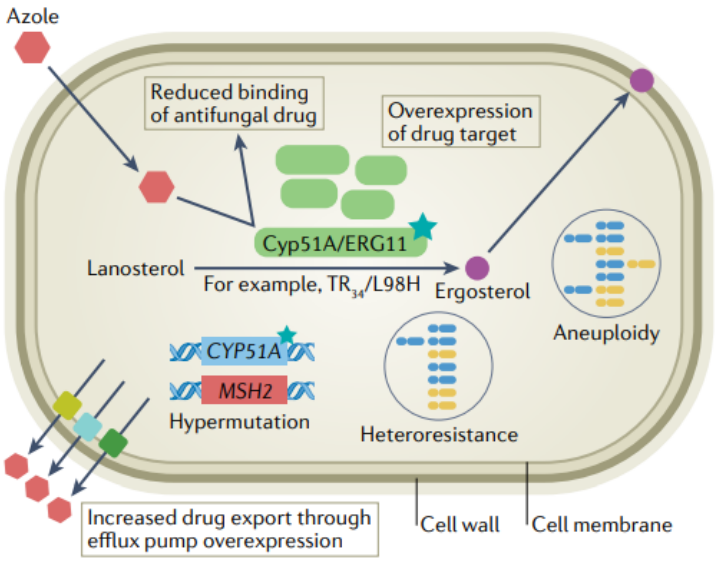

Figure 2.2 - *Schematic representation of the mechanisms of resistance to azole-based drugs*[88].

Some fungal species can be intrinsically resistant, also known as primary or innate resistant, which means that the organism is naturally resistant to antifungal agents. Conversely, in other cases, resistance appears to be acquired (secondary resistance), which means that the organism has rapidly adapted to counteract the action of the antifungal agent[89,90]. For example, *C. glabrata* exhibits innate resistance (primary resistance), a characteristic contributing to its ability to overcome *C. albicans* infections in many patients receiving chronic azole treatments. This phenomenon has led to a notable increase in fungal infections caused by *C. glabrata*[87,88,91]. The development of

novel drugs to fight these *C. glabrata* infections is thus of utmost importance[92].

The role of compounds containing metals has been central in the last century since the discovery of auranofin and cisplatin, which paved the way for the testing of metal-containing compounds in many areas of medicine[93,94]. In recent decades, organometallic compounds have been explored in the development of antimicrobial and anticancer agents due to the role that these metals can provide, namely, in coordination and redox disruption.

In the field of antimicrobial agents, a recent high-throughput screening of both organic and organometallic molecules for a vast array of microorganisms has been reported[95]. This study revealed that the probability of an organometallic compound exhibiting activity is nine times greater than that of an organic molecule. Contrary to common belief, despite their enhanced activity, organometallic compounds are not more toxic than organic molecules to human cells. Indeed, a compound containing nickel as a metal centre was found to be particularly active against a particular fungal species, *Cryptococcus deuterogattii*[96].

In line with this, the development of NHCs based on bioactive ligands is particularly promising[10]. One such example is xanthines (3,7-dihydropurine-2,6-diones), such as caffeine, theophylline, and theobromine, which are purine derivatives widely found in nature[53,97,98]. Xanthines and their derivatives have been found to have many pharmacological properties, interact directly with human receptors, or inhibit microbial chitinase and enhance the activity of common antimicrobial agents[99–101]. Xanthines can

easily form N-heterocyclic carbenes upon suitable modifications[102], as discussed previously. Indeed, complexes bearing NHCs based on xanthines have been shown to be effective as anticancer agents[102–106] and antimicrobial agents[54,55]. In this chapter, the synthesis of nickel complexes bearing NHC ligands based on xanthines and their activity on *Candida* yeasts are described.

2.2. Results and Discussion

2.2.1. Synthesis of Xanthinium Salts

Ligand precursors were synthesized using caffeine and theophylline as starting materials. Caffeine was methylated using a previously established procedure with methyl iodide (Scheme 2.1a)[107]. Modifications beyond methylation are difficult to attain due to the lower nucleophilicity of N9 when compared to imidazole derivatives[42,44]. For this reason, we opted to modify N7 starting from theophylline (Scheme 2.1b). Theophylline was reacted with isopropyliodide, octyliodide or allylbromide in the presence of a base and subsequently quaternized with methyl iodide, yielding compounds **3a**, **3b** and **3c** in 59%, 26% and 21% yield, respectively. The methylation of compound **2c** was more challenging because the compound undergoes degradation and forms an oil that is difficult to purify.

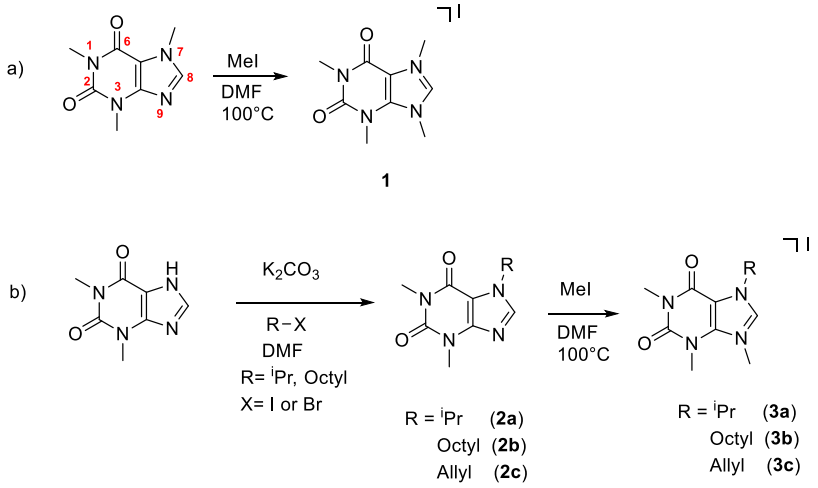

Scheme 2.1 - *Synthesis of ligand precursors **1**-**3**.*

To overcome this, the reaction conditions were modified by reducing the temperature to 70°C and increasing the amount of methyl iodide used, affording **3c** in 29% yield. Only iodide was used as a counter ion due to the greater propensity of halide salts to form more stable nickel Cp compounds[108]. The compounds were characterized by ^{1}H NMR, and a significant downfield shift at H8 upon methylation was observed for the xanthinium salts compared to their corresponding precursors (2.40 ppm for **3a**, 2.67 for **3b** and 1.30 for **3c**), in agreement with what has been observed for imidazolium salts versus imidazole[109].

The synthesis of bis-xanthinium salts was also pursued, aiming to obtain the corresponding bis-NHC compounds. Accordingly, theophylline was first reacted with diiodomethane in DMF in the presence of K_2CO_3 (Scheme 2.2) for 18 hours. The success of the reaction was confirmed by ^{1}H NMR, where

the ratio of the CH_2 linker group to the methyl groups of theophylline was 2:6.

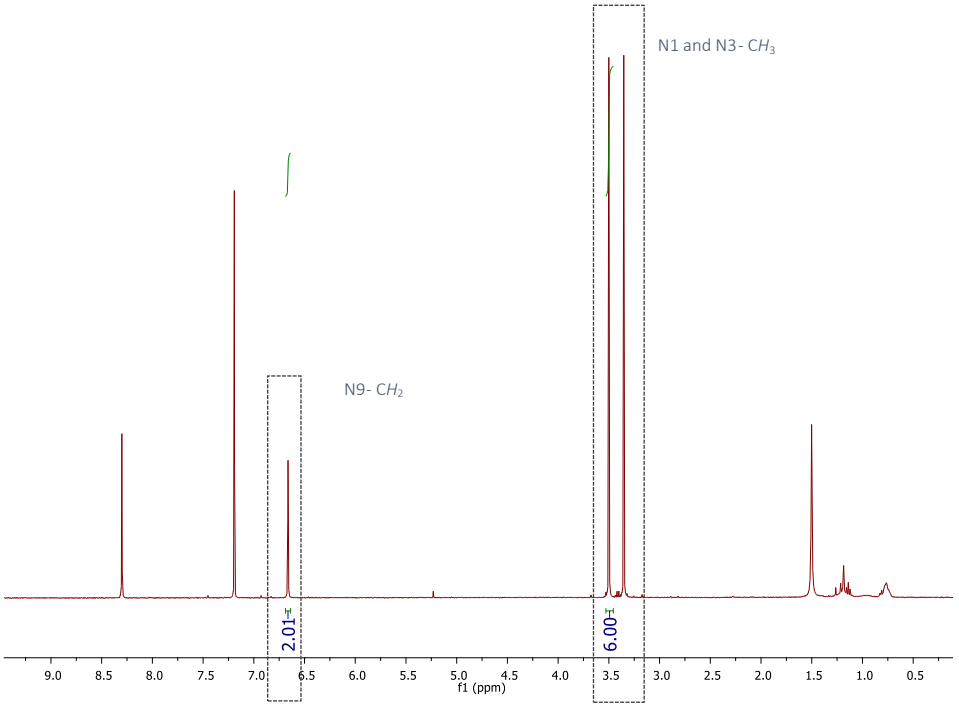

Figure 2.3 - *^{1}H NMR spectrum of compound* ***4.***

Several subsequent attempts to methylate and quaternize bis-theophylline were performed with methyl triflate. However, under these conditions, only the monomethylated compound was obtained (Scheme 2.2). The formation of the monomethylated compound was evident from ^{1}H NMR due to the loss of symmetry of the xanthine rings in the final compound, in which the methyl signals of the xanthine backbone and H8 resonate at different ppm. In compound **4**, the methyl groups and the two H8 protons of the theophylline moiety are magnetically equivalent, while in compound **5,** the H8 proton of the methylated xanthine undergoes a downfield shift of 1.25 ppm, while the

H8 proton of the unmethylated ring remains essentially unchanged. We were unable to induce full methylation of **4**; thus, metallation was not attempted.

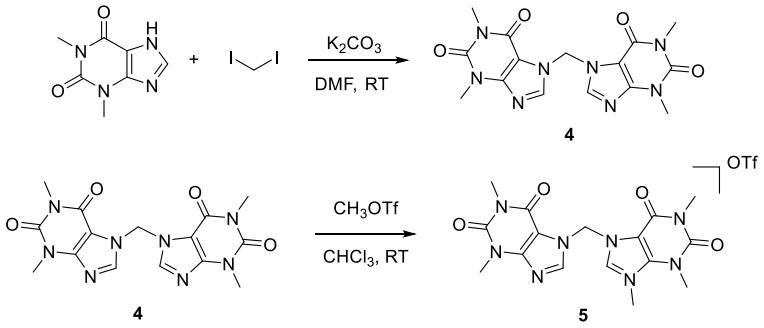

Scheme 2.2 - *Synthesis of the dixanthine **4** and dixantinium salt **5**.*

We then considered the derivatization of theophylline with 2-bromomethyl pyridine to allow for the formation of bidentate ligands since the formation of the bis-xanthinium salt was unsuccessful. Thus, theophylline was reacted with 2-bromomethyl pyridine in DMF in the presence of K_2CO_3 (Scheme 2.3). The reaction was successful (yield 64%), as confirmed by ^1H NMR in which the pyridine protons resonate at 8.48 (H_α), 7.78 (H_γ), 7.30 (H_σ) and 7.25 (H_β) ppm. The CH_2 linker resonates at 5.59 ppm, and the theophylline signals are found at 7.95 ppm for H8 and at 3.44 and 3.16 ppm for the two CH_3. Subsequent methylation was more complex since the pyridine nitrogen competes with the N9 of theophylline, which was found to be less nucleophilic, thus yielding compound **8**. The methylation of the pyridine ring was confirmed by ^1H NMR, in which a shift was observed for the H_α of the pyridine, from 8.49 ppm to 9.09 ppm.

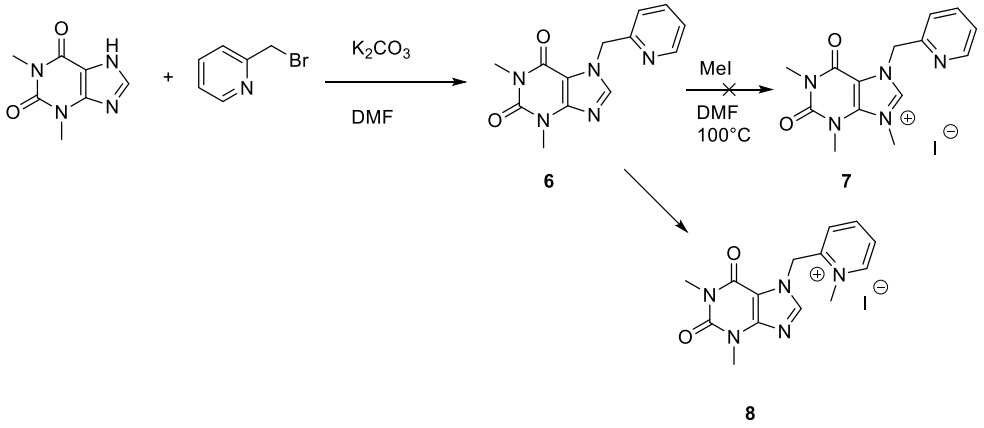

Scheme 2.3 - *Synthesis of compound **6** and attempts at methylation at the xanthine ring.*

To circumvent this problem, nitrogen protection of pyridine with *meta*-chloro-perbenzoic acid (*m*-CPBA) was performed, yielding compound **9** in quantitative yield (Scheme 2.4), in which the pyridine ring was oxidized, as confirmed by a slight shift upfield of the H_α of the pyridine ring (from 8.49 to 8.34 ppm) in ^{1}H NMR. Compound **9** was then methylated with trimethyl oxonium tetrafluoroborate in dichloromethane at room temperature. Pyridine deprotection was subsequently performed with molybdenum hexacarbonyl, leading to the formation of compound **11** in very low yields (10%) after purification by chromatography. Characterization of compound **11** by ^{1}H NMR revealed that H8 underwent a downfield shift typical of N9 methylation, from 8.20 ppm to 9.53 ppm, thus confirming the success of the reaction. Nevertheless, due to the number of synthetic steps required for the synthesis of **11** and the very low yields obtained, the reactivity of this compound with nickel was not examined.

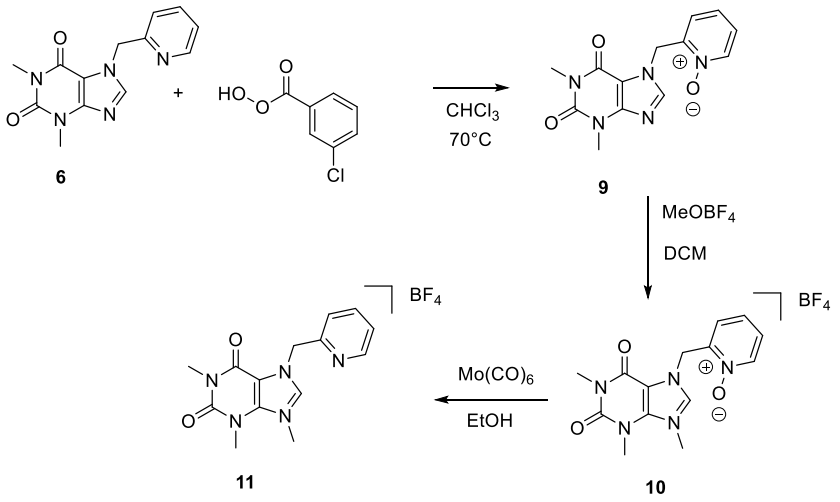

Scheme 2.4 - *Synthesis of compound **11**.*

Xanthines are purines and bear similarities with purine nucleobases. With the aim of evaluating the reactivity of purine nucleobases, ligand precursors based on guanine were also synthesized. Guanine was selected due to the facile derivatization of N7, which is the most nucleophilic position, in contrast to adenine, for which N1 is more nucleophilic[34]. Dimethyl guanine and methyl guanosine were synthesized from the corresponding precursors by methylation in DMF with methyliodide, following procedures previously employed by our group[11,31]. In the case of guanosine, methylation is preceded by protection at the ribose ring by an acetate group to avoid side reactions[11]. Additionally, we considered the use of guanosine-based compounds such as acyclovir. Acyclovir is a commonly used nucleoside analogue that is widely employed as an antiviral agent, act blocks the DNA synthesis of the virus and. Acyclovir was first methylated with dimethyl sulfate since earlier attempts to achieve methylation with methyliodide were

not successful. The hydroxyl group was then protected with acetate, providing compound **16** in 70% yield.

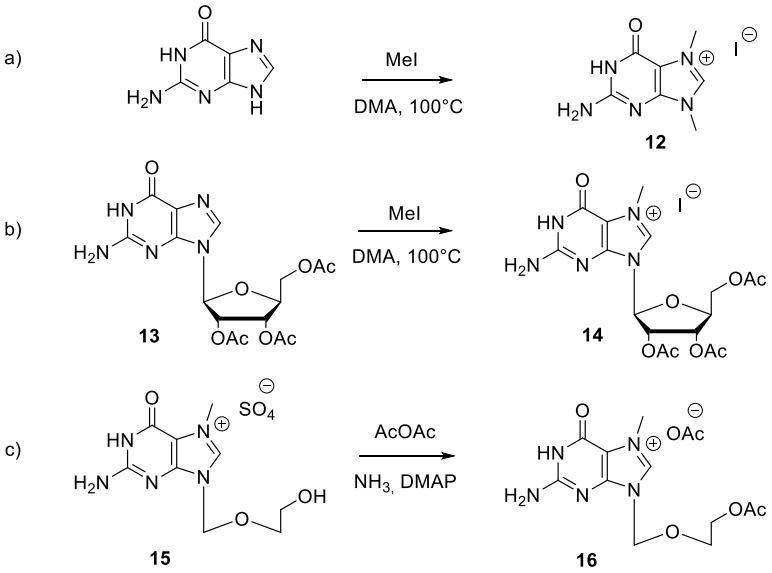

Scheme 2.5 - *Synthesis of guanosine derivatives as ligand precursors: a) dimethylguanine, b) N7-methyl guanosine, and c) N7-methyl acyclovir.*

The success of the reactions was confirmed by ^{1}H NMR spectroscopy for compounds **12** and **14**, which is similar to the chemical shifts previously reported[11,31]. For compound **16**, the acyclovir derivative, methylation leads to a new signal for the methyl group at 4.02 ppm, and H8 resonates at 9.36 ppm. During the protection of acyclovir, the excess of acetic anhydride used in the reaction mixture leads to an exchange of the counter anion from sulfate to acetate, as confirmed by the corresponding signal at 3.37 ppm.

In summary, we successfully synthesized seven ligand precursors comprising methyl caffeine and theophylline derivatives bearing an isopropyl,

an octyl and an allyl group at N7, and guanosine derivatives dimethyl guanine, N7-methyl guanosine and methyl acyclovir.

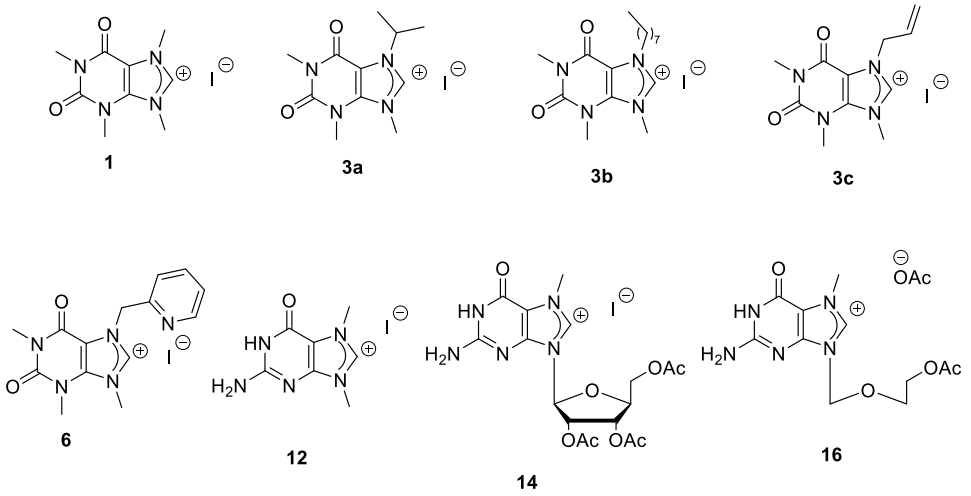

Figure 2.4 - *Ligand precursors successfully synthetized.*

In addition to these compounds, we also attempted to synthesize two other derivatives of theophylline: one containing two theophylline molecules linked by a CH_2 bridge and another derivatized with a methyl pyridine. The former was not successfully methylated, while methylation of the latter was obtained in very low yields. The ligand precursors displayed in Figure 2.4 were examined for their reactivity with nickelocene, which will be discussed in the following section.

2.2.2. Synthesis of nickel complexes bearing methyl caffeine N-heterocyclic carbenes.

The nickel NHC complexes were synthesized following previously described procedures employed for imidazolium[110–116] and triazolium

salts[112,117,118]. Thus, methylcaffeine **1** was reacted with nickelocene at 100°C for 2 hours in DMF. Analysis of the mixture by ^{1}H NMR spectroscopy confirmed the disappearance of H8 at 9.27 ppm and the formation of a mixture of two compounds in a 4/1 ratio, as indicated by the integrals of the corresponding CH_3 protons.

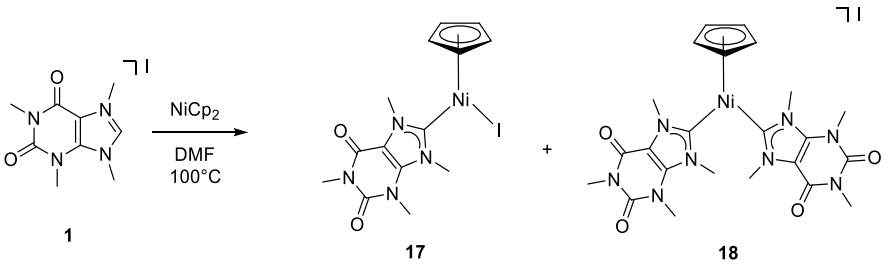

Scheme 2.6 - *Synthesis of compounds **17** and **18**.*

Further NMR analysis indicated the formation of mono- and bis-carbene complexes, as indicated by the ratios of the integrals of the Cp protons and those of the methyl groups of the xanthine ligand, with a 1/1 ratio for monocarbene and a 1/2 ratio for biscarbene. Liquid–liquid extraction was performed by adding water and DCM to the mixture in DMF, allowing for the separation of the two complexes. Specifically, the biscarbene **18** is soluble in a water/DMF mixture, allowing it to migrate into the aqueous layer, while monocarbene **17** remains in the organic layer.

Characterization of compound **17** by ^{1}H NMR in $CDCl_3$ showed the Cp ligand at 5.38 ppm, with the four methyl groups of xanthine (4.69, 4.49, 3.80 and 3.36 ppm) at a 3:5 ratio with respect to Cp. For compound **18**, the Cp ligand resonates at 5.51 ppm, with the methyl groups of the caffeine moiety

at 4.71, 4.38, 3.96 and 3.33 ppm and a ratio of 6:5 for Me:Cp. According to the $^{13}C\{1H\}$ NMR spectra, the carbenic carbon C8 in monocarbene **17** resonates at 179 ppm and at 189 ppm for biscarbene **18**, in agreement with values found for similar complexes[110,111]. The formation of a biscarbene under these conditions is not unusual and has been reported previously for imidazolium and triazolium salts[112,119].

To evaluate the conditions under which the biscarbene **18** is formed, the reaction was monitored by ^{1}H NMR, and the kinetic profile of the reaction was studied (Figure 2.5). The cyclopentadienyl anion acts as an internal base to deprotonate the C8-H of methyl caffeine, which then binds to the metal center. Upon protonation, the four protons of the dienic system show peaks at 6.57 and 6.47 ppm. The formation of two complexes is clear from the signals of the cyclopentadienyl groups of both complexes (at 5.44 ppm for monocarbene and at 5.76 ppm for biscarbene), even at t=0, measured a few minutes after preparation. After 30 min, biscarbene **18** was already present; thus, it started to form prior to total consumption of the ligand precursor. After 2 h, the ligand precursor is already consumed, indicating the formation of mono- and bis-carbene at a 4:1 ratio. After four hours, the spectrum becames less clear and with lower resolution, probably due to the formation of paramagnetic species, but the presence of both mono- and biscarbene was evident. Further heating of the mixture shows that after the total consumption of the starting material, the concentration of **18** continues to increase. This increase was concomitant with the decrease in the concentration of monocarbene **17**.

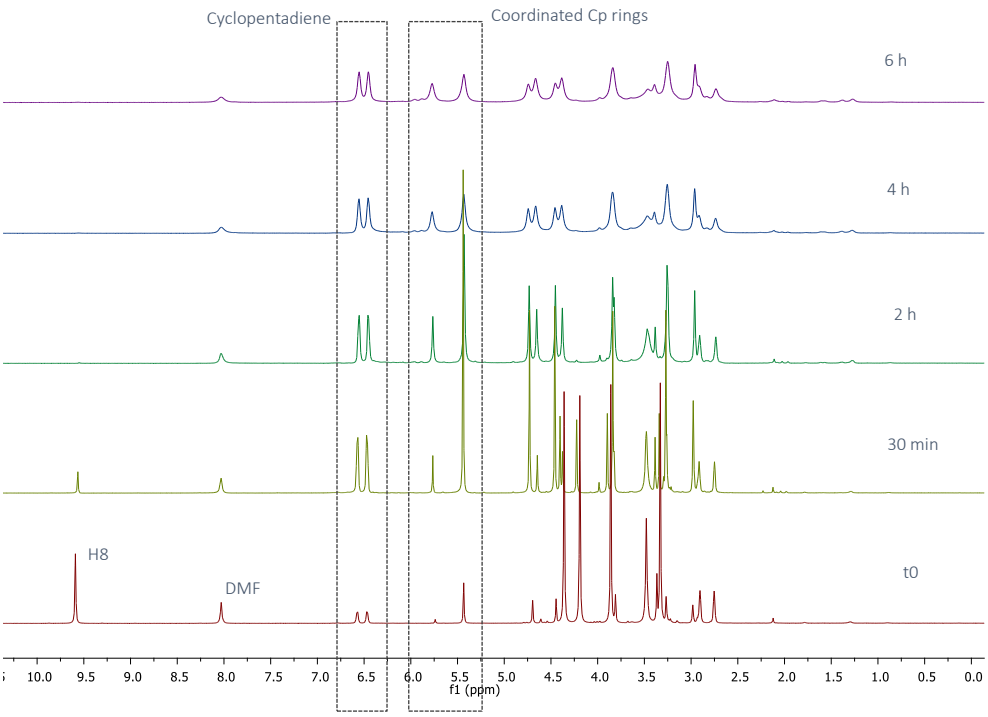

Figure 2.5 - *^{1}H NMR spectrum of the reaction of compound **1** with nickelocene in DMF-d_7, at 100°C at different times.*

This is evident from the graphic in Figure 2.6, which shows that the concentration of **18** increases with the decreasing in the concentration of **17**. Additionally, after approximately 8 hours, a plateau in the formation of both complexes is reached, probably indicating that the maximum conversion to compound **18** has been achieved.

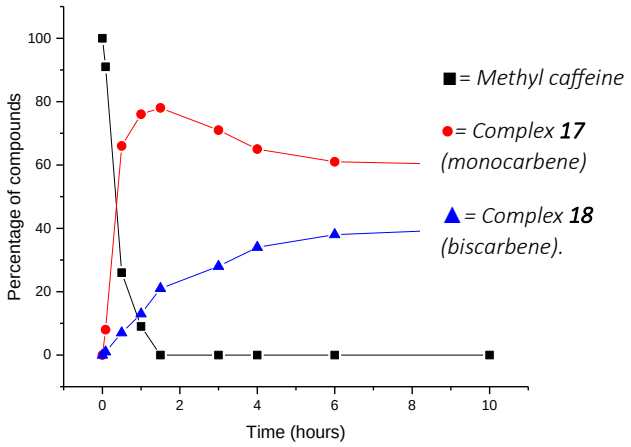

Figure 2.6 - *Variation of concentrations of the compounds **1**, **17** and **18** with time*

The reaction was also monitored at 80°C under less concentrated conditions to determine whether the formation of biscarbene could be avoided. By decreasing the temperature and the concentration of the initial mixture, the formation of biscarbene decreased.

Methyl caffeine was also reacted with nickelocene using a microwave reactor, but the reaction was not successful, probably because the conditions required to achieve an inert atmosphere were not ideal.

2.2.3. Synthesis of Nickel complexes bearing NHCs derived from theophylline.

The theophylline derivatives **3a** and **3b** were subjected to similar reaction conditions to those applied for methyl caffeine **1**. Compound **3a** was reacted in DMF at 100°C, resulting in a mixture of compounds. The ^{1}H NMR spectrum of the final mixture, obtained by precipitation with ether and subsequent filtration, was difficult to interpret due to poor resolution, probably resulting from the presence of paramagnetic byproducts. Despite this, the presence of more than one compound was evident. Due to the absence of the corresponding peak relative to H8 of the starting material **3a**, one of the compounds was hypothesized to be a carbene. The mixture was then purified by chromatography, after which it was possible to isolate the two compounds. One of the compounds was monocarbene complex **19**, and the other was demethylated ligand **2a** (Scheme 2.7).

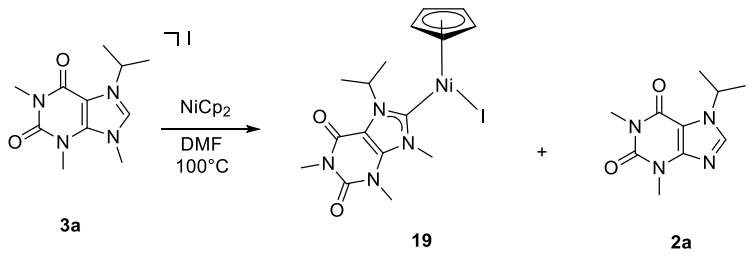

Scheme 2.7 – *Reaction of **3a** with nickelocene.*

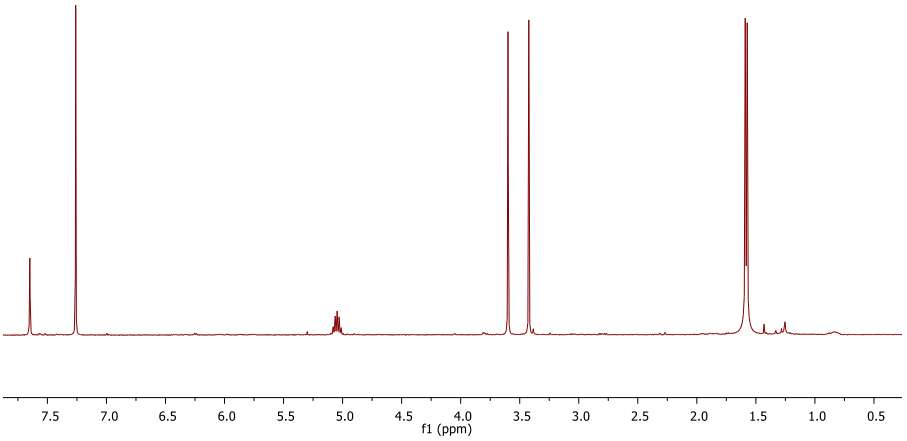

Figure 2.7 - *^{1}H NMR spectrum of compound **2a** resulting from demethylation*

.

The formation of compound **2a** results from demethylation of the ligand precursor, most likely as a consequence of the generation of free carbene, as observed by Bertrand and Albrecht for imidazolium[120] and triazolium salts[112], respectively.

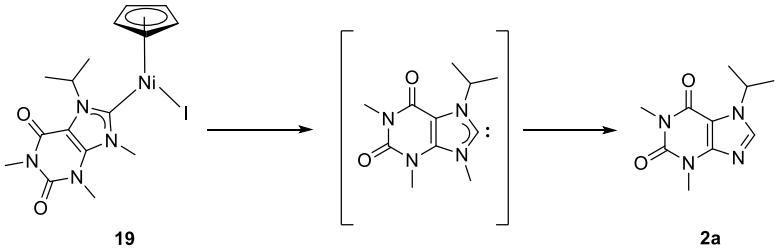

Figure 2.8 - *Formation of the demethylated side-product.*

Compound **19** was also analysed by NMR spectroscopy in $CDCl_3$. According to the ^{1}H NMR spectrum, the Cp ligand resonates at 5.38 ppm, and the rotation of Ni-xanthine is hindered. In complex **19,** this is reflected by the splitting

pattern of CH_3 of the isopropyl moiety, which results in two doublets at 1.72 and 1.68 ppm. According to the $^{13}C\{^1H\}$ NMR data, the carbenic carbon resonance resonates at 177.8 ppm, with a shift of 1.2 ppm with respect to that of complex **17.**

The reaction progress and formation of the demethylated compound were monitored by ^1H NMR (Figure 2.9). Like what was observed with methyl caffeine, the H8 signal at 9.77 ppm was used to determine the consumption of the starting material. In general, the broad singlet at 6.72 ppm, corresponding to the proton of the isopropyl CH group, increased concomitantly with the two signals corresponding to free cyclopentadiene (at 6.57 and 6.47 ppm). As can be observed, compound **2a** starts to form after 1 h (the H8 peak at 8.24 ppm). The starting material **3a** is still available prior to demethylation. This finding agrees well with what was reported for similar systems where demethylation occurs[112,120]. Most likely, the free carbene undergoes demethylation before reacting to form a biscarbene, which could be due to a slower rate of reaction with monocarbene **19**. This could also be the result of the steric hindrance imposed by the N7 substituent . Indeed, the formation of the biscarbene, could be hindered due to the difficulty in accommodating two xanthine ligands with bulky substituents at N7, such as an isopropyl.

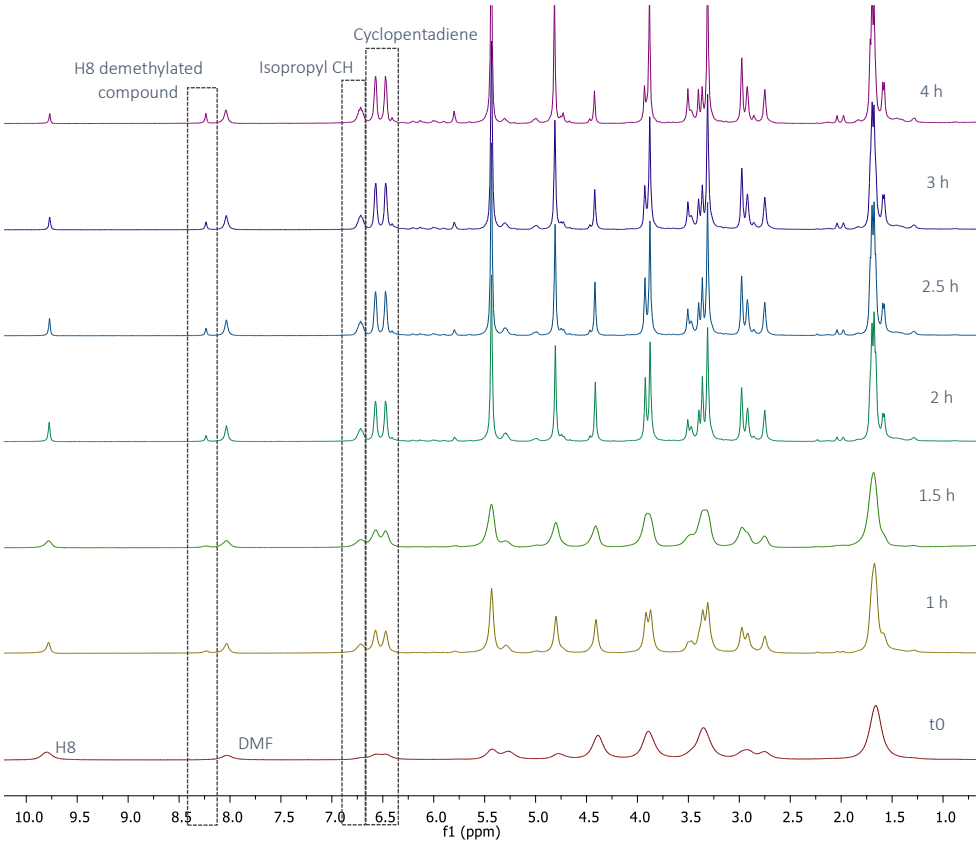

Figure 2.9 - *^{1}H NMR spectrum of the reaction of compound **1** with nickelocene in DMF-d_7 at 100°C at different times..*

Following these results, the reaction was performed at 60°C. Decreasing the reaction temperature to 60°C prevented the formation of the demethylated product **2a** and increased the yield of the reaction from 15% to 39%, even though it required longer reaction times (from 16 hours to 72 hours).

The same strategy was employed for compound **3b**. Nickelocene was reacted with **3b** directly at 60°C, affording compound **20** (Scheme 2.8).

Increasing the temperature leads to significant decomposition, and a mixture of unidentifiable products is obtained. At 60°C, some decomposition was observed, but the major compound was monocarbene **20**. The formation of biscarbene or a demethylated compound was not detected.

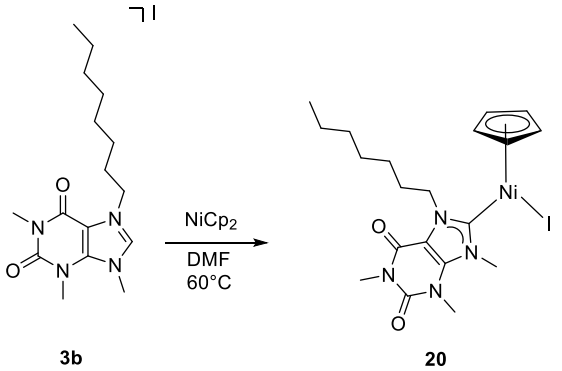

Scheme 2.8 - *Synthesis of compound **20**.*

Characterization of complex **20** was performed by ^{1}H NMR and $^{13}C\{1H\}$ NMR in $CDCl_3$. The signal corresponding to the Cp ligand can be observed at 5.37 ppm. Additionally, the rotation around the Ni-C8 bond appears to be hindered by the octyl side chain. The hindered rotation is evidenced by the inequivalence of the N-CH_2 protons, which exhibit an AA'BB' system pattern for the NCH_2CH_2 group, with signals at 5.05 and 4.81 ppm. As for the $^{13}C\{^{1}H\}$ NMR data, the carbenic carbon resonates at 178.0 ppm, closely resembling the values observed for complexes **19** and **17**.

The remaining theophylline derivatives **3c** and **6** were also reacted with nickelocene. For allyl derivative **3c,** the reaction was conducted in DMF at 100°C (Scheme 2.9), and samples of the reaction mixture were periodically analysed to monitor the ongoing reaction. Nevertheless, the ^{1}H NMR

spectrum had poor resolution, probably due to the presence of paramagnetic side products, as noted previously. Several attempts to separate the mixture through chromatography were performed, but no identifiable product was obtained. Possible outcomes of this reaction were the formation of the Ni-NHC compound, as for the previous theophylline derivatives, and/or the formation of a cyclometallated compound where the allyl moiety coordinates with the nickel centre via a double bond (Scheme 2.9). A similar compound has been reported in the literature for an imidazole analogue[121], but in the case of **3c**, no such compound was observed.

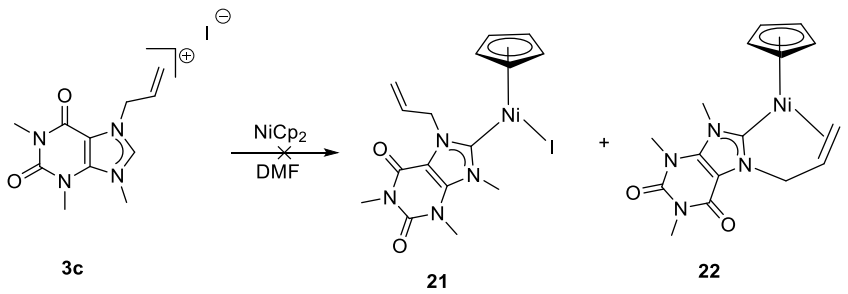

3c **21** **22**

Scheme 2.9 - *Attempt of synthesis of complexes **21** and **22**.*

The reactivity of compound **6** with $NiCp_2$ was also investigated. After 24 hours at 100°C in DMF (Scheme 2.10), the reaction mixture changed from a intense green typical of nickelocene to a bright purple suspension. However, attempts to isolate any compound from the suspension were unsuccessful, as was the case for the allyl derivative **3c**.

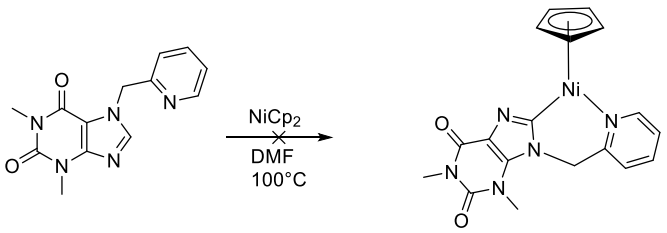

6 23

Scheme 2.10 - *Attempt of synthesis of complex **23**.*

Our working hypothesis was that coordination with pyridine nitrogen could facilitate the formation of a bidentate ligand, also promoting the formation of a C_8-Ni bond, but no such compound was observed in the crude reaction.

2.2.4. Synthesis of nickel complexes bearing NHCs derived from guanine.

The guanine derivatives **12**, **14** and **16** were also reacted with nickelocene. With dimethyl guanine **12** and N7-methyl guanosine **14,** the reaction was first performed under the same conditions used for the xanthine precursors (in DMF at 100°C). For dimethyl guanine **12**, ^{1}H NMR analysis of the reaction showed that no reaction with nickelocene occurred, and the guanine compound was recovered completely. For N7-methyl guanosine **14**, analysis via ^{1}H NMR of the crude reaction showed degradation of the ligand precursor, and the formation of nickel-guanosine compounds was not observed. The degradation of methyl guanosine was associated with high temperature, as noted previously for reactions with platinum with the same ligand precursor[31]. Lowering the reaction temperature to 50° still leads to partial

degradation of the ligand precursor. The reaction was repeated several times using different solvents for both methyl guanosine and dimethyl guanine. First, the solvent was changed from DMF to toluene, and the reactions were performed at 100°C. These reactions led, again, to degradation of the starting material, which contrasts with the reactivity of this ligand precursor with $Pt(PPh_3)_4$ under the same conditions[31]. A second attempt was performed in THF at 70°C. Also in this case, for both dimethyl guanine and N7-methyl guanosine, no reaction occurred. Finally, the two ligand precursors were reacted with nickelocene in dioxane at 90°C. Analysis of the crude product by ^1H NMR revealed a spectrum with poor resolution, in which it was possible to observe the H8 peak of the ligand precursor, indicating that most of the ligand was still intact and that the expected carbene was not formed. All these reaction conditions are summarized in Table 2.1.

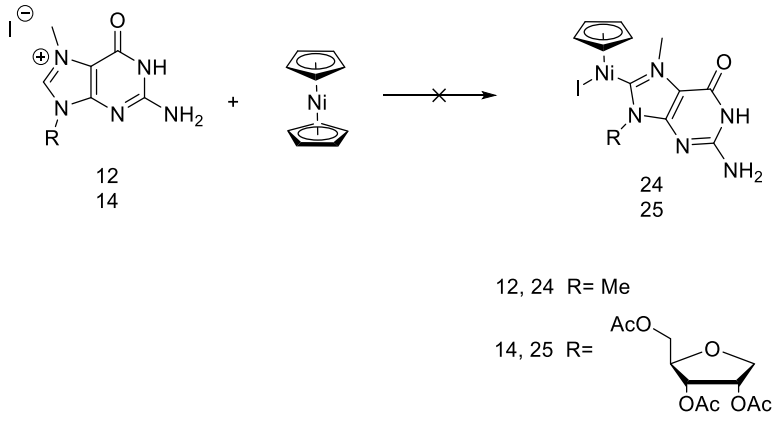

Scheme 2.11 – *Reaction of guanine derivatives **12** and **14** with nickelocene.*

Table 2.1 – *Reaction conditions tested for the reaction of compounds **12** and **14** with nickelocene (NR= Not Reacted).*

Solvent	Conditions	Products
DMF	0.1 M; 100°C	NR
DMF	0.03 M; 50°C	NR
Toluene	0.02 M; 100°C	NR
THF	0.16 M; 70°C	NR
Dioxane	0.1 M; 90°C	NR

Similar results were obtained with methylated acyclovir **16**. Compound **16** was reacted with nickelocene in DMF, and KI was added to the reaction as a halogen source, with the aim of providing a coordinating anion, similar to the other nickel compounds. The reaction was first performed at 100°C, and ^{1}H NMR analysis revealed mostly starting material and some impurities, suggesting degradation with temperature, as observed for methyl guanosine.

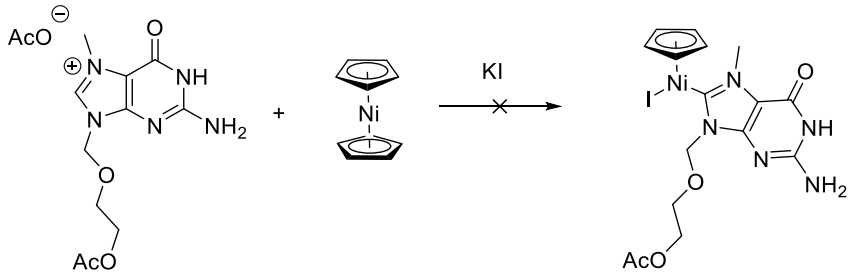

Scheme 2.12 - *Reaction of compound **16** with nickelocene.*

When the temperature was decreased to 70°C, no improvement was observed. The formation of complex **26** was therefore not successful, as was the case for methyl guanosine and dimethyl guanine.

The reactivity observed among the three guanosine derivatives probably reflects the distinct electronic distributions between guanine and xanthine derivatives. This discrepancy may arise from the presence of a more oxidized ring in xanthines, the different substitution patterns of the purine ring, or a combination of both factors. Interestingly, previous studies by our group on dimethyl guanine and methyl guanosine with platinum(0) precursors have shown that these compounds can react by oxidative addition even more effectively than imidazolium salts but fail to react via base-assisted deprotonation with iridium or through transmetalation[11,31].

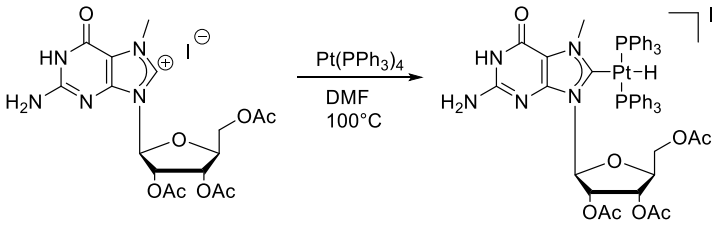

Scheme 2.13 - *Reaction of methyl guanosine with platinum(0).*

In the next chapter, the reactivity of 7-methylguanosine with gold via base-assisted deprotonation will be discussed. Clearly, these compounds are highly sensitive to the reactivity of the metal itself and the conditions employed.

2.2.5. Solid-state Structure of the Nickel Complexes.

Crystals of complexes **17** and **19**, suitable for single-crystal X-ray diffraction, were obtained by slow evaporation of their corresponding CH_2Cl_2/Et_2O solutions, allowing unambiguous determination of their molecular structure. Figures 2.10 and 2.11 depict their ORTEP diagrams, with the most relevant bond distances (Å) and angles (°) reported in Table 2.2. The molecular structures of complexes **17** and **19** are very similar, presenting a Ni(II) centre bonded to an iodide ligand, a η^5-ciclopentadienyl (η^5-Cp) group and a purine ligand. The geometry around the metal centre can be described as a slightly distorted trigonal plane, considering that the η^5-Cp ring centroid, the iodide and the carbenoid atom C8 of the purine are located at the vertices of the triangle.

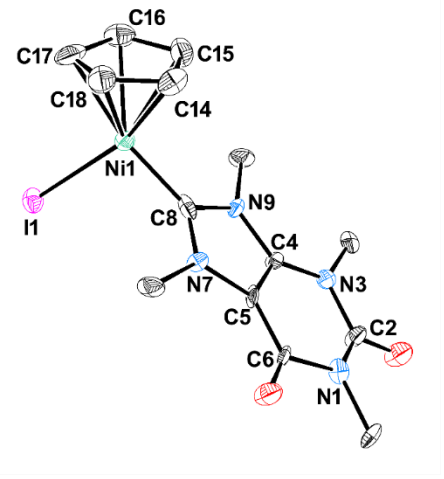

Figure 2.10 - *ORTEP representation of complex **17**, using 50% level ellipsoids. Hydrogen atoms are omitted for clarity.*

In fact, the sum of the bond angles between these ligands is *ca.* 360°, but there are deviations from the ideal 120° bond angles, as, for example, in the

I1–Ni1–C8 angles (96.4(4)° for **17** and 96.54(7)° for **19**). The dihedral angles ω between I1–Ni1–C8 and the η^5-Cp plane are similar at **17** and **19°**, with values of 87.7(6)° and 89.40(13)°, respectively (Table 1). On the other hand, when comparing the dihedral angles φ between I1–Ni1–C8 and the caffeine plane in both complexes, it is possible to observe a difference of approximately 10° (79.0(3)° for **17** and 89.76(6)° for **19**). However, in the case of the dihedral angle χ between the η^5-Cp and caffeine planes, this difference decreases to ~5° (35.4(5)° for **17** and 40.38(11)° for **19**). Ni1–$C8_{purine}$ and Ni1–I1 are 1.865(15) Å and 2.503(2) Å in **17** and 1.870(3) Å and 2.4993(4) Å in **19**, comparable to other [Ni(η^5-Cp)(NHC)I] derivatives already reported in the literature[114–116].

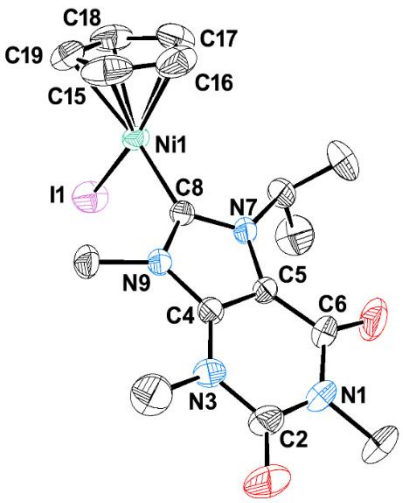

Figure 2.11 – *ORTEP representation of complex **19**, using 50% level ellipsoids. Hydrogen atoms are omitted for clarity.*

Table 2.2 - *Selected bond distances (Å) and angles (°) for complexes **17** and **19**.*

	17	**19**
Bond distances		
Ni1–I1	2.503(2)	2.4993(4)
Ni1–C8	1.865(15)	1.870(3)
Ni1–C14	2.084(17)	
Ni1–C15	2.128(15)	2.114(3)
Ni1–C16	2.153(16)	2.053(3)
Ni1–C17	2.108(14)	2.141(3)
Ni1–C18	2.173(16)	2.119(3)
Ni1–C19		2.155(3)
Bond angles		
I1–Ni1–C8	96.4(4)	96.54(7)
C8–Ni1–E1[a]	99.7(6)	97.59(12)
C8–Ni1–E2[b]	98.2(5)	100.05(10)
ω [c]	87.7(6)	89.40(13)
φ [d]	79.0(3)	89.76(6)
χ [e]	35.4(5)	40.38(11)

[a] *E1 corresponds to C14 (**17**) or C16 (**19**);* [b] *E2 corresponds to C17 (**17**) or C18 (**19**);* [c] *dihedral angle between I1–Ni1–C8 and the η^5-Cp plane;* [d] *dihedral angle between I1–Ni1–C8 and the caffeine plane;* [e] *dihedral angle between the η^5-Cp and caffeine planes.*

2.2.6. Antifungal activity of the complexes.

The antifungal activity of all the nickel compounds (**17-20**) was tested on the medically relevant yeasts *Candida albicans* and *Candida glabrata*. The activity was evaluated by measuring the minimal inhibitory concentration at 50% (MIC_{50}), which corresponds to the lowest concentration of a compound in a medium that inhibits the growth of 50% of the population of the microorganism. The MIC_{50} range was determined according to CLSI guidelines after 24 and 48 h[122]. Nickel acetate and potassium iodide were tested as controls. For reference, to ascertain the role of the xanthine moiety, two NHCs based on imidazole (**27**) and benzimidazole (**28**), previously reported by Crabtree's group, were also examined, as was fluconazole, a common antifungal currently used in the clinic.

The compounds were serially diluted in DMSO, and 5 µl was added to the wells of a 96-well plate containing 95 µl of RPMI medium. The compound concentrations ranged from 2.5 mM to 4.9 µM. Cellular suspensions of *C. glabrata* or *C. albicans* (3x103 cfu/ml) were prepared from fresh cultures grown overnight on YPD agar medium, and 100 µl was added to each well. Growth in RPMI medium was recorded after 24 and 48 h at 30°C (*Candida albicans*) or 37°C (*Candida glabrata*) by measuring the OD600. The growth conditions without drugs but with solvent (mock control) were used as the normalization condition after background (in RPMI medium) subtraction. The MIC was defined as the drug concentration range where the relative OD600 fell below 50% of the mock control. At least three independent assays were performed for each compound and strain.

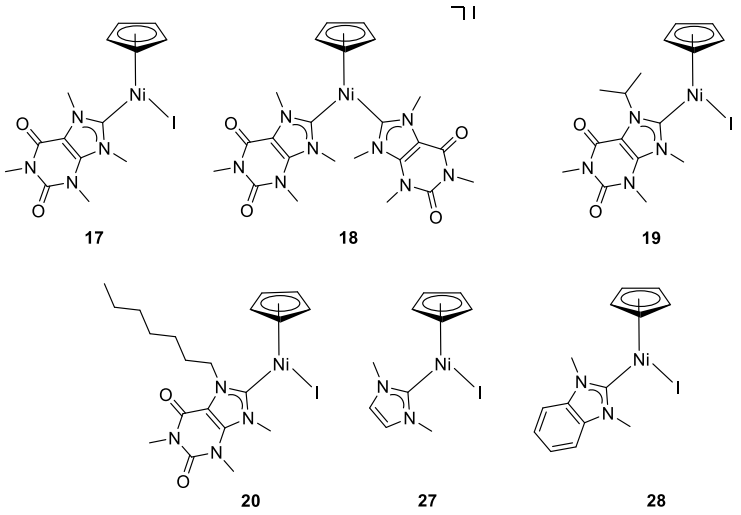

Figure 2.12 - *Nickel compounds evaluated for antifungal activity.*

With the exception of compound **18**, all the nickel complexes were active against *C. albicans* and *C. glabrata* (Table 2.3). Monocarbenes **19** and **20** were similarly active against both yeasts, while **17** and **18** were more effective against *C. glabrata*. All the nickel NHC complexes had greater antifungal activity than did their ligand precursors (MICs of **1**–**17, 1**–**18**, **3a**–**19** and **3b**–**20**), which were generally not active (except for **3b**). Variation in the side chain at position N7 did not seem to significantly influence antifungal activity (MICs of **17**, **19** and **20**).

Table 2.3 - *Minimum inhibitory concentration (MIC) of nickel complexes* ***17–20, 27, 28*** *and the corresponding ligand precursors.*

	MIC_{50} (μM)			
	C. glabrata		*C. albicans*	
Compound	24 h	48 h	24 h	48 h
1	625-312.5	NA	NA	NA
3a	625-312.5	NA	NA	NA
3b	312.5-156.25	312.5-156.25	1250-625	2500-1250
17	78-39	156.25-78	156.25-78	625-312.5
18	78-39	156.25-78	1250-625	NA
19	78-39	312.5-156.25	156.25-78	312.5-156.25
20	39-19.5	156.25-78	78-39	312.5-156.25
27	78-39	312-156.25	312.5-156.25	625-312.5
28	78-39	156.25-78	156.25-78	312.5-156.25
Fluconazole	26-13	52-26	1.6-0.8	1.6-0.8
$Ni(OAc)_2$	156.25-78	312.5-156.25	625-312.5	1250-625

NA – not active

Interestingly, biscarbene **18** was strongly active against *C. glabrata* and was only slightly active or not active after 24 h and 48 h, respectively, for *C. albicans.* Seemingly, the presence of more than one NHC ligand and/or the influence of the overall charge of the nickel cation yields a selective antifungal compound for *C. glabrata*. This could imply different mechanistic effects of

this compound on different *Candida sp*. strains. Such specificity is highly important given that *C. glabrata* strains are less susceptible to available antifungal drugs used to treat invasive candidiasis[123]. When examining the activities of compounds **27** and **28**, we observed that their antifungal behaviors were similar to those of compounds **17, 19** and **20,** with compound **27** being the least active of the series for *C. albicans*. Thus, the antifungal activity cannot be specifically ascribed to the xanthine moiety and is probably the result of the nickel-NHC connectivity. Finally, nickel acetate was used as a control, and after 24 hours, at concentrations equimolar to or greater than those of the other tested compounds, it was effective against *C. glabrata* and *C. albicans* but was far less effective for the latter. The antifungal activity of fluconazole was greater than that of the other tested agents. We nevertheless emphasize that several mechanisms of resistance are known to exist for fluconazole and that the development of effective alternatives is highly important.

2.2.7. Toxicity of the nickel complexes to human cells.

We also tested the cytotoxic effects of the complexes on HeLa cells[124,125]. The lowest concentration of nickel acetate tested (39 µM) reduced the viability of the HeLa cells by 30%. Complex **20** strongly affected cell viability by almost 100% when concentrations near the MIC were used for *C. glabrata* (Figure 4). Complex **27** decreased cellular viability by almost 50%, while for complex **19,** cellular viability was affected by 20 to 30% for concentrations within the range of the corresponding MIC for *C. glabrata*. Seemingly,

increasing the number of carbons in the substituent at N7 leads to a significant increase in cytotoxicity in HeLa cells.

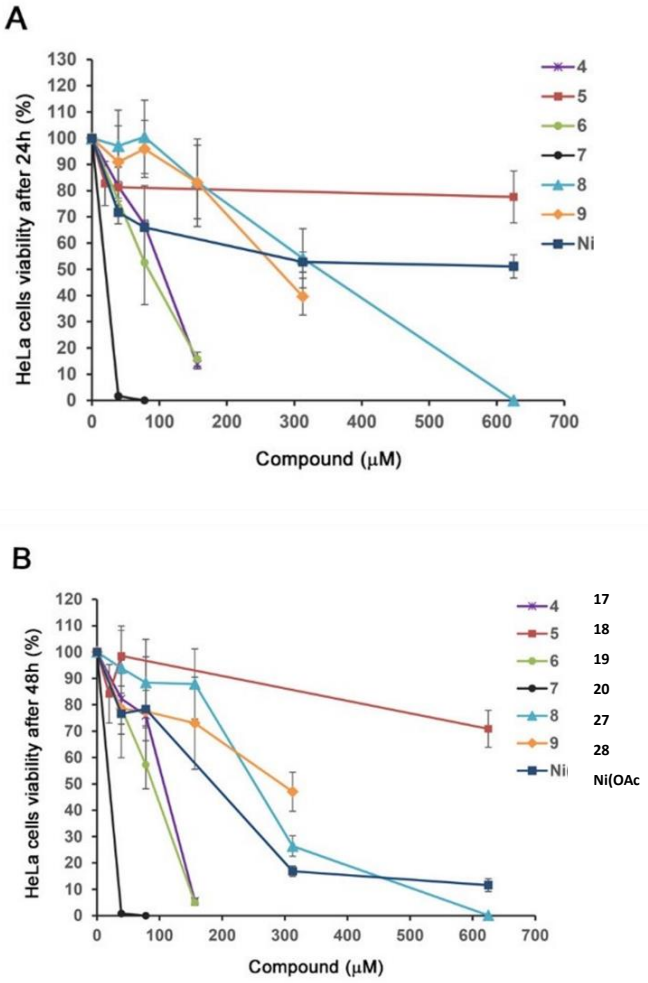

Figure 2.13 - *The cytotoxicities of compounds* ***17, 18, 19, 20, 27, 28*** *and* $Ni(OAc)_2$ *toward HeLa cells was evaluated after 24 h (A) and 48 h (B).*

Cellular viability was assessed using the MTT assay, and the values are expressed as the percentage of viable cells relative to the untreated control. Complex **18** showed the lowest cellular toxicity, with a reduction in cell

viability of 20% at all the concentrations tested. For concentrations in the range of the *C. glabrata* MIC_{50} (78-39 µM), the complex toxicity remained low even after 48 h of treatment (Figure 2.13). Therefore, of the series of compounds tested, complex **18** is the most promising because it has specific antifungal activity against *C. glabrata* combined with lower toxicity toward human cells.

2.3. Conclusions

In summary, a series of nickel complexes, **17–20,** were synthesized. Methyl caffeine yields mono- and bis-carbene nickel complexes, whereas theophylline derivatives, with isopropyl and octyl substituents at N7, yield only monocarbene complexes. The theophylline derivatives bearing an allyl substituent or the benzyl pyridine substituent did not lead to the formation of a nickel complex, and the same occurred when guanosine derivatives were used as ligand precursors. All the complexes were tested for antifungal activity, and complexes **17**, **19** and **20** were found to be active as antifungal agents against both *C. glabrata* and *C. albicans*. Compound **20** is very toxic to HeLa cells, and **17** and **19** also exhibit toxicity. The biscarbene derivative **18** is highly selective for *C. glabrata* but has almost no antifungal activity against *C. albicans.* Complex **18** also has low toxicity towards HeLa cells, making complex **18** a promising candidate for the selective treatment of candidiasis associated with *C. glabrata*, which is often very difficult to treat.

2.4. Experimental

The syntheses of the complexes were carried out under an inert atmosphere of N_2 using Schlenk techniques. All ^{1}H and $^{13}C\{^{1}H\}$ NMR spectra were recorded at room temperature on Bruker spectrometers (400 MHz and 500 MHz), and chemical shifts were referenced to $SiMe_4$ (δ in ppm, *J* in Hz) and H_3PO_4. The synthesis of theophylline derivatives was adapted from a published procedure[126]. Methyl caffeine was synthesized according to the synthetic procedure described in reference[107]. Mass Spectroscopy and Elemental Analysis were performed by the UniMass Laboratory at Instituto de Tecnologia Química e Biológica, Portugal.

2.4.1. Compound 2a

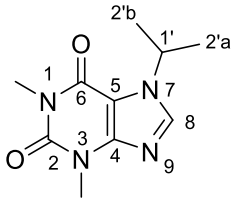

Theophylline (500 mg, 2.80 mmol) and K_2CO_3 (1.50 mg, 11.0 mmol) were suspended in DMF (20 ml), and the mixture was stirred for 3 hours. Subsequently, 2-iodopropane (550 µl, 5.55 mmol) was added to the mixture, and the reaction was stirred overnight at room temperature. The final mixture was diluted with water (10 ml) and extracted with CH_2Cl_2 (3×30 ml). The organic layer was separated and dried with Na_2SO_4. The filtrate was evaporated to dryness under vacuum, affording compound **2a** as a white powder (428 mg, 69% yield). The characterization can be found in the literature[127].

2.4.2. Compound 2b

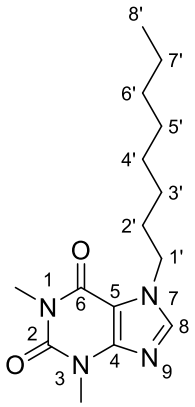

Theophylline (250 mg, 1.38 mmol) and K_2CO_3 (770 mg, 5.55 mmol) were suspended in DMF (5 ml), and the mixture was stirred for 3 hours. Subsequently, 1-iodooctane (300 µl, 1.67 mmol) was added to the mixture, and the mixture was stirred overnight at room temperature. The final mixture was diluted with water (2.5 ml) and extracted with CH_2Cl_2 (3 × 10 ml). The organic layer was separated and dried with Na_2SO_4. The filtrate was evaporated to dryness under vacuum. The mixture was then purified by column chromatography with an AcOEt:Toluene mixture (6:4) as the eluent, affording compound **2b** as a colorless oil (379 mg, 99% yield).

^{1}H NMR (400 MHz, $CDCl_3$): δ 7.54 (s, 1H, H-8); 4.28 (t, 2H, H-1', $^3J_{H\text{-}1',\,H\text{-}2'}$ = 7.2 Hz); 3.59 (s, 3H, N3-C*H*$_3$); 3.41 (s, 3H, N1-C*H*$_3$); 1.87 (m, 2H, H-2'); 1.36–1.18 (m, 10H, H-3' to H-7'); 0.87 (m, 3H, H-8') ppm.

^{13}C{^{1}H} NMR (100 MHz, $CDCl_3$): δ 155.2 (C-6); 151.8 (C-2); 148.9 (C-4); 140.8 (C-8); 107.1 (C-5); 47.5 (C-1'); 31.8 (*C*H$_2$); 31.0 (C-2'); 29.9 (N3-*C*H$_3$); 29.2 (*C*H$_2$); 29.1 (*C*H$_2$); 28.1 (N1-*C*H$_3$); 26.5 (C-3'); 22.7 (C-7'); 14.2 (C-8') ppm.

HRMS-ESI (m/z): $[M\text{-}+H]^+$ calc. for $C_{15}H_{24}N_4O_2$ 293.1972 Found 293.1970.

2.4.3. Compound 2c

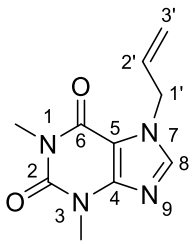

Theophylline (500 mg, 2.7 mmol) and K_2CO_3 (1.5 g, 10 mmol) were suspended in DMF (10 ml), and the mixture was stirred for 3 hours. Subsequently, allyl bromide (480 µl, 5.5 mmol) was added to the mixture, and the reaction was stirred overnight at room temperature. The final mixture was diluted with water (5 ml) and extracted with CH_2Cl_2 (3 × 20 ml). The organic layer was separated and dried with Na_2SO_4. The filtrate was evaporated to dryness under vacuum, affording compound **2c** as a white solid (591 mg, 99% yield). The characterization has been previously reported [128].

2.4.4. Compound 4

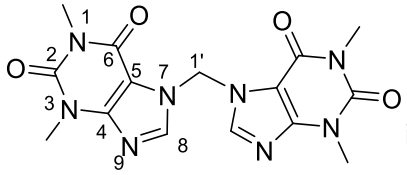

Theophylline (500 mg, 2.77 mmol) and K_2CO_3 (1.5 g, 11.1 mmol) were suspended in DMF (6 ml), and the mixture was stirred for 3 hours. Subsequently, diiodomethane (225 µl, 2.77 mmol) was added to the mixture, and the mixture was stirred overnight at room temperature. The final mixture was diluted with water (2.5 ml) and extracted with CH_2Cl_2 (3 × 10 ml). The organic layer was separated and dried with Na_2SO_4. The filtrate was evaporated to dryness under vacuum, affording compound **2b** as a white solid (208.5 mg, 36% yield). The characterization has been previously reported [129].

2.4.5. Compound 6

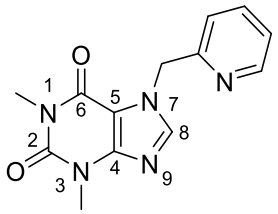

Theophylline (1 g, 5.6 mmol) and K_2CO_3 (3 g, 22 mmol) were suspended in DMF (10 ml), and the mixture was stirred for 3 hours. Subsequently, 2-(bromomethyl)pyridine (1.5 g, 5.6 mmol) was added to the mixture, and the reaction mixture was stirred overnight at room temperature. The final mixture was diluted with water (6 ml) and extracted with CH_2Cl_2 (3 × 20 ml). The organic layer was separated and dried with Na_2SO_4. The filtrate was evaporated to dryness under vacuum, affording compound **4** as a white solid (979 mg, 64.5% yield). The characterization has been previously reported.[126]

2.4.6. Compound 3a

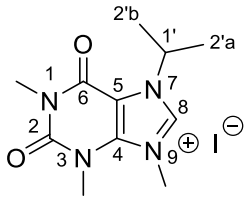

Compound **2a** (1.7 g, 7.7 mmol) was dissolved in DMF (13 ml), and methyl iodide (1.4 ml, 23 mmol) was added to the solution. The mixture was heated at 100°C overnight. After cooling, Et_2O (15 ml) was added to induce the formation of a precipitate. The solid was separated by filtration, washed with Et_2O and dried, yielding compound **3a** as a yellow powder in 59% yield (1.7 g).

^{1}H NMR (400 MHz, $CDCl_3$): δ 10.59 (s, 1H, H-8); 5.35 (sept, 1H, H-1', $^3J_{H\text{-}1',\ H\text{-}2'}$ = 6.8 Hz); 4.54 (s, 3H, N9-CH_3); 3.88 (s, 3H, N3-CH_3); 3.42 (s, 3H, N1-CH_3); 1.75 (d, 6H, H-2', $^3J_{H\text{-}2',\ H\text{-}1'}$ = 6.8 Hz) ppm

$^{13}C\{^1H\}$ NMR (100 MHz, $CDCl_3$): δ 153.1 (C-6); 150.1 (C-2); 139.9 (C-4); 138.1 (C-8); 107.7 (C-5); 54.5 (C-1'); 38.9 (N9-*C*H_3); 32.4 (N3-*C*H_3); 29.3 (N1-*C*H_3); 22.9 (2×*C*H_3, C-2') ppm.

HRMS-ESI (m/z): $[M+H]^+$ calc. for $C_{11}H_{17}N_4O_2$ 237.1346. Found 237.1345.

2.4.7. Compound 3b

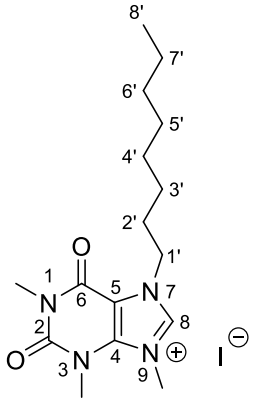

Compound **2b** (549 mg, 1.97 mmol) was dissolved in DMF (7 ml), methyl iodide (615 µl, 9.80 mmol) was added to the solution, and the mixture was heated at 100°C for 24 hours. After cooling, Et_2O (10 ml) and pentane (10 ml) were added to induce the formation of an oily precipitate. The oil was subsequently decanted and purified by column chromatography using a mixture of AcOEt:MeOH (8:2) as the eluent, affording compound **3b** as a waxy yellow solid in 26% yield (199 mg).

^1H NMR (400 MHz, $CDCl_3$): δ 10.21 (s, 1H, H-8); 4.56 (t, 2H, H-1', $^3J_{H\text{-}1',\ H\text{-}2'}$ = 7.6 Hz); 4.46 (s, 3H, N9-CH_3); 3.88 (s, 3H, N3-CH_3); 3.41 (s, 3H, N1-CH_3); 2.00 (quint, 2H, H-2', $^3J_{H\text{-}2',\ H\text{-}1'}$ = 7.6 Hz); 1.42-1.26 (m, 10H, H3' to H7'); 0.86 (m, 3H, H-8') ppm.

$^{13}C\{^1H\}$ NMR (100 MHz, $CDCl_3$): δ 153.1 (C-6); 150.2 (C-2); 139.6 (C-4); 138.8 (C-8); 108.0 (C-5); 50.2 (C-1'); 39.1 (N9-*C*H_3); 32.5 (N1-*C*H_3); 31.8 (*C*H_2); 30.2 (C-2'); 29.2 (2×*C*H_2, N3-*C*H_3 + *C*H_2); 29.0 (*C*H_2); 26.4 (*C*H_2); 22.7 (*C*H_2); 14.2 (C-8') ppm.

HRMS-ESI (m/z): $[M]^+$ Calc. for $C_{16}H_{27}N_4O_2$ 307.2128. Found 307.2128.

2.4.8. Compound 3c

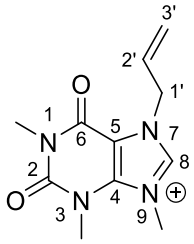

Compound x (115 mg, 0.520 mmol) was dissolved in DMF (2.5 ml), methyl iodide (142 µl, 4.5 mmol) was added to the solution, and the mixture was heated at 70°C for 24 hours. After cooling, Et_2O (10 ml) and pentane (10 ml) were added to induce the formation of an oily precipitate. The supernatant was removed, and additional Et_2O and pentane were added to afford compound x as a yellow solid in 29% yield (53 mg). The characterization has been previously reported [130].

2.4.9. Compound 14

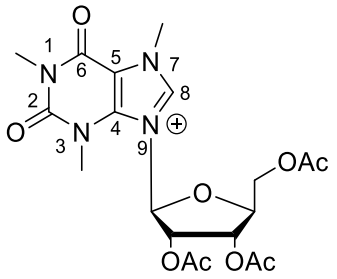

2',3',5'-Tri-O-acetylguanosine (500 mg, 1.22 mmol) was suspended in N,N-dimethylacetamide (6 mL), methyl iodide (228 µL, 3.66 mmol) was added, and the reaction mixture was stirred at room temperature for 24 hours. The addition of Et2O (200 mL) resulted in the appearance of an oily solid, and stirring was continued for ca. 1 h. The liquid was then removed, the oil was diluted in MeOH, 200 mL of Et2O was added, and the suspension was stirred for ca. 6 hours. This process was repeated 2 more times to yield compound x as a light-yellow solid (595 mg, 88%). The characterization has been previously reported [11].

2.4.10. Compound 15

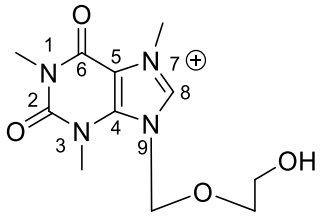

Acyclovir (1.13 g, 5 mmol) was dissolved in DMF (10 ml), and dimethyl sulfate (620 µL, 6.5 mmol) was added to the solution. The reaction mixture was stirred overnight at room temperature. The mixture was cooled to 0°C, and 20 ml of acetone was added to yield compound x as a white precipitate in 74% yield (1.44 g). The characterization has been previously reported [131].

2.4.11. Compound 16

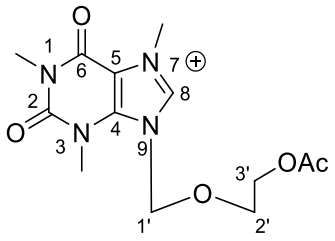

Methyl acyclovir (compound **15**; 100 mg, 0.346 mmol) was suspended in acetic anhydride (30 µL), DMAP (9 mg, 0.069 mmol) was added, and the reaction mixture was stirred overnight at room temperature. The addition of Et2O (20 mL) resulted in the appearance of a white precipitate, which was then suspended in DCM and filtered, affording compound 16 in 70% yield (83 mg).

^{1}H NMR (400 MHz, $CDCl_3$): δ 12.93 (bs, 1H, N*H*); 9.22 (s, 1H, H-8); 7.20 (bs, 2H, NH_2); 5.52 (s, 1H, H-1'); 4.44 (t, 2H, H-3', $^{3}J_{H\text{-}3',\,H\text{-}2'}$ = 4.4 Hz); 4.13 (t, 2H, H-2', $^{3}J_{H\text{-}2',\,H\text{-}3'}$ = 4.4 Hz); 4.03 (s, 3H, N7-CH_3); 1.99 (s, 3H, OAc-CH_3) ppm.

^{13}C{^{1}H} NMR (100 MHz, $CDCl_3$): δ 170.7 (C-2); 159.9 (C-8); 158.9 (OAc-*C*O); 150.5 (C-6); 137.2 (C-4); 107.9 (C-5); 74.1 (C-1'); 67.9 (C-2'); 63.0 (C-3'); 35.9 (N7-*C*H_3); 21.0 (OAc-*C*H_3) ppm.

2.4.12. Compound 17

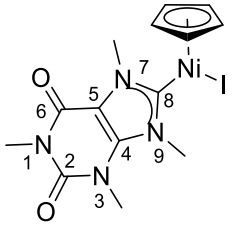

A Schlenk tube was charged with methyl caffeine (compound **1,** 110 mg, 0.330 mmol) and nickelocene (61.0 mg, 0.330 mmol). After the addition of DMF (9 ml), the reaction mixture was heated at 100°C for 2 hours. After cooling, the mixture was diluted with CH_2Cl_2 (13 ml) and washed with H_2O (7×7 ml) to remove DMF. The organic layer was separated, dried with Na_2SO_4 and filtered. The filtrate was evaporated to dryness under vacuum, affording compound **4** as a dark red powder (164 mg, 54%). Compound **4** was recrystallized by slow evaporation of a saturated solution of **4** in CH_2Cl_2/Et_2O.

^{1}H NMR (400 MHz, $CDCl_3$): δ 5.38 (s, 5H, C_5H_5); 4.69 (s, 3H, N7-C*H*$_3$); 4.49 (s, 3H, N9-C*H*$_3$); 3.80 (s, 3H, N1-C*H*$_3$); 3.36 (s, 3H, N3-C*H*$_3$) ppm.

^{13}C{^{1}H} NMR (100 MHz, $CDCl_3$): δ 179.3 (C-8); 152.6 (C-6); 150.6 (C-2); 140.9 (C-4); 111.8 (C-5); 92.5 (*C*$_5$H$_5$); 40.8 (N9-*C*H$_3$); 39.1 (N7-*C*H$_3$); 32.2 (N3-*C*H$_3$); 28.7 (N1-*C*H$_3$) ppm.

HRMS-ESI (m/z): $[M\text{-}I+CH_3CN]^+$ calc. for $C_{16}H_{20}N_5O_2Ni$ 372.0964 Found 372.0973.

Anal. Calcd for $C_{14}H_{17}IN_4O_2Ni$: C, 36.64; H, 3.73; N, 12.21. Found: C, 36.89; H, 3.99; N, 12.13.

2.4.13. Compound 18

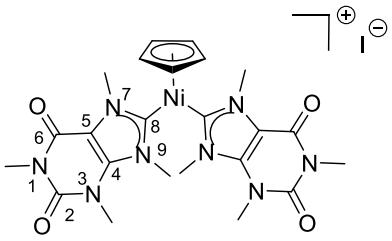

Following the procedure described for compound **6**, the aqueous phase was evaporated to dryness, first with the addition of isopropanol to facilitate water removal and subsequently with the addition of heptane to remove residual DMF. Compound **7** was isolated as a pale green solid in 13% (24 mg)

^{1}H NMR (400 MHz, $CDCl_3$): δ 5.52 (s, 5H, C_5H_5); 4.76 (br s, 6H, N9-CH_3); 4.39 (s, 6H, N7-CH_3); 3.97 (s, 6H, N3-CH_3); 3.34 (s, 6H, N1-CH_3) ppm.

^{13}C{^{1}H} NMR (100 MHz, $CDCl_3$): δ 170.9 (C-8); 152.9 (C-6); 150.6 (C-2); 142.3 (C-4); 112.0 (C-5); 92.8 (C_5H_5); 41.0 (N9-CH$_3$); 39.0 (N7-CH$_3$); 33.6 (N3-CH$_3$); 28.7 (N1-CH$_3$) ppm.

HRMS-ESI (m/z): $[M+H]^+$ calc. for $C_{23}H_{29}N_8O_4Ni$ 539.1660. Found 539.1671.

Anal. Calcd for $C_{23}H_{29}IN_8O_4Ni$: C, 41.41; H, 4.38; N, 16.80. Found: C, 41.63; H, 4.70; N, 16.92.

2.4.14. Compound 19

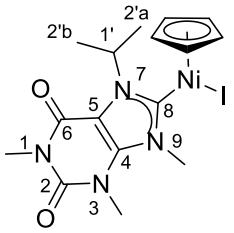

A Schlenk tube was charged with the isopropyl theophylline derivative (compound **3a,** 100 mg, 0.270 mmol) and nickelocene (52.0 mg, 0.270 mmol). After the addition of DMF (2.7 ml), the reaction mixture

was heated at 60°C for 3 days. After cooling, the mixture was diluted with CH_2Cl_2 (10 ml) and washed with H_2O (6×5 ml) to remove DMF. The organic layer was separated, dried with Na_2SO_4 and filtered. The filtrate was evaporated to dryness under vacuum, affording compound **8** as a dark red powder (52 mg, 39%). Compound **8** was recrystallized by slow evaporation of a saturated solution of **8** in CH_2Cl_2/Et_2O.

^{1}H NMR (400 MHz, $CDCl_3$): δ 6.65 (sept, 1H, H-1', $^3J_{H\text{-}1',\ H\text{-}2'}$ = 6.9 Hz); 5.38 (s, 5H, C_5H_5); 4.75 (s, 3H, N9-C*H*$_3$); 3.82 (s, 3H, N3-C*H*$_3$); 3.39 (s, 3H, N1-C*H*$_3$); 1.72 (d, 1H, H-2'a, $^3J_{H\text{-}2',\ H\text{-}1'}$ = 6.9 Hz); 1.68 (d, 1H, H-2'b, $^3J_{H\text{–}2',\ H\text{-}1'}$ =6.9 Hz) ppm.

^{13}C{^{1}H} NMR (100 MHz, $CDCl_3$): δ 177.8 (C-8); 151.5 (C-6); 150.5 (C-2); 142.6 (C-4); 111.1 (C-5); 92.7 (*C*$_5$H$_5$); 59.3 (C-1'); 41.3 (N9-*C*H$_3$); 32.6 (N3-*C*H$_3$); 29.2 (N1-*C*H$_3$); 21.1 (C-2'a); 20.2 (C-2'b).

HRMS-ESI (m/z): $[M\text{-}I+CH_3CN]^+$ calc. for $C_{18}H_{23}N_5O_2Ni$ 400.1277. Found 400.1275.

Anal. Calcd for $C_{16}H_{20}IN_4O_2Ni$: C, 39.55; H, 4.15; N, 11.53. Found: C, 39.60; H, 4.10; N, 11.69.

2.4.15. Compound 20

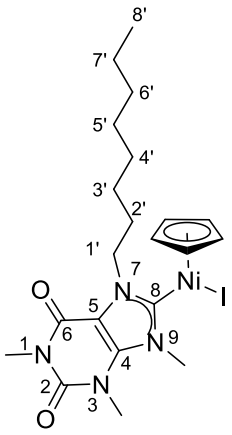

A Schlenk tube was charged with the octyl theophylline derivative (compound **3b,** 72.0 mg, 0.160 mmol) and nickelocene (30.5 mg, 0.160 mmol). After the addition of DMF (1.6 ml), the reaction mixture was heated at 60°C overnight. After cooling, the mixture was diluted with CH_2Cl_2 (6 ml) and washed with H_2O (7×7 ml) to remove DMF. The organic layer was separated, dried with Na_2SO_4 and filtered. The filtrate was evaporated to dryness under vacuum. The solid residue was purified by chromatography using a mixture of CH_2Cl_2:Et_2O (1:1) as the eluent to afford compound **9** as a red solid in 36% yield (32 mg).

^{1}H NMR (400 MHz, $CDCl_3$): 5.37 (s, 5H, C_5H_5); 5.05 (td, AA'BB', 1H, H-1$_a$', $^3J_{H\text{-}2,\ H\text{-}1a'}$ = 4.9 Hz, $^2J_{H\text{-}1a',\ H\text{-}1b'}$ = 12 Hz); 4.81 (td, AA'BB', 1H, H-1'b $^3J_{H\text{-}1b',\ H\text{-}2'}$ = 4.9 Hz, $^2J_{H\text{-}1a',\ H\text{-}1b'}$ = 12 Hz); 4.72 (s, 3H, N9-*CH$_3$*); 3.79 (s, 3H, N3-*CH$_3$*); 3.36 (s, 3H, N1-*CH$_3$*); 2.14 (m, 1H, H-2'a); 1.72 (m, 1H, H-2'b); 1.62-1.18 (m, 10H, H-3–H-7'); 0.89 (m, 3H, H-8' ppm).

^{13}C{^{1}H} NMR (100 MHz, $CDCl_3$): δ 178.0 (C-8); 152.1 (C-6); 150.6 (C-2); 141.4 (C-4); 111.2 (C-5); 92.6 (*C*$_5$H$_5$); 52.5 (C-1'); 41.1 (N9-*C*H$_3$); 32.3 (N3-*C*H$_3$); 32.0 (*C*H$_2$); 30.1 (C-2'); 29.4 (2×*C*H$_2$); 29.3 (*C*H$_2$); 28.7 (*C*H$_2$); 27.1 (N1-*C*H$_3$); 22.8 (C-7'); 14.3 (C-8') ppm.

HRMS-ESI (m/z): $[M\text{-}I+CH_3CN]^+$ calc. for $C_{23}H_{34}N_5O_2Ni$ 470.2060. Found 470.2066.

Anal. Calcd for $C_{21}H_{31}IN_4O_2Ni$: C, 45.28; H, 5.61; N, 10.06. Found: C, 45.08; H, 5.93; N, 9.77.

2.4.16. Single-Crystal X-ray Crystallography

Crystals suitable for single-crystal X-ray analysis of compounds **17** and **19** were selected, covered with Fomblin (polyfluoro ether oil) and mounted on a nylon loop. The data were collected at 110 K or at room temperature on a Bruker D8 Venture diffractometer equipped with a Photon 100 CMOS detector using graphite monochromated Mo-Kα radiation (λ=0.71073 Å). The data were processed using the APEX3 suite software package, which includes integration and scaling (SAINT), absorption corrections (SADABS)[132] and space group determination (XPREP). Structure solution and refinement were performed using direct methods with the programs SHELXT 2014/5 and SHELXL (version 2018/3)[133,134] built in the APEX and WinGX-Version 2021.3[135] software packages. All nonhydrogen atoms were refined anisotropically. All the hydrogen atoms were inserted in idealized positions and allowed to refine riding on the parent carbon atom.

Table 2.4 - *Main crystal data for compound **17**.*

Empirical formula	C14 H17 I N4 Ni O2
Formula weight	458.92
Temperature	110(2) K
Wavelength	0.71073 Å
Crystal system	Orthorhombic

Space group	P 21 21 21
Unit cell dimensions	a = 6.0892(5) Å α= 90°.
	b = 13.8298(9) Å β= 90°.
	c = 18.5881(12) Å γ= 90°.
Volume	1565.35(19) $Å^3$
Z	4
Density (calculated)	1.947 Mg/m3
Absorption coefficient	3.224 mm^{-1}
F(000)	904
Crystal size	0.200 x 0.100 x 0.080 mm3
Theta range for data collection	2.640 to 27.620°.
Index ranges	-7<=h<=7,-18<=k<=17,-23<=l<=23
Reflections collected	12426
Independent reflections	3586 [R(int) = 0.1081]
Completeness to theta = 25.242°	99.5%
Absorption correction	Semiempirical from equivalents
Max. and min. transmission	0.7456 and 0.4490
Refinement method	Full-matrix least-squares on F^2
Data/restraints/parameters	3586/0/205
Goodness-of-fit on F^2	1.039
Final R indices [I>2sigma(I)]	R1 = 0.0661, wR2 = 0.1350

R indices (all data)	R1 = 0.1078, wR2 = 0.1520
Absolute structure parameter	0.47(8)
Extinction coefficient	0.0135(15)
Largest diff. peak and hole	2.216 and-2.197 e.$Å^{-3}$

Table 2.5 - *Main crystal data for compound **19**.*

Empirical formula	C16 H21 I N4 Ni O2
Formula weight	486.98
Temperature	296(2) K
Wavelength	0.71073 Å
Crystal system	Monoclinic
Space group	P 21/c
Unit cell dimensions	a=8.7196(10) Å α= 90°.
	b=11.6325(12) Å β= 97.780(4)
	c=20.059(3) Å γ= 90°.
Volume	2015.8(4) $Å^3$
Z	4
Density (calculated)	1.605 Mg/m^3
Absorption coefficient	2.508 mm^{-1}
F(000)	968.0
Crystal size	0.400 x 0.300 x 0.100 mm3

Theta range for data collection	2.696 to 33.836°.
Index ranges	-12<=h<=13,-18<=k<=18,-31<=l<=31
Reflections collected	52325
Independent reflections	8075 [R(int) = 0.0777]
Completeness to theta = 25.242°	99.4%
Absorption correction	Semiempirical from equivalents
Max. and min. transmission	0.7467 and 0.4703
Refinement method	Full-matrix least-squares on F^2
Data/restraints/parameters	8075/0/221
Goodness-of-fit on F^2	1.048
Final R indices [I>2sigma(I)]	R1 = 0.0524, wR2 = 0.1320
R indices (all data)	R1 = 0.0903, wR2 = 0.1445
Absolute structure parameter	n/a
Extinction coefficient	0.0135(15)
Largest diff. peak and hole	1.823 and-1.341 e.$Å^{-3}$

2.4.17. Antifungal activity

The fungal strains used in this assay, *Candida glabrata* and *Candida albicans*, were maintained on yeast peptone dextrose (YPD) agar plates and grown at 37°C or 30°C, respectively. The assay was carried out in RPMI-1640 medium at pH 7. The minimum inhibitory concentrations (MICs) of *Candida*

glabrata and *Candida albicans* were determined by conducting broth microdilution assays in accordance with the CLSI (Clinical Laboratory and Standards Institute) standard methods M27- A3 for yeasts. The drug concentrations ranged from 2.5 mM to 9.8 µM. Growth in RPMI medium was recorded after 24 h and 48 h at 30°C (*Candida albicans*) or 37°C (*Candida glabrata*) by measuring the OD_{600}. The growth condition without drugs was used as the normalization condition after background (in RPMI medium) subtraction. The concentrations of the drugs for which the relative ODs fell less than 50% of the no-drug conditions were considered the MIC_{50}. At least three independent assays were performed for each chemical and strain.

2.4.18.Cytotoxicity assays

HeLa cells were seeded at a density of $5x10^4$ cells/mL in DMEM supplemented with 10% foetal bovine serum and cultured at 37°C with 5% CO_2 for 24 h. The medium was discarded, the medium was replaced with fresh medium supplemented with each drug, and the cells were incubated again at 37°C with 5% CO_2 for 24 h and 48 h. The concentrations used for each drug were the ones for which *Candida* sp. were susceptible according to the MIC_{50}. Untreated HeLa cells were used as controls. The effect of the drugs on the viability of the HeLa cells was assessed using the MTT (thiazolyl blue tetrazolium bromide) method. The cells were incubated with 500 µg/mL MTT and left in the dark for 2 h. After the incubation, DMSO was used to solubilize the precipitate formed by MTT, and the absorbance was read at 570 nm. Cell viability was determined in relation to that of the control group. Biological quadruplicates were used in all the assays.

CHAPTER 3

GUANOSINE-BASED GOLD N-HETEROCYCLIC CARBENES

Introductory notes

Figure numbering

The numbering of the figures, schemes and tables shown here in Chapter 3 is independent of the use of the other chapters.

Published paper

2. The majority of the content of this chapter is summarized in the following submitted preprint: Francescato, G.; Orsini, G.; Petronilho, A.; Gold Mono and Bis N-Heterocyclic Carbenes based on mRNA cap0. DOI: 10.26434/chemrxiv -2024-bt0dw-v2

Author contributions

The author of this thesis performed all the experiments reported in this chapter, as well as the chemical characterization.

3.1. Introduction

N7-methylguanosine is also known as the cap of messenger RNA (mRNA) or cap0. This cap is present at position 5’ in the mRNA of all eukaryotic cells and certain viruses but is absent in prokaryotes. The formation of a 5' cap is the initial co-transcriptional modification performed on messenger RNA (mRNA). The 5' cap is a distinguishing feature of transcripts produced by RNA polymerase II in eukaryotes and viral mRNA[136,137]. As a cap, N7-methyl guanosine is linked to the first nucleoside of the nascent transcript via an inverted 5'-5' triphosphate bridge[138].

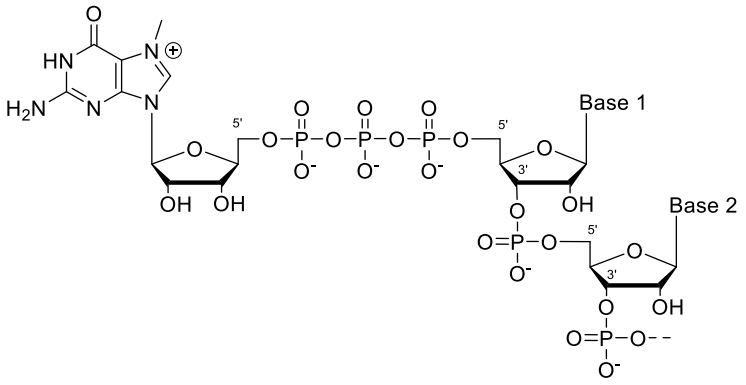

Figure 3.1 - *N7-methylguanosine linked to the first nucleoside via an inverted 5'-5' triphosphate bridge.*

Cap formation occurs through three sequential enzymatic steps performed by three enzymes: RNA triphosphatase (which cleaves RNA from one phosphate group), RNA guanylyltransferase (which caps RNA with guanosine monophosphate (GMP), and RNA guanine-N7 methyltransferase (which methylates the guanosine nucleobase)[139].

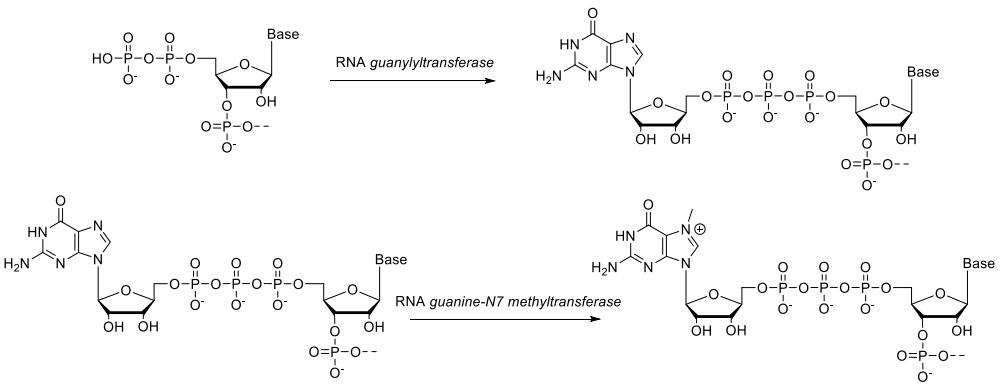

Scheme 3.1 - *Enzymatic formation of N7-methyl guanosine, RNA cap0.*

The modification leading to the formation of cap0 is crucial for various biological processes, including mRNA regulation and maturation, as it is essential for RNA splicing. RNA splicing is the process in which noncoding sequences of RNA (introns) are excised from the RNA chain, allowing the coding sequences of RNA (exons) to be joined together, forming messenger RNA[140]. The presence of methyl guanosine at the 5' end of the mRNA chain is also fundamental for the export of RNA, as it protects RNA from degradation by exoribonucleases[141]. Finally, the 5' cap0 region is essential for translation, as it serves as a signal for the initiation of translation, starting from the 5' end and progressing toward the coding region of the mRNA for protein synthesis. This signal is particularly crucial considering that the recruitment of mRNA represents a limiting step in the translation process[142,143].

In addition to its translational significance, the process of guanosine methylation is also relevant from an organometallic perspective, as it increases the acidity of C8-H (Fig 3.2). Thus, the imidazolium ring in the structure of methyl guanosine is indeed an NHC precursor.

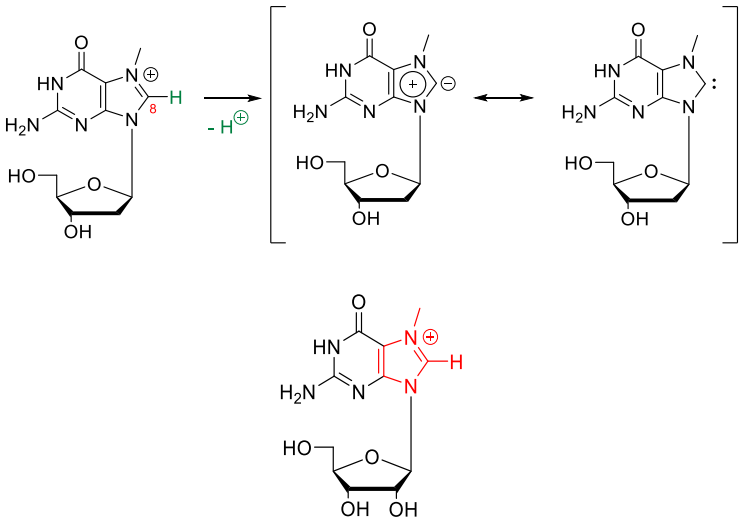

Figure 3.2 - *N7-Methyl guanosine has an increased acidity of the C8-H (top) and contains an imidazolium ring (bottom).*

The potential reactivity of cap0 mRNA toward platinum has already been assessed and studied in our laboratory. In a previous study, we demonstrated the possibility of methyl guanosine undergoing metalation with tetrakis(triphenylphosphine)platinum(0), affording a complex with potential anticancer activity[11,31]. This research underscores the importance of understanding the reactivity of a biological compound capable of interacting with numerous proteins while also highlighting the potential for identifying a novel pharmaceutical target within the mRNA cap0. In this context, the reactivity of N-7-methylguanosine as an NHC precursor, namely, its reactivity with gold, has never, to the best of our knowledge, been explored by other groups.

The use of gold as a medicinal agent can be traced back to ancient times, but its modern application in medical contexts can be attributed to the bacteriologist Robert Koch. In 1890, Koch reported the antimicrobial activity

of gold cyanide against *tubercle bacilli* in vitro. After the discoveries of Robert Koch, in 1920, Jacques Forestier reported that gold possesses antirheumatic properties[144]. Thus, auranofin has emerged as a medication for the treatment of rheumatoid arthritis that functions to reduce inflammation and disease progression[49].

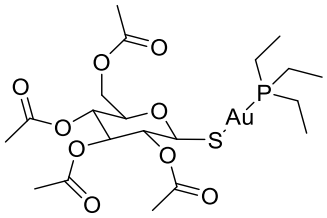

Figure 3.3 - *Auranofin.*

Although the exact mechanism of action of this orally administered compound is not well understood, it is believed that due to gold's strong affinity for elements such as sulfur and selenium, it can interact with proteins containing amino acids such as cysteine and selenocysteine[145–148]. Notably, proteins such as thioredoxin reductase and glutathione peroxidase, which are vital for cellular function, appear to be significantly inhibited by gold(I) complexes[149].

The interaction between gold complexes and these proteins has motivated many research groups to explore new gold(I) compounds capable of interacting with sulfur- or selenium-containing enzymes. This has led to the synthesis of gold complexes containing NHC carbenes, with the aim of developing pharmacologically active compounds, especially for antitumour applications. The idea of a possible antitumour application arises from the role of thioredoxin reductase (TrxR). Thioredoxin reductase is an enzyme that

plays a crucial role in maintaining the cellular redox balance by reducing oxidized thioredoxin to its active form. In cancer cells, thioredoxin reductase is often overexpressed because it contributes to the survival and proliferation of cells with aberrant redox activity. By inhibiting TrxR, the cellular redox system is disrupted, leading to increased levels of reactive oxygen species (ROS) and oxidative stress. These alterations can trigger various downstream events, including the induction of apoptosis (programmed cell death) in cancer cells[150]. In this sense, gold compounds containing NHC are attractive due to the stability of the NHC and the vast range of side groups that can be incorporated into it. In line with this, the reactivity of gold compounds toward TrxR appears to vary based on the derivatization of NHC: compounds with N-methyl groups exhibit greater reactivity toward the enzyme than compounds derivatized with bulky side chains[151].

In addition to the aforementioned points, some gold compounds are able to interact with DNA via noncovalent interactions. When these gold complexes contain two NHCs (bisNHCs), the complexes can interact with a specific secondary DNA structure known as the G-quadruplex (G4). The G-quadruplex structure is formed by repetitive guanine sequences, where four guanosine molecules coordinate through Hoogsteen sites to establish hydrogen bonds, creating a planar and cyclic structure called a G-quartet. A G- quartet constitute the building block of the G-quadruplexes, and by stacking one on top of the other, G-quadruplexes form. The presence of cations, such as K^+, promotes the formation of this structure[152].

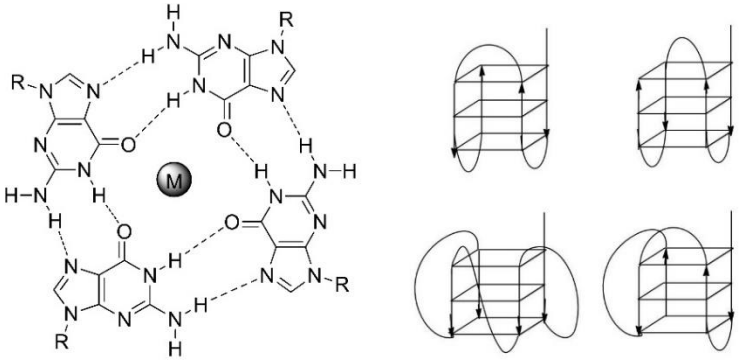

Figure 3.4 - *Left: G-quartets are formed by Hoogsteen hydrogen bonds; Right: G-quartets stacked on top of the other formed G-quadruplexes.*

The G4 is a structure that can be found in the entire human genome but is particularly present before promoter regions of oncogenes and in telomeres. The promoter regions of oncogenes are DNA sequences in which RNA polymerase initiates the transcription of the gene in question. The G4 structures of these regions appear to be able to regulate transcription[153]. Telomeres, on the other hand, are the terminal part of the chromosome and are a region of DNA in which the sequence TTAGGG (T=thymine; A=adenine, G=guanosine) is repeated; this region is intended to protect the DNA since DNA polymerase is unable to replicate the DNA sequence down to the last base[154,155]. Therefore, from replication to replication, telomeres are shortened. When telomere elongation is necessary, the enzyme telomerase intervenes. The latter is responsible for lengthening the telomere by adding sequences in which guanosine is repeated (TTAGGG), which is why the G-quadruplex is particularly present in this region of the chromosome[156,157]. The enzyme telomerase is particularly active in cancer cells, which have longer telomeres than healthy cells and therefore have a high concentration of G4 structures[62,154]. In summary, stabilizing G-quadruplex structures means

intervening by blocking the transcription of oncogenes when the structures are present in the promoter regions of oncogenes. By stabilizing G4 the unwinding of such structure is impeded, this blocks the action of telomerases and, as a consequence, the telomere elongation. In addition, these structures also arrest DNA polymerase during the replication process, causing instability, which leads to apoptosis or prevents cell replication[61–63,65,66,155,156,158].

In recent publications, Casini and coworkers presented a study on the synthesis of gold biscarbenes derived from caffeine, which demonstrated selective activity against cancer cells, specifically ovarian cancer cells[63,65]. The synthesis of the gold complexes was inspired by previous work from Monchaud, who demonstrated that a gold(I) biscarbene based on methyl caffeine is able to interact with G-quadruplexes[159].

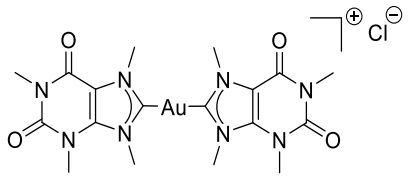

Figure 3.5 - *The complex proposed by Monchaud and coworkers.*

Building upon the resemblance between caffeine and N-7-methyl guanosine, we explored the metalation of guanosine with gold. Our objective was to obtain gold carbenes incorporating mRNA cap0 for dual purpose. First, we aimed to gain insights into the reactivity of these compounds within the cellular environment. Second, we aimed to investigate the potential antitumour activity of the complexes due to their potential to interact with G-quadruplexes. This study holds promise for advancing our understanding

of mRNA cap0 reactivity and therapeutic potential of derived complexes in combating tumours.

3.2. Results and discussion

Earlier examples from our group showed that the metalation of unprotected nucleosides leads to the formation of a myriad of compounds[11], while the protection of ribose generally results in more selective reactions. Additionally, protecting the ribose ring can increase the solubility in less polar solvents[160]. Therefore, protected methyl guanosine was synthesized using previously established procedures[31]. Accordingly, guanosine was first protected at the sugar moiety with acetate groups by reacting with acetic anhydride using pyridine as the solvent. Protection was followed by methylation at N7 with methyl iodide in DMA, yielding compound **1**.

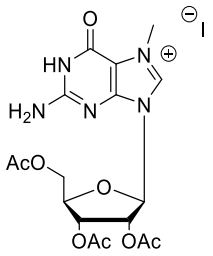

1

Figure 3.6 - *Ligand precursor based on guanosine.*

The ligand precursor was then reacted with $Au(SMe_2)Cl$ at room temperature, employing DMF as the solvent, in the presence of potassium carbonate for 3 days (Scheme 3.2). Following this time, ^1H NMR analysis in

DMSO-d_6 of the reaction mixture showed complete consumption of the methylguanosine salt **1**, as noted by the disappearance of the H8 resonance. It was possible to identify two main compounds, as evidenced by the presence of two N7-methyl groups at 4.09 and 3.98 ppm in a 1:9 ratio; this was also the case for the ribose protons, although some of the signals overlapped. The new compounds do not show any signals in the region corresponding to H8, strongly indicating the presence of two guanosine carbenes in the mixture.

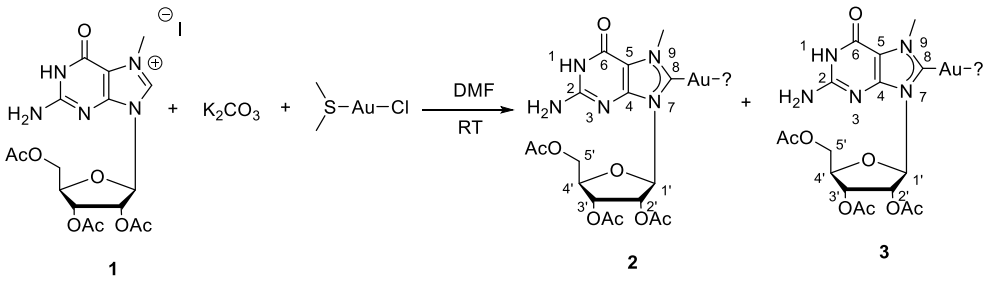

Scheme 3.2 - *Reaction of methyl guanosine **1** with the gold(I) precursor.*

At this stage, it was not possible to distinguish whether the mixture corresponded to a mono- and a biscarbene (Scheme 3.3a) or a mixture of two gold(I) compounds bearing, for instance, two different halogens (chloride or iodide) as shown in Scheme 3.3b. Nevertheless, it was possible to identify a major product (compound **2**) and a minor one (compound **3**), and the mixture allowed for partial characterization of the two guanosine compounds. The broad signal between 7.43 and 6.96 ppm corresponds to the NH_2 of both compounds. The H1' resonates at 6.37 ppm for compound **3** and at 6.27 ppm for compound **2**. For H2', the order is reversed, with compound **2** resonating at a lower field (6.12 ppm) and compound **3**

resonating at 5.97 ppm. For compound **2**, H3' resonates at 5.63 ppm, H4' resonates at 4.36 ppm between the two diasterotopic protons of H5', which are located at 4.46 and 4.25 ppm. For compound **3** H3' is visible at 5.70 ppm, while the remaining signals are overlapped with those of compound **2**. In the $^{13}C\{1H\}$ NMR spectrum, the hypothetical carbenic carbons were not visible in this first analysis. Nevertheless, in the 2D HMBC spectrum, it was possible to observe interactions with both the N7 methyl groups and ^{13}C. In particular, the methyl group of compound **2** shows a cross-peak at 172.2 ppm, while for compound **3**, a cross-peak can be found at 184.8 ppm. These two values agree well with those reported in the literature for mono- and bis-carbenes of gold(I)[161].

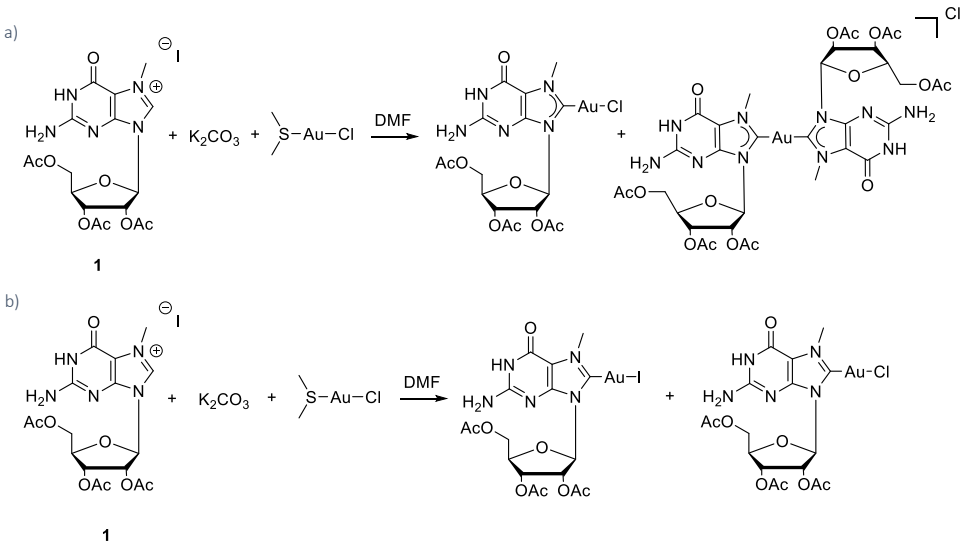

Scheme 3.3 - *Possible products of the reaction of 7-methylguanosine **1** with $Au(SMe_2)Cl$.*

A diffusion-ordered spectroscopy (DOSY) experiment performed on the mixture revealed that the minor compound, compound **3**, had a higher

molecular weight and, alongside the value found for $^{13}C\{1H\}$ NMR, we hypothesized that compound **3** corresponded to a gold biscarbene. However, for gold compounds, carbene chemical shifts in $^{13}C\{1H\}$ NMR show significant variations depending on the halogen trans to the NHC[162]. To exclude the hypothesis of halogen scrambling (Scheme 3.3b), we also examined the reaction using a poorly coordinating anion, BF_4[161]. Thus, the protected guanosine was methylated using trimethyloxonium tetrafluoroborate for 3 hours in dry DCM, leading to the formation of compound **4** in 63% yield. The formation of compound **4** was confirmed by ^1H NMR, in which H8 resonates at 9.34 ppm, a value similar to that of the iodide salt **1**.

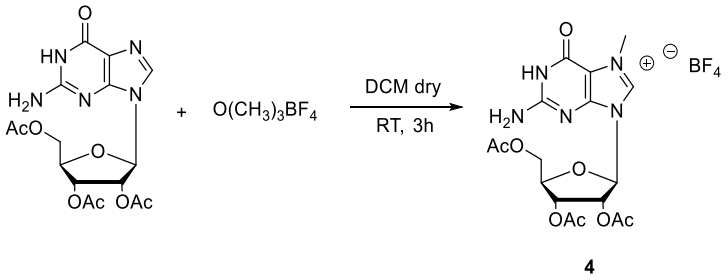

Scheme 3.4 - *Synthesis of the ligand precursor 2',3',5'-tri-O-acetyl-7-methylguanosine bearing BF_4 (**4**).*

Compound **4** was then reacted with $Au(SMe_2)Cl$ in DMF under the same conditions as those used previously. Analysis of the reaction mixture by ^1H NMR after 3 days showed the presence of two products, as indicated by the absence of H8 signals and the presence of two methyl groups at N7 in a 3:2 ratio (compounds **2** and **3**). All the signals for the two complexes fall in the same region as those previously described for the reaction with **1**. A

substantial difference in the ratio between **2** and **3** was observed, as the amount of complex **3** present in the mixture increased from 10% to 40%. We speculate that this difference can be attributed to an increase in solubility when BF_4 is used as an anion for the biscarbene compound.

The presence of more than one complex, even when using the BF_4 ligand precursor **4**, further supported our assumption that the two complexes were likely a gold monocarbene and a gold biscarbene (Figure 3.7), already inferred by the values found for $^{13}C\{1H\}$ NMR.

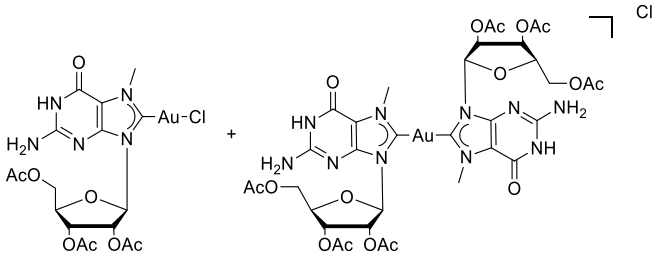

Figure 3.7 - *Gold mono and biscarbene complexes of 7-methylguanosine.*

Following the preliminary studies and characterization, the reaction was replicated on a larger scale in DMF. After completion, diethyl ether was added to induce complete precipitation of the mixture and simultaneously facilitate DMF removal. The precipitate was then dried under vacuum, and the mixture was analysed by ^{1}H NMR. The isolated solid showed very poor solubility and was partially soluble only in DMF and DMSO. Due to the low solubility of the mixture, chromatography-based separation was not feasible, and all attempts to separate the mixture by other methodologies (crystallization, coprecipitation) were unsuccessful. Due to this, we decided to further

examine the initial reaction conditions to determine if it was possible to selectively form each of the compounds.

To better understand the mechanism of their formation, the reaction (Scheme 3.5) was monitored by ^{1}H NMR (Figure 3.8). Compound **1** was reacted with Au(SMe$_2$)Cl in the presence of 1 equivalent of K_2CO_3. The reaction was carried out in an NMR tube in DMF-d_7 under nitrogen.

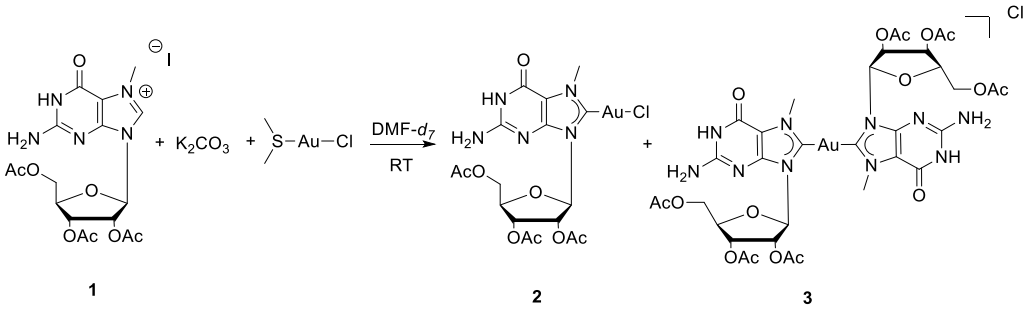

Scheme 3.5 - *Reaction of N7-Methyl guanosine **1** with Au(SMe$_2$)Cl.*

The reaction was analysed by ^{1}H NMR after preparation (t0), after 10 hours and 48 hours, after 3 days and 5 days and after 10 days (Figure 2) to evaluate the stability of the solution.

As can be inferred from Figure 3.8, at t0 (which was measured a few minutes after the preparation of the sample), compound **1** was already reacting, and at least one new compound was formed (new signal at 4.09 ppm). This new signal at 4.09 ppm is indicative of a new methyl group bound to N7, as this group is located slightly upfield than that of compound **1** (4.24 ppm).

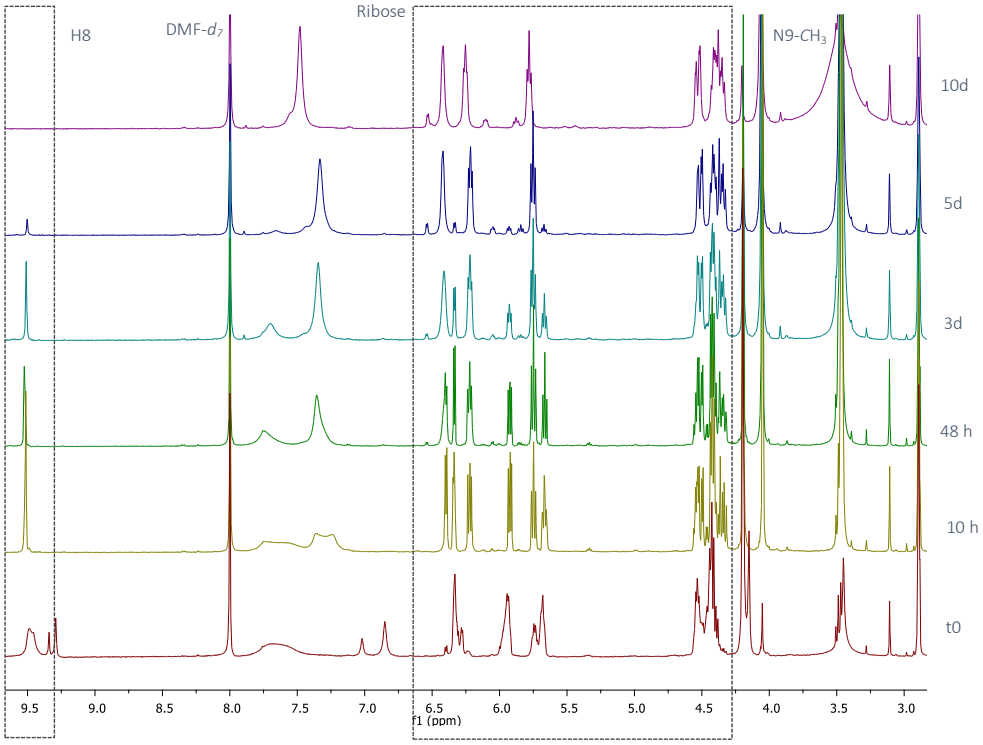

Figure 3.8 - *^{1}H NMR spectrum of the reaction of **1** in DMF-d_7 with Au(SMe_2)Cl and K_2CO_3 at room temperature at different times.*

The appearance of the new signal is concomitant with the partial disappearance of the C8-*H* peak at 9.41 ppm. Nevertheless, at t0, there are three peaks in the H8 region (9.6-9.3 ppm), suggesting the presence of different reaction intermediates[162,163]. Dimethyl sulfide, from Au(SMe_2)Cl, is released during the reaction, resulting in a distinct, constant signal at 2.08 ppm throughout the reaction, which was omitted for clarity. After 10 hours, the ^{1}H NMR spectrum was clearer, allowing to better identify the signals of the two compounds in the reaction mixture; one was the ligand precursor, compound **1,** and the other was a new species, compound **2**, in a 1:1 ratio. In the H8 region, only one signal was identified, corresponding to unreacted

compound **1**. The presence of just one signal at 9.53 ppm (H8) also suggested that the new compound lacked the proton at C8, in agreement with the formation of NHC complexes of guanosine ligands bound to gold via C8, as discussed above. After 2 days, the ratio of compound **1** to compound **2** changed, with compound **2** representing 61% of the mixture. Additionally, in the region of the sugar moiety, a new set of signals was observed, confirming the formation of a second compound, compound **3**. This new set of signals was particularly evident after 3 days, which was the timeframe used for previous experiments. At this stage, the percentage of the starting material **1** is 25%, while that of compound **2** reaches 70%, and compound **3** accounts for the remaining 5%. The difference between the slower reactivity observed under these conditions to that observed previously can be ascribed to the lack of stirring for these measurements since the reaction was performed in an NMR tube. It should be noted that during the reaction, the formation of a precipitate, which increased over time was observed. The ratios described correspond exclusively to what is determined in solution. After 5 days, ^{1}H-NMR showed that starting material **1** was almost completely consumed (8%), and compound **2** and compound **3** were present in a 9:1 ratio. The amount of compound **3** increased slightly, facilitating the identification of the corresponding signals, as evidenced by the signals at 6.57, 6.11 and 5.89 ppm, corresponding to H1', H2' and H3', respectively, which are slightly shifted with respect to the ^{1}H NMR in DMSO-d_6, as expected.

After 10 days, the starting material was completely consumed, and the methyl groups of the new compounds **2** and **3** were clearly distinguishable. Considering the evolution of the reaction mixture and the absence of any

signal for H8, the mixture shows the presence of two different compounds bound to the metal via C8, one major (compound **2**) and one minor (compound **3**) (N7-methyl at 4.09 and 4.23 ppm, respectively, in DMF-d_7) in a 9:1 ratio, in agreement with previous observations.

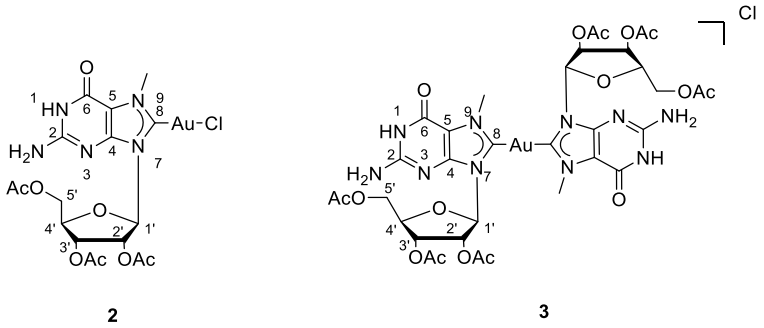

2 **3**

Figure 3.9 – *Gold mono- and biscarbene **2** and **3**.*

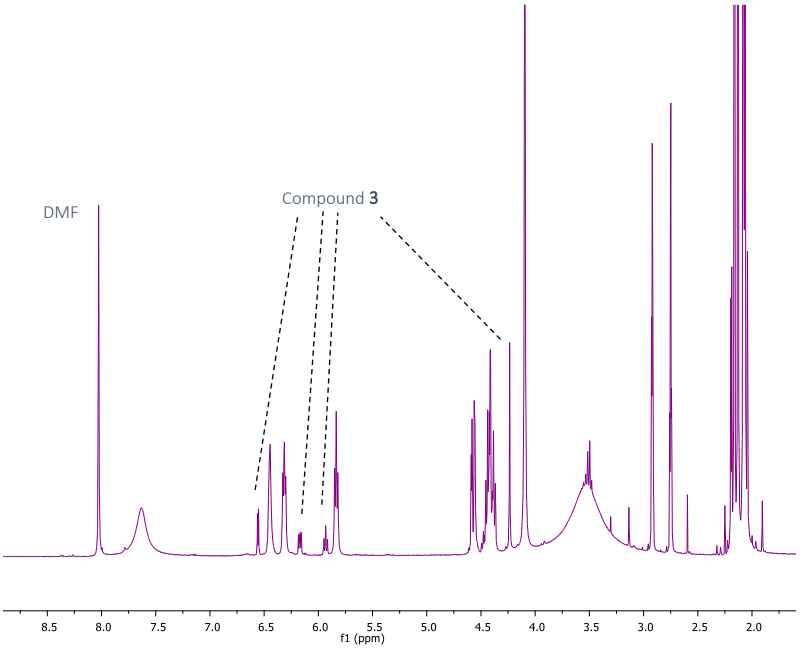

Figure 3.10 - *^{1}H NMR spectrum of the monocarbene **2** and biscarbene **3** in the final reaction mixture.*

The reaction mixture was further examined using $^{13}C\{^1H\}$ NMR and 2D HMBC and HSQC. The $^{13}C\{^1H\}$ NMR spectrum of compound **2** shows a peak attributed to a gold(I) carbene at 174.2 ppm, which agrees well with the previous value. Although the carbenic carbon of compound **3** is not visible due to the low concentration of the compound, once again, in the 2D HMBC spectrum, a cross peak between the methyl group at N7 is visible at 185.2 ppm, further confirming the formation of **3**.

Overall, these measurements indicate that it is not possible to avoid the formation of compound **3** prior to the total consumption of the ligand precursor **1**.

3.2.1. Inducing Selectivity: Variation of the Reaction Conditions

Given the failure to separate the mixture we explored some variations of the reaction conditions. For example, different solvents were considered. Acetonitrile was selected due to the many examples in the literature using this solvent for the formation of gold NHCs using gold(I) and K_2CO_3 as a base[149,164–166]. Thus, compound **1**, $Au(SMe_2)Cl$ and K_2CO_3 were suspended in acetonitrile, and the mixture was heated at 70°C for several hours (Scheme 3.6) . Even at this temperature, three days were needed to reach completion. The analysis of the mixture again revealed the formation of the two carbenes, at a ratio of 9:1 of mono- vs biscarbene, similar to previous conditions.

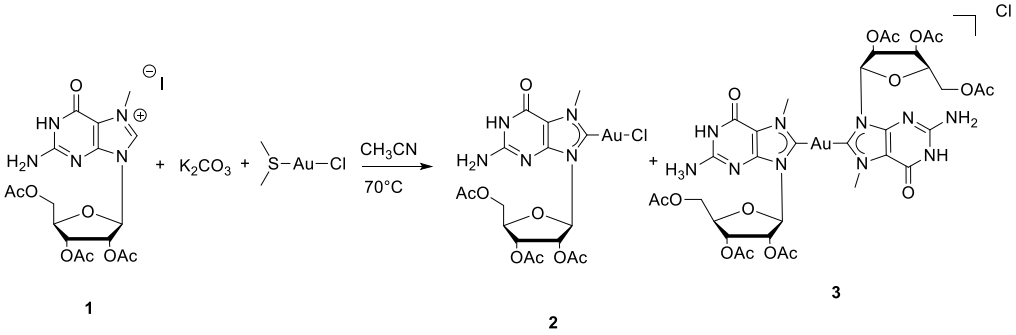

Scheme 3.6 - *Reaction of N7-methyl guanosine with gold(I) in acetonitrile.*

To examine a solvent with properties similar to those of DMF, we conducted the reaction in deuterated DMSO. This allowed us to monitor the progress of the reaction effectively. Thus, the ligand precursor was suspended in DMSO-d_6, with 1 equiv. of gold(I) and 1 equiv. of K_2CO_3 and this mixture was reacted at room temperature.

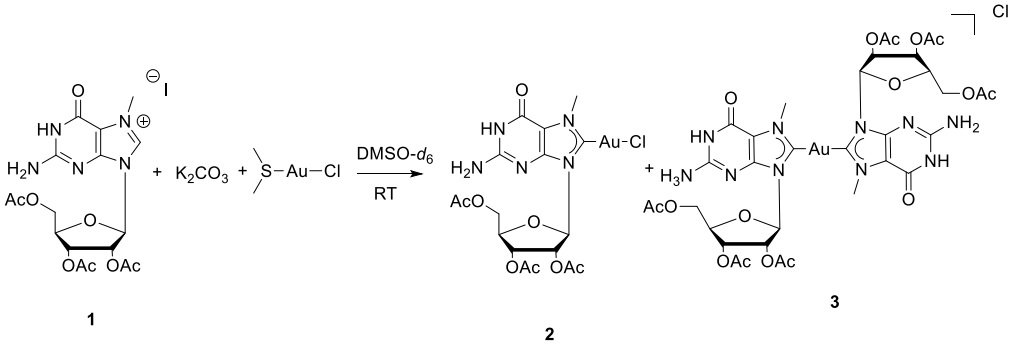

Scheme 3.7 - *Reaction of N7-methyl guanosine with gold(I) in deuterated DMSO.*

NMR analysis of the reaction allowed to conclude that changing the solvent from DMF to DMSO lead to a similar outcome, with a final mixture containing compound **2** and **3** in a ratio 9:1 (Scheme 3.7). Finally, the

reactivity of compound **1** in acetone was explored. Previous work from Collado and Nolan showed that gold NHCs can be formed using K_2CO_3 starting from the corresponding imidazolium salts in acetone[162,167]. Accordingly, for gold compounds, the formation of monocarbene occurs through the formation of an anion aurate (Scheme3.8), in which the gold precursor binds to the halogen of the ligand precursor, after the loss of the dimethyl sulfide ligand[162]. Evidence of the formation of this anion is obtained by inspecting the ^{1}H NMR, which generally shows a significant upfield shift in the C2-H signal of the imidazolium salt. Importantly, if an excess of base is used, bis-NHCs complexes can also be formed due to the formation of a gold acetonyl complex from the monocarbene [167–170].

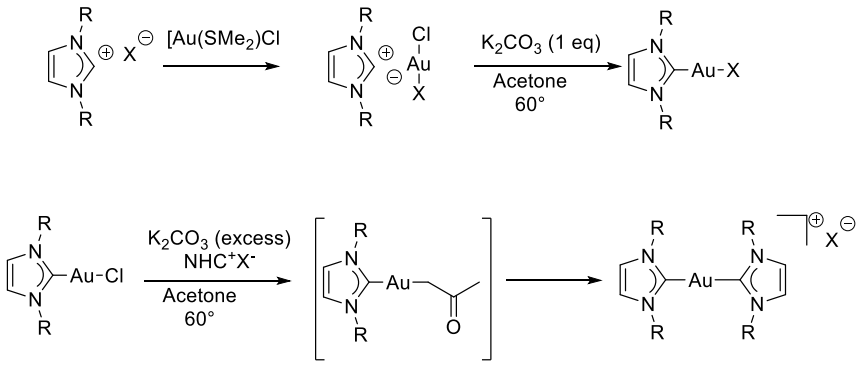

Scheme 3.8 - *Synthesis of gold mono- and bis carbenes in acetone as described by Nolan and Collado.*

This methodology was tested on guanosine salt **1,** aiming to selectively obtain the gold monocarbene **2**. ^{1}H NMR spectra for the mixture of **1** and $AuCl(SMe_2)$, in the absence and presence of K_2CO_3 were recorded. In the absence of the base, the ^{1}H NMR spectrum shows a very small shift of H8, from 9.53 ppm to 9.30 ppm (an upfield shift of 0.23 ppm). This difference is

not as significant as that observed by Nolan for imidazolium salts, probably suggesting that the aurate anion does not form under these conditions.

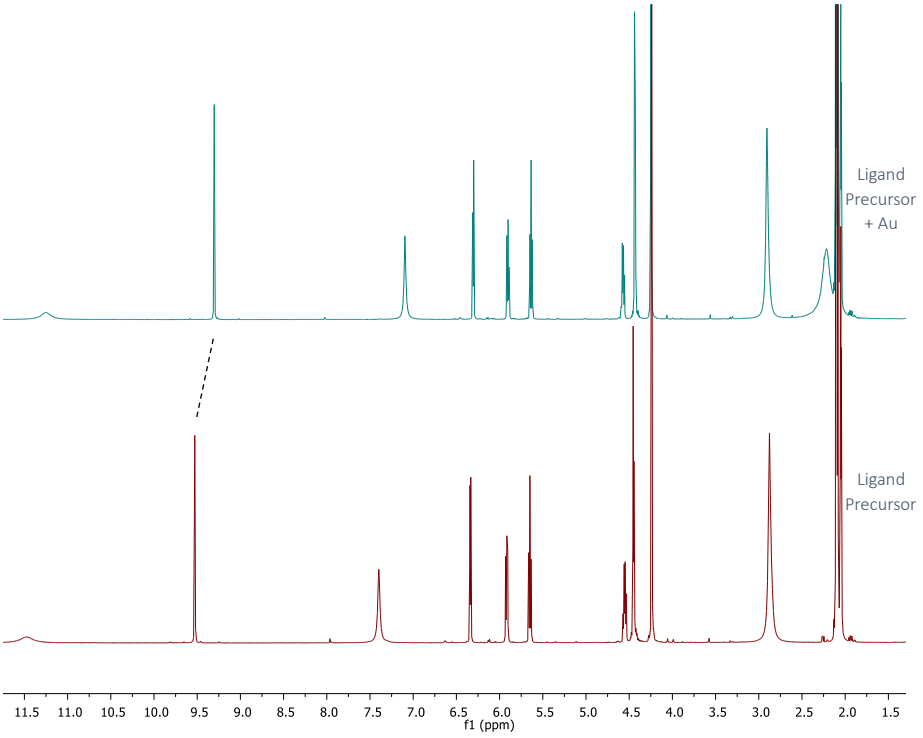

Figure 3.11 - *^{1}H NMR of compound **1** in acetone (top) and in the presence of $AuSMe_2(Cl)$ (bottom)*

After adding the base, analysis of the mixture at different times allowed to observe that N7-methyl guanosine does not react in acetone in a similar mode to that reported by Nolan and co-workers for imidazolium salts. In this case, the reaction led to a mixture of unidentified compounds. Thus, with this approach is not possible to selectively synthetize the monocarbene and the biscarbene complexes.

Finally, transmetallation procedures were attempted. Transmetallation is a very common route for selectively synthesizing either mono- or bis-carbenes of gold utilizing silver[171,172]as discussed in chapter 1. The stoichiometry of the reaction can be adjusted to facilitate the formation of mono- or bis-carbenes, which then are transmetallated to gold.

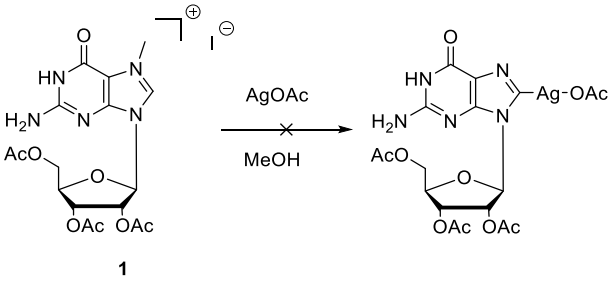

Scheme 3.9 – *Reaction of **1** with AgOAc.*

Thus, the ligand precursor **1** was reacted with silver acetate in methanol at room temperature, but no reaction for the formation of the NHC took place. Similar results were obtained when employing silver oxide. In both cases a precipitate can be observed, but probably corresponds to the formation of the silver halide salts since the C8-H remain intact.

3.2.2. Inducing Selectivity: Variation of the Stoichiometry

Several reports on the synthesis of gold NHCs highlight that stoichiometry can be important to achieve selectivity[173]. For example, Gabbiani and co-workers used 2 equivalents of the ligand precursor versus gold, leading to the formation of the corresponding gold biscarbene exclusively[64,174]. Therefore,

our strategy was to examine whether a change in the stoichiometry of **1** vs $Au(SMe_2)Cl$ had any influence on the ratio of the mixture obtained.

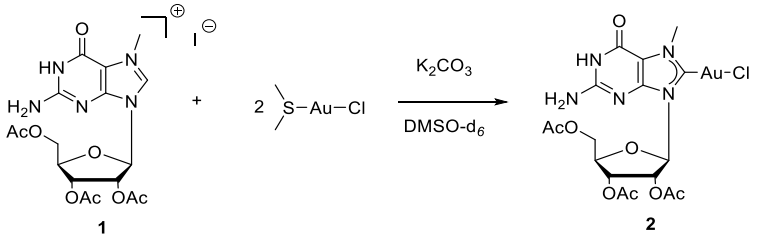

Scheme 3.10 - *Reaction of **1** in DMF with 2 equivalents of $Au(SMe_2)Cl$ in the presence of K_2CO_3.*

The reaction with gold was repeated by changing the reaction stoichiometry; in this case, 2 equivalents of $Au(SMe_2)Cl$ were reacted with 1 equivalent of the ligand precursor **1**. The reaction was carried out in an NMR tube in deuterated DMSO to enable monitorization by ^1H NMR. The sample was analysed at t0 (within minutes of preparation), after 3 hours, after 5.5 hours, after 24 hours and after 2 days.

At t0, the spectrum is unclear, and many of the signals are broad. After 3 hours, ^1H NMR showed that monocarbene **2** was the major compound in the mixture. Integration with respect to compound **1** indicated that **2** represented 78% of the mixture. After 5 hours, compound **1** was almost completely consumed, and after 24 hours, gold monocarbene compound **2** was the only product present, and no signs of compound **3** were observed.

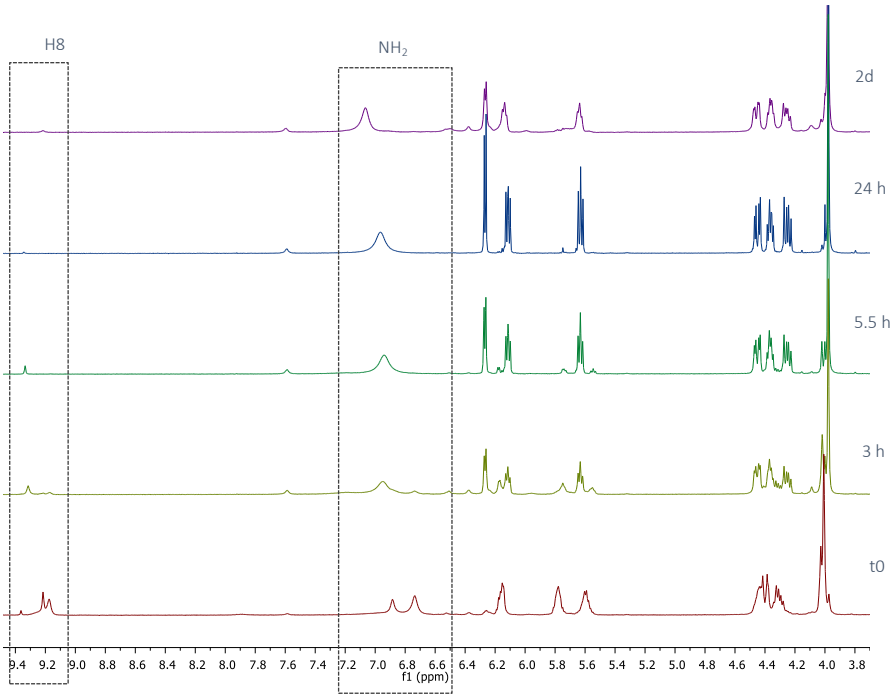

Scheme 3.11 - *^{1}H NMR spectrum of the reaction of **1** in DMSO-d_6 with 2 equivalents of Au(SMe$_2$)Cl in the presence of K_2CO_3 at room temperature at different times.*

During the reaction, a pink–brown precipitate formed, while the solution turned from colourless to intensely yellow. After filtration, attempts to analyse the solid by ^{1}H NMR were unsuccessful due to its insolubility. ^{1}H NMR analysis of the mother liquor confirmed the presence of compound **2** exclusively. Compound **2** can be isolated by precipitation using several solvents (such as water, diethyl ether or dichloromethane) without jeopardizing the stability of the compound. Compound **2** is soluble in DMSO, DMF, and DMA. Complete characterization of **2** was performed. The ^{13}C{^{1}H} NMR spectrum revealed the presence of a peak at 172.2 ppm corresponding to the carbenic carbon C8, which is in accordance with what observed for the mixture of both compounds 2 and 3 discusses above. Is possible to identify

all the ribose carbons, with C1' resonating at 89.8 ppm, followed by the C4' at 79.6 ppm. The C2', C3' and C5' resonate at 71.3, 69.9 and 62.7 ppm, respectively.

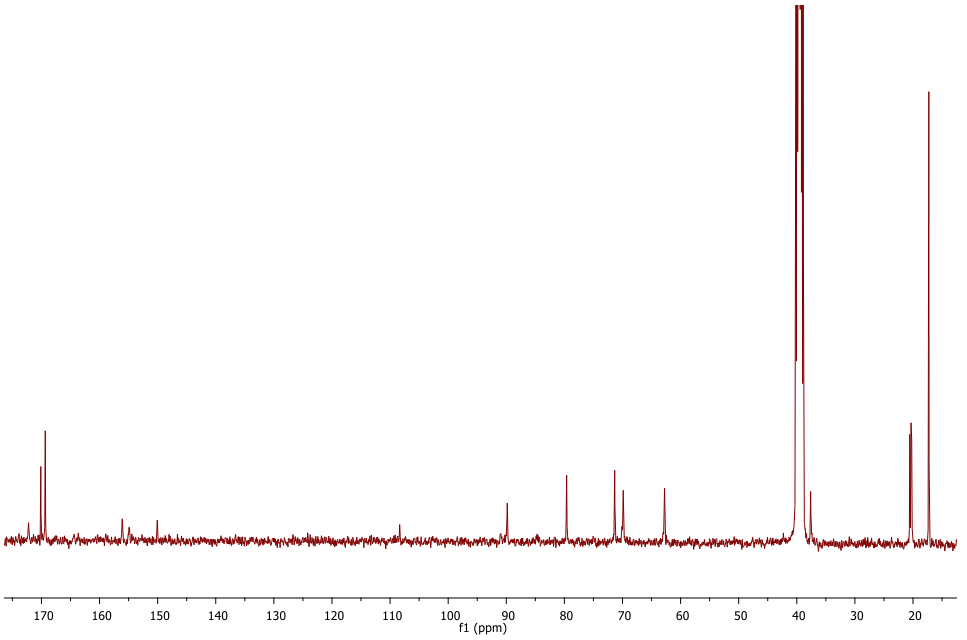

Figure 3.12 - *$^{13}C\{^{1}H\}$ NMR spectrum of gold monocarbene (complex **2**) in DMSO-d_6.*

The reaction was scaled up successfully, and after appropriate work-up, compound **2** was isolated as a white powder in 34% yield. Analysis of the solid by high-resolution mass spectrometry showed a peak at 694.0370, corresponding to the monocarbene **2** bearing a chloride in trans plus a potassium cation. Mass spectrometry also showed that the halogen bound to gold is chloride and not iodide. This indicates that formation of the aurate anion by reaction with the iodide of **1** probably did not take place[162]. This is also in line with what was previously observed for the reaction performed in acetone, for which no aurate was formed, as inferred by ^{1}H NMR.

Following the previous approach employed for the monocarbene complex, the reaction was carried out using 2 equivalents of ligand precursor and 1 equivalent of chloro(dimethylsulfide)gold(I) (Scheme 3.12). This experiment was expected to confirm the selective formation of compound **3**.

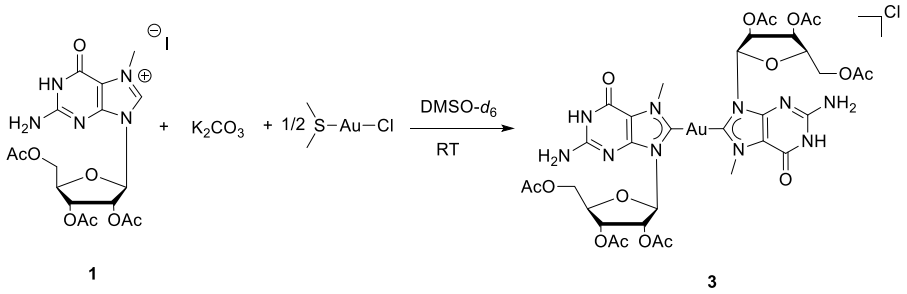

Scheme 3.12 - *Reaction of **1** in DMF with 0.5 equivalents of $Au(SMe_2)Cl$ in the presence of K_2CO_3.*

Once again, the reaction was carried out in deuterated DMSO and in an NMR tube to allow for monitorization by ^{1}H NMR. The sample was analysed at t0 (a few minutes after preparation), after 1 hour, after 3.5 hours, after 24 hours, after 2 days and after 3 days.

At t0, a change in the composition of the mixture with respect to the starting material, **1**, is already noted. A new peak at 6.37 ppm (H1') is clearly visible. Integration with respect to the starting material indicated that the new compound accounted for 37% of the mixture. After 1 h, gold biscarbene **3** was the predominant compound in the mixture, with an 8:2 ratio with respect to **1**. After 3.5 hours, no significant changes were noted. Changes in the composition of the mixture appear after 24 hours, when the starting material **1** is practically absent.

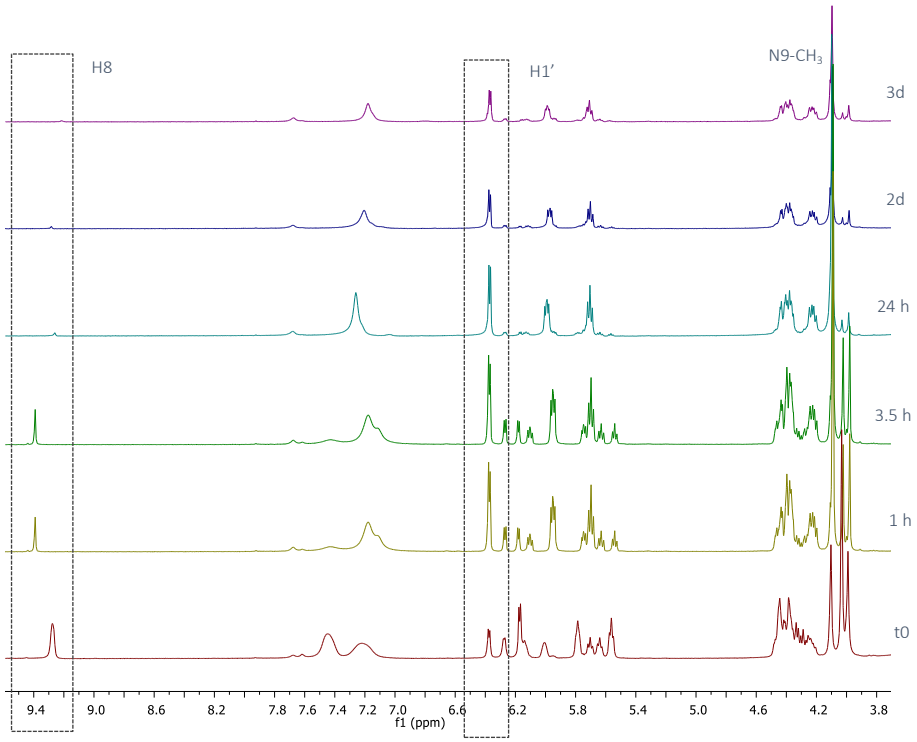

Scheme 3.13 - *^{1}H NMR spectrum of the reaction of **1** in DMSO-d_6 with 0.5 equivalents of $Au(SMe_2)Cl$ in the presence of K_2CO_3 at room temperature at different times.*

Further analysis after 2 and 3 days revealed no changes, demonstrating that complex **3** is stable in DMSO solutions during this time. Interestingly, as the reaction progresses, a large amount of flocculent white precipitate is formed. ^{1}H NMR analysis of the isolated precipitate confirmed that this solid correspond to the biscarbene **3**, and therefore, compound **3** tends to precipitate upon formation. Thus, is probably the reason for which the reaction became apparently slower. Complete NMR analysis of the solid allowed for its full characterization. The $^{13}C\{^{1}H\}$ NMR spectrum confirmed the presence of a peak at 184.8 ppm, corresponding to the C8 carbenic carbon. As stated previously, this value is consistent with those reported in the

literature for gold biscarbenes[161]. For the ribose signals C1' resonates at 89.8 ppm and C4' at 79.6 ppm. C2', C3' and C5' resonate at 71.3, 69.9 and 62.7, respectively.

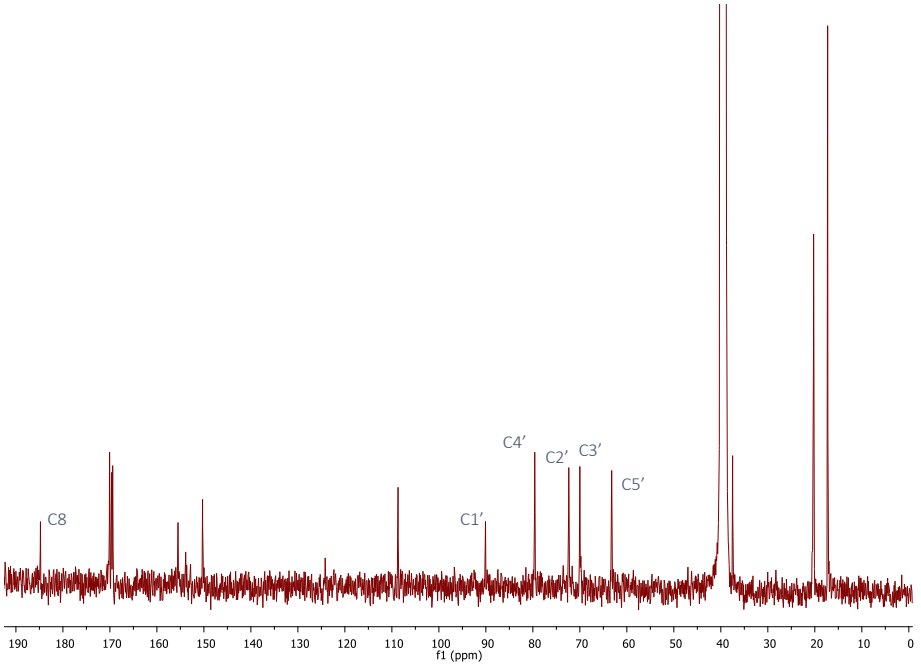

Figure 3.13 - *$^{13}C\{^{1}H\}$ NMR spectrum of complex **3** in DMSO-d_6.*

In addition to $^{13}C\{1H\}$ NMR analysis, 2D NMR experiments have also been performed. Among these, NOESY analysis revealed a cross-peak between the CH_3 group in N7 and the H1' position of the ribose. This interaction enabled to determine the relative conformation of the NHCs, a conformation previously documented in the literature for compounds of this nature[65], as illustrated in Figure 3.14. Following this, the reaction was scaled up successfully, and compound **3** was isolated as a yellowish precipitate in 48% yield. High resolution mass spectrometry confirmed that compound **3** is

indeed a biscarbene, with a peak at 1043.2438 corresponding to the biscarbene cation.

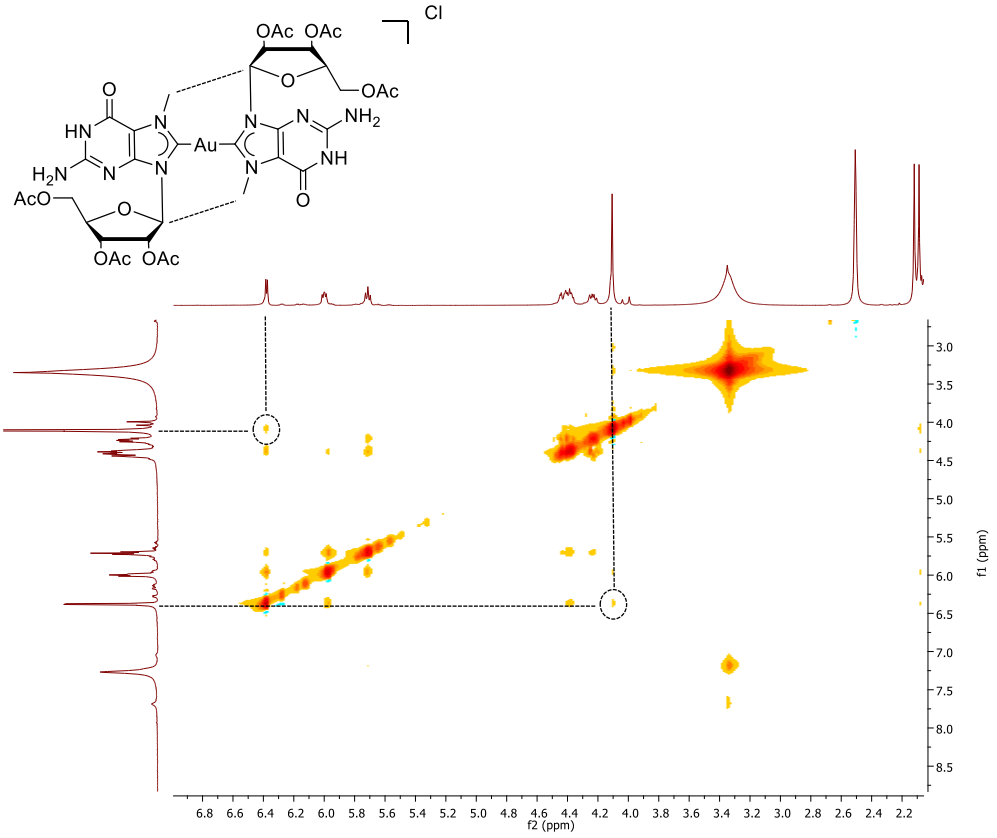

Figure 3.14 - *NOESY spectrum of biscarbene complex **5**.*

Despite successful isolation of biscarbene complex **3** and comprehensive NMR characterization, a persistent challenge was found: the insolubility of **3** in all the tested solvents. While biscarbene does exhibit marginal solubility, which allows for NMR analysis, it falls short in providing sufficient solubility for further biological testing.

3.2.3. Selective Synthesis of Gold Mono and Bis Carbenes with unprotected 7-methylguanosine

Attempts to deprotect compounds **2** and **3** were not successful. Compound **2** was stirred in the presence of HCl, but the acetate groups remained intact even after 24 hours. Also, under these conditions, we observed no hydrolysis of the sugar. As for compound **3**, due to the poor solubility, deprotection also revealed unattainable. Previous work from our group on metal complexes bearing nucleosides has shown that guanosine proligands require protection when reacting by C-X or C-H oxidative addition to Pt(0) or Pd(0). Contrastingly, for similar reactions, uridine proligands react cleanly without requiring the protection of the sugar. Given the difficulties to find a suitable deprotection method, most probably driven by the low solubility of the compounds in suitable solvents for deprotection, we explored the reactivity of the unprotected guanosine ligand, compound **5** (Scheme 3.14). Compound **5** was first reacted with gold in a 1:1 ratio in the presence of K_2CO_3. The reaction was first performed in DMF, expecting a difference in solubility due to the unprotected OH groups.

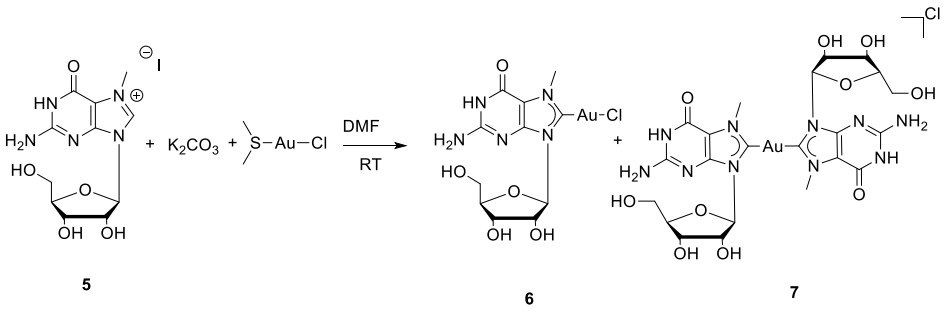

5 **6** **7**

Scheme 3.14 - *Reaction of **5** in DMF with 1 equivalent of $Au(SMe_2)Cl$ in the presence of K_2CO_3.*

After 3 days, diethyl ether was added to the reaction mixture to obtain a precipitate. This precipitate was revealed to be a highly insoluble mixture of two carbenes, as was the case for the mixture obtained with **1**. Nevertheless, in the case of unprotected guanosine, the corresponding biscarbene forms in lower amounts that with **1** but can still be observed. Therefore, the strategy employed to obtain compounds **2** and **3** selectively was also used for compound **5**. Thus, 2 equiv. of $Au(SMe_2)Cl$ was used to obtain the monocarbene compound **6** (Scheme 3.15).

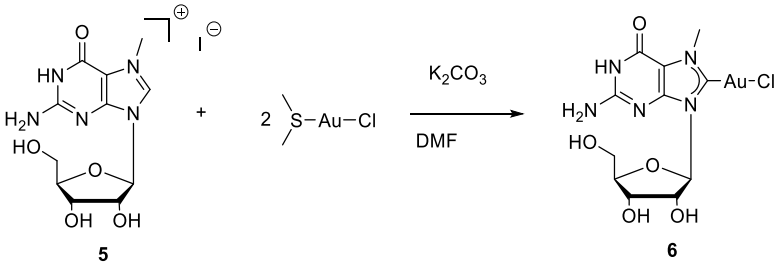

5 **6**

Scheme 3.15 - *Reaction of **5** with 2 equivalents of $Au(SMe_2)Cl$ in the presence of K_2CO_3.*

The reaction required two and a half days to reach completion, and yielded cleanly the gold monocarbene (13 mg, 19%), compound **6**, as depicted in Scheme 3.15. Compound **6** was characterised by ^1H NMR. The broad signal ranging from 7.20 to 6.88 ppm corresponds to the NH_2 group of compound **6**. The H1' resonates at 6.08 ppm, while H2' can be found at 5.07 ppm. The three OH groups exhibit resonances at 5.48, 5.16, and 4.99 ppm, but specific assignments cannot be obtained.

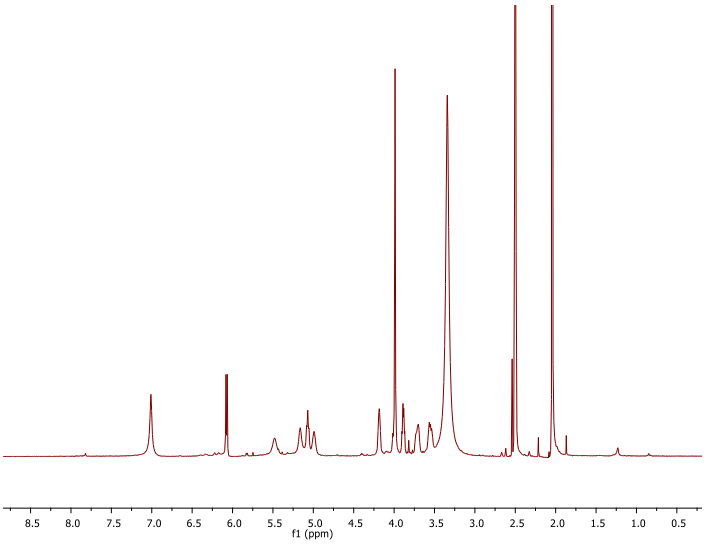

Figure 3.15 - *^{1}H NMR spectrum of gold monocarbene (compound **6**) in DMSO-d_6.*

The remaining four protons of the sugar moiety resonate at 4.18 and 3.88 ppm (H3' and H4', respectively) and at 3.70 and 3.55 ppm (H5'). Finally, the NCH_3 group resonates at 3.99 ppm. In the $^{13}C\{^{1}H\}$ NMR spectrum, the C8 is observed at 172.7 ppm, in line with the value found for **2**. High resolution mass spectrometry (HRMS) showed a peak at 568.0051, corresponding to the monocarbene **2** bearing a chloride in trans plus a potassium cation.

Following our earlier approach to form the biscarbene with protected guanosine, the reaction was performed using 2 equivalents of **5** (Scheme 3.16). The reaction was stirred at room temperature for 3 days and, also in this case, the gold biscarbene **7** was formed and was the only compound detected in the reaction crude. Compound **7** was isolated as a white powder in 45% yield.

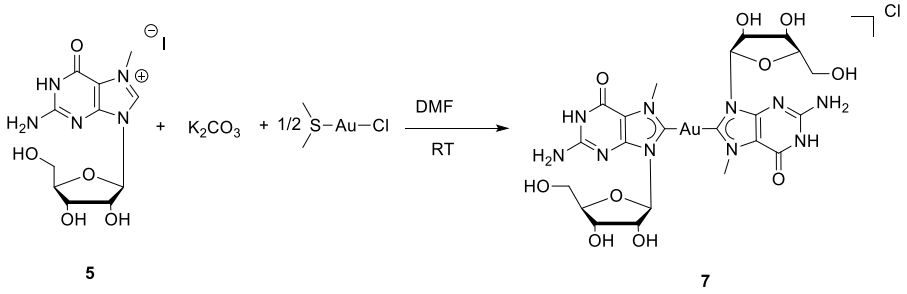

Scheme 3.16 - *Reaction of **5** in DMF with 0.5 equivalents of $Au(SMe_2)Cl$ in the presence of K_2CO_3.*

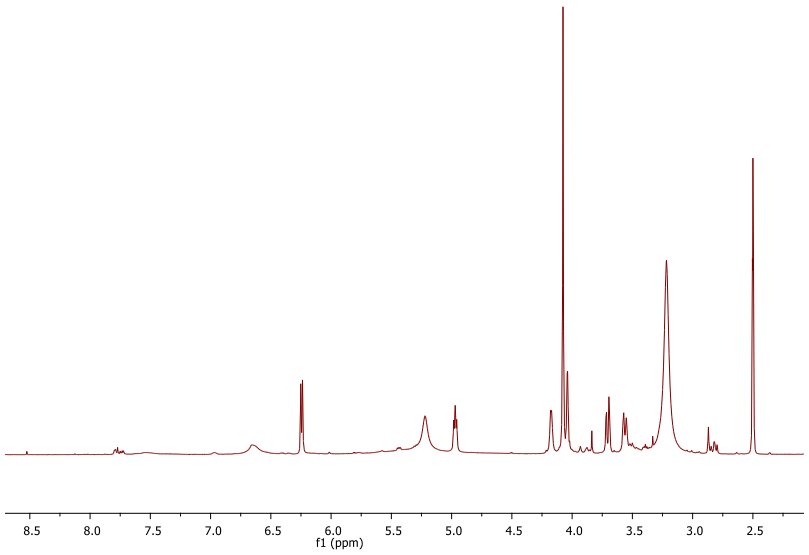

Figure 3.16 - *^1H NMR spectrum of gold biscarbene (compound **7**) in DMSO-d_6.*

The doublet visible at 6.24 ppm corresponds to the anomeric proton H1', which is followed by a broad signal (5.22 ppm), corresponding to the NH_2 signal. The triplet of H2' resonates at 4.97 ppm, and the remaining signals of the sugar resonate at 4.17, 4.03, 3.70 and 3.56 ppm for the protons at positions 3', 4' and 5', respectively. The N7-methyl group resonates at 4.08 ppm; in this case, it was not possible to observe the OH groups. The $^{13}C\{^1H\}$

NMR spectrum was recorded at 50ºC to avoid precipitation. The carbenic C8 resonates at 182.1 ppm, a value similar to that of compound **3**. HRMS further confirmed that compound **7** is the gold biscarbene bearing unprotected guanosine as NHC, as it shows a peak at 791.1800 corresponding to the biscarbene cation.

3.3. Conclusions

In conclusion, the reaction of N7-methyl guanosine **1** (mRNA cap0) with $Au(SMe_2)Cl$ has been thoroughly investigated. The ribose ring was first protected to avoid the possible interaction of the metal precursor with the free -OH, as was already observed in previous studies with 7-methyl guanosine. The ligand precursor was then reacted with 1 equiv. of $Au(SMe_2)Cl$ leading to the formation of a mixture of two complexes. Analysis of this final mixture revealed that the two products corresponded to a mono- and a bis-carbene (complex **2** and **3** respectively), with the monocarbene being the major product in solution. The reaction was tested with different solvents, with no improvement in the selectivity. The selective synthesis of complex **2** or complex **3** was achieved by a changing the stoichiometry of the reaction and thus modifying the gold:guanosine ratio. The use of 2 equiv. of $Au(SMe_2)Cl$ yielded the monocarbene **2** selectively, while the use of 2 equiv. of N7-Methyl guanosine afforded the biscarbene **3** as the only product obtained.

The same conditions were applied to deprotected N7-methyl guanosine **5**. $Au(SMe_2)Cl$ reacts with compound **5** in DMF or DMSO, leading to the formation of the monocarbene **6** with only small amounts of the

corresponding bis-NHC complex. As is the case with the protected ligand precursor **1,** modifying the stoichiometry of the reactions leads to the selective formation of compounds **6** and **7** in moderate yields.

Hence, four gold complexes bearing as NHC based on mRNA cap0 were successfully synthetised.

3.4. Experimental

The syntheses of the complexes were carried out under an inert atmosphere of N_2 using Schlenk techniques. All ^{1}H and $^{13}C\{^{1}H\}$ NMR spectra were recorded on Bruker spectrometers (400 MHz and 500 MHz), and chemical shifts were referenced to $SiMe_4$ (δ in ppm, J in Hz) and H_3PO_4. The ligand precursors were synthesized according to the synthetic procedure described previously[11,31]. Mass Spectroscopy and Elemental Analysis were performed by the UniMass Laboratory at Instituto de Tecnologia Química e Biológica, Portugal.

3.4.1. Compound 2

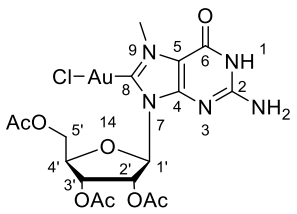

A Schlenk tube was charged with methylated and protected guanosine (Compound **1**, 65 mg, 0.12 mmol), K_2CO_3 (16 mg, 0.12 mmol) and disulfide gold chloride (70 mg, 0.23 mmol). After the addition of DMF (3 ml), the reaction mixture was stirred at room

temperature for 3 days. The reaction mixture was then filtered through alumina, and the solvent was removed under air flux. The resulting reddish powder was suspended in DCM and filtered. The mother liquors were evaporated, and then acetone was added, affording compound **2** as a white powder (27 mg, 34%).

^{1}H NMR (400 MHz, DMSO-*d*$_6$): δ 11.80 (bs, 1H, N1-*H*); 7.07 (bs, 2H, C2-N*H*$_2$); 6.27 (d, 1H, H-1', $^{3}J_{H\text{-}1',\ H\text{-}2'}$ = 5.12 Hz); 6.14 (dd, 1H, H-2', $^{3}J_{H\text{-}2',\ H\text{-}1'}$ = 5.12 Hz, $^{3}J_{H\text{-}2',\ H\text{-}3'}$ = 6.16 Hz); 5.64 (t, 1H, H-3', $^{3}J_{H\text{-}3',\ H\text{-}2'}$ = 6.16 Hz, $^{3}J_{H\text{-}3',\ H\text{-}4'}$ = 6.16 Hz); 4.46 (m, 1H, H-5'); 4.37 (m, 1H, H-4'); 4.27 (m, 1H, H-5'); 3.98 (s, 3H, N7-C*H*$_3$); 2.11 (s, 3H, Ac-C*H*$_3$); 2.07 (s, 3H, Ac-C*H*$_3$); 2.02 (s, 3H, Ac-C*H*$_3$) ppm.

^{13}C{^{1}H} NMR (100 MHz, DMSO-*d*$_6$): δ 172.2 (C-8); 170.1 (Ac-*C*O); 169.3 (2C, Ac-*C*O); 156.1 (C-2 or C-6); 154.9 (C-2 or C-6); 150.1 (C-4); 108.3 (C-5); 89.8 (C-1'); 79.6 (C-4'); 71.3 (C-2'); 69.9 (C-3'); 62.7 (C-5'); 37.6 (N7-*C*H$_3$); 20.5 (Ac-*C*H$_3$); 20.3 (Ac-*C*H$_3$); 20.2 (Ac-*C*H$_3$) ppm.

HRMS-ESI (m/z): $[M+K]^+$ Calc. for. $C_{17}H_{21}O_8N_5AuCl$: 694.0375. Obs: 694.0370

3.4.2. Compound 3

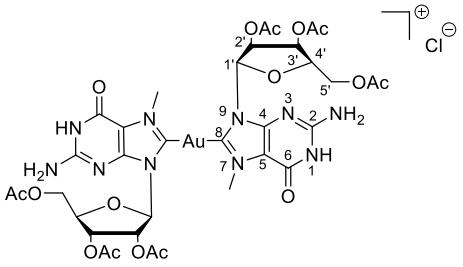

A Schlenk tube was charged with methylated and protected guanosine (Compound **1**, 138 mg, 0.25 mmol), K_2CO_3 (41 mg, 0.3 mmol) and disulfide gold chloride (29 mg, 0.1 mmol). After the addition of DMF (1.5 ml), the mixture was stirred

at room temperature for 3 days. The solvent was removed from the final suspension using air flux, affording compound **3** as a white powder (200 mg, 48%).

^{1}H NMR (400 MHz, DMSO-*d*$_6$): δ 12.21 (bs, 1H, N1-*H*); 7.26 (bs, 2H, C2-N*H*$_2$); 6.37 (d, 1H, H-1', $^{3}J_{H\text{-}1',\ H\text{-}2'}$ = 4.27 Hz); 5.99 (dd, 1H, H-2', $^{3}J_{H\text{-}2',\ H\text{-}1'}$ = 4.27 Hz, $^{3}J_{H\text{-}2',\ H\text{-}3'}$ = 6.4 Hz); 5.70 (dd, 1H, H-3', $^{3}J_{H\text{-}3',\ H\text{-}2'}$ = 6.4 Hz, $^{3}J_{H\text{-}3',\ H\text{-}4'}$ = 6.26 Hz); 4.48-4.32 (m, 2H, H-5'+ H-4'); 4.23 (m, 1H, H-5'); 4.10 (s, 3H, N7-C*H*$_3$); 2.11 (s, 3H, Ac-C*H*$_3$); 2.08 (s, 3H, Ac-C*H*$_3$); 1.95 (s, 3H, Ac-C*H*$_3$) ppm.

^{13}C{^{1}H} NMR (100 MHz, DMSO-*d*$_6$): δ 184.8 (C-8); 170.1 (Ac-*C*O); 169.6 (Ac-*C*O); 169.4 (Ac-*C*O); 155.5 (C-2 or C-6); 150.3 (C-4); 108.7 (C-5); 90.1 (C-1'); 79.6 (C-4'); 72.4 (C-2'); 69.9 (C-3'); 63.2 (C-5'); 37.5 (N7-*C*H$_3$); 20.4 (Ac-*C*H$_3$); 20.3 (2C, Ac-*C*H$_3$); ppm.

HRMS-ESI (m/z): [M]$^{+}$ Calc. for. $C_{34}H_{42}O_{16}N_{10}Au$: 1043.2440. Obs: 1043.2438

3.4.3. Compound 6

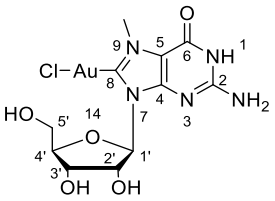

A Schlenk tube was charged with methylated guanosine (Compound **5**, 56 mg, 0.12 mmol), K_2CO_3 (16 mg, 0.12 mmol) and disulfide gold chloride (70 mg, 0.23 mmol). After the addition of DMF (3 ml), the reaction mixture was stirred at room temperature for 3 days. The reaction mixture was then filtered through alumina, and the solvent was removed under air flux. The resulting reddish powder was suspended in DCM and

filtered. The mother liquors were evaporated, and then acetone was added, affording compound **6** as a white powder (13 mg, 19%).

^{1}H NMR (400 MHz, DMSO-*d*$_6$): δ 11.92 (bs, 1H, N1-*H*); 7.01 (bs, 2H, C2-N*H*$_2$); 6.07 (m, 1H, H-1'); 5.48 (m, 1H, O*H*); 5.16 (m, 1H, O*H*); 5.07 (m, 2H, H-2'+ O*H*); 4.18 (m, 1H, H-3'); 3.99 (s, 3H, N7-C*H*$_3$); 3.90 (m, 1H, H-4'); 3.70 (m, 1H, H-5'); 3.55 (m, 1H, H-5'); ppm.

^{13}C{^{1}H} NMR (100 MHz, DMSO-*d*$_6$): δ 172.4 (C-8); 155.8 (C-2 or C-6); 154.9 (C-2 or C-6); 150.4 (C-4); 108.3 (C-5); 91.4 (C-1'); 86.1 (C-4'); 71.6 (C-2'); 70.7 (C-3'); 62.2 (C-5'); 37.6 (N7-*C*H$_3$) ppm.

HRMS-ESI (m/z): [M+K]$^{+}$ Calc. for. $C_{11}H_{15}O_5N_5AuCl$: 568.0058; Obs: 568.0051

3.4.4. Compound 7

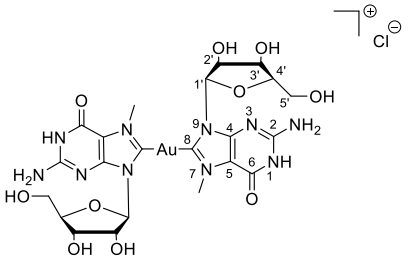

A Schlenk tube was charged with methylated guanosine (Compound **5**, 106 mg, 0.25 mmol), K_2CO_3 (41 mg, 0.3 mmol) and disulfide gold chloride (29 mg, 0.1 mmol). After the addition of DMF (1.5 ml), the mixture was stirred at room temperature for 3 days. The solvent was removed from the final suspension using air flux, affording compound **7** as a white powder (144 mg, 45%).

^{1}H NMR (400 MHz, DMSO-*d*$_6$): δ 6.24 (d, 1H, H-1', $^{3}J_{H\text{-}1',\ H\text{-}2'}$ = 7.2 Hz); 5.22 (bs, 2H, C2-N*H*$_2$); 4.97 (t, 1H, H-2', $^{3}J_{H\text{-}2',\ H\text{-}1'} = {}^{3}J_{H\text{-}2',\ H\text{-}3'}$ = 6.17 Hz); 4.17 (m, 1H,

H-3'); 4.08 (s, 3H, N7-CH_3); 4.03 (m, 1H, H-4'); 3.70 (m, 1H, H-5'); 3.56 (m, 1H, H-5'); ppm.

$^{13}C\{^1H\}$ NMR (100 MHz, DMSO-d_6): δ 182.1 (C-8); 162.8 (C-6); 161.4 (C-2); 149.6 (C-4); 110.3 (C-5); 93.1 (C-1'); 87.1 (C-4'); 71.9 (C-2'); 71.3 (C-3'); 62.4 (C-5'); 36.5 (N7-CH$_3$) ppm.

HRMS-ESI (m/z): $[M]^+$ Calc. for. $C_{22}H_{30}O_{10}N_{10}Au$: 791.1806; Obs: 791.1800

CHAPTER 4

URACIL-BASED CYCLOMETALATED COMPLEXES

Introductory notes

Figure numbering

The numbering of the figures, schemes and tables shown here in Chapter 3 is independent of the use of the other chapters.

Author contributions

The author of this thesis performed the majority of the experiments reported in this chapter, as well as the chemical characterization. Catarina Roque completed some of the synthesis of the complexes and catalytic measurements. The in catalytic experiments were conducted with the laboratory of Dr. Ligia O. Martins from ITQB NOVA, under the guidance of André Taborda. X-ray diffraction data acquisition and analysis were performed by Dr. Clara Gomes from NOVA FCT, Portugal.

4.1. Introduction

Hydrogenation reactions involve the addition of hydrogen to a molecule; traditionally, this kind of transfer occurs due to the use of molecular hydrogen. Currently, hydrogenation reactions take advantage of the use of a catalyst; in some of this process, the use of molecular hydrogen (H_2) is avoided, as a separate proton donor (alcohols, ethers, etc.) serves as the hydrogen source, and the catalyst transfers protons to a proton acceptor, this kind of reactions are called transfer hydrogenation reactions[175]. As a result, the proton donor is oxidized, while the proton acceptor is reduced. Metal-catalysed transfer hydrogenation can occur via two mechanisms: direct and indirect pathways. In the direct pathway, the metal catalyst, the proton donor, and the acceptor form a complex simultaneously, allowing the donor to transfer protons directly to the acceptor. Conversely, in the indirect pathway, the metal initially forms a complex with the donor, generating one or two hydrides. Subsequently, the complex coordinates the acceptor to transfer one or two hydrogens[176].

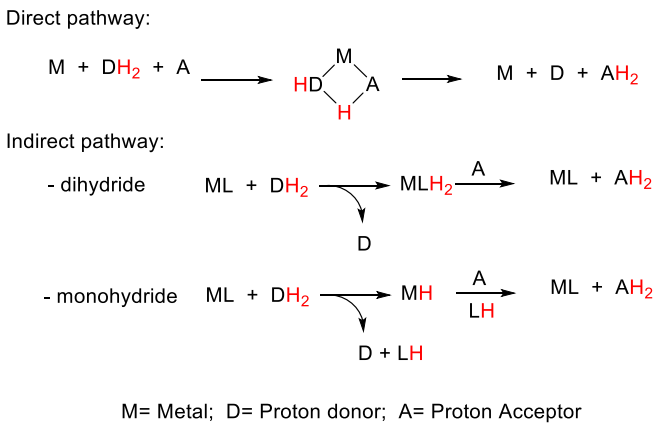

Scheme 4.1 - *Schematic representation of the two possible pathways for transfer hydrogenation reactions.*

This catalytic reaction was discovered in 1903 by Knoevenagel, who used palladium black as a catalyst[177]. Subsequent advancements in these reactions included the exploration of late-transition metals as catalysts. In the 1960s, Henbest, Mitchell, and their colleagues used an iridium complex containing a hydride to catalyze transfer hydrogenation reactions[178]. Subsequently, during the 1970s, Sasson and Blum demonstrated the viability of utilizing a ruthenium catalyst for transfer hydrogenation reactions[175,179].

The isolation of the first NHC by Arduengo et al. in the early 1990s[6] significantly impacted the field of organometallic catalysis. NHCs have emerged as extensively utilized ligands for developing catalysts containing iridium, ruthenium, or rhodium[180]. Notably, an advantage of NHCs lies in their ability to form a stable bond with the metal centre and in the possibility of being functionalized with different substituents. These substituents can, for instance, bear a donor group, such as pyridine, pyrimidine, phosphines, carboxylates, and ethers, which can readily and reversibly dissociate to

facilitate the bonding of the metal to the proton donor or the proton acceptor. Iridium, ruthenium, and rhodium catalysts containing a bidentate ligand with an NHC became widely used for their application in transfer hydrogenation [175,176,180,181].

This type of catalytic reaction also occurs inside cells due to enzyme catalysis. Transfer hydrogenation enzymes perform transfer hydrogenation with NAD^+, an important co-factor in different metabolic pathways. These enzymes catalyse the reduction of NAD^+ to NADH[182]. The presence of NAD^+ inside the cell is fundamental for maintaining the redox balance in the cell environment. The maintenance of this equilibrium is crucial for the cell to maintain the presence/formation of ROS due to different factors: external (environmental, viral or microbial infections) or internal (stress, aging)[183]. In addition to the formation of ROS, which causes oxidative stress, the accumulation of reducing species causes the so-called reductive stress, which is as harmful as oxidative stress[183,184]. Maintaining the cellular redox balance is critical for cell survival. In the case of cancer cells, this condition is fundamental, because they suffer continuous oxidative stress. Consequently, any disturbance in the NAD^+/NADH ratio presents an additional challenge in this already dysregulated redox environment, and it is nearly impossible for cancer cells to correct this imbalance[185]. In this context, metal catalysts capable of catalysing transfer hydrogenation reactions have emerged as appealing tools for causing excessive reduction of NAD^+ to NADH[186,187]. This depletion of NAD^+ causes reductive stress, posing a significant challenge for cancer cells to compensate for, eventually leading to cancer cell death[185].

The ability of metal complexes to induce the reduction of NAD^+ was exploited by several groups. Steckhan et al. described in 1991 the ability of rhodium complexes to catalyse the regioselective reduction of NAD^+ to 1,4-NADH [188]. Subsequently, Fish et al. elucidated the mechanism behind the reduction of NAD^+ to NADH in aqueous media aided by metal catalysts[189]. Following these advancements, various research groups have actively contributed to the development of the so-called catalytic drugs. These efforts predominantly involved cyclometalated compounds featuring iridium, ruthenium, rhodium, or osmium as the metal center, comprising an arene group and a bidentate chelating group.

In 2015, Sadler coined the term catalytic drug, exploiting the ability of metal catalysts to perform reactions inside the cell to promote a pharmacologic effect, for example in the induction of reductive stress. In these works, compounds such as [(η6-arene)Ru(ethylenediamine)Cl]PF_6 and [Os(arene)(p-toluenesulfonyl)-1,2-diphenylethylenediamine)][190,191] (Figure 4.1) were explored. Osmium-based catalysts primarily facilitate the reduction of pyruvate to lactate, leading to lactate accumulation and subsequent metabolic dysfunction, culminating in cell death[192]. Other groups also participate in the search for new catalysts for the catalysis of transfer hydrogenation reaction for the reduction of NAD^+ to NADH. For example, Macchioni, which developed different iridium complexes[186], and Casini, which works on ruthenium complexes bearing phosphine groups[187].

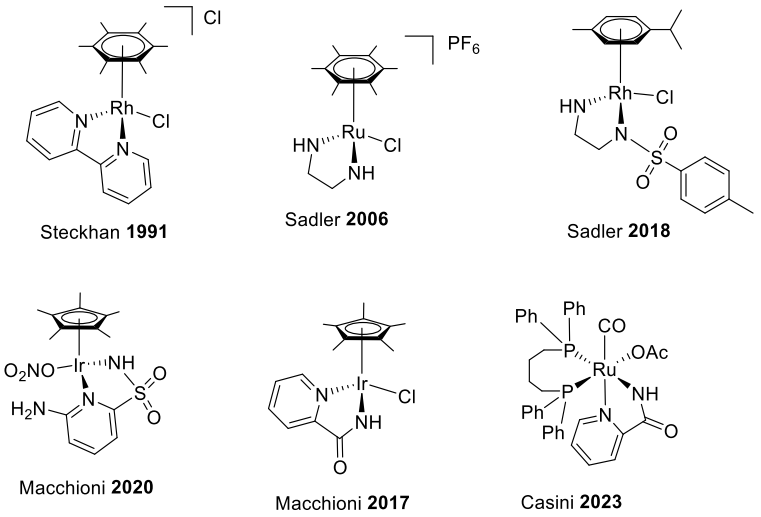

Figure 4.1 - *Examples of cyclometallated arene complexes of iridium, ruthenium and rhodium capable to catalize the readuction of NAD⁺.*

Considering the need for a bidentate chelating group, we considered that the derivatization of a pyrimidine nucleobase could provide suitable ligand precursors for transfer hydrogenation catalysts. In addition, the development of synthetic approaches for the metalation of pyrimidines is very challenging, and examples of such methods are very scarce. Our group recently explored the reactivity of halogenated pyrimidines with platinum by oxidative addition [27].

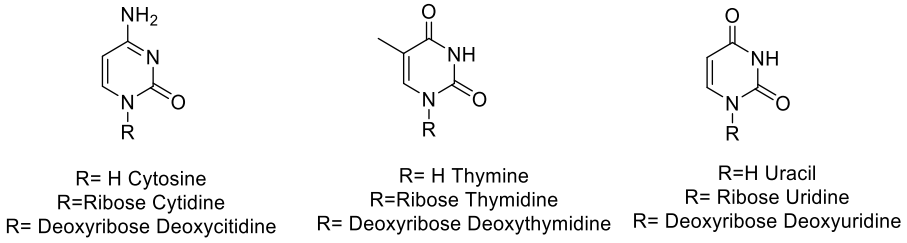

Figure 4.2 - *Pyrimidine nucleobases and nucleosides.*

Nevertheless, it is possible to derivatize the pyrimidine ring with a pendant group able to form a NHC, such as an imidazole or a triazole ring. When the pyrimidine nucleobase is deprived of the sugar moiety, nitrogen is also available to form a bond with the metal, allowing for the possibility of forming a cyclometalated NHC complex.

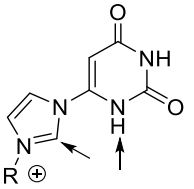

Figure 4.3 - *Uracil functionalised with an imidazolium salt.*

In this chapter, we explore the reactivity of the uracil based ligands, as depicted in Figure 4.3, to synthesize cyclometalated complexes capable of catalyzing the reduction of NAD^+ to NADH in aqueous environment. Upon elucidating their catalytic potential, these compounds will be tested in cancer cells and fungi to determine their activity within the cellular environment.

4.2. Results and discussion

4.2.1. Study of the reactivity of compound 1

The ligand precursor was synthesized following an established procedure reported by Schmidt and coworkers. Thus, 6-chlorouracil was suspended in chlorobenzene, methyl imidazole was added, and the reaction mixture was refluxed for 7 hours at 135°C[193].

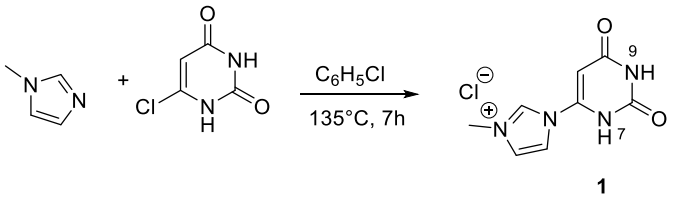

Scheme 4.2 - *Synthesis of the ligand precursor.*

As described previously, in the ^{1}H NMR spectrum of compound **1** the signals of the imidazole ring resonate as triplets as they couple among them with similar coupling constants (1.84 Hz). In addition to this, compound **1** ^{1}H NMR lacks the signal relative to the proton in N7, probably due to its high acidity, while the proton in N9 resonates at 11.16 ppm as a broad singlet[193].

The behaviour of compound **1** was examined by ^{1}H NMR at different pH values in D_2O to ascertain the acidity of the ligand and to verify the rate of deuteration at different positions. It is important to note that the proton at N7 always undergoes deuteration. The measurements were performed in acidic, neutral, and basic pH (pH 2, 7 and 13, respectively).

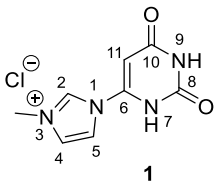

Figure 4.4 - *The ligand precursor **1.***

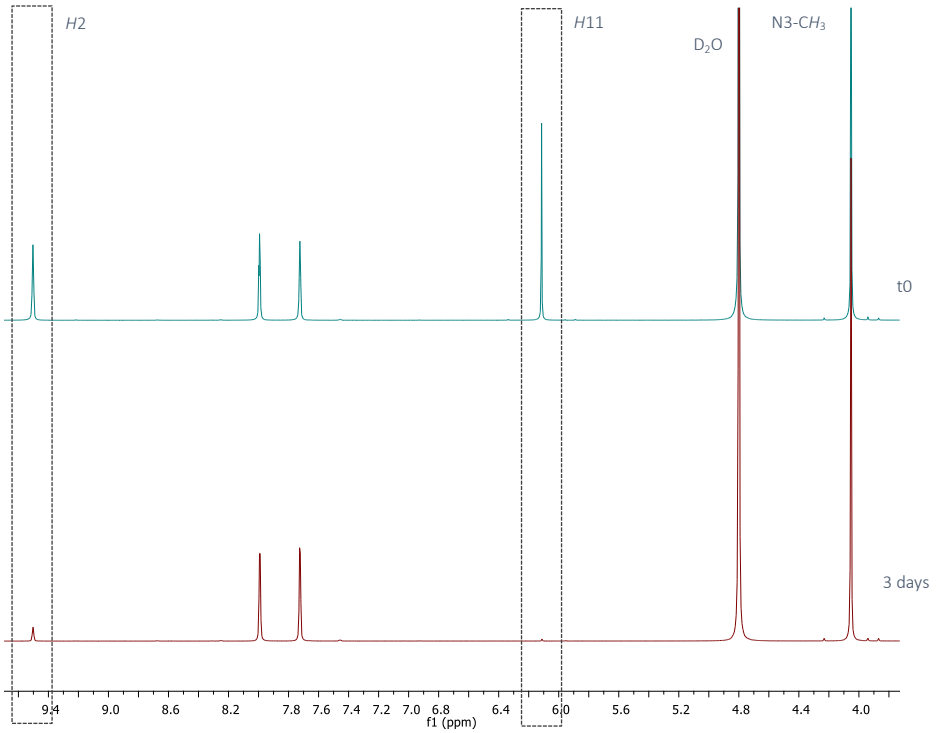

Figure 4.5 - *Deuteration of compound **1** at pH 7 - ^{1}H NMR spectra of the compound in D_2O at t0 (top) and after 3 days (bottom).*

At pH 7, after 4 hours, H11 was 33% deuterated and this percentage increased to 70% after 12 hours, reaching 89% after 24 hours. The H2 has a slower deuteration rate, with only 12% deuteration after 4 hours and 28% after 12 hours. After 24 hours, the deuteration of H2 reaches 48%. After 3 days H11 is almost completely deuterated (98%) and H2 also reached high levels of deuteration (85%).

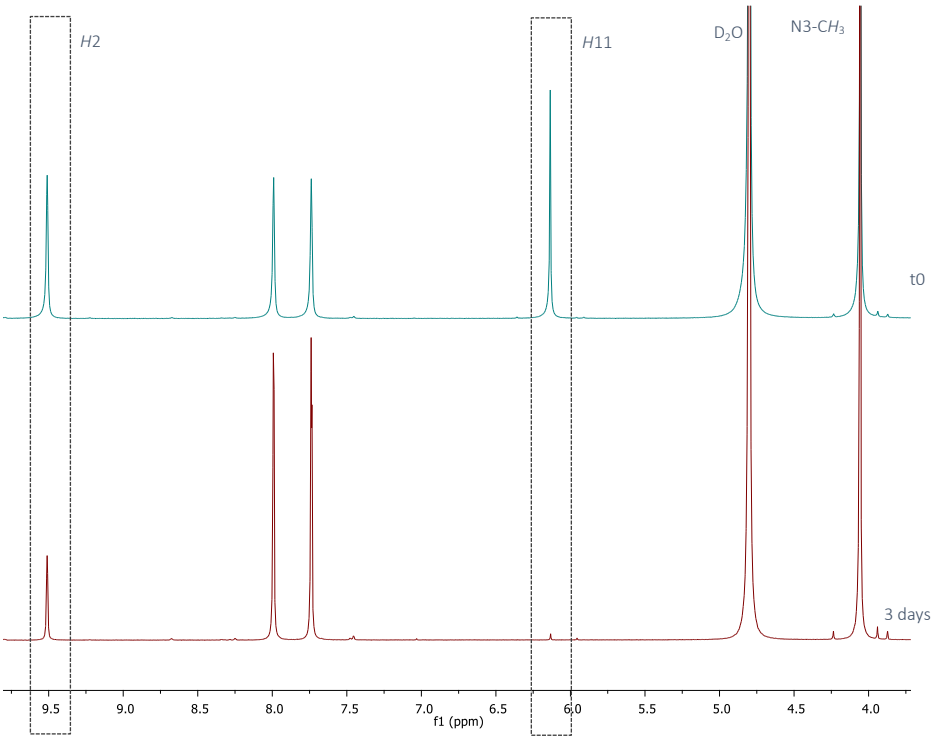

Figure 4.6 - *Deuteration of compound **1** at pH 2 - ^{1}H NMR spectra of the compound in DCl (1M in D_2O) at t0 (top) and after 3 days (bottom).*

At pH 2, H11 is the fastest proton to undergo deuteration, with a rate similar to that observed at pH 7 (39% after 4 hours, 72% after 12 hours and 90% after 24 hours). After 3 days, H11 was almost not visible in the NMR spectrum. H2 undergoes deuteration but much more slowly than H11 and also at a slower rate than at pH 7. After 12 hours, H2 is 23% deuterated, and after 24 hours, the deuteration increases to 33%, reaching 69% after 3 days.

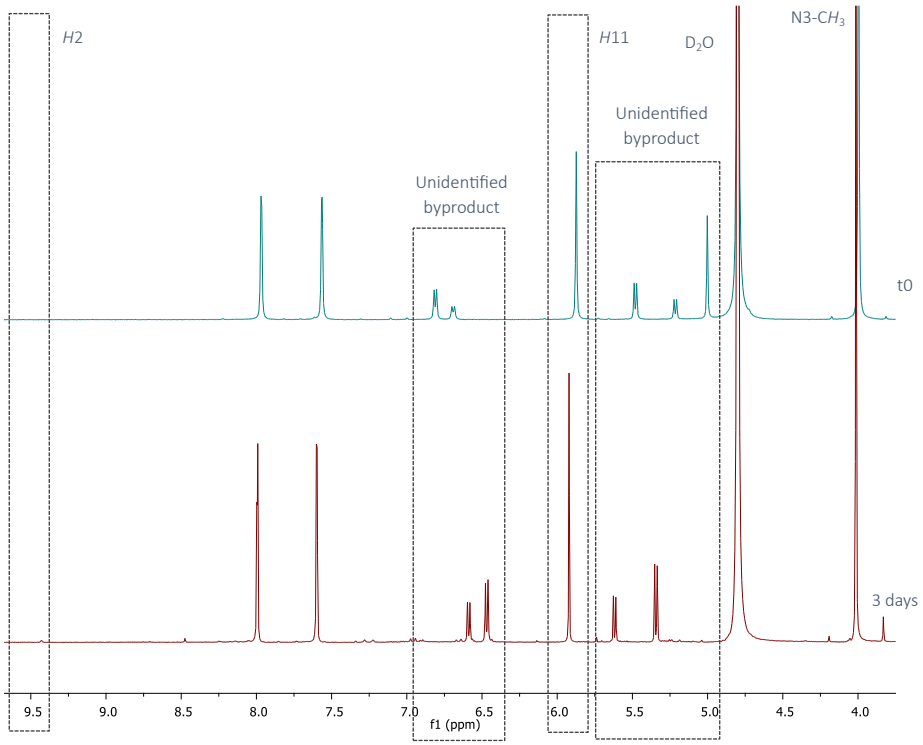

Figure 4.7 - *Deuteration of compound **1** at pH - ^{1}H NMR spectra of the compound in NaOD (1M in D_2O) at t0 (top) and after 3 days (bottom).*

Under basic conditions (pH 13) after the addition of the deuterated solvent, H2 is immediately deuterated, indicating that H2 is the most basic proton within the imidazole ring. The addition of the basic solvent also caused the formation of some unidentified byproducts already present at t0, which increased after 3 days.

No deuteration was observed for H4 or H5. Clearly, when comparing the acidity of H2 versus H5, the latter is less acidic. This agrees well with the behaviour described for imidazolium salts[194–196].

The different stability properties of compound **1** at pH 2 and pH 13 suggest different mechanisms of deuteration in acidic and basic media. A deuteration/deprotonation mechanism is probably involved under acidic conditions, following local charge densities within the aromatic rings. At high pH, a deprotonation/deuteration process is suggested by the different rates of deuteration, which reflect the acidity of the protons within the heterocycles.

Studies by Schmidt et al.[193] also showed that compound **1** can be converted to the corresponding betaine upon treatment with a base. The corresponding betaine is in tautomeric equilibrium with the ylide and its corresponding neutral carbene (Scheme 4.3). To confirm whether compound **1** could generate a "bottleable carbene", we proceeded with deprotonation of compound **1**. Thus, compound **1** was reacted with NaOAc in DMSO-d_6 to afford the corresponding betaine. The variation in the chemical shifts of the obtained betaine **1a** was in accordance with the published spectra[193].

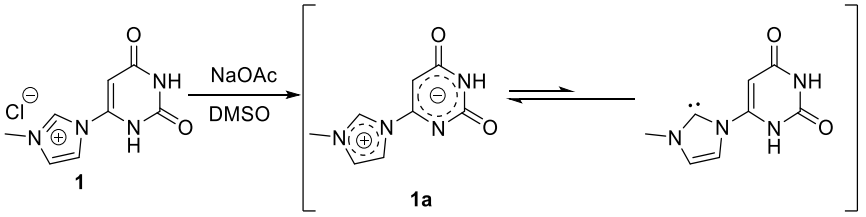

Scheme 4.3 - *Synthesis of the betaine **1a** from the imidazolium salt **1**.*

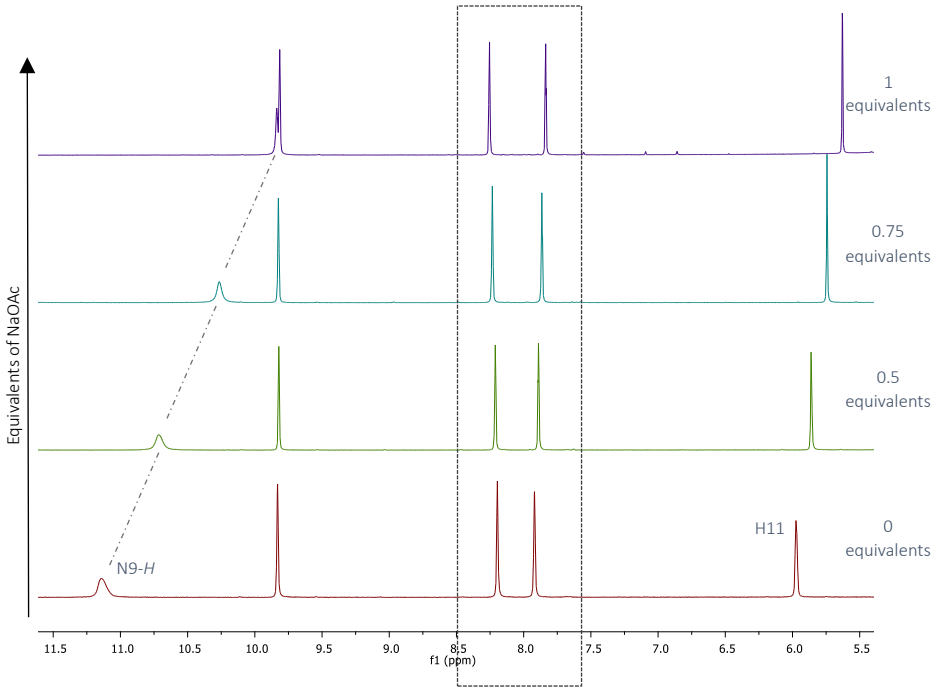

Figure 4.8 - *^{1}H NMR spectra of compound **1** with different equivalents of NaOAc.*

We observe that N9 does not undergo deprotonation, even after the addition of a large excess of NaOAc. When compound **1** is completely deprotonated at N7 the N9-*H* of the pyrimidine ring changes significantly, shifting 1.3 ppm upfield, with H11 shifting 0.3 ppm upfield. H4 and H5 resonate as triplets, coupling between them and with H2.

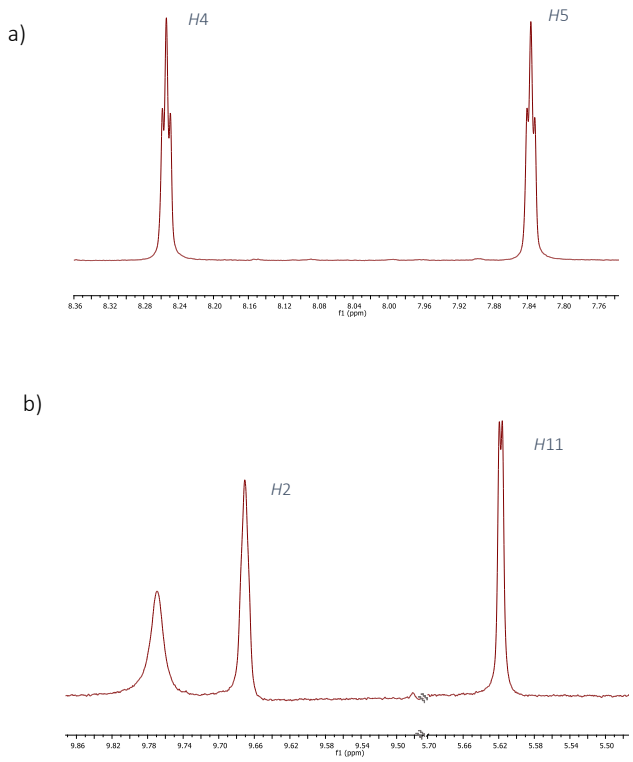

Figure 4.9 - *Section of the ^{1}H NMR spectrum of compound **1a:** a) protons H4 and H5; b) The protons H11 and H2.*

H2 appears as a broad singlet and according to the 2D COSY spectrum, H2 couples with H11, which resonates as a doublet (J_{HH}=1.32 Hz), showing additional J_{HH} couplings beyond 5 bonds. Schmidt et al. suggested that this occurs due a planar conformation assumed by the betaine **1a**, optimizing the overlap of its *p* orbitals between the positive and the negative portion of the molecule[193].

With these reactivity studies it can be inferred that in compound **1** the most acidic position is C2-H2 and that the compound can easily form the

corresponding betaine, providing access to the free carbene. Therefore, for compound **1**, it is possible perform reactions with metal precursors starting from the imidazolium salt **1** or from the betaine **1a**. Both possibilities were evaluated and are described in the next sections.

4.2.2. Reactivity of the ligand precursor with metals

Compound **1** was reacted with $[IrCp^*Cl_2]_2$ following the reaction conditions previously established[197]. Thus, compound **1** was suspended in methanol, along with $[IrCp^*Cl_2]_2$ in an inert atmosphere at 80°C for 16 hours. The mixture was then dried under vacuum and resuspended in a small amount of DCM. The solid was filtered through celite and rinsed with DCM to remove excess of the metal precursor. ^{1}H NMR analysis of the reaction crude revealed that the compound was bound to iridium via C5 instead of C2 (Scheme 4.4), thus the ligand is bound as an abnormal NHC. Abnormal carbenes are nonclassical N-heterocyclic carbenes characterized in which the carbene is located at C4 or C5 position of the imidazole ring rather than C2. The term abnormal refers to their mesoionic nature; in fact, for canonical NHCs, it is possible to write a neutral resonance structure when drawn in the free form; by contrast, for abnormal carbenes, it is not possible to draw a neutral resonance structure. Upon coordination to a metal, an abnormal carbene displays similar properties, but tends to exhibit a stronger sigma-donor character than canonical NHCs[198].

The formation of the abnormal carbene was evidenced due to the presence of H2 and the absence of H5. Additionally, H4 underwent an upfield shift of 1.85 ppm from 7.92 to 6.07 ppm, while H2 shifted downfield, from 9.83 ppm to 10.2 ppm. The signals of the pyrimidine ring remain essentially unchanged. $^{13}C\{^{1}H\}$ NMR revealed a signal at 130.6 ppm, corresponding to the metalated C5, a value consistent with that of other abnormal iridium carbenes described in the literature[199,200].

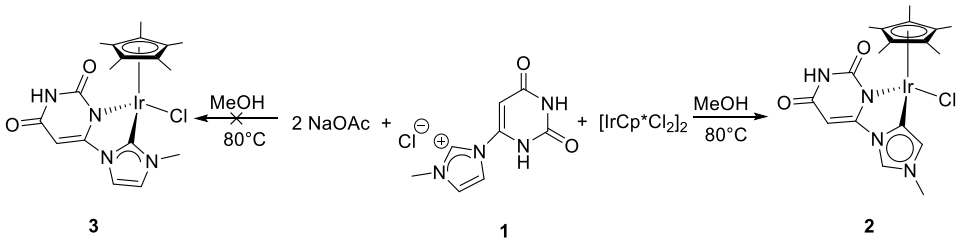

Scheme 4.4 - *Reaction of compound **1** with $[IrCp^*Cl_2]_2$ yielding the abnormal carbene.*

Earlier work from Choudhury's group on a similar system also led to the formation of an abnormal NHC[197]. The authors promoted the formation of an abnormal carbene by substitution of the imidazole ring with a methyl group at C2. This substitution forces, in principle, the formation of an abnormal carbene, via C5 (scheme 4.4). However, the methyl group at position C2 could also undergo metalation.

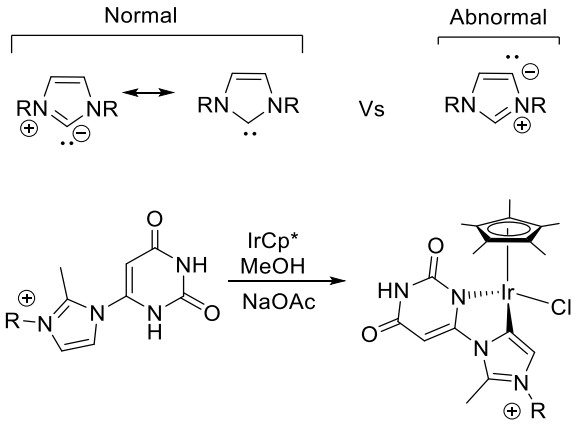

Scheme 4.5 - *Synthesis of the abnormal carbene reported by Choudhury and co-workers.*

This reactivity was already observed by Peris[201], Albrecht[196] and other groups[202,203], which showed how the C-H activation of an imidazole ring with methyl at C2 also be exocyclic and not occur at C5. When metalation occurs at C5, resulting from Csp^2-H activation, the reaction is endocyclic, while metalation of the exocyclic methyl group at C2 leads to Csp^3-H activation. The activation of C2-H or C5-H position depends on the conditions used, as exocyclic metalation occurs only when a base is used[204]. The conditions used by Choudry and coworkers involve the use of a base; nevertheless, metalation occurs only at C5. Comparing these results with the outcome of the reaction of **1** with iridium to form compound **2**, It could be suggested that Csp^2-H activation at position 5 is preferred in both cases.

As the ligand precursor was synthesized in its betainic form **1a**, which is in tautomeric equilibrium with the free normal carbene, **1a** was reacted with $[IrCp^*Cl_2]_2$ in methanol at 80°C. ^{1}H NMR analysis shows that the reaction yields again the abnormal carbene **2**. This suggests that the first step of the

cyclometallation is probably the formation of the N-Ir bond, followed by the C5-H activation, via cyclometallation.

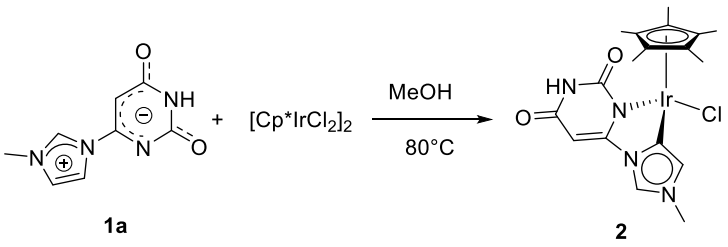

Scheme 4.4 - *Reaction of betaine with a pentamethylcyclopentadienyl iridium dichloride dimer.*

Our results indicate the preferential formation of the abnormal carbene, starting from either the imidazolium salt or the corresponding betaine. This observation seems to support that the formation of complex **2** is thermodynamically favoured in these reactions.

We then considered examining the behaviour of different metal precursors to determine the role of the metal centre. We started by examining ruthenium, employing $[Ru(p\text{-cymene})Cl_2]_2$. The reaction conditions employed were the same as those used for $[IrCp^*Cl_2]_2$ (Scheme 4.7).

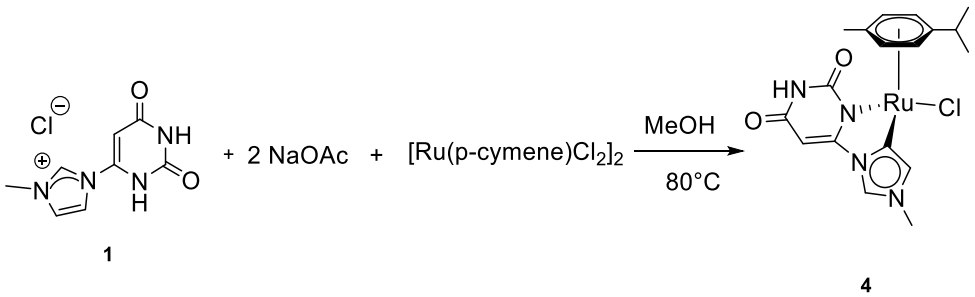

Scheme 4.5 - *Reaction of **1** with $[Ru(p\text{-cymene})Cl_2]_2$.*

The reaction afforded complex **4** in 53% yield. Complex **4** revealed to be unstable in DMSO or $CDCl_3$, thus MeOD was employed for NMR characterization, nevertheless the complex has a low solubility in methanol, thus **4** was characterized with a 800MHz NMR apparatus for faster and more sensitive characterization of the compound in DMSO-d_6. For compound **4**, ^{1}H NMR revealed a similar outcome to that of **2**, with H5 absent, while the H2 resonates at 9.52 ppm, confirming the formation of an abnormal carbene at C5. An upfield shift is noted for H2 when compared to **1**, which resonates at 9.62 ppm. H4 resonates at 7.44 ppm and all the other signals do not suffer significant shifts with respect to **1.** $^{13}C\{^1H\}$ NMR shows the carbenic C5 at 158.6 ppm, 28 ppm downfield in respect to the iridium abnormal carbene **2**.

The reaction of $[Ru(p\text{-cymene})Cl_2]_2$ with the betaine **1a** was also evaluated (Scheme 4.8). ^{1}H NMR analysis of the reaction revealed that, in this case, the reaction leads to the formation of a mixture of normal and abnormal carbenes, with the normal carbene being the major product at a 5:2 ratio. Indeed, three sets of signals were present: normal carbene, abnormal carbene and unreacted starting material.

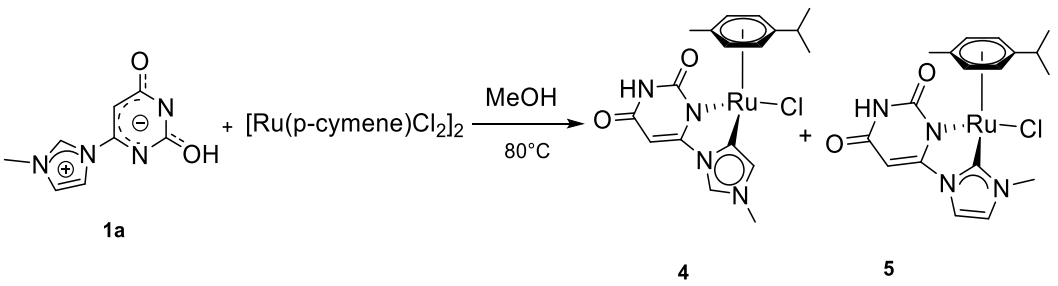

Scheme 4.6 - *Reaction of the betaine **1a** with $[Ru(p\text{-cymene})Cl_2]_2$ yields complexes **4** and **5**.*

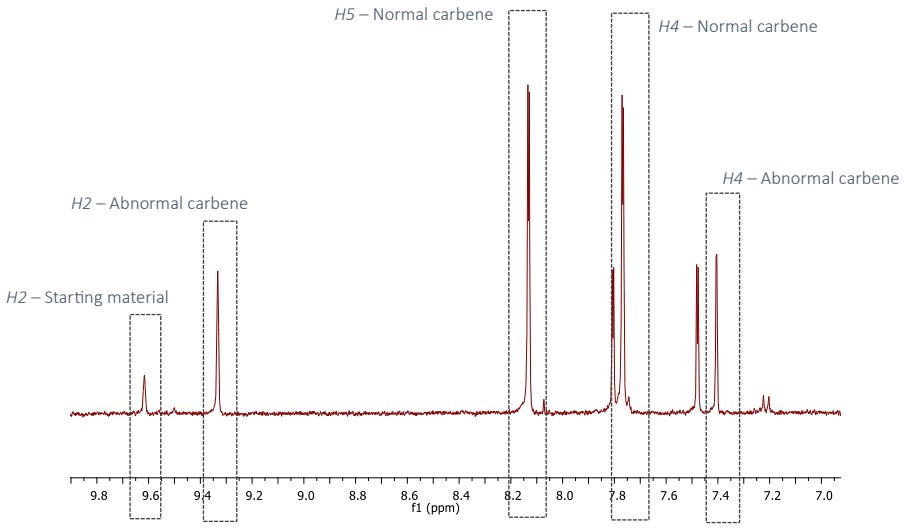

Figure 4.10 - *Section of the ^{1}H NMR of the reaction of the betaine **1a** with $[Ru(p\text{-cymene})Cl_2]_2$.*

For the normal carbene complex **5**, the ^{1}H NMR characterization was conducted in MeOD, in which H4 and H5 resonate as doublets at 8.13 and 7.77 ppm, respectively. The signal at 7.44 ppm corresponds to H4 of the abnormal carbene complex **4**, which also maintains the H2 signal at 9.52 ppm as was noticed for the reaction in Scheme 4.7. The unreacted starting material **1a** has the H2 signal partially deuterated, and this is also reflected in H4 and H5, which resonate as doublets at 7.80 and 7.48 ppm, respectively. Complex **5** was also characterized by $^{13}C\{^{1}H\}$ NMR, in which the carbenic carbon resonance was 186.6 ppm, slightly downfield in respect to complex **4** (158.6 ppm showed in Scheme 4.7).

Clearly, for iridium, metalation at C5 is preferred even when starting from the betaine **1a.** For ruthenium, while in the presence of a base the abnormal carbene is formed preferentially, when starting from the betaine both normal

(complex **5**) and abnormal (complex **4**) carbenes are formed with the former being the major species.

To better understand the role of the cyclometallation in the previous reactions, we evaluated the reactivity of **1a** with gold(I). $Au(SMe_2)Cl$ was chosen due to the facile generation of a vacant site upon loss of the disulfide ligand. When $Au(SMe_2)Cl$ reacts with betaine **1a** (Scheme 4.9), a normal NHC gold complex is formed exclusively. The formation of the normal carbene was confirmed by ^{1}H NMR (Figure 4.11). The signal at 11.97 ppm corresponds to N9-*H*, while the two signals at 7.78 and 7.62 ppm correspond to H5 and H4, respectively (Figure 4.11).

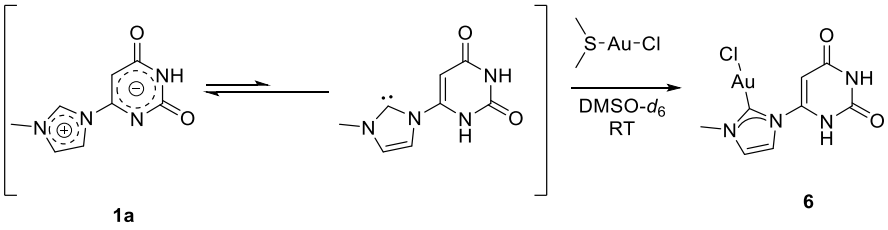

Scheme 4.7 - *Reaction of the betaine **1a** with $Au(SMe_2)Cl$ to yield compound **6**.*

The remaining signals are the pyrimidine ring proton H11 at 5.99 ppm and the methyl group of the imidazole ring at 3.83 ppm. The N7-*H* can be seen at 11.57 ppm as a very broad peak. The $^{13}C\{^{1}H\}$ NMR spectrum shows the carbenic carbon at 168.6 ppm.

The formation of a normal carbene exclusively with gold(I) where cyclometallation does not take place, suggests that cyclometallation does impact the formation of normal and abnormal NHCs with iridium and ruthenium.

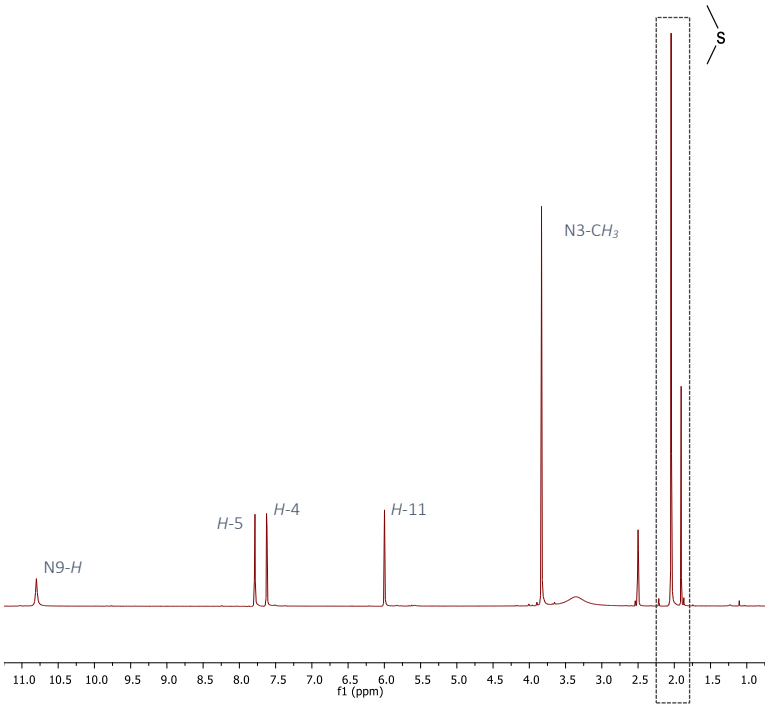

Figure 4.11 - *^{1}H NMR of compound **6**.*

Considering that silver(I) also forms linear compounds that are widely used for transmetalation reactions, we set out to form a normal carbene for iridium and ruthenium via transmetallation. In this case, compound **1** was reacted with silver oxide, and subsequently reacted with iridium or ruthenium. The ligand precursor **1** was therefore reacted with Ag_2O in DCM at room temperature for 24 hours in the absence of light. After this time, $[IrCp^*Cl_2]_2$ or $[Ru(p\text{-cymene})Cl_2]_2$ was added (Schemes 4.10 and 4.11). The reactions were stirred for another 24 hours. After this time and appropriate work-up, ^{1}H NMR analysis showed that the reaction leads to a mixture containing the cyclometalated normal carbenes **3** and **5** in 60% and 28% yield respectively.

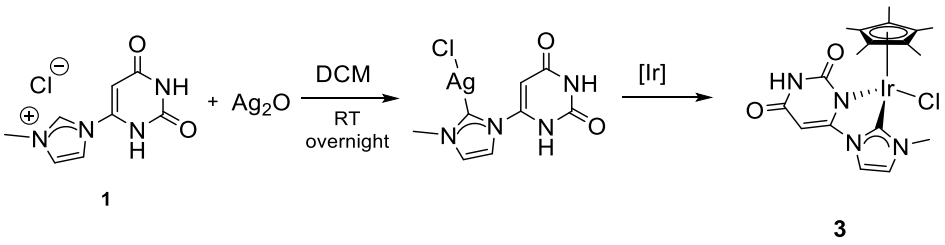

Scheme 4.8 – *Reaction of **1** with Ag_2O and $[IrCp^*Cl_2]_2$.*

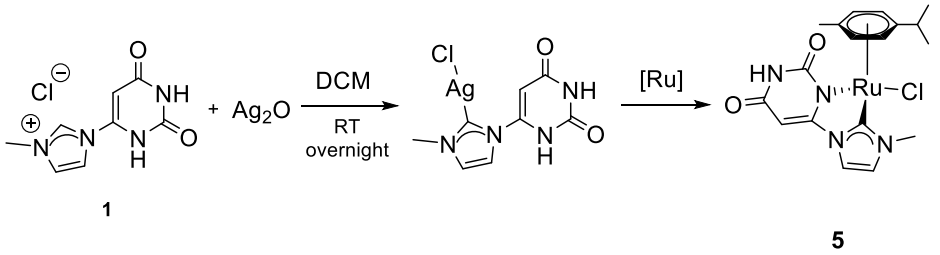

Scheme 4.9 - *Reaction of **1** with Ag_2O and $[Ru(p\text{-}cym)Cl_2]_2$.*

After purification by column chromatography, the compounds were fully characterized by NMR. For the iridium complex, ^{1}H NMR revealed the disappearance of the proton at C2 and the two doublets of the protons at C5 and C4 at 8.34 and 7.83 ppm, respectively (^3J= 2.22 Hz). The protons of the pyrimidine ring resonate at 10.85 ppm for the N*H* at position 9 and at 6.11 ppm for the proton at C11. The $^{13}C\{^1H\}$ NMR spectrum showed the carbenic carbon at 154.1 ppm, a shift to lower fields with respect to the abnormal carbene, which resonates at 130.6 ppm ($\Delta\delta$= 23.5ppm), in accordance with the values described in the literature[205]. In addition, coupling between the methyl groups of Cp* and the carbenic carbon was observed via HMBC spectroscopy. The ^{1}H NMR of the ruthenium complex agree with the values already described for complex **5** (Scheme 4.8).

4.2.3. Variation of the wingtip of the imidazole

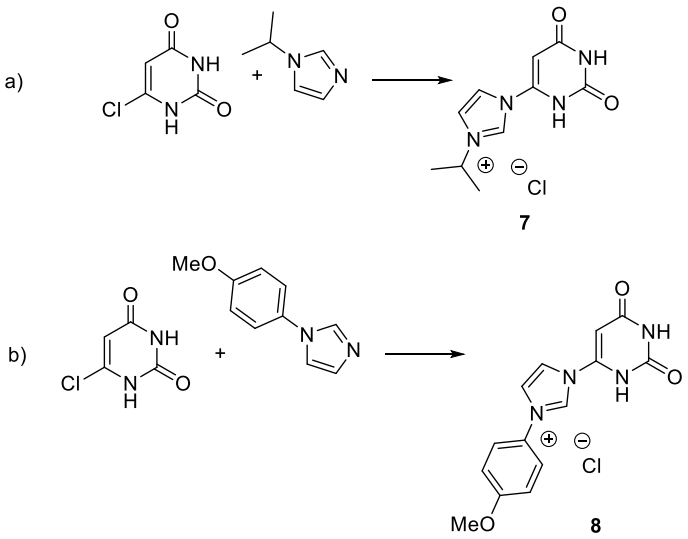

Scheme 4.10 - *Synthesis of ligand precursors with different side chains on the imidazole ring (a-isopropyl; b-anisole).*

The reactivity of the ligand precursor was also studied with different wingtips at the imidazole ring. 6-chloro uracil was reacted with an imidazole ring substituted with an isopropyl or an anisole at N1. Thus, the imidazole derivatives and 6-chloro uracil were suspended in chlorobenzene and the reaction was refluxed at 135°C for 7 hours (Scheme 4.12). Analysis of the ^{1}H NMR showed that H2 resonates at 9.81 ppm for compound **7**, similar to the value found for compound **1** (9.83 ppm). H5 and H4 of complex **7** resonate at 8.25 and 8.10 ppm, respectively. The three signals resonate as triplets with a coupling constant of 1.85 Hz. The chemical shifts for the protons of the pyrimidine ring are similar to those found for compound **1**. In the $^{13}C\{^{1}H\}$ NMR spectrum, C2 resonates at 134.8 ppm, while C4 and C5 resonate at 121.3 and 120.3 ppm, respectively.

For compound **8**, H2 resonates at 10.22 ppm compared to 9.83 ppm for the methyl derivative **1** and 9.81 ppm for the isopropyl derivative **7**. For H5 and H4 the signals are very close to one another and resonate at lower fields with respect to **1** (8.43 and 8.40 ppm). Due to the proximity of the two signals, the two triplets appear distorted, but it is still possible to calculate a coupling constant of 1.86 Hz. The signals of the pyrimidine ring remain essentially unchanged with respect to compounds **1** and **7**. The $^{13}C\{^{1}H\}$ NMR shows that C2, C4 and C5 resonated at 134.3, 122.0 and 120.4 ppm, respectively.

Compounds **7** and **8** were reacted with the iridium and ruthenium precursors. Compound **7** and $[IrCp^*Cl_2]_2$ were suspended in methanol and refluxed at 80°C overnight.

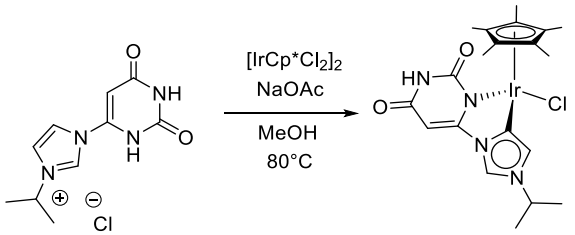

7 **9**

Scheme 4.11 - *Reaction of compound **7** with $[IrCp^*Cl_2]_2$.*

^{1}H NMR indicates that the reaction afforded, again, the corresponding abnormal carbene **9** in 58% yield, where H2 resonates at 9.96 ppm, a slight downfield shift of 0.15 ppm with respect to **7** (9.81 ppm). H4 underwent a shift of 0.63 ppm, from 8.10 ppm in **7** to 7.47 ppm in **9**. The signals for both H2 and H4 resonate as doublets with a coupling constant of 1.12 Hz. The proton H11 of the pyrimidine ring and the isopropyl substituent do not suffer

significant changes upon metalation. The $^{13}C\{^{1}H\}$ NMR spectrum showed the carbenic carbon at 130.9 ppm, in line with the previous value found for iridium abnormal carbene **2**.

Compound **7** was also reacted with ruthenium, following the conditions employed for the methyl derivative (Scheme 4.14).

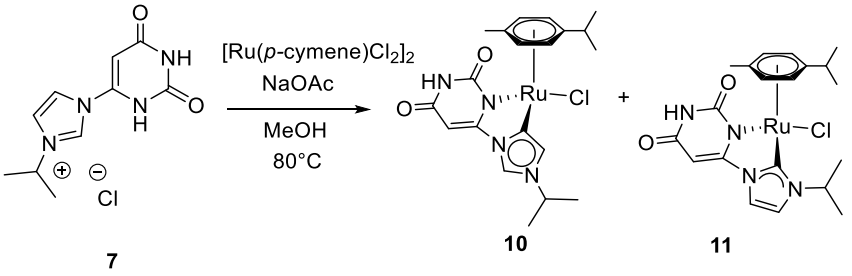

7 **10** **11**

Scheme 4.12 - *Reaction of compound **7** with $[Ru(p\text{-cymene})Cl_2]_2$.*

In this case, the reaction led to a mixture of abnormal and normal carbenes, with compound **10** representing the major the product (61% of the final mixture). Compound **11** is present in only 27% of the mixture, and there is still some unreacted starting material (12%).

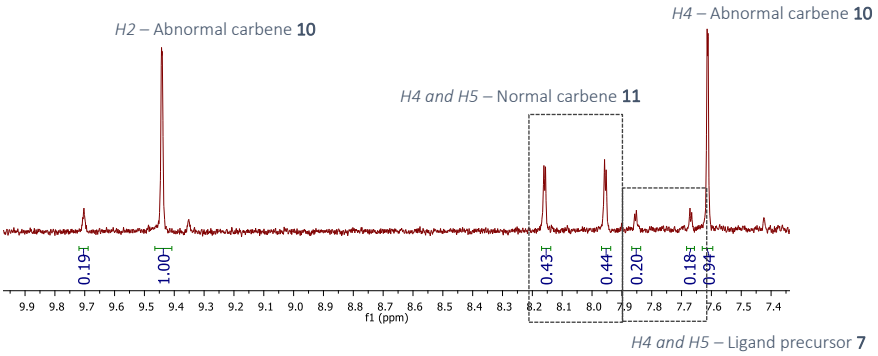

Figure 4.12 - *^{1}H NMR spectrum of reaction of compound **7** with $[Ru(p\text{-cymene})Cl_2]_2$.*

The mixture was purified by column chromatography allowing for the separation and characterization of the complexes **10** and **11**.

Complex **10** revealed to be unstable in DMSO or $CDCl_3$, thus **10** was characterized with a 800 MHz NMR apparatus for faster and more sensitive characterization of the compound in DMSO-d_6. ^{1}H NMR shows the absence of H5, while H2 and H4 resonate at 9.56 and 7.66 ppm respectively. In this case the resolution of the spectra did not allow to calculate the coupling constant between the two protons which appear as broad singlets. $^{13}C\{^1H\}$ NMR shows the carbenic C5 at 159.0 ppm, in accordance with the shift observed for complex **4**. For compound **11** the two imidazole ring protons (H4 and H5) resonate as doublets at 7.65 and at 7.85 ppm respectively, coupling with each other with $^3J_{HH}$ of 2.28 Hz, shifting slightly upfield compared to the corresponding signals in the ligand precursor (8.10 and 8.25 ppm for H4 and H5 respectively). The other protons of the pyrimidine ring did not suffer significative shifts. In the $^{13}C\{^1H\}$ NMR the carbenic carbon of compound **11** resonates at 183.8 ppm.

Following this, the anisole derivative **8** was also examined. Thus, compound **8** was reacted with $[IrCp^*Cl_2]_2$ in methanol at 80°C in the presence of 2 equivalents of NaOAc (Scheme 4.15). After purification by column chromatography, analysis by ^{1}H NMR of the final product allowed for the identification of the abnormal carbene in 18% yield.

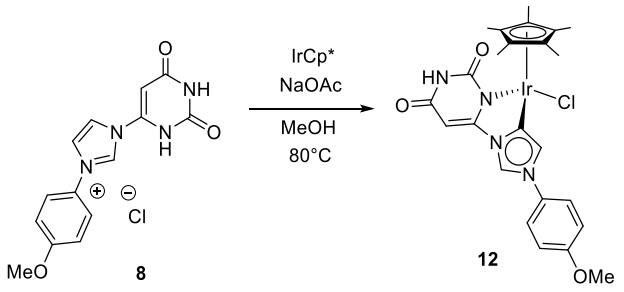

Scheme 4.13 - *Reaction of compound **8** with $[IrCp^*Cl_2]_2$.*

^{1}H NMR showed that H2 was still present in the final product, resonating at 10.33 ppm as a doublet (J_{HH}=1.2 Hz). H4 signal undergoes an upfield shift of 0.64 ppm, from 8.40 to 7.76 ppm, upon metalation. Both signals undergo a slight lowfield shift with respect to **9** (10.07 and 7.48 ppm for H2 and H4, respectively) and **2** (10.19 and 7.30 ppm for H2 and H4, respectively). The other signals did not show significant shifts. According to the ^{13}C{^{1}H} NMR, the carbenic C5 resonates at 131.4 ppm, consistent with the previous values of complexes **9** and **2**, which resonate at 130.9 and 130.6 ppm, respectively.

Compound **8** was also reacted with $[Ru(p\text{-cymene})Cl_2]_2$ in methanol at 80°C with 2 equivalents of NaOAc overnight, also in this case the reaction afforded the abnormal carbene (21% yield, Scheme 4.16).

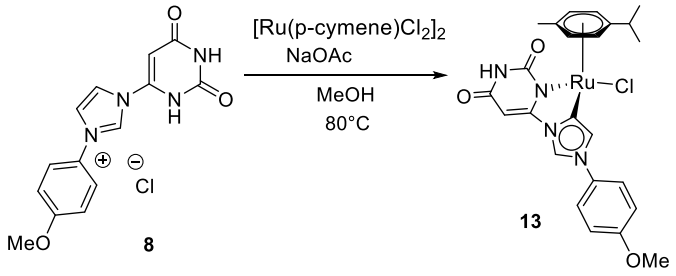

Scheme 4.14 - *Reaction of compound **8** with $[Ru(p\text{-cymene})Cl_2]_2$.*

The formation of **13** was confirmed by ^{1}H NMR, which shows the signal of H2 at 10.05 ppm, a doublet coupled with H4 (8.05 ppm), with a J_{HH} of 1.12Hz. In the $^{13}C\{^{1}H\}$ NMR spectrum the carbenic C5 resonates at 159.8 ppm.

Following our previous observations regarding the formation the formation of normal NHCs via transmetalation, we explored the reactivity of **7** and **8** under similar conditions. Thus, the isopropyl derivative **7** was suspended in DCM with Ag_2O and stirred at room temperature for 24 hours. Subsequently, $[Ir(Cp^*)_2Cl_2]$ or $[Ru(p\text{-cymene})_2Cl_2]$ were added (Scheme 4.17). Using this approach the corresponding normal carbenes **11** and **14** were obtained in 28% and 34% yield respectively, after purification by cromatography.

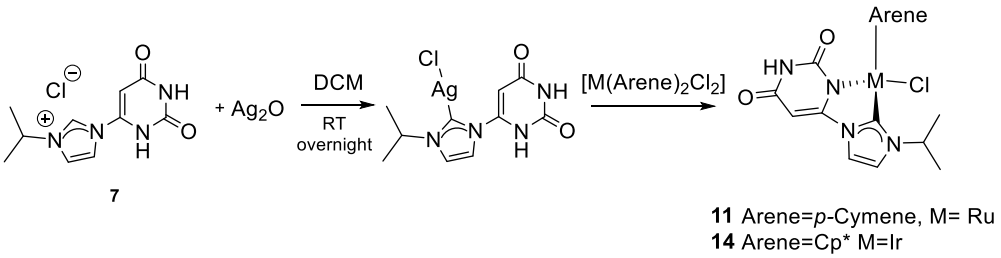

Scheme 4.15 - Formation of compounds **11** and **14** by *transmetallation.*

The complexes were fully characterized and in the case of the ruthenium complex (**11**), NMR was recorded in MeOD due to the instability of the *p*-cymene ligand in other solvents, such as DMSO or $CDCl_3$. The two imidazole ring protons resonate at 7.85 ppm and 7.65 ppm for H5 and H4, respectively in complex **11** as was already noted above. According to the $^{13}C\{^{1}H\}$ NMR spectrum, the carbenic carbon resonates at 183.8 ppm when bound to ruthenium. As for the Iridium complex (complex **14**) the two imidazole

protons H4 and H5 resonate as doublets at 8.17 and 8.47 ppm respectively with a coupling constant of 6.5 Hz. The other signals in the ^{1}H NMR did not show any relevant shift. In the $^{13}C\{^{1}H\}$ NMR spectrum the carbenic carbon resonates at 152.9 ppm, a value similar to that observed for complex **3** (154.1 ppm).

Compound **8,** was reacted under the same conditions, leading to the corresponding compounds **15** and **16** (Scheme 4.18) in 24% and 18% yield respectively.

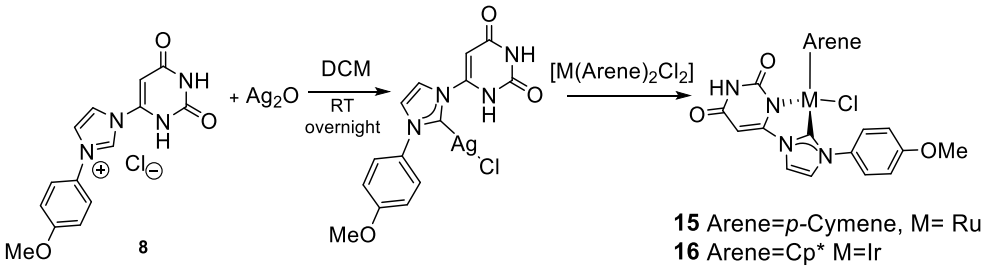

Scheme 4.16 - Formation of compounds **15** and **16** by *transmetallation.*

Analysis of the products, after column chromatography confirm the formation of the normal carbene exclusively for both metals. As for complex **15** complete NMR characterization was afforded in DMSO-d_6 at 800MHz. In the ^{1}H NMR H4 and H5 resonate at 8.23 and 7.89 ppm respectively (J_{HH}= 2 Hz). While $^{13}C\{^{1}H\}$ NMR shows the carbenic carbon at 184.2 ppm, in line with the others ruthenium normal carbenes **5** and **11** (186.6 and 183.8 ppm respectively). On the other hand, complex **16** was unstable in both $CDCl_3$ and DMSO-d_6, and not sufficiently soluble in MeOD, thus it was not possible for us to have a complete characterization of the complexes. Nevertheless a 1H NMR was recorded, showing no trace of H2 and the resonance of H4 at 8.29

as a doublet (J_{HH}= 2.5 Hz), H5 is probably resonating under the signal of the aromatic anisole protons. In addition to the 1H NMR analysis, complex **16**, was also analysed by elemental analysis, which confirm the purity of the compound (Anal. Calcd for C24H26ClIrN4O3: C, 44.61; H, 4.06; N, 8.67. Found: C, 44.70; H, 3.74; N, 8.89).

4.2.4. Solid-state Structures

Crystals of complexes of **3**, **4** and **5** suitable for single-crystal X-ray diffraction, were obtained by slow evaporation of their corresponding MeOH solutions, allowing unambiguous determination of their molecular structure. Figures 1, 2 and 3 depict their ORTEP diagrams, with the most relevant bond distances (Å) and angles (°) reported in Table 4.1. The molecular structures of complexes **4** and **5** are, as expected very similar, presenting a Ru(II) centre bonded to a chloride ligand, a *p*-cymene (*p*-cym) group and a cyclometalated ligand with the imidazole ring bound via C2 or C5. Complex **3** also has a similar structure to that of complexes **4** and **5**. The geometry around the metal centre can be described as piano stool for all three complexes.

In complex **3,** the bond distances C1-Ir1 and N3-Ir1 are 2.005 Å and 2.106 Å, respectively, while the distance between the iridium and the Cp* ring centroid is 1.819 Å. The bite angle of the chelate five-member ring (C1-Ir1-N3) is 75.36°, while the centroid has an angle of 133.98° with C1 and of 129.52° with N3. The dihedral angle between the centroid plane and the chelate plane is 131.01°.

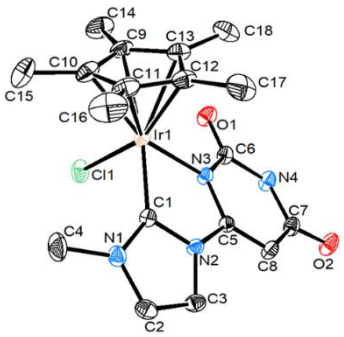

Figure 4.13 - *ORTEP representation of complex **3**, using 30% level ellipsoids. Hydrogen atoms are omitted for clarity.*

In complexes **4** and **5,** the bond distances between C1-Ru1 and N3-Ru1 are similar, being 2.025 Å and 2.107 Å, respectively, for compound **4** and 2.024 Å and 2.1201 Å, respectively, for compound **5**. Thus, the connectivity via C2 or C5 does not seem to influence the bond distances; this difference in connectivity seems to be more reflected in the distance between Ru1 and the Cymene centroid, which is 1.688 Å for the abnormal carbene (complex **4**) and slightly longer in the normal carbene (complex **5**): 1.715 Å. The bite angle in the chelate ring (C1-Ru1-N3) is similar for both complexes, being 76.68° and 75.68° for complexes **4** and **5,** respectively. The dihedral angle between the chelate plane and the cymene plane is 69.60° for the abnormal carbene complex **4** and is slightly smaller for the normal carbene complex **5** (55.77°). The relevant bond distances and angles are shown in Table 4.1.

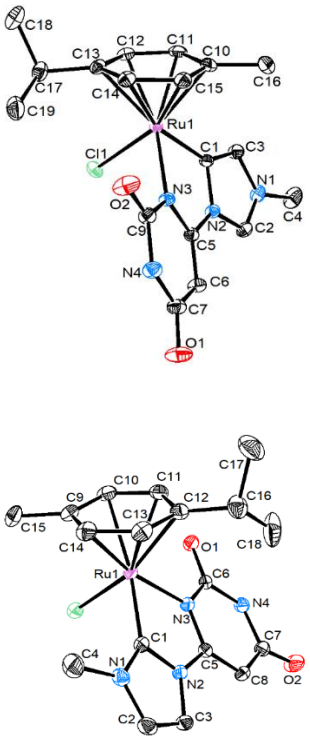

Figure 4.14 - *ORTEP representation of complex **4** (top) and **5** (bbottom), using 30% level ellipsoids. Hydrogen atoms are omitted for clarity.*

Table 4.1 - *Selected bond distances (Å) and angles (°) for complexes **3**, **4** and **5**.*

	3	**4**	**5**
Bond distances			
M1–C1	2.005(3)	2.025(4)	2.024(2)
M1–N3	2.106(3)	2.107(4)	2.1201(2)
M1–Cl1	2.4098(9)	2.4282(12)	2.4337(6)
M1–C9	2.229(4)	2.228(5)	2.179(2)

M1–C10	2.173(4)	2.242(5)	2.178(2)
M1–C11	2.167(4)	2.242(5)	2.180(2)
M1–C12	2.132(4)	2.227(5)	2.269(2)
M1–C13	2.240(4)	2.177(5)	2.253(2)
M1–C14		2.216(5)	2.158(2)
Bond angles			
C1–M1–N3	96.4(4)	76.68(8)	75.68
N3–Ir1–E1[a]	129.52		
N3–Ru1–E2[b]		132.13	120.46
C1–Ir1–E1[a]	133.98		
C1–Ru1–E2[b]		132.36	131.04
ω [c]	131.01	62.60	55.77

*M corresponds to Ir (**3**) or Ru (**4** and **5**). [a] E1 corresponds to the centroid of Cp*; [b] E2 corresponds to the centroid of the p-Cymene; [c] dihedral angle between the chelate planes and the arene plane.*

4.2.5. Catalytic activity of the complexes on the reduction of NAD^+

The ability of the synthetized cyclometalated complexes to catalyze hydrogen transfer reactions was studied by evaluating the reduction of NAD^+ to NADH. The purpose of this study was to obtain preliminary data on the possibility of carrying out the abovementioned catalysis within the cellular

environment. This would lead to a redox imbalance and eventually to cell death. Healthy cells are able to compensate for the redox imbalance, while cancer cells, which are already dealing with intense redox activity, stressed to accommodate such imbalance[185].

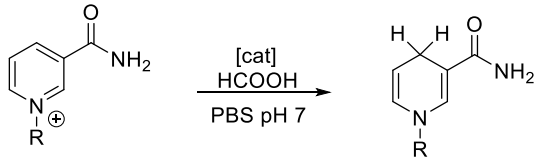

Scheme 4.17 - *Catalytic reduction of NAD^+ to NADH by transfer hydrogenation.*

The catalytic tests were conducted in a UV microplate spectrophotometer, which enables monitoring the formation of NADH, by reading the correspondent absorbance at 340 nm, as reported in the literature[186,187].

For all the experiments, the absorbance at 340 nm was recorded at regular time points (varying according to the quantity of the samples), reflecting the concentration of NADH. As a result, a curve of the concentration of NADH vs time is produced. The interpolation of the curve allows to calculate the slope of the linear range of the curve, which is directly proportional to the rate of the reaction.

In a first stage, only the complexes based on ligand precursor 1 were tested (Fig 4.16).

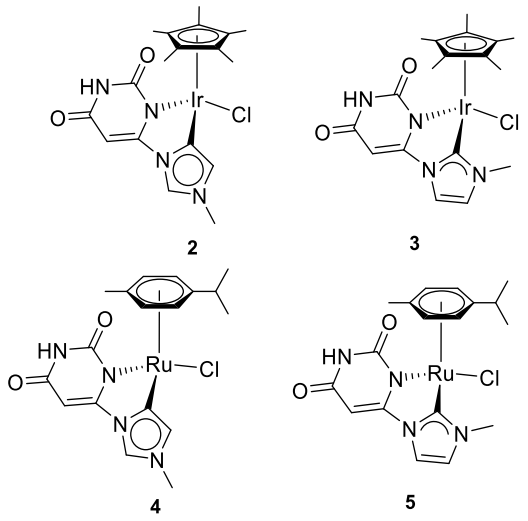

Figure 4.15 - *Cyclometalated complexes used for the reduction of NAD^+.*

A first experiment was done by changing the catalyst concentration; thus, the catalyst loading was tested between 0.5 and 10%. The reactions were conducted at pH 7 using formic acid as a proton donor under the following conditions: 1 mM NAD, 5 mM formic acid and phosphate buffer, to mantain the desired pH, following a procedure described in the literature[187]. A control experiment with no catalyst or without NAD^+ was also performed to ensure that a variation in the absorbance was not due to the medium. Similarly, in the absence of a catalyst the NADH absorbance did not increase, indicating that no transfer hydrogenation occurred. In the absence of NAD^+ an increase of the absorbance was not observed.

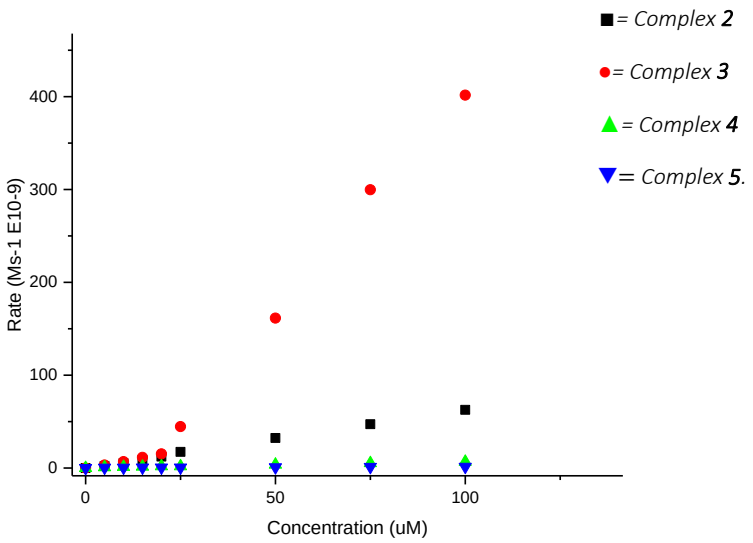

Graphic 4.1 - *Variation of the rate of the reaction of reduction of NAD^+ to NADH with the catalyst loading*

According to Graphic 4.1, Complex **3** was the fastest at any of the catalysts loadings tested, and complex **2** shows some activity, albeit lower than **3**. The results of the present study highlighted the very low activity of the ruthenium catalysts **4** and **5**, which could be due to the saturation of the catalyst or to its inability to catalyse this kind of reduction. Furthermore, ruthenium catalysts have proven to be unstable in some NMR solvents, such as chloroform and DMSO. In DMSO, ruthenium compounds can lose the p-cymene group, and this instability could be linked to the lack of catalytic activity[206].

Further catalytic tests were performed. Next, we investigated the impact of the variations in NAD concentration. To prevent an excessively high NAD-to-catalyst for very low NAD concentrations, the experiment was performed

using a catalyst concentration of 5 µm, while NAD concentrations ranged from 0.001 mM to 5 mM.

With respect to the iridium catalysts **2** and **3**, at the lowest NAD concentrations (up to 0.01 mm), determining the slope of the curve in the graph of concentration of the NADH vs time proved challenging. This could be due to the time required for the addition of the catalyst to each well, as this amount of time might be sufficient for complete depletion of the substrate. Second, the instrument might struggle to detect minor absorbance changes for these low NAD^+ concentrations, especially when compared to significant absorbance fluctuations in other wells. Concentrations of NAD^+ ranging from 0.025 mM to 0.75 mM allowed for the calculation of the rate within a narrow time frame (different for every NAD concentration). Beyond this time range, complete substrate consumption likely occurred, preventing any further increase in absorbance relative to NADH formation. On the other hand, ruthenium catalysts **4** and **5** showed no significant activity at any of the tested NAD concentrations, confirming the results of previous experiments. Considering all of these factors, the catalytic profile was obtained for each complex.

Inspecting Graphic 4.2, it is evident that high concentrations of NAD^+ inhibit the catalytic activity. This decrease in activity could be attributed to catalyst saturation. For example, a stable complex could be formed between the catalyst and either the starting material or the final product; examples of this phenomenon have been described in the literature for iridium catalysts[186].

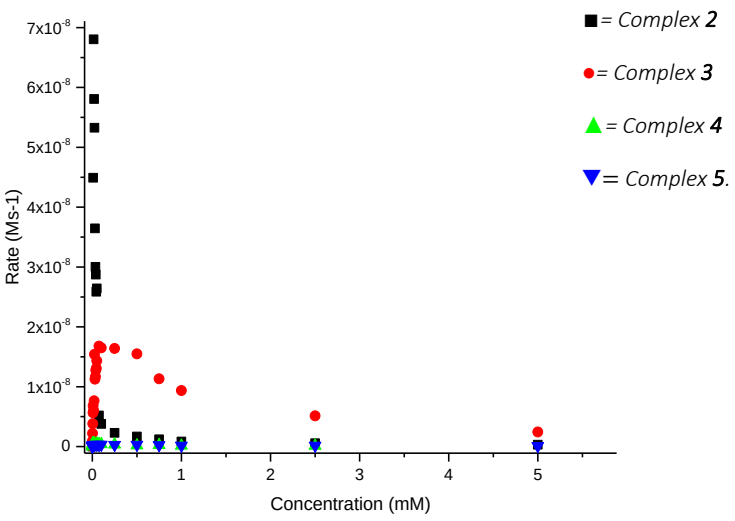

Graphic 4.2 – *Variation of the rate of reduction of NAD^+ to NADH with the substrate concentration (NAD^+).*

A focus on the measurements for the lowest concentrations of NAD^+ (highest catalyst loading), depicted in Graphic 4.3 showed a narrow window of activity for complex **2** compared to that of complex **3**. In addition, the focus on the lowest NAD^+ concentrations allowed us to observe an initial increase in the activity for lower NAD^+ concentrations (especially for complex **3**). This phenomenon has already been reported in the literature by Macchioni and coworkers[186]. Complexes **4** and **5** showed only residual catalytic activity, indicating that the iridium catalysts outperformed the ruthenium catalysts.

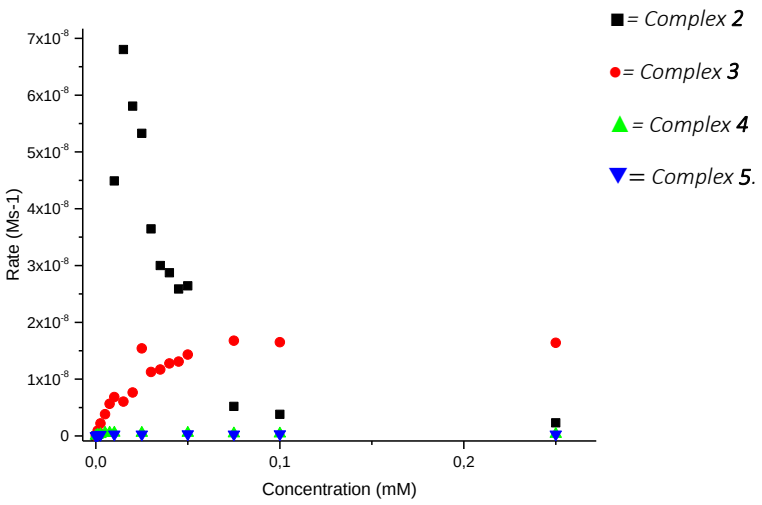

Graphic 4.3 – *Variation of the rate of reduction of NAD^+ to NADH with the substrate concentration (NAD^+) – concentrations between 0 and 0.25 mM.*

As for the iridium complexes, the analysis of one compound per time allows some considerations. Compound **2** showed the best catalytic performance at a concentration of 0.015 mM with a rate of $6.8x10^{-8}$ MxS^{-1}. This corresponds to a very high catalyst loading (33.33%), which leads to a TON of 0.3 and a TOF of 41.5 h^{-1}. In addition, complex **2** has a very narrow window of catalytic activity, as it reaches nearly zero with a catalyst loading under 10% (NAD^+ concentration higher than 0.05 mM).

Compound **3** reached a maximum rate of $1.6x10^{-8}$ MxS^{-1}, for a wide range of concentrations of NAD^+ (0.075 to 0.25 mM). At higher NAD+ concentrations, the catalyst still maintained acceptable catalytic activity, decreasing until a concentration of 0.75 mM of NAD^+ (0.6% catalyst loading) was reached. The TON and TOF were calculated for three different catalyst

loadings at which the catalyst has a significant catalytic activity: 6.6%, 5% and 2%.

Table 4.2 – *TON and TOF for different catalyst loading of complexes **2** and **3**.*

Catalyst	Catalyst loading	NAD+ concentration	TON	TOF
2	33.33%	0.015 mM	0.3	41.5 h^{-1}
3	6.6%	0.075 mM	1.5	23.1 h^{-1}
3	5%	0.1 mM	2	22.2 h^{-1}
3	2%	0.25 mM	5	6.4 h^{-1}

For comparative purposes, cyclometalated complexes synthesized with different imidazole derivatives were also tested for their ability to catalyse the reduction of NAD^+ to NADH.

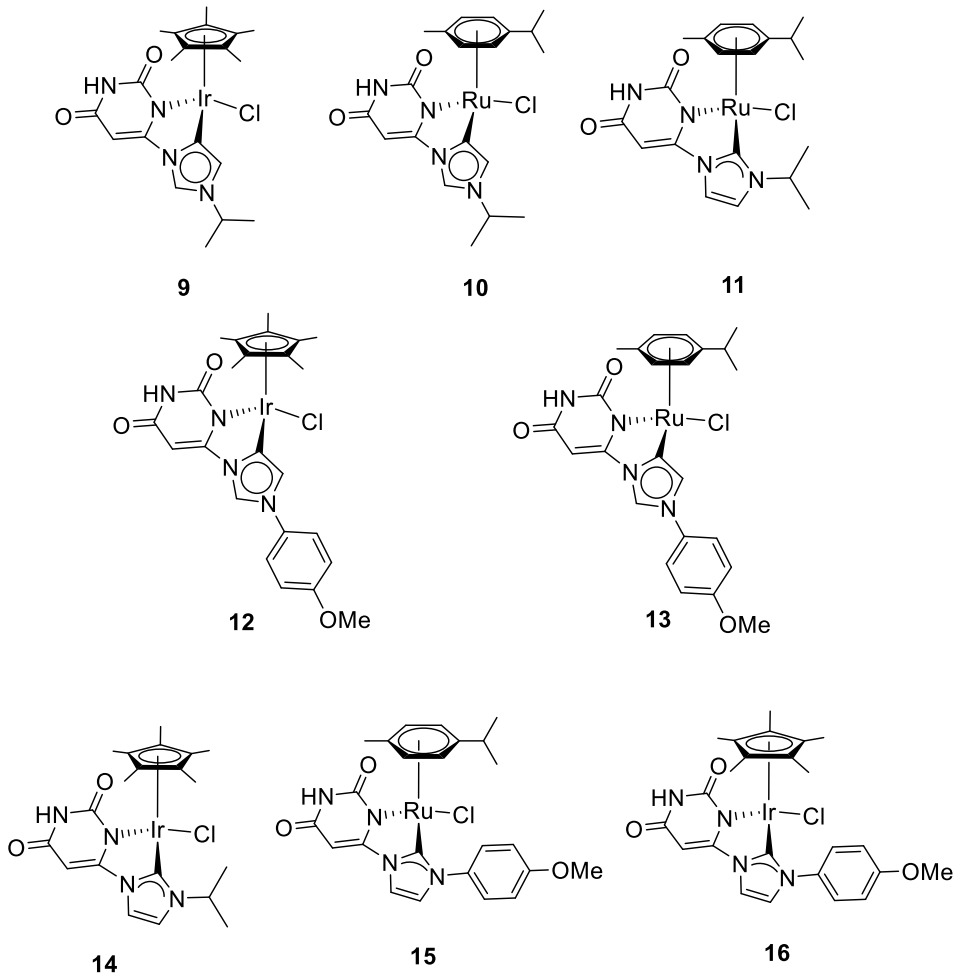

Figure 4.16 - *Cyclometalated complexes of iridium and ruthenium, with imidazole wingtip different than methyl, tested for their ability to catalyse the reduction of NAD^+ to NADH.*

The compounds were tested by directly varying the NAD^+ concentration and maintaining the catalyst concentration as described above (5 µM).

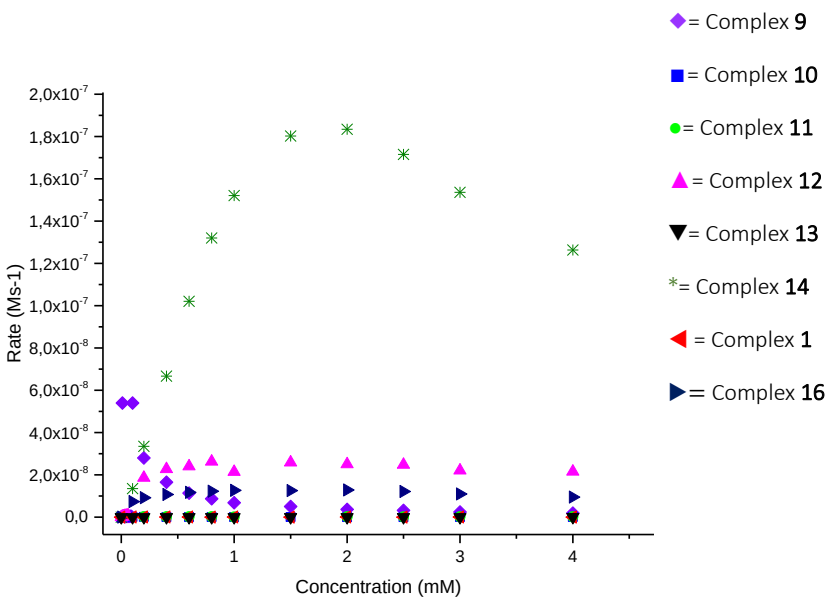

Graphic 4.4 – *Variation of the rate of reduction of NAD^+ to NADH with substrate concentration (NAD^+) – concentrations between 0 and 4 mM.*

The Graphic 4.4 shows the catalytic activities of complexes **9**-**16**. As expected, the ruthenium catalysts (**10, 11, 13, 15**) showed only residual activity, while for the iridium catalysts the N-substituent proved to influence the catalytic activity. The iridium complexes bearing an anisole substituent (complexes **12** and **16**) did not show relevant catalytic activity in all the conditions evaluated. For the iridium complexes bearing an isopropyl group (complexes **9** and **14**) the dependence between the carbene type and catalytic activity was confirmed, as observed previously with complexes **2** and **3**. Specifically, complex **14,** the normal NHC, performed better than the abnormal compound **9**. Complex **14** induced a very high catalytic activity for a wide range of catalyst loadings, while complex **9** showed a sharp profile.

This profile may be due to a saturation of the catalyst as already discussed for complex **2**.

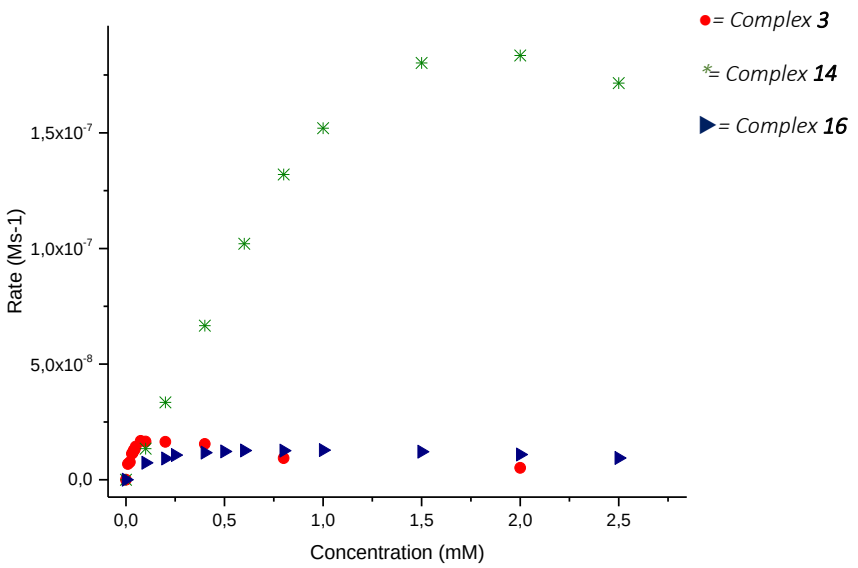

Graphic 4.5 – *Variation of the rate of reduction of NAD^+ to NADH with substrate concentration (NAD^+).*

Graphic 4.5 compares the catalytic activity of the iridium normal NHCs (complexes **3**, **14** and **16**) and shows that complex **14** presents the best catalytic activity, being more active than **3** and **16** at any NAD^+ concentration. In addition, it shows a maximum rate of $1.52x10^{-7}$ Ms^{-1}, 10 times faster than **3** ($1.6x10^{-8}$ MxS^{-1}) and at lower catalyst loading (0.5% compared to 6.6%). Furthermore, at this catalyst loading the complex possess a TON of 20 and a TOF of 299 h^{-1}, the higher of all the tested complexes. The more relevant TON and TOF of all the iridium complexes tested in this series are summarised in Table 4.3.

Table 4.3 - More relevant *TON and TOF corresponding to different catalyst loading of complexes **9**, **12**, **14** and **16**.*

Catalyst	Catalyst loading	NAD+ concentration	TON	TOF
9	5%	0.1 mM	2	57 h^{-1}
9	2.5%	0.2 mM	4	40 h^{-1}
12	0.83%	0.6 mM	12	33 h^{-1}
12	0.62%	0.8 mM	16	27 h^{-1}
14	0.5%%	1 mM	20	299 h^{-1}
14	0.33%	1.5 mM	30	253 h^{-1}
14	0.25%	2 mM	40	194 h^{-1}
14	0.2%	2.5 mM	50	152 h^{-1}
16	62%	0.8 mM	16	9 h^{-1}

Finally, Graphic 4.6 compares the activity of the iridium abnormal NHCs (complexes **2**, **9** and **12**). As it can be observed, complex **12** (bearing an anisole substituent) maintains activity over a greater range of NAD concentrations than complex **2** and **9**. This could be the result of a general decrease in the activity, but probably the best conditions for this catalyst require further insights that were not further pursued due to time constraints.

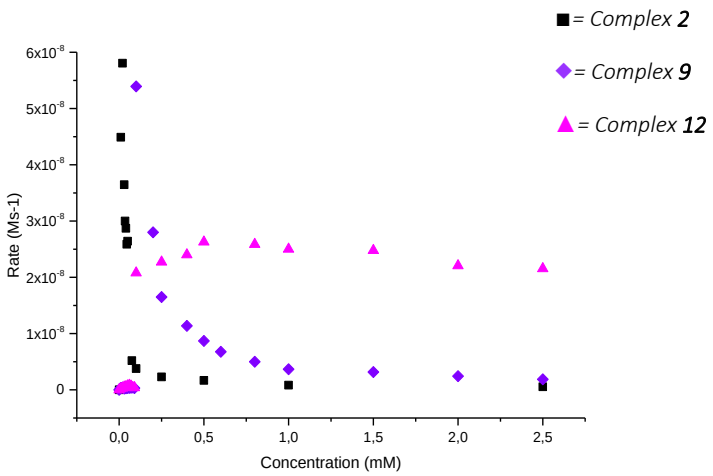

Graphic 4.6 - *Variation of the rate of reduction of NAD⁺ to NADH with substrate concentration (NAD⁺) – concentrations between 0 and 2.5 mM.*

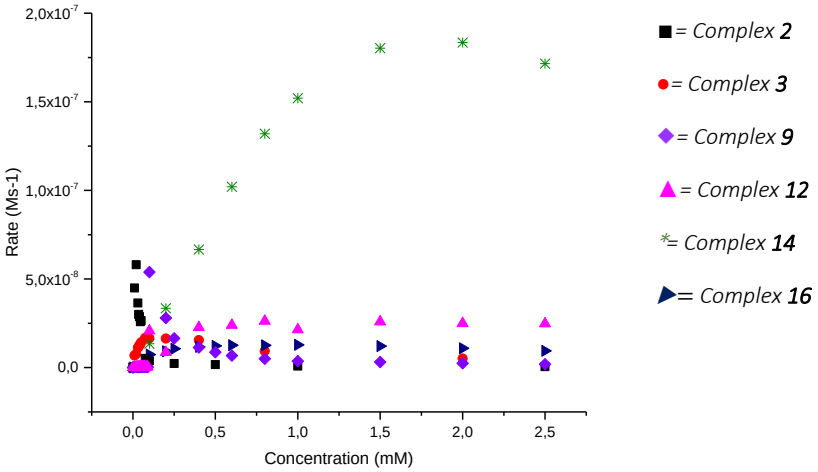

Graphic 4.7 - *Dependence of the rate of reduction of NAD⁺ to NADH with the substrate concentration (NAD⁺) – concentrations between 0 and 2.5 mM.*

Graphic 4.7 compares the activity of all the iridium catalysts tested. The three abnormal iridium NHCs (complexes **2**, **9** and **12**) showed low catalytic activity when compared to the activity showed by the corresponding normal carbenes (complexes **3**, **14** and **16**). Among the iridium normal carbenes, complex **14**, which has an isopropyl group as side chain, showed to be the best catalyst for catalysing the reduction of NAD^+ to NADH. The reason of the influence of the side chain on the imidazole ring was not investigated, but we can speculate that a more hindering substituent do not allow to form a stable bond with either the starting material or the final product. Thus, the catalyst is not poisoned and its activity increases. Further insights on this reactivity will be pursued.

4.2.6. Conclusions

In conclusion, we synthesized an uracil ligand precursor derivatized with a methyl imidazole ring (compound **1**) that can undergo cyclometallation. The behaviour of the ligand precursor at different pH values and its capacity to form the corresponding betaine were evaluated. Compound **1** was reacted with $[IrCp^*Cl_2]_2$ and $[Ru(p\text{-cymene})Cl_2]_2$ through cyclometallation. Although the studies on compound **1** demonstrated a higher acidity at position 2 of the imidazole ring, the cyclometallation reaction resulted in the formation of an abnormal carbene bound to the metal via C5. The ligand precursor also reacted with the two metal precursors in its betaine form, confirming the reactivity via C5 in the case of reaction with iridium and leading to a mixture of abnormal and normal carbenes in the case of ruthenium. To obtain a more in-depth understanding, the betaine **1a** was reacted with $Au(SMe_2)Cl$ and

afforded the formation of the normal carbene only, via C2. Considering this, we concluded that the driving force for the formation of the abnormal carbenes is cyclometallation. The cyclometallated normal carbenes can be obtained via silver transmetallation reactions with both iridium and ruthenium .

The reactivity of ligand precursors with different substituents on the imidazole ring was also explored; namely, isopropyl imidazole and anisole imidazole were used. When reacted with $IrCp^*Cl_2]_2$ and $[Ru(p\text{-cymene})Cl_2]_2$ the different ligand precursors confirmed the reactivity already observed for compound **1**.

All the cyclometallated complexes were tested for their ability to catalyse the reduction of NAD^+ to NADH, demonstrating a direct dependence of activity on the type of metal and the type of connectivity between the carbene carbon and metal (via C5 or via C2). In fact, iridium complexes have proven to be much better catalysts than ruthenium-containing complexes, regardless of the type of ligand precursor. In addition, among the iridium-containing complexes, the complexes containing imidazole bound via C2 (normal carbene), proved to be the best catalyst of the series. Among the iridium normal carbenes, the complex bearing an isopropyl substituent at the imidazole ring performed 10 times better than the other catalysts.

4.3. Experimental

The syntheses of the complexes were carried out under an inert atmosphere of N_2 using Schlenk techniques. All ^1H and $^{13}C\{^1H\}$ NMR spectra

were recorded at room temperature on Bruker spectrometers (400 MHz and 800 MHz), and chemical shifts were referenced to $SiMe_4$ (δ in ppm, *J* in Hz) and H_3PO_4. The ligand precursors were synthesized according to the synthetic procedure described previously[193]. Mass Spectroscopy and Elemental Analysis were performed by the UniMass Laboratory at Instituto de Tecnologia Química e Biológica, Portugal.

4.3.1. Compound 1

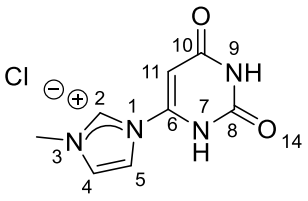

6-Chlorouracil (500 mg, 3.41 mmol) was suspended in chlorobenzene (20 ml), and methyl imidazole (0.816 ml, 10.23 mmol) was added. The mixture was heated for 7 hours. After cooling, the suspension was filtered, and the solid was washed with a hot mixture of AcOEt/EtOH (5:1). The precipitate was dissolved it in water and the mixture precipitated with acetone, affording compound **1** as a white powder (595 mg, 77%).

^{1}H NMR (400 MHz, DMSO-d_6): δ 11.16 (bs, 1H, N9-*H*); 9.83 (s, 1H, H-2); 8.19 (t, 1H, H-5, $^3J_{H\text{-}5,\,H\text{-}4} = {}^4J_{H\text{-}5,\,H\text{-}2}$= 1.84 Hz); 7.92 (s, 1H, $^3J_{H\text{-}4,\,H\text{-}5} = {}^4J_{H\text{-}4,\,H\text{-}2}$= 1.84 Hz); 5.98 (s, 1H, H-11); 3.93 (s, 3H, N3-CH_3) ppm

^{13}C{^{1}H} NMR (100 MHz, DMSO-d_6): δ 164.1-152.4 (C-8; C-10); 146.5 (C-6); 136.8 (C-2); 124.3 (C-4); 120.3 (C-5); 91.1 (C-11); 36.4 (N3-*C*H_3) ppm.

4.3.2. Compound 1a

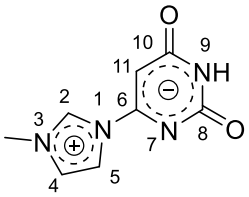

1a

Compound **1** (200 mg, 0.87 mmol) was suspended in methanol (21 ml), and NaOAc (143 mg, 1.74 mmol) was added. The mixture was stirred at room temperature for 2 hours. The obtained suspension was filtered and compound **1a** was isolated as a white powder in 88% yield (148 mg). The characterization has been previously reported[193].

4.3.3. Compound 7

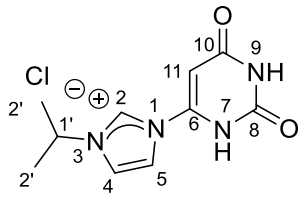

6-Chlorouracil (250 mg, 1.71 mmol) was suspended in chlorobenzene (11 ml), and isopropyl imidazole (0.546 ml, 5.12 mmol) was added. The mixture was heated for 7 hours. After cooling, the suspension was filtered, and the solid was washed with a hot mixture of AcOEt/EtOH (5:1). The precipitate was dissolved it in water and the mixture precipitated with acetone, affording compound **7** as a white powder (90 mg, 21%).

^{1}H NMR (400 MHz, DMSO-d_6): δ 10.87 (bs, 1H, N9-*H*); 9.81 (s, 1H, H-2); 8.25 (t, 1H, H-5, $^3J_{H\text{-}5,\ H\text{-}4} = {}^4J_{H\text{-}5,\ H\text{-}2}$= 1.85 Hz); 8.10 (s, 1H, H-4, $^3J_{H\text{-}4,\ H\text{-}5} = {}^4J_{H\text{-}4,\ H\text{-}2}$= 1.85 Hz); 5.95 (s, 1H, H-11); 4.69 (sept, 1H, H-1', $^3J_{H\text{-}1',\ H\text{-}2'}$ = 6.65 Hz); (d, 6H, H-2', $^3J_{H\text{-}2',\ H\text{-}1'}$ = 6.65 Hz) ppm

$^{13}C\{^1H\}$ NMR (100 MHz, DMSO-d_6): δ 164.6-153.5 (C-8; C-10); 144.3 (C-6); 134.7 (C-2); 121.3 (C-4); 120.3 (C-5); 89.42 (C-11); 53.3 (C-1'); 22.0 (2C, C-2') ppm.

4.3.4. Compound 8

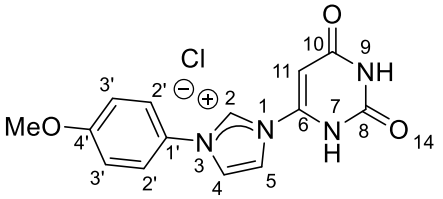

6-Chlorouracil (250 mg, 1.71 mmol) was suspended in chlorobenzene (11 ml), and anisole imidazole (891 mg, 5.12 mmol) was added. The mixture was heated for 7 hours. After cooling, the suspension was filtered, and the solid was washed with a hot mixture of AcOEt/EtOH (5:1). The precipitate was dissolved it in water and the mixture precipitated with acetone, affording compound **8** as a white powder (381 mg,69 %).

^1H NMR (400 MHz, DMSO-d_6): δ 11.66 (bs, 1H, N9-*H*); 10.22 (s, 1H, H-2); 8.42 (t, 1H, H-5, $^3J_{H\text{-}5,\,H\text{-}4} = {}^4J_{H\text{-}5,\,H\text{-}2}$= 1.86 Hz); 8.40 (s, 1H, $^3J_{H\text{-}4,\,H\text{-}5} = {}^4J_{H\text{-}4,\,H\text{-}2}$= 1.86 Hz); 7.80 (d, 2H, H-2', ^3J= 9.1 Hz); 7.21 (d, 2H, H-3', ^3J= 9.1 Hz); 5.99 (s, 1H, H-11); 3.85 (s, 3H, OMe-CH_3) ppm.

$^{13}C\{^1H\}$ NMR (100 MHz, DMSO-d_6): δ 165.0 (2C, C-8, C-10); 160.3 (C-4'); 134.4 (C-2); 127.5 (C-1'); 123.7 (C-2'); 122.0 (C-4); 120.4 (C-5); 115.1 (C-3'); 88.6 (C-11); 55.8 (Anisol-CH_3) ppm.

4.3.5. Complex 2

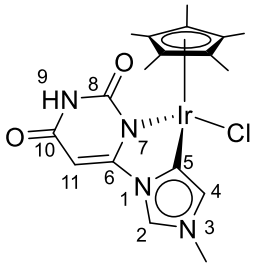

A Schlenk tube was charged with compound **1** (40 mg, 0.139 mmol), $[IrCp^*Cl_2]_2$ (77 mg, 0.97 mmol) and sodium acetate (23 mg, 0.277 mmol). After the addition of methanol (13 ml), the mixture was refluxed for 24 hours. After cooling, the mixture was dried under vacuum, and washed with DCM to remove the unreacted metal precursor. Yielding complex **2** in 88% yield (68 mg), as an orange solid.

^{1}H NMR (400 MHz, DMSO-d_6): δ 10.86 (bs, 1H, N9-*H*); 10.19 (d, 1H, H-2, $^4J_{H\text{-}2,\ H\text{-}4}$= 1.06 Hz); 7.30 (d, 1H, H-4, $^4J_{H\text{-}4,\ H\text{-}2}$= 1.06 Hz); 6.07 (s, 1H, H-11); 3.91 (s, 3H, N3-CH_3); 1.62 (s, 15H, CH_3 Cp) ppm.

^{13}C{^{1}H} NMR (100 MHz, DMSO-d_6): δ 164.9; 155.5; 155.1 (C-6; C-8; C-10); 135.7 (C-2); 130.6 (C-5); 124.1 (C-4); 95.8 (Cp); 85.0 (C-11); 35.9 (N3-CH$_3$); 8.7 (CH$_3$ Cp) ppm.

4.3.6. Complex 3

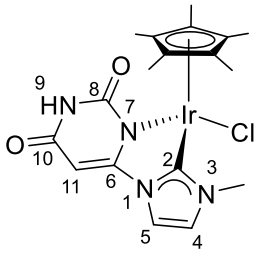

A Schlenk tube was charged with compound **1** (56 mg, 0.245 mmol) and silver oxide (73.4 mg, 0.245 mmol). After the addition of dichloromethane (6 ml), the mixture was stirred in the dark at room temperature. After 24 hours, $[IrCp^*Cl_2]_2$ (97 mg, 0.122 mmol) was added to the mixture, and the mixture was stirred at room temperature for an additional 24 hours. The mixture was then filtered through celite and the celite was rinsed with dichloromethane

and methanol. The mother liquors were dried and purified by column chromatography (97:3 DCM:MeOH), affording complex **3** in 60% yield (82 mg).

^{1}H NMR (400 MHz, DMSO-d_6): δ 10.85 (bs, 1H, N9-*H*); 8.34 (d, 1H, H-5, $^{3}J_{H\text{-}5,\ H\text{-}4}$= 2.22 Hz); 7.83 (d, 1H, H-4, $^{3}J_{H\text{-}4,\ H\text{-}5}$= 2.22 Hz); 6.11 (s, 1H, H-11); 3.94 (s, 3H, N3-CH_3); 1.81 (s, 15H, CH_3 Cp) ppm.

^{13}C{^{1}H} NMR (100 MHz, DMSO-d_6): δ 164.8-155.3-155.2 (C-6; C-8; C-10); 154.1 (C-2); 126.9 (C-4); 118.8 (C-5); 97.6 (Cp); 86.1 (C-11); 37.8 (N3-CH$_3$); 9.0 (CH$_3$ Cp) ppm.

Anal. Calcd for $C_{18}H_{22}ClIrN_4O_2$: C, 39.02; H, 4.00; N, 10.11. Found: C, 39.20; H, 4.31; N, 9.98.

4.3.7. Complex 4

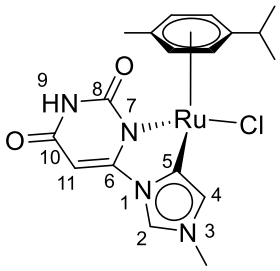

A Schlenk tube was charged with compound **1** (40 mg, 0.139 mmol), [Ru(*p*-cymene)Cl$_2$]$_2$ (59 mg, 0.097 mmol) and sodium acetate (23 mg, 0.277 mmol). After the addition of methanol (13 ml), the mixture was refluxed for 24 hours. After cooling, the mixture was dried under vacuum, and washed with DCM to remove the unreacted metal precursor. The resulting orange solid was purified by column chromatography (97:3 DCM:MeOH), affording complex **4** in 53% yield (34 mg).

^{1}H NMR (800 MHz, DMSO-d_6): δ 10.27 (bs, 1H, N9-*H*); 9.52 (d, 1H, H-2, $^{4}J_{H\text{-}2,\ H\text{-}4}$= 1.12 Hz); 7.44 (d, 1H, H-4, $^{4}J_{H\text{-}4,\ H\text{-}2}$= 1.12Hz); 5.82 (d, 1H, *p*-cym, $^{3}J_{H,H}$= 5.52 Hz); 5.74 (d, 1H, *p*-cym, $^{3}J_{H,H}$= 5.68 Hz); 5.70 (s, 1H, H-11); 5.51 (d, 1H, *p*-cym, $^{3}J_{H,H}$= 5.52 Hz); 5.11 (d, 1H, *p*-cym, $^{3}J_{H,H}$= 5.68 Hz); 3.86 (s, 3H, N3-C*H*$_3$); 2.42 (sept, 1H, C*H* *p*-cym, $^{3}J_{H,H}$= 6.92 Hz); 1.93 (s, 3H, C*H*$_3$ *p*-cym); 1.02 (d, 3H, C*H*$_3$ *p*-cym, $^{3}J_{H,H}$= 6.92 Hz); 0.88 (d, 3H, C*H*$_3$ *p*-cym, $^{3}J_{H,H}$= 6.92 Hz); ppm.

^{13}C{^{1}H} NMR (200 MHz, DMSO-d_6): δ 165.2-156.8-156.4 (C-6; C-8; C-10); 158.6 (C-5); 131.9 (C-2); 125.2 (C-4); 88.3 (*p*-cym); 87.6 (*p*-cym); 82.7 (C-11); 82.4 (*p*-cym); 81.2 (*p*-cym); 35.2 (N3-*C*H$_3$); 30.3 (*C*H *p*-cym); 22.7 (C*H*$_3$ *p*-cym); 21.4 (C*H*$_3$ *p*-cym); 18.4 (C*H*$_3$ *p*-cym) ppm.

Anal. Calcd for $C_{18}H_{21}ClN_4O_2Ru$: C, 46.80; H, 4.58; N, 12.13. Found: C, 46.60; H, 4.58; N, 12.13.

4.3.8. Complex 5

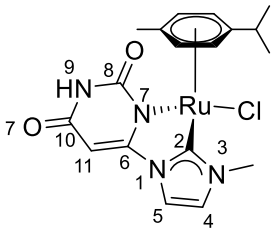

A Schlenk tube was charged with compound **1** (56 mg, 0.245 mmol) and silver oxide (73 mg, 0.245 mmol). After the addition of dichloromethane (6 ml), the mixture was stirred in the dark at room temperature. After 24 hours, [Ru(*p*-cymene)Cl_2]$_2$ (75 mg, 0.122 mmol) was added to the mixture, and the reaction was stirred at room temperature for an additional 24 hours. The mixture was then filtered through celite and the celite was rinsed with dichloromethane and methanol.

The mother liquors were dried and purified by column chromatography (97:3 DCM:MeOH), affording complex **5** in 28% yield (32 mg).

^{1}H NMR (400 MHz, MeOD): δ 7.81 (d, 1H, H-5, $^{3}J_{\text{H-5, H-4}}$= 2.08 Hz); 7.48 (d, 1H, H-4, $^{3}J_{\text{H-4, H-5}}$= 2.08 Hz); 6.18 (d, 1H, p-cym, $^{3}J_{H,H}$= 5.84 Hz); 6.10 (m, 2H, p-cym); 5.78 (s, 1H, H-11); 5.43 (d, 1H, p-cym, $^{3}J_{H,H}$= 5.84 Hz); 4.11 (3H, N3-CH_3); 2.34 (sept, 1H, C*H* p-cym, $^{3}J_{H,H}$= 6.88 Hz); 2.16 (s, 3H, CH_3 p-cym); 0.96 (m, 6H, CH_3 p-cym) ppm.

^{13}C{^{1}H} NMR (100 MHz, MeOD): δ 186.6 (C-2); 171.8-168.9-158.9 (C-6; C-8; C-10); 127.1 (C-4); 117.6 (C-5); 86.8 (*p*-cym); 84.5 (C-11); 38.6 (N3-*C*H$_3$); 32.4 (*C*H *p*-cym); 22.7 (*C*H$_3$ *p*-cym); 19.3 (*C*H$_3$ *p*-cym) ppm.

4.3.9. Complex 6

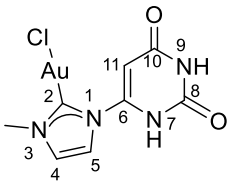

An NMR tube was charged with compound **1a** (9.6 mg, 0.05 mmol) and S(Me)$_2$AuCl (14.7 mg, 0.05 mmol) and degassed. DMSO-d_6 was added, and the mixture was reacted at room temperature and monitored periodically by NMR. After two days, the reaction afforded complete conversion of the starting material to complex **6**.

^{1}H NMR (400 MHz, DMSO-d_6): δ 11.97 (bs, 1H, N7-*H*); 10.80 (bs, 1H, N9-*H*); 7.79 (d, 1H, H-5, $^{3}J_{\text{H-5, H-4}}$= 1.96 Hz); 7.62 (d, 1H, H-4, $^{3}J_{\text{H-4, H-5}}$= 1.96 Hz); 5.99 (s, 1H, H-11); 3.83 (s, 3H, N3-CH_3) ppm.

$^{13}C\{^1H\}$ NMR (100 MHz, DMSO-d_6): δ 168.6 (C-2); 164.7 (C-8/C-10); 153.9 (C-8/C-10); 152.0 (C-6); 123.2 (C-4); 121.1 (C-5); 92.9 (C-11); 38.5 (N3-CH$_3$) ppm.

4.3.10.Complex 9

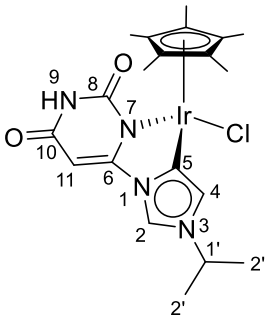

A Schlenk tube was charged with compound **7** (50 mg, 0.190 mmol), [IrCp*Cl$_2$]$_2$ (77 mg, 0.097 mmol) and sodium acetate (32 mg, 0.389 mmol). After the addition of methanol (19 ml), the mixture was refluxed for 24 hours. After cooling, the mixture was dried under vacuum, and washed with DCM to remove the unreacted metal precursor. Pentane was added to the mother liquor, affording complex **9** as an orange precipitate in 58% yield (65 mg).

^1H NMR (400 MHz, DMSO-d_6): δ 10.82 (bs, 1H, N9-*H*); 9.96 (d, 1H, H-2, $^4J_{H\text{-}2,\ H\text{-}4}$= 0.96 Hz); 7.47 (d, 1H, H-4, $^4J_{H\text{-}4,\ H\text{-}2}$= 0.96 Hz); 6.15 (s, 1H, H-11); 4.62 (sept, 1H, H-1', $^3J_{H\text{-}1',\ H\text{-}2'}$ = 6.50 Hz); 1.55 (d, 6H, H-2', $^3J_{H\text{-}2',\ H\text{-}1'}$ = 6.50 Hz); 1.78 (s, 15H, CH_3 Cp) ppm.

$^{13}C\{^1H\}$ NMR (100 MHz, DMSO-d_6): δ 164.8-155.5-155.0 (C-6; C-8; C-10); 133.5 (C-2); 130.9 (C-5); 121.1 (C-4); 95.8 (Cp); 85.2 (C-11); 52.6 (*C*-1'); 22.3 (*C*-2'); 8.7 (*C*H$_3$ Cp) ppm.

Anal. Calcd for $C_{20}H_{26}ClIrN_4O_2$: C, 41.27; H, 4.50; N, 9.62. Found: C, 41.40; H, 4.49; N, 9.21.

4.3.11.Complex 14

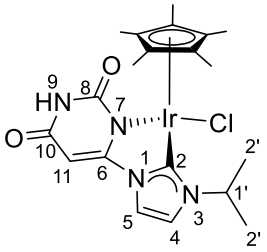

A Schlenk tube was charged with compound **7** (56 mg, 0.218 mmol) and silver oxide (65 mg, 0.218 mmol). After the addition of dichloromethane (5.5 ml), the mixture was stirred in the dark at room temperature. After 24 hours, $[IrCp^*Cl_2]_2$ (87 mg, 0.109 mmol) was added to the mixture, and the reaction mixture was stirred at room temperature for an additional 24 hours. The mixture was then filtered through celite and the celite was rinsed with dichloromethane and methanol. The mother liquors were dried and purified by column chromatography (97:3 DCM:MeOH), affording complex **14** in 28% yield (46 mg).

^{1}H NMR (400 MHz, DMSO-*d*$_6$): δ 10.89 (bs, 1H, N9-*H*); 8.45 (d, 1H, H-5, $^3J_{H\text{-}5,\ H\text{-}4}$= 2.28 Hz); 8.17 (d, 1H, H-4, $^3J_{H\text{-}4,\ H\text{-}5}$= 2.28 Hz); 6.13 (s, 1H, H-11); 4.48 (sept, 1H, H-1', $^3J_{H\text{-}1',\ H\text{-}2'}$= 6.5 Hz); 1.80 (s, 15H, C*H*$_3$ Cp); 1.68 (d, 3H, H-2', $^3J_{H\text{-}2',\ H\text{-}1'}$= 6.5 Hz); 1.40 (d, 3H, H-2', $^3J_{H\text{-}2',\ H\text{-}1'}$= 6.5 Hz) ppm.

^{13}C{^{1}H} NMR (100 MHz, DMSO-*d*$_6$): δ 164.7-155.6-154.8 (C-6; C-8; C-10); 152.9 (C-2); 122.2 (C-4); 120.1 (C-5); 97.6 (Cp); 86.4 (C-11); 52.6 (C-1'); 23.6 (C-2'); 22.8 (C-2'); 9.0 (*C*H$_3$ Cp) ppm.

Anal. Calcd for $C_{20}H_{26}ClIrN_4O_2$: C, 41.27; H, 4.50; N, 9.62. Found: C, 41.06; H, 4.13; N, 9.35.

4.3.12.Complex 10

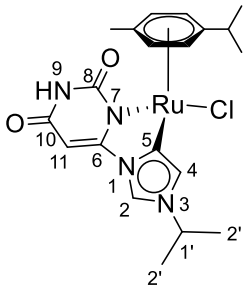

A Schlenk tube was charged with compound **7** (40 mg, 0.156 mmol), $[Ru(p\text{-cymene})Cl_2]_2$ (69.0 mg, 0.109 mmol) and sodium acetate (25 mg, 0.312 mmol). After the addition of methanol (16 ml), the mixture was refluxed for 24 hours. After cooling, the mixture was dried under vacuum, and washed with DCM to remove the unreacted metal precursor. The resulting orange solid was purified by column chromatography (97:3 DCM:MeOH), affording complex **10** in 84% yield (64 mg).

^{1}H NMR (800 MHz, DMSO-d_6): δ 10.26 (bs, 1H, N9-H); 9.56 (bs, 1H, H-2); 7.66 (bs, 1H, H-4); 5.86 (d, 1H, *p*-cym, $^{3}J_{H,H}$= 5.68 Hz); 5.79 (m, 2H, H-11 + *p*-cym); 5.44 (d, 1H, *p*-cym, $^{3}J_{H,H}$= 5.68 Hz); 5.15 (d, 1H, *p*-cym, $^{3}J_{H,H}$= 5.68 Hz); 4.57 (sept, 1H, H-1', $^{3}J_{H\text{-}1',H\text{-}2'}$= 6.56 Hz); 2.42 (sept, 1H, C*H p*-cym, $^{3}J_{H,H}$=6.72); 1.93 (s, 3H, *p*-cym CH_3); 1.54 (d, 6H, H-2', $^{3}J_{H\text{-}2',H\text{-}1'}$= 6.56 Hz); 1.02 (d, 3H, CH_3 *p*-cym, $^{3}J_{H,H}$=6.72); 0.86 (d, 3H, CH_3 *p*-cym, $^{3}J_{H,H}$=6.72) ppm.

^{13}C{^{1}H} NMR (200 MHz, DMSO-d_6): δ 165.4-156.9-156.3 (C-6; C-8; C-10); 159.0 (C-5); 129.8 (C-2); 122.1 (C-4); 88.5 (*p*-cym); 87.5 (*p*-cym); 82.9 (C-11); 82.0 (*p*-cym); 80.8 (*p*-cym); 51.8 (C-1'); 30.3 (*C*H *p*-cym); 22.5 (2C, C-2'); 22.5 (CH_3 *p*-cym); 21.5 (CH_3 *p*-cym) ppm.

4.3.13.Complex 11

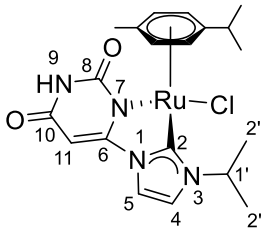

A Schlenk tube was charged with compound **7** (56 mg, 0.218 mmol) and silver oxide (65 mg, 0.218 mmol). After the addition of dichloromethane (6 ml), the mixture was stirred in the dark at room temperature. After 24 hours, $[Ru(p\text{-cymene})Cl_2]_2$ (67 mg, 0.109 mmol) was added to the mixture, and the reaction was stirred at room temperature for an additional 24 hours. The mixture was then filtered through celite and the celite was rinsed with dichloromethane and methanol. The mother liquors were dried and purified by column chromatography (97:3 DCM:MeOH), affording complex **11** in 34% yield (37 mg).

^{1}H NMR (400 MHz, MeOD): δ 7.85 (d, 1H, H-5, $^{3}J_{H\text{-}5,\ H\text{-}4}$= 2.28 Hz); 7.65 (d, 1H, H-4, $^{3}J_{H\text{-}4,\ H\text{-}5}$= 2.28 Hz); 6.16(m, 1H, *p*-cym); 6.08 (m, 1H, *p*-cym); 5.97 (m, 1H, *p*-cym); 5.80 (s, 1H, H-11); 5.41 (m, 1H, *p*-cym); 5.05 (sept, 1H, H-1', $^{3}J_{H\text{-}1',\ H\text{-}2'}$= 6.2 Hz); 2.34 (sept, 1H, C*H* *p*-cym); 2.16 (d, 3H, H-2', $^{3}J_{H\text{-}2',\ H\text{-}1'}$= 6.2 Hz); 1.50 (d, 3H, H-2', $^{3}J_{H\text{-}2',\ H\text{-}1'}$= 6.2 Hz); 0.98 (m, 6H, CH_3 p-cym) ppm.

^{13}C{^{1}H} NMR (100 MHz, MeOD): δ 183.8 (C-2); 168.9-159.6 (C-8; C-10); 158.8 (C-6); 120.4 (C-4); 117.3 (C-5); 91.8-91.3-87.11 (*p*-cym); 80.8 (C-11); 53.7 (C-1'); 32.4 (*C*H *p*-cym); 24.1 (C-2'); 23.2 (C-2'); 22.8 (*C*H_3 *p*-cym); 19.4 (*C*H_3 *p*-cym) ppm.

Anal. Calcd for $C_{20}H_{25}ClN_4O_2Ru$: C, 49.03; H, 5.14; N, 11.43. Found: C, 49.40; H, 4.99; N, 11.43.

4.3.14.Complex 12

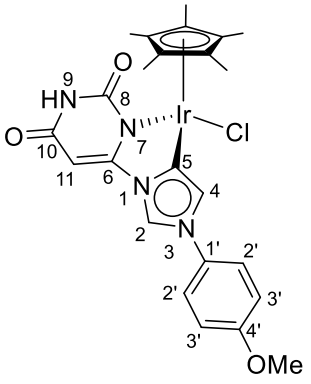

A Schlenk tube was charged with compound **8** (50 mg, 0.156 mmol), $[IrCp^*Cl_2]_2$ (62 mg, 0.078 mmol) and sodium acetate (25 mg, 0.312 mmol). After the addition of methanol (15 ml), the mixture was refluxed for 24 hours. After cooling, the mixture was dried under vacuum, and washed with DCM to remove the unreacted metal precursor. Pentane was added to the mother liquor, affording complex **12** as an orange precipitate in 28% yield (28 mg).

^{1}H NMR (400 MHz, DMSO-d_6): δ 10.89 (bs, 1H, N9-*H*); 10.33 (d, 1H, H-2, $^4J_{H\text{-}2,\ H\text{-}4}$= 1.2 Hz); 7.83 (d, 2H, H-2', ^3J= 9.02 Hz); 7.76 (d, 1H, H-4, $^4J_{H\text{-}4,\ H\text{-}2}$= 1.2 Hz); 7.24 (d, 2H, H-3', ^3J= 9.02 Hz); 6.20 (s, 1H, H-11); 3.87 (s, 1H, O-CH_3); 1.78 (s, 15H, CH_3 Cp) ppm.

^{13}C{^{1}H} NMR (100 MHz, DMSO-d_6): δ 164.8-155.4-154.9 (C-6; C-8; C-10); 160.3 (C-1'-C-4'); 133.4 (C-2); 131.4 (C-5); 123.3 (C-3'); 121.2 (C-4); 115.0 (C-2'); 96.0 (Cp); 85.6 (C-11); 55.8 (O-CH_3); 8.7 (CH_3 Cp) ppm

4.3.15.Complex 16

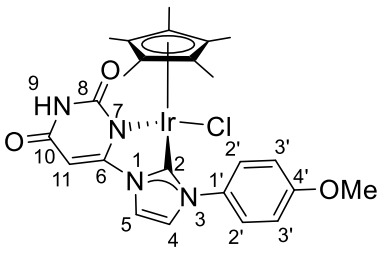

A Schlenk tube was charged with compound **8** (56 mg, 0.175 mmol) and silver oxide (52 mg, 0.175 mmol). After the addition of dichloromethane (4 ml), the mixture was stirred in the dark at

room temperature. After 24 hours, $[IrCp^*Cl_2]_2$ (65 mg, 0.087 mmol) was added to the mixture, and the reaction was stirred at room temperature for an additional 24 hours. The mixture was then filtered through celite and the celite was rinsed with dichloromethane and methanol. The mother liquors were dried and purified by column chromatography (97:3 DCM:MeOH), affording complex **16** in 18% yield (19.8 mg).

Anal. Calcd for $C_{24}H_{26}ClIrN_4O_3$: C, 44.61; H, 4.06; N, 8.67. Found: C, 44.70; H, 3.74; N, 8.89.

4.3.16.Complex 13

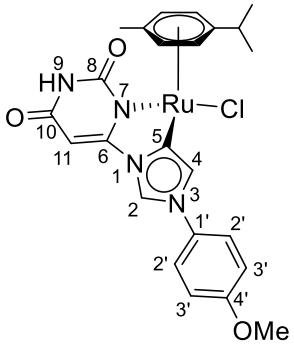

A Schlenk tube was charged with compound **8** (50 mg, 0.156 mmol), $[IrCp^*Cl_2]_2$ (61.0 mg, 0.330 mmol) and sodium acetate (25 mg, 0.312 mmol). After the addition of methanol (4 ml), the mixture was refluxed for 24 hours. After cooling, the mixture was dried under vacuum, and washed with DCM to remove the unreacted metal precursor. The resulting orange solid was purified by column chromatography (97:3 DCM:MeOH), affording complex **13** in 21% yield (18 mg).

^{1}H NMR (800 MHz, DMSO-d_6): δ 10.33 (bs, 1H, N9-*H*); 10.05 (d, 1H, H-2, $^4J_{H\text{-}2,\ H\text{-}4}$= 1.1 Hz); 8.05 (d, 1H, H-4, $^4J_{H\text{-}4,\ H\text{-}2}$= 1.1 Hz); 7.81 (d, 2H, H-2', ^3J= 8.9 Hz); 7.22 (d, 2H, H-3', ^3J= 8.9 Hz); 5.93 (d, 1H, *p*-cym, ^3J= 5.8 Hz); 5.91 (s, 1H, H-11); 5.83 (d, 1H, *p*-cym, ^3J= 5.8 Hz); 5.53 (d, 1H, *p*-cym, ^3J= 5.8 Hz); 5.25 (d, 1H, *p*-cym, ^3J= 5.8 Hz); 3.86 (s, 1H, O-CH_3); 2.47 (sept, 1H, C*H p*-cym, ^3J= 6.9

Hz); 1.96 (s, 3H, CH_3 p-cym); 1.06 (d, 3H, CH_3 *p*-cym, ^3J= 6.9 Hz); 0.91 (d, 3H, CH_3 *p*-cym, ^3J= 6.9 Hz); ppm.

^{13}C{^{1}H} NMR (200 MHz, DMSO-d_6): δ 165.3-156.7-156.3 (C-6; C-8; C-10); 159.9 (C-1'; C-4'); 159.8 (C-5); 129.7 (C-2); 128.2 (C-1'; C-4'); 122.8 (C-2'; C-3'); 122.3 (C-4); 115.2 (C2'; C-3'); 101.4 (*p*-cym); 100.6 (*p*-cym); 88.5 (*p*-cym); 87.7 (*p*-cym); 83.5 (C-11); 82.3 (*p*-cym); 81.3 (*p*-cym); 55.7 (O-*C*H$_3$); 30.3 (*C*H *p*-cym); 22.6-21.5 (*C*H$_3$ *p*-cym); 18.4 (*C*H$_3$ *p*-cym) ppm.

4.3.17.Complex 15

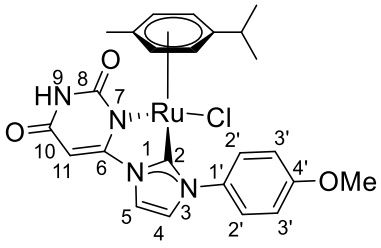

A Schlenk tube was charged with compound **8** (56 mg, 0.175 mmol) and silver oxide (52 mg, 0.175 mmol). After the addition of dichloromethane (4 ml), the mixture was stirred in the dark at room temperature. After 24 hours, [Ru(*p*-Cym)Cl$_2$]$_2$ (54 mg, 0.087 mmol) was added to the mixture, and the reaction was stirred at room temperature for an additional 24 hours. The mixture was then filtered through celite and the celite was rinsed with dichloromethane and methanol. The mother liquors were dried and purified by column chromatography (97:3 DCM:MeOH), affording complex **15** in 24% yield (23 mg).

^{1}H NMR (800 MHz, DMSO-d_6): δ 10.34 (bs, 1H, N9-*H*); 8.23 (d, 1H, H-4, $^3J_{H\text{-}4,\ H\text{-}5}$= 2 Hz); 7.89 (d, 1H, H-5, $^3J_{H\text{-}5,\ H\text{-}4}$= 2 Hz); 7.78 (d, 2H, H-3', ^3J= 8.8 Hz); 7.24

(d, 2H, H-2', ^{3}J= 8.8 Hz); 5.87 (s, 1H, H-11); 5.77 (bs, 1H, *p*-cym); 5.67 (bs, 1H, *p*-cym); 4.94 (bs, 1H, *p*-cym); 4.57 (bs, 1H, *p*-cym); 3.88 (s, 1H, O-CH_3); 2.19 (m, 1H, C*H* *p*-cym); 1.98 (s, 3H, CH_3 p-cym); 0.81 (m, 6H, CH_3 *p*-cym) ppm.

$^{13}C\{^{1}H\}$ NMR (200 MHz, DMSO-d_6): δ 184.2 (C-2); 165.3-157.1-156.3 (C-6; C-8; C-10); 159.7 (C-4'); 132.4 (C-1'); 127.4 (C-3'); 125.7 (C-5); 116.9 (C-4); 114.7 (C-2'); 83.4 (C-11); 55.7 (O-*C*H_3); 30.5 (*C*H *p*-cym); 22.2 (*C*H_3 *p*-cym); 18.7 (*C*H_3 *p*-cym) ppm.

4.3.18.Single-Crystal X-ray Crystallography

Crystals suitable for single-crystal X-ray analysis of compounds **3**, **4** and **5** were selected, covered with Fomblin (polyfluoro ether oil) and mounted on a nylon loop. The data were collected at 110 K or at room temperature on a Bruker D8 Venture diffractometer equipped with a Photon 100 CMOS detector using graphite monochromated Mo-Kα radiation (λ=0.71073 Å). The data were processed using the APEX3 suite software package, which includes integration and scaling (SAINT), absorption corrections (SADABS)[132] and space group determination (XPREP). Structure solution and refinement were performed using direct methods with the programs SHELXT 2014/5 and SHELXL (version 2018/3)[133,134] built in the APEX and WinGX-Version 2021.3[135] software packages. All nonhydrogen atoms were refined anisotropically. All the

hydrogen atoms were inserted in idealized positions and allowed to refine riding on the parent carbon atom.

Table 4.4 - *Main crystal data for compound **3**.*

Empirical formula	C18 H22 Cl Ir N4 O2
Formula weight	554.04
Temperature	293(2) K
Wavelength	0.71073 Å
Crystal system	Monoclinic
Space group	C 2/c
Unit cell dimensions	a = 19.3385(17) Å α= 90°.
	b = 14.4948(17) Å β= 120.044(6)°.
	c = 16.1794(18) Å γ= 90°.
Volume	3925.9(8) $Å^3$
Z	8
Density (calculated)	1.875 Mg/m3
Absorption coefficient	6.957 mm^{-1}
F(000)	2144
Crystal size	0.200 x 0.160 x 0.100 mm3
Theta range for data collection	1.949 to 33.026°.
Index ranges	-29<=h<=29,-22<=k<=22,-24<=l<=24
Reflections collected	128823
Independent reflections	7407 [R(int) = 0.0805]

Completeness to theta = 25.242°	99.5%
Absorption correction	Semiempirical from equivalents
Max. and min. transmission	0.7465 and 0.5472
Refinement method	Full-matrix least-squares on F^2
Data/restraints/parameters	7407/1/245
Goodness-of-fit on F^2	1.056
Final R indices [I>2sigma(I)]	R1 = 0.0322, wR2 = 0.0704
R indices (all data)	R1 = 0.0590, wR2 = 0.0778
Extinction coefficient	n/a
Largest diff. peak and hole	1.940 and-1.176 e.$Å^{-3}$

Table 4.5 - *Main crystal data for compound **4.***

Empirical formula	C19 H21 Cl N3 O2 Ru
Formula weight	459.91
Temperature	293(2) K
Wavelength	0.71073 Å
Crystal system	Monoclinic
Space group	P 21/n
Unit cell dimensions	a=7.8750(4) Å α= 90°.
	b=12.9930(6) Å β= 99.718(2)°.

	c=17.9843(10) Å γ= 90°.
Volume	1813.75(16) $Å^3$
Z	4
Density (calculated)	1.684 Mg/m^3
Absorption coefficient	1.031 mm^{-1}
F(000)	932
Crystal size	0.260 x 0.240 x 0.200 mm3
Theta range for data collection	2.298 to 28.287°.
Index ranges	-10<=h<=10,-17<=k<=17,-23<=l<=23
Reflections collected	72225
Independent reflections	4499 [R(int) = 0.0585]
Completeness to theta = 25.242°	99.8%
Absorption correction	Semiempirical from equivalents
Max. and min. transmission	0.820 and 0.775
Refinement method	Full-matrix least-squares on F^2
Data/restraints/parameters	4499/0/235
Goodness-of-fit on F^2	1.092
Final R indices [I>2sigma(I)]	R1 = 0.0297, wR2 = 0.0790
R indices (all data)	R1 = 0.0339, wR2 = 0.0804
Extinction coefficient	n/a
Largest diff. peak and hole	0.785 and-0.473 $e.Å^{-3}$

Table 4.6 - *Main crystal data for compound **5**.*

Empirical formula	C18 H23 Cl N4 O3 Ru
Formula weight	479.92
Temperature	110(2) K
Wavelength	0.71073 Å
Crystal system	Monoclinic
Space group	P 2/c
Unit cell dimensions	a = 12.5668(13) Å α= 90°.
	b = 7.0766(8) Å β= 99.239(4)°.
	c = 22.013(2) Å γ= 90°.
Volume	1932.2(3) $Å^3$
Z	4
Density (calculated)	1.650 Mg/m3
Absorption coefficient	0.976 mm^{-1}
F(000)	976
Crystal size	0.400 x 0.260 x 0.200 mm^3
Theta range for data collection	1.875 to 26.458°.
Index ranges	-15<=h<=15,-8<=k<=8,-27<=l<=27
Reflections collected	85138
Independent reflections	3953[R(int) = 0.0618]
Completeness to theta = 25.242°	99.7%

Absorption correction	Semiempirical from equivalents
Max. and min. transmission	0.829 and 0.696
Refinement method	Full-matrix least-squares on F^2
Data/restraints/parameters	3953/0/251
Goodness-of-fit on F^2	1.102
Final R indices [I>2sigma(I)]	R1 = 0.0479, wR2 = 0.1530
R indices (all data)	R1 = 0.0512, wR2 = 0.1563
Extinction coefficient	n/a
Largest diff. peak and hole	1.309 and-0.688 e.$Å^{-3}$

4.3.19. Catalytic measurements

The reaction was monitored by UV-Vis spectroscopy, following the formation of the absorption band of NADH centred at 340 nm (ε = 6220 M^{-1} cm^{-1}), using a multimode microplate reader Biotek synergy Neo 2 (Agilent). Turnover frequency [TOF = moles of NADH/(moles of catalyst per unit time)] values were obtained by deriving the TON versus t linear trends in the first 10 % of reaction progress.

CONCLUSIONS AND OUTLOOK

Conclusions and Future perspectives

In this thesis, we addressed the problem of finding new bioactive molecules containing metals, basing the rationale on different mechanisms of action for both microbial infections and cancer treatment.

In Chapter Two, we proposed a new antifungal agent based on nickel complexes bearing caffeine NHCs. The biscarbene complex **18** proved to be an excellent candidate for the selective treatment of *C. glabrata*, for which a patent has been filed. Further experiments with the caffeine biscarbene complex as a scaffold are currently being performed in collaboration with the laboratory of Dr. Catarina Pimentel. These studies include investigating the antimicrobial activity of different nickel biscarbenes and conducting in vivo studies. The discovery of the selective activity of nickel biscarbenes on *C. glabrata* is of utmost importance for understanding a mechanism of action that could circumvent the innate antifungal resistance of this species.

In Chapter Three, we explored the synthesis of new gold complexes bearing guanosine derivatives as NHCs. The synthesis of the complexes proved to be difficult due to the solubility of the products. Nevertheless, the gold monocarbenes, once isolated, allowed for solubilization in specific solvents, and will enable tests for their anticancer activity. In the future, further studies on the cytotoxicity will need to be performed. Similar structures proved to be very active and selective against ovarian cancer cell lines, and we expect a similar or better outcome due to the presence of a nucleobase in the metal complex. Furthermore, studies on reactivity of

gold(I) with guanosine bearing different side chains than methyl at N7 could be conducted, as well as their interference with G-quadruplexes.

In Chapter Four, we proposed to exploit a key aspect of iridium and ruthenium cyclometallated compounds, namely their ability to catalyze transfer hydrogenation reactions. Such reactions can occur within the cellular environment and cause reductive stress. These types of compounds constitute the so-called catalytic drugs; thus, the synthesized compounds were tested for their ability to reduce NAD^+ to NADH. We found a dependence of the catalytic activity on the metal, the wingtip of the imidazole ring, and the type of carbene (normal or abnormal). The best catalyst proved to be the iridium complex bearing a normal carbene with an isopropyl group as a wingtip (complex **14**). These preliminary trials on catalytic activity allow us to understand whether we can expect any cytotoxic activity on tumour cell lines or microbials. All the cyclometalated complexes are currently being tested on fungi and will also be tested on cancer cell lines as well as on healthy cells to understand their safety profile. Finally, different side chains for the imidazole ring, or different metal centres can be explored to further increase catalytic activity and, thus, bioactivity.

List of compounds

Chapter 2

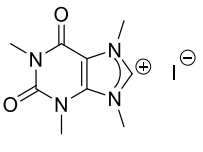

1

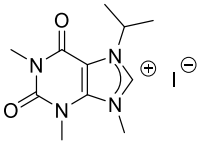

3a

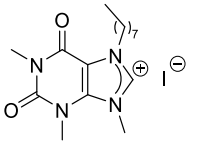

3b

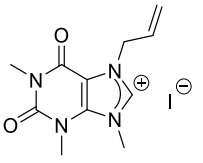

3c

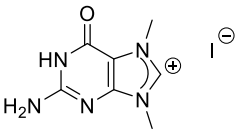

12

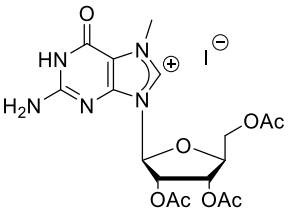

14

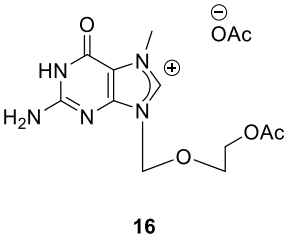

16

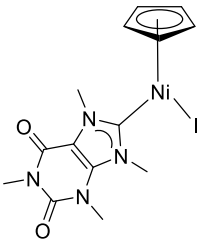

17

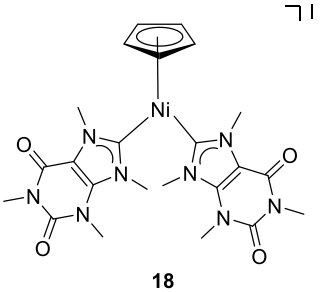

18

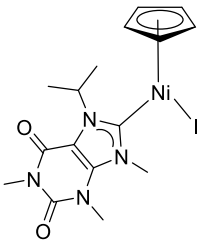

19

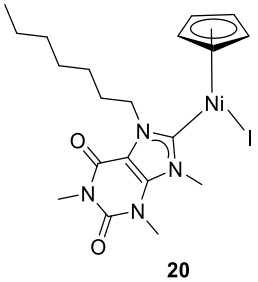

20

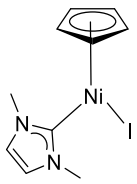

27

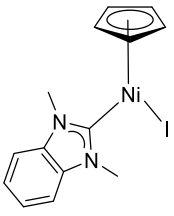

28

Chapter 3

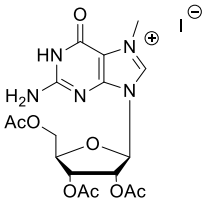

1

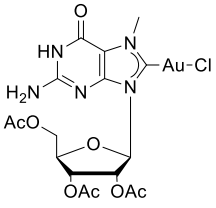

2

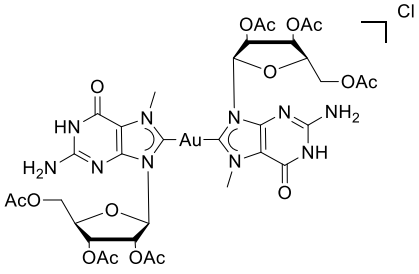

3

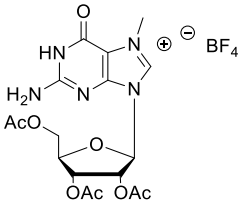

4

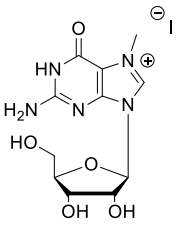

5

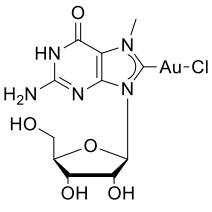

6

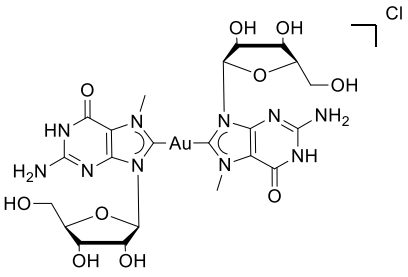

7

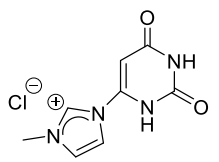

1

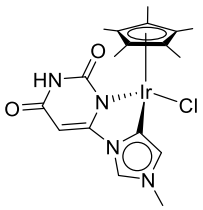

2

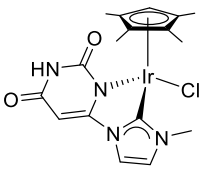

3

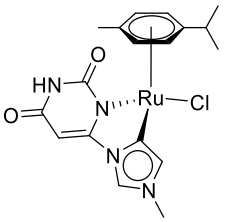

4

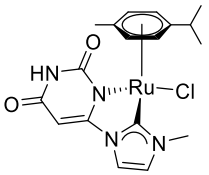

5

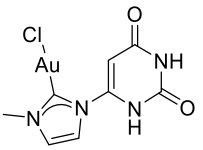

6

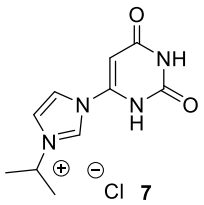

7

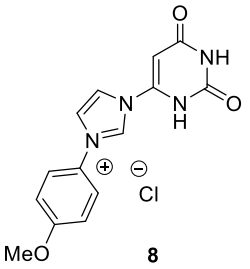

8

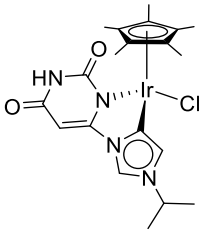

9

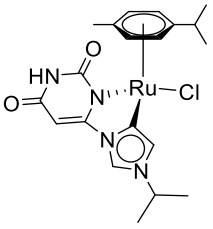

10

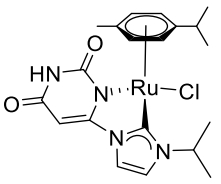

11

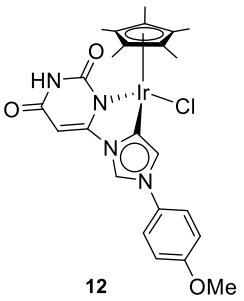
HN
O
O
N
Ir
Cl
N
N
OMe

12

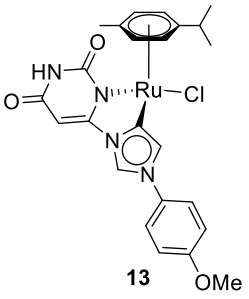
HN
O
O
N
Ru
Cl
N
N
OMe

13

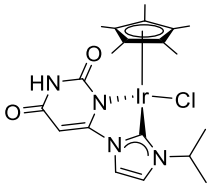
HN
O
O
N
Ir
Cl
N
N

14

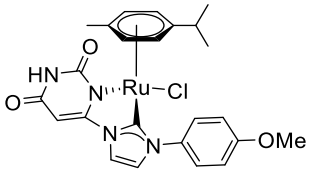
HN
O
O
N
Ru
Cl
N
N
OMe

15

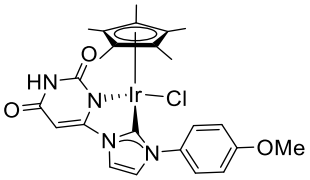
HN
O
O
N
Ir
Cl
N
N
OMe

16

BIBLIOGRAPHY

1. Munz, D. Pushing Electrons - Which Carbene Ligand for Which Application? *Organometallics* 2018, *37* (3), 275–289.

2. Scattolin, T.; Logvinov, A. A.; Tzouras, N. V.; Cazin, C. S. J.; Nolan, S. P. Advances in the Synthesis and Applications of N-Heterocyclic Carbene Metal Complexes with a Focus on the Weak Base Route. *Organometallics* 2023, *42* (19), 2692–2730.

3. Bourissou, D.; Guerret, O.; Gabbaï, F. P.; Bertrand, G. Stable Carbenes. *Chem Rev* 2000, *100* (1), 39–91.

4. Qi, X.; Lan, Y. Recent Advances in Theoretical Studies on Transition-Metal-Catalyzed Carbene Transformations. *Acc Chem Res* 2021, *54* (14), 2905–2915.

5. Line Pauling, B. The Structure of Singlet Carbene Molecules. *J. Chem. Soc., Chem. Commun* 1980, No. 15, 688–689.

6. Arduengo, A. J.; Harlow, R. L.; Kline, M. A Stable Crystalline Carbene. *J Am Chem Soc* 1991, *113* (1), 361–363.

7. Huynh, H. V. Electronic Properties of N-Heterocyclic Carbenes and Their Experimental Determination. *Chem Rev* 2018, *118* (19), 9457–9492.

8. Hopkinson, M. N.; Richter, C.; Schedler, M.; Glorius, F. An Overview of N-Heterocyclic Carbenes. *Nature* 2014, 510, 485–496.

9. Ott, I. Metal N-Heterocyclic Carbene Complexes in Medicinal Chemistry. *Adv Inorg Chem* 2020, *75*, 121–148.

10. Hanif, M.; Hartinger, C. G. Anticancer Metallodrugs: Where Is the next Cisplatin? *Future Med Chem* 2018, *10* (6), 615–617.

11. Leitão, M. I. P. S.; Herrera, F.; Petronilho, A. N-Heterocyclic Carbenes Derived from Guanosine: Synthesis and Evidences of Their Antiproliferative Activity. *ACS Omega* 2018, *3* (11), 15653–15656.

12. Moore, L. D.; Le, T.; Fan, G. DNA Methylation and Its Basic Function. *Neuropsychopharmacology* 2013, 38, 23–38.

13. Lewandowska, J.; Bartoszek, A. DNA Methylation in Cancer Development, Diagnosis and Therapy- Multiple Opportunities for Genotoxic Agents to Act as Methylome Disruptors or Remediators. *Mutagenesis* 2011, 26 (4), 475–487.

14. Gates, K. S. An Overview of Chemical Processes That Damage Cellular DNA: Spontaneous Hydrolysis, Alkylation, and Reactions with Radicals. *Chemical Research in Toxicology* 2009, 22 (11), 1747–1760.

15. Tomasz, M.; Olson, J.; Mercado, C. M. Mechanism of the Isotopic Exchange of the C-8 Hydrogen of Purines in Nucleosides and in Deoxyribonucleic Acidt. *Biochemistry* 1972, 11 (7), 1235–1241

16. Drabløs, F.; Feyzi, E.; Aas, P. A.; Vaagbø, C. B.; Kavli, B.; Bratlie, M. S.; Peña-Diaz, J.; Otterlei, M.; Slupphaug, G.; Krokan, H. E. Alkylation Damage in DNA and RNA- Repair Mechanisms and Medical Significance. *DNA Repair* 2004, 3 (11), 1389–1407.

17. Hemminki, K.; Koskinen, M.; Rajaniemi, H.; Zhao, C. DNA Adducts, Mutations, and Cancer. *Regulatory Toxicology and Pharmacology* 2000, *32* (3), 264–275.

18. Garner, R. C. The Role of DNA Adducts in Chemical Carcinogenesis. *Mutat Res* 1998, *402*, 67–75.

19. Salpin, J.-Y.; Haldys, V.; Latrous, L.; Guillemin, J.-C.; Tortajada, J.; Léon, E.; Mó, O.; Yáñez, M.; Yáñez, Y.; Merced Montero-Campillo, M. Alkylation of Uracil and Thymine in the Gas Phase through Interaction with Alkylmercury Compounds. *Int J Mass Spectrom* 2019, *436*, 153–165.

20. Tretyakova, N.; Villalta, P. W.; Kotapati, S. Mass Spectrometry of Structurally Modified DNA. *Chemical Reviews* 2013, 113 (4), 2395–2436.

21. Tomasz, M. Extreme Lability of the C-8 Proton: A Consequence of 7-Methylation of Guanine Residues in Model Compounds and in DNA and Its Analytical Application. *Biochimica et Biophysica Acta (BBA) - Nucleic Acids and Protein Synthesis* 1970, *199* (1), 18–28.

22. Gates, K. S.; Nooner, T.; Dutta, S. Biologically Relevant Chemical Reactions of M-Alkylguanine Residues in DNA. *Chem Res Toxicol* 2004, *17* (7), 839–856.

23. Kowalski, K. Organometallic Nucleosides-Synthesis, Transformations, and Applications. *Coord Chem Rev* 2020, *432*, 213705.

24. Schollhorn, H.; Thewait, U.; Lippert, B. Ptlll Co-Ordination through C(5) of I-Methyluracil: The First Example of a Pt-Nucleobase Complex Containing a Pt-C Bond. *J. Chem. Soc., Chem. Commun.* 1986, 3, 258-260.

25. Romanelli, A.; Iacovino, R.; Piccialli, G.; Ruffo, F.; De Napoli, L.; Pedone, C.; Blasio, B. Di; Messere, A. Reactions of Pd(PPh3)4 with 3′,5′-Di-O- Acetylthymidine: Oxidative Addition of Pd(PPh3)4 on Thymidine N3 and C4 Atoms. *Organometallics* 2005, *24* (14), 3401–3406.

26. De Napoli, L.; Iacovino, R.; Messere, A.; Montesarchio, D.; Piccialli, G.; Romanelli, A.; Ruffo, F.; Saviano, M. Synthesis of Platinum(II) Complexes of Thymidine and 1-Methyl-Thymine (1-MeThy); Crystal Structure of Cis-[PtCl(1-MeThy)-(PPh 3) 2]. *J. Chem. Soc* 1999, 1945–1949.

27. Leitão, M. I. P. S.; Orsini, G.; Murtinheira, F.; Gomes, C. S. B.; Herrera, F.; Petronilho, A. Synthesis, Base Pairing Properties, and Biological Activity Studies of Platinum(II) Complexes Based on Uracil Nucleosides. *Inorg Chem* 2023, *62* (40), 16412–16425.

28. Schuster, O.; Yang, L.; Raubenheimer, H. G.; Albrecht, M. Beyond Conventional N-Heterocyclic Carbenes: Abnormal, Remote, and Other Classes of NHC Ligands with Reduced Heteroatom Stabilization. *Chem Rev* 2009, *109* (8), 3445–3478.

29. Brackemeyer, D.; Hervé, A.; Schulte To Brinke, C.; Jahnke, M. C.; Hahn, F. E. A Versatile Methodology for the Regioselective C8-Metalation of Purine Bases. *J Am Chem Soc* 2014, *136* (22), 7841–7844.

30. Kampert, F.; Brackemeyer, D.; Tan, T. T. Y.; Ekkehardt Hahn, F. Selective C8-Metalation of Purine Nucleosides via Oxidative Addition. *Organometallics* 2018, *37* (22), 4181–4185.

31. Leitão, M. I. P. S.; Gonzalez, C.; Francescato, G.; Filipiak, Z.; Petronilho, A. On the Reactivity of MRNA Cap0: C-H Oxidative Addition of 7-Methylguanosine to Pt and Base Pairing Studies. *Chemical Communications* 2020, *56* (87), 13365–13368.

32. Mcguinness, D. S.; Cavell, K. J.; Yates, B. F. Unprecedented C-H Bond Oxidative Addition of the Imidazolium Cation to Pt 0 : A Combined Density Functional Analysis and Experimental Study. *Chem. Commun.* 2001, 355–356.

33. Leitão, M. I. P. S.; Turos-Cabal, M.; Sanchez-Sanchez, A. M.; Gomes, C. S. B.; Herrera, F.; Martin, V.; Petronilho, A. Antitumor Activity and Reductive Stress by Platinum(II) N-Heterocyclic Carbenes Based on Guanosine**. *Chemistry - A European Journal* 2023, *29* (40).

34. Leitão, M. I. P. S.; Francescato, G.; Gomes, C. S. B.; Petronilho, A. Synthesis of Platinum(II) N-Heterocyclic Carbenes Based on Adenosine. *Molecules* 2021, *26* (17), 5384.

35. Price, C.; Elsegood, M. R. J.; Clegg, W.; Rees, N. H.; Houlton, A. Evidence for Directed Metalation: A Structural Intermediate in the Formation of a Novel C-Bound Adenine Complex of Ruthenium. *Angewandte Chemie Int. Ed.* 1997, *36* (16), 1762–1764.

36. Brackemeyer, D.; Schulte To Brinke, C.; Roelfes, F.; Hahn, F. E. Regioselective C8-Metalation of N-Phosphine Tethered Adenine Derivatives via C8-H Activation. *Dalton Transaction commun.* 2017, *46*, 4510–4513.

37. Hille, R.; Nishino, T. Xanthine Oxidase and Xanthine Dehydrogenase. *The FASEB Journal* 1995, *9* (11), 995–1003.

38. Belotti, D.; Kampert, F.; Jahnke, M. C.; Hahn, F. E. Oxidative Addition of a 8-Bromotheobromine Derivative to D10metals. *Zeitschrift fur Naturforschung - Section B Journal of Chemical Sciences* 2021, *76* (3–4), 227–235.

39. Krentzien, H. J.; Clarke, M. J.; Taube, H. Crystal Structure of a Compound Featuring Caffeine Bound at C8 to Ruthenium (III). *Bioinorg Chem* 1975, *4* (2), 143–151.

40. Clarke, M. J.; Taube, H. Nitrogen-Bound and Carbon-Bound Xanthine Complexes of Ruthenium Ammines. *J Am Chem Soc* 1975, *97* (6), 1397–1403.

41. Beck, W.; Kottmair, N. Neue Übergangsmetallkomplexe Mit Nuclein-Basen Und Nucleosiden. *Chem Ber* 1976, *109* (3), 970–993.

42. Kascatan-Nebioglu, A.; Panzner, M. J.; Garrison, J. C.; Tessier, C. A.; Youngs, W. J. Synthesis and Structural Characterization of N-Heterocyclic Carbene Complexes of Silver(I) and Rhodium(I) from Caffeine. *Organometallics* 2004, *23* (8), 1928–1931.

43. Mokfi, M.; Rust, J.; Lehmann, C. W.; Mohr, F. Facile N9-Alkylation of Xanthine Derivatives and Their Use as Precursors for N-Heterocyclic Carbene Complexes. *Molecules* 2021, *26* (12), 3705.

44. Schü Tz, J.; Herrmann, W. A. Purine-Based Carbenes at Rhodium and Iridium I. *J. of Organometallic Chemistry* 2004, 689 (19), 2995-2999

45. Mohammadi, E.; Movassagh, B. Synthesis of Polystyrene-Supported Pd(II)-NHC Complex Derived from Theophylline as an Efficient and Reusable Heterogeneous Catalyst for the Heck-Matsuda Cross-Coupling Reaction. *J Mol Catal A Chem* 2016, 158–167.

46. Scattolin, T.; Caligiuri, I.; Canovese, L.; Demitri, N.; Gambari, R.; Lampronti, I.; Rizzolio, F.; Santo, C.; Visentin, F. Synthesis of New Allyl Palladium Complexes Bearing Purine-

Based NHC Ligands with Antiproliferative and Proapoptotic Activities on Human Ovarian Cancer Cell Lines. *Dalton Trans.* 2018, *47* (38), 13616–13630.

47. Colotti, G.; Ilari, A.; Boffi, A.; Morea, V. Metals and Metal Derivatives in Medicine. *Mini-Reviews in Medicinal Chemistry* 2013, *13* (2), 211–221.

48. Rai, M.; Yadav, A.; Gade, A. Silver Nanoparticles as a New Generation of Antimicrobials. *Biotechnol Adv* 2009, *27* (1), 76–83.

49. Kean, W. F.; Hart, L.; Buchanan, W. W. *Auranofin*; *British Journal of Rheumatology* 1997, 36, 560-572.

50. Rosenberg, B.; VanCamp, L.; Trosko, J. E.; Mansour, V. H. Platinum Compounds: A New Class of Potent Antitumour Agents. *Nature* 1969, *222* (5191), 385–386.

51. Mohammadi, S.; Maghsoudloo, M.; Maroufi, M. Micro Nano Bio Aspects Antioxidant, Antineurodegenerative, Anticancer, and Antimicrobial Activities of Caffeine and Its Derivatives: Micro and Nano Aspects. *Micro Nano Bio Aspects* 2023, *2023* (3), 32–37.

52. Singh, N.; Shreshtha, A. K.; Thakur, M. S.; Patra, S. Xanthine Scaffold: Scope and Potential in Drug Development. *Heliyon* 2018, *4* (10), e00829.

53. Monteiro, J. P.; Alves, M. G.; Oliveira, P. F.; Silva, B. M. Structure-Bioactivity Relationships of Methylxanthines: Trying to Make Sense of All the Promises and the Drawbacks. *Molecules* 2016, *21* (8), 974.

54. Kascatan-Nebioglu, A.; Melaiye, A.; Hindi, K.; Durmus, S.; Panzner, M. J.; Hogue, L. A.; Mallett, R. J.; Hovis, C. E.; Coughenour, M.; Crosby, S. D.; Milsted, A.; Ely, D. L.; Tessier, C. A.; Cannon, C. L.; Youngs, W. J. Synthesis from Caffeine of a Mixed N-Heterocyclic Carbene-Silver Acetate Complex Active against Resistant Respiratory Pathogens. *J Med Chem* 2006, *49* (23), 6811–6818.

55. Kascatan-Nebioglu, A.; Panzner, M. J.; Tessier, C. A.; Cannon, C. L.; Youngs, W. J. N-Heterocyclic Carbene–Silver Complexes: A New Class of Antibiotics. *Coord Chem Rev* 2007, *251* (5–6), 884–895.

56. Vanlalveni, C.; Lallianrawna, S.; Biswas, A.; Selvaraj, M.; Changmai, B.; Rokhum, S. L. Green Synthesis of Silver Nanoparticles Using Plant Extracts and Their Antimicrobial Activities: A Review of Recent Literature. *RSC Adv* 2021, *11* (5), 2804–2837

57. Anees Ahmad, S.; Sachi Das, S.; Khatoon, A.; Tahir Ansari, M.; Afzal, M.; Saquib Hasnain, M.; Kumar Nayak, A. Bactericidal Activity of Silver Nanoparticles: A Mechanistic Review. *Mater Sci Energy Technol* 2020, *3*, 756–769.

58. Mohamed, H. A.; Lake, B. R. M.; Laing, T.; Phillips, R. M.; Willans, C. E. Synthesis and Anticancer Activity of Silver(i)–N-Heterocyclic Carbene Complexes Derived from the Natural Xanthine Products Caffeine, Theophylline and Theobromine. *Dalton Transaction* 2015, *44* (16), 7563–7569.

59. Holmes, J.; Kearsey, R. J.; Paske, K. A.; Singer, F. N.; Atallah, S.; Pask, C. M.; Phillips, R. M.; Willans, C. E. Tethered N-Heterocyclic Carbene-Carboranyl Silver Complexes for Cancer Therapy. *Organometallics* 2019, *38* (12), 2530–2538.

60. Khanna, S.; Jana, B.; Saha, A.; Kurkute, P.; Ghosh, S.; Verma, S. Targeting Cytotoxicity and Tubulin Polymerization by Metal–Carbene Complexes on a Purine Tautomer Platform. *Dalton Transactions* 2014, *43* (26), 9838–9842.

61. Moreno-Alcántar, G.; Picchetti, P.; Casini, A. Gold Complexes in Anticancer Therapy: From New Design Principles to Particle-Based Delivery Systems. *Angewandte Chemie – Int. Ed.* 2023, 62, e2022180.

62. Casini, A.; Sun, R. W. Y.; Ott, I. Medicinal Chemistry of Gold Anticancer Metallodrugs. In *Metallo-Drugs: Development and Action of Anticancer Agents*; Walter de Gruyter GmbH, 2018, 199–217.

63. Wragg, D.; de Almeida, A.; Bonsignore, R.; Kühn, F. E.; Leoni, S.; Casini, A. On the Mechanism of Gold/NHC Compounds Binding to DNA G-Quadruplexes: Combined Metadynamics and Biophysical Methods. *Angewandte Chemie* 2018, *130* (44), 14732–14736.

64. Estrada-Ortiz, N.; Guarra, F.; de Graaf, I. A. M.; Marchetti, L.; de Jager, M. H.; Groothuis, G. M. M.; Gabbiani, C.; Casini, A. Anticancer Gold N-Heterocyclic Carbene Complexes: A Comparative in Vitro and Ex Vivo Study. *ChemMedChem* 2017, *12* (17), 1429–1435.

65. Bertrand, B.; Stefan, L.; Pirrotta, M.; Monchaud, D.; Bodio, E.; Richard, P.; Le Gendre, P.; Warmerdam, E.; De Jager, M. H.; Groothuis, G. M. M.; Picquet, M.; Casini, A. Caffeine-Based Gold(I) N-Heterocyclic Carbenes as Possible Anticancer Agents: Synthesis and Biological Properties. *Inorg Chem* 2014, *53* (4), 2296–2303.

66. Meier-Menches, S. M.; Neuditschko, B.; Zappe, K.; Schaier, M.; Gerner, M. C.; Schmetterer, K. G.; Del Favero, G.; Bonsignore, R.; Cichna-Markl, M.; Koellensperger, G.; Casini, A.; Gerner, C. An Organometallic Gold(I) Bis-N-Heterocyclic Carbene Complex with Multimodal Activity in Ovarian Cancer Cells. *Chemistry - A European Journal* 2020, *26* (67), 15528–15537.

67. Zhang, J.-J.; Muenzner, J. K.; Abu El Maaty, M. A.; Karge, B.; Schobert, R.; Wölfl, S.; Ott, I. A Multi-Target Caffeine Derived Rhodium(I) N-Heterocyclic Carbene Complex: Evaluation of the Mechanism of Action. *Dalton Transactions* 2016, *45*, 13161.

68. Zhang, J.-J.; Che, C.-M.; Ott, I. Caffeine Derived Platinum(II) N-Heterocyclic Carbene Complexes with Multiple Anti-Cancer Activities. *J. Organometallic Chemistry* 2014, 782 (15), 37-41.

69. Perlin, D. S.; Rautemaa-Richardson, R.; Alastruey-Izquierdo, A. The Global Problem of Antifungal Resistance: Prevalence, Mechanisms, and Management. *Lancet* 2017, 17 (12), 383-392.

70. Denning, D. W.; Bromley, M. J. How to Bolster the Antifungal Pipeline: Few Drugs Are Coming to Market, but Opportunities for Drug Development Exist. *Science* 2015, *347* (6229), 1414–1416.

71. Azie, N.; Neofytos, D.; Pfaller, M.; Meier-Kriesche, H. U.; Quan, S. P.; Horn, D. The PATH (Prospective Antifungal Therapy) Alliance® Registry and Invasive Fungal Infections: Update 2012. *Diagnostic Microbiology and Infectious Disease* 2012, 73 (4), 293–300.

72. Gupta, A. K.; Venkataraman, M.; Renaud, H. J.; Summerbell, R.; Shear, N. H.; Piguet, V. The Increasing Problem of Treatment-Resistant Fungal Infections: A Call for Antifungal Stewardship Programs. *Int. J. of Dermatology 2021, 60 (12),* e474-e479.

73. Cowen, L. E.; Sanglard, D.; Howard, S. J.; Rogers, P. D.; Perlin, D. S. Mechanisms of Antifungal Drug Resistance. *Cold Spring Harb Perspect Med* 2015, *5* (7).

74. Morita, Y.; Teixeira, M. C.; Keniya, M.; Sanglard, D. Emerging Threats in Antifungal-Resistant Fungal Pathogens. 2016, *3*, 1.

75. Musial, C. E.; Cockerill, F. R.; Roberts, G. D. Fungal Infections of the Immunocompromised Host: Clinical and Laboratory Aspects. *Clin Microbiol Rev* 1988, *1* (4), 349–364.

76. Baddley, J. W.; Patel, M.; Bhavnani, S. M.; Moser, S. A.; Andes, D. R. Association of Fluconazole Pharmacodynamics with Mortality in Patients with Candidemia. *Antimicrob Agents Chemother* 2008, *52* (9), 3022–3028.

77. Alexander, B. D.; Johnson, M. D.; Pfeiffer, C. D.; Jiménez-Ortigosa, C.; Catania, J.; Booker, R.; Castanheira, M.; Messer, S. A.; Perlin, D. S.; Pfaller, M. A. Increasing Echinocandin Resistance in Candida Glabrata: Clinical Failure Correlates With Presence of FKS Mutations and Elevated Minimum Inhibitory Concentrations. *Clinical Infectious Diseases* 2013, 56 (12), 1724–1732.

78. Pappas, P. G.; Lionakis, M. S.; Cavling Arendrup, M.; Ostrosky-Zeichner, L.; Jan Kullberg, B. Invasive Candidiasis. *Nature* 2018, *4*.

79. Teixeira, M. M.; Carvalho, D. T.; Sousa, E.; Pinto, E. New Antifungal Agents with Azole Moieties. *Pharmaceuticals* 2022, *15* (11), 1427.

80. Maertens, J. A. History of the Development of Azole Derivatives. *Clinical Microbiology and Infection* 2004, *10* (1), 1–10.

81. Heel, R. C.; Brogden, R. N.; Carmine, A.; Morley, P. A.; Speight T. M.; Avery G. S.; Ketoconazole: A Review of its Therapeutic Efficacy in Superficial and Systemic Fungal Infections. *Drugs* 1982, 23, 1-36.

82. Allen, D.; Wilson, D.; Drew, R.; Perfect, J. Azole Antifungals: 35 Years of Invasive Fungal Infection Management. *Expert Rev Anti Infect Ther* 2015, *13* (6), 787–798.

83. Shafiei, M.; Peyton, L.; Hashemzadeh, M.; Foroumadi, A. History of the Development of Antifungal Azoles: A Review on Structures, SAR, and Mechanism of Action. *Bioorg Chem* 2020, 104, 104240.

84. Sheehan, D. J.; Hitchcock, C. A.; Sibley, C. M. Current and Emerging Azole Antifungal Agents. *Clin Microbiol Rev* 1999, *12* (1), 40–79.

85. Georgopapadakou, N. H.; Walsh, T. J. Antifungal Agents: Chemotherapeutic Targets and Immunologic Strategies. *Antimicrob Agents Chemother* 1996, *40* (2), 279–291.

86. Odds, F. C.; Brown, A. J. P.; Gow, N. A. R. Antifungal Agents: Mechanisms of Action. *Trends in Microbiology* 2003, 11 (6), 271-279.

87. White, T. C.; Marr, K. A.; Bowden, R. A. Clinical, Cellular, and Molecular Factors That Contribute to Antifungal Drug Resistance. *Clin Microbiol Rev* 1998, *11* (2), 382–402.

88. Fisher, M. C.; Alastruey-Izquierdo, A.; Berman, J.; Bicanic, T.; Bignell, E. M.; Bowyer, P.; Bromley, M.; Brüggemann, R.; Garber, G.; Cornely, O. A.; Gurr, S. J.; Harrison, T. S.;

Kuijper, E.; Rhodes, J.; Sheppard, D. C.; Warris, A.; White, P. L.; Xu, J.; Zwaan, B.; Verweij, P. E. Tackling the Emerging Threat of Antifungal Resistance to Human Health. *Nat Rev Microbiol* 2022, *20* (9), 557–571.

89. Fidel, P. L.; Vazquez, J. A.; Sobel, J. D. Candida Glabrata: Review of Epidemiology, Pathogenesis, and Clinical Disease with Comparison to C. Albicans. *Clin Microbiol Rev* 1999, *12* (1), 80–96.

90. Healey, K. R.; Zhao, Y.; Perez, W. B.; Lockhart, S. R.; Sobel, J. D.; Farmakiotis, D.; Kontoyiannis, D. P.; Sanglard, D.; Taj-Aldeen, S. J.; Alexander, B. D.; Jimenez-Ortigosa, C.; Shor, E.; Perlin, D. S. ARTICLE Prevalent Mutator Genotype Identified in Fungal Pathogen Candida Glabrata Promotes Multi-Drug Resistance. *Antimicrob Agents Chemother.* 2019, 63 (1), e01692-18.

91. Perfect, J. R.; Ghannoum, M. Emerging Issues in Antifungal Resistance. *Infect Dis Clin North Am* 2020, *34* (4), 921–943.

92. Fisher, M. C.; Hawkins, N. J.; Sanglard, D.; Gurr, S. J. Worldwide Emergence of Resistance to Antifungal Drugs Challenges Human Health and Food Security. *Science* 2018, 360 (6390), 739-742.

93. Frei, A.; Verderosa, A. D.; Elliott, A. G.; Zuegg, J.; Blaskovich, M. A. T. Metals to Combat Antimicrobial Resistance. *Nature Reviews Chemistry* 2023, *7* (3), 202–224.

94. Lin, Y.; Betts, H.; Keller, S.; Cariou, K.; Gasser, G. Recent Developments of Metal-Based Compounds against Fungal Pathogens. *Chem Soc Rev* 2021, *50* (18), 10346–1040.

95. Frei, A.; Zuegg, J.; Elliott, A. G.; Baker, M.; Braese, S.; Brown, C.; Chen, F.; G. Dowson, C.; Dujardin, G.; Jung, N.; King, A. P.; Mansour, A. M.; Massi, M.; Moat, J.; Mohamed, H. A.; Renfrew, A. K.; Rutledge, P. J.; Sadler, P. J.; Todd, M. H.; Willans, C. E.; Wilson, J. J.; Cooper, M. A.; Blaskovich, M. A. T. Metal Complexes as a Promising Source for New Antibiotics. *Chem Sci* 2020, *11* (10), 2627–2639.

96. Frei, A.; Elliott, A. G.; Kan, A.; Dinh, H.; Bräse, S.; Bruce, A. E.; Bruce, M. R.; Chen, F.; Humaidy, D.; Jung, N.; King, A. P.; Lye, P. G.; Maliszewska, H. K.; Mansour, A. M.; Matiadis, D.; Muñoz, M. P.; Pai, T. Y.; Pokhrel, S.; Sadler, P. J.; Sagnou, M.; Taylor, M.; Wilson, J. J.; Woods, D.; Zuegg, J.; Meyer, W.; Cain, A. K.; Cooper, M. A.; Blaskovich, M. A. T. Metal Complexes as Antifungals? From a Crowd-Sourced Compound Library to the First in Vivo Experiments. *JACS Au* 2022, *2* (10), 2277–2294.

97. Faudone, G.; Arifi, S.; Merk, D. The Medicinal Chemistry of Caffeine. *J Med Chem* 2021, *64* (11), 7156–7178.

98. Monteiro, J.; Alves, M. G.; Oliveira, P. F.; Silva, B. M. Pharmacological Potential of Methylxanthines: Retrospective Analysis and Future Expectations. *Crit Rev Food Sci Nutr* 2019, *59* (16), 2597–2625.

99. Singh, N.; Kumar Shreshtha, A.; Thakur, M. S.; Patra, S. Xanthine Scaffold: Scope and Potential in Drug Development. *Heliyon* 2018, *4*, 829.

100. Schüttelkopf, A. W.; Andersen, O. A.; Rao, F. V.; Allwood, M.; Lloyd, C.; Eggleston, I. M.; Van Aalten, D. M. F. Screening-Based Discovery and Structural Dissection of a Novel Family 18 Chitinase Inhibitor. *Journal of Biological Chemistry* 2006, *281* (37), 27278–27285.

101. Hayallah, A. M.; Elgaher, W. A.; Salem, O. I.; Abdel Alim, A. A. M. Design and Synthesis of Some New Theophylline Derivatives with Bronchodilator and Antibacterial Activities. *Arch Pharm Res* 2011, *34* (1), 3–21.

102. Eslava-Gonzalez, I.; Valdés, H.; Teresa Ramírez-Apan, M.; Hernandez-Ortega, S.; Rosario Zermeño-Ortega, M.; Avila-Sorrosa, A.; Morales-Morales, D. Synthesis of Theophylline-Based Iridium(I) N-Heterocyclic Carbene Complexes Including Fluorinated-Thiophenolate Ligands. Preliminary Evaluation of Their in Vitro Anticancer Activity. *Inorganica Chim Acta* 2020, *507*, 119588.

103. Mohamed, H. A.; Lake, B. R. M.; Laing, T.; Phillips, R. M.; Willans, C. E. Synthesis and Anticancer Activity of Silver(I)–N-Heterocyclic Carbene Complexes Derived from the Natural Xanthine Products Caffeine, Theophylline and Theobromine. *Dalton Transactions* 2015, *44*, 7563.

104. Zhang, J.-J.; Che, C.-M.; Ott, I. Caffeine Derived Platinum(II) N-Heterocyclic Carbene Complexes with Multiple Anti-Cancer Activities. *J. of Organometalloc Chemistry* 2014, 782, 37-41

105. Zhang, J.-J.; Muenzner, J. K.; Abu El Maaty, M. A.; Karge, B.; Schobert, R.; Wölfl, S.; Ott, I. A Multi-Target Caffeine Derived Rhodium(I) N-Heterocyclic Carbene Complex: Evaluation of the Mechanism of Action. 2016, *45*, 13161.

106. Holmes, J.; Kearsey, R. J.; Paske, K. A.; Singer, F. N.; Atallah, S.; Pask, C. M.; Phillips, R. M.; Willans, C. E. Tethered N-Heterocyclic Carbene-Carboranyl Silver Complexes for Cancer Therapy. *Organometallics* 2019, *38* (12), 2530–2538.

107. Luo, F. T.; Lo, H. K. Short Synthesis of Bis-NHC-Pd Catalyst Derived from Caffeine and Its Applications to Suzuki, Heck, and Sonogashira Reactions in Aqueous Solution. *J Organomet Chem* 2011, *696* (6), 1262–1265.

108. Banach; Guńka, P. A.; Zachara, J.; Buchowicz, W. Half-Sandwich Ni(II) Complexes [Ni(Cp)(X)(NHC)]: From an Underestimated Discovery to a New Chapter in Organonickel Chemistry. *Coordination Chemistry Reviews* 2019, 389, 19–58.

109. Vellé, A.; Cebollada, A.; Macías, R.; Iglesias, M.; Gil-Moles, M.; Sanz Miguel, P. J. From Imidazole toward Imidazolium Salts and N-Heterocyclic Carbene Ligands: Electronic and Geometrical Redistribution. *ACS Omega* 2017, *2* (4), 1392–1399.

110. Włodarska, A.; Kozioł, A.; Dranka, M.; Gryff-Keller, A.; Szczeciński, P.; Jurkowski, J.; Pietrzykowski, A. Synthesis, Structure, and Solution Dynamic Behavior of Nickel Complexes Bearing a 1,3-Diallyl-Substituted NHC Ligand. *Organometallics* 2015, *34* (3), 577–581.

111. Hahn, E. F.; Heidrich, B.; Hepp, A.; Pape, T. Coordination Compounds of N,N 0-Olefin Functionalized Imidazolin-2-Ylidenes. *J. Organometallic Chemistry* 2007, 692, 4630–4638.

112. Wei, Y.; Petronilho, A.; Mueller-Bunz, H.; Albrecht, M. Mesoionic Triazolylidene Nickel Complexes: Synthesis, Ligand Lability, and Catalytic C-C Bond Formation Activity. *Organometallics* 2014, *33* (20), 5834–5844.

113. Kelly, R. A.; Scott, N. M.; Díez-González, S.; Stevens, E. D.; Nolan, S. P. Simple Synthesis of CpNi(NHC)Cl Complexes. *Organometallics* 2005, *24* (14), 3442–3447.

114. Ritleng, V.; Barth, C.; Brenner, E.; Milosevic, S.; Chetcuti, M. J. Synthesis, Structure, and Solution Dynamics of Pentamethylcyclopentadienyl Nickel Complexes Bearing N-Heterocyclic Carbene Ligands. *Organometallics* 2008, *27* (16), 4223–4228.

115. Oertel, A. M.; Ritleng, V.; Chetcuti, M. J.; Veiros, L. F. C-H Activation of Acetonitrile at Nickel: Ligand Flip and Conversion of N-Bound Acetonitrile into a C-Bound Cyanomethyl Ligand. *J Am Chem Soc* 2010, *132* (39), 13588–13589.

116. Luca, O. R.; Thompson, B. A.; Takase, M. K.; Crabtree, R. H. Synthesis and Electrochemistry of a Series of Cyclopentadienyl Ni N-Heterocyclic Carbene Compounds. *J. of Organometallic Chemistry* 2013, 730, 79–83.

117. Wei, Y.; Liu, S. X.; Mueller-Bunz, H.; Albrecht, M. Synthesis of Triazolylidene Nickel Complexes and Their Catalytic Application in Selective Aldehyde Hydrosilylation. *ACS Catal* 2016, *6* (12), 8192–8200.

118. Mejuto, C.; Royo, B.; Guisado-Barrios, G.; Peris, E. Rhodium, Iridium and Nickel Complexes with a 1,3,5-Triphenyl-Benzene Tris-MIC Ligand. Study of the Electronic Properties and Catalytic Activities. *Beilstein J. Org. Chem* 2015, *11*, 2584–2590.

119. Włodarska, A.; Gołaszewska-Gajda, J.; Dranka, M.; Pietrzykowski, A. Synthesis, Characterization and Catalytic Activity of Nickel NHC Complexes. *Molecular Catalysis* 2017, *440*, 25–35.

120. Guisado-Barrios, G.; Bouffard, J.; Donnadieu, B.; Bertrand, G. Crystalline 1H-l,2,3-Triazol-5-Ylidenes: New Stable Mesoionic Carbenes (MICs). *Angewandte Chemie - International Edition* 2010, *49* (28), 4759–4762.

121. Włodarska, A.; Kozioł, A.; Dranka, M.; Gryff-Keller, A.; Szczeciński, P.; Jurkowski, J.; Pietrzykowski, A. Synthesis, Structure, and Solution Dynamic Behavior of Nickel Complexes Bearing a 1,3-Diallyl-Substituted NHC Ligand. *Organometallics* 2015, *34* (3), 577–581.

122. Kidd, S. E.; Crawford, L. C.; Halliday, C. L. Antifungal Susceptibility Testing and Identification. *Infectious Disease Clinics* 2021, *35* (2), 313–339.

123. Ben-Ami, R. Treatment of Invasive Candidiasis: A Narrative Review. *J. Fungi* 2018, 4(3).

124. Schoonen, W. G. E. J.; Westerink, W. M. A.; De Roos, J. A. D. M.; Débiton, E. Cytotoxic Effects of 100 Reference Compounds on Hep G2 and HeLa Cells and of 60 Compounds on ECC-1 and CHO Cells. I Mechanistic Assays on ROS, Glutathione Depletion and Calcein Uptake. *Toxicol In Vitro* 2005, 19(4), 505-16.

125. Gaspar-Cordeiro, A.; da Silva, S.; Aguiar, M.; Rodrigues-Pousada, C.; Haas, H.; Lima, L. M. P.; Pimentel, C. A Copper(II)-Binding Triazole Derivative with Ionophore Properties Is Active against Candida Spp. *Journal of Biological Inorganic Chemistry* 2020, *25* (8), 1117–1128.

126. Tan, T. T. Y.; Hahn, F. E. Synthesis of Iridium(III) and Rhodium(III) Complexes Bearing C8-Metalated Theophylline Ligands by Directed C-H Activation. *Organometallics* 2019, *38* (9), 2250–2258.

127. Soltani Rad, M. N.; Behrouz, S.; Najafi, H. N7-Tosyltheophylline (TsTh): A Highly Efficient Reagent for the One-Pot Synthesis of N7-Alkyltheophyllines from Alcohols. *Synthesis* 2014, *46* (10), 1380–1388.

128. Daly, J. W.; Padgett, W. L.; Shamim, M.T. Analogues of Caffeine and Theophylline: Effect of Structural Alterations on Affinity at Adenosine Receptors. *Journal of Medicinal Chemistry* 1986, 29 (7), 1305-1308.

129. Kaußler, C.; Wragg, D.; Schmidt, C.; Moreno-Alcántar, G.; Jandl, C.; Stephan, J.; Fischer, R. A.; Leoni, S.; Casini, A.; Bonsignore, R. "dynamical Docking" of Cyclic Dinuclear Au(I) Bis-N-Heterocyclic Complexes Facilitates Their Binding to G-Quadruplexes. *Inorg Chem* 2022, *61* (50), 20405–20423.

130. Wang, M.; Wang, Z.; Zhang, J.; Fei, T.; Zhang, J. Synthesis and Properties of Bio-Renewable Ionic Salts Derived from Theophylline as Green Hypergolic Fuels. *J Mol Liq* 2023, *372*.

131. De Clercq, E.; Walker, R. T.; Ellis, G. P.; West, G. B.; Chu, C. K.; Cutler, S. J. ; M. J.; Hatfield, P. W.; Balzarini, J.; Fyfe, J. A.; Keller, P. M.; Furman, P. A.; Miller, R. L.; Elion, G. B.; Miller, W. H. Collaborative DHPG Treatment Study Group. *Journal of Medicinal Chemistry* 1988, 31, 1351-1355.

132. Krause, L.; Herbst-Irmer, R.; Sheldrick, G. M.; Stalke, D. Comparison of Silver and Molybdenum Microfocus X-Ray Sources for Single-Crystal Structure Determination. *J Appl Crystallogr* 2015, *48* (1), 3–10.

133. Sheldrick, G. M. Crystal Structure Refinement with SHELXL. *Acta Crystallogr C Struct Chem* 2015, *71* (1), 3–8.

134. Hübschle, C. B.; Sheldrick, G. M.; Dittrich, B. ShelXle: A Qt Graphical User Interface for SHELXL. *J Appl Crystallogr* 2011, *44* (6), 1281–1284.

135. Farrugia, L. J. WinGX and ORTEP for Windows: An Update. *J Appl Crystallogr* 2012, *45* (4), 849–854.

136. Specificites, A. S.; Martin, S. A.; Moss, B. mRNA Guanylyltransferase and mRNA (Guanine-7-)-Methyltransferase from Vaccinia Virions; *J. Of Biological Chemistry* 1976, 251 (23), 7313-7321.

137. Banerjee, A. K. 5'-Terminal Cap Structure in Eucaryotic Messenger Ribonucleic Acids; *Microbiological Review* 1980, 44, 175-205.

138. Shatkin, A. J. *Capping of Eucaryotic MRNAs. Cell* 1976, 9, 645-653.

139. Shuman, S. Structure, Mechanism, and Evolution of the MRNA Capping Apparatus. *Progress in Nucleic Acid Research and Molecular Biology* 2001, 66, 1-40.

140. RNA Splicing | Learn Science at Scitable. https://www.nature.com/scitable/topicpage/rna-splicing-introns-exons-and-spliceosome-12375/ (accessed 4/01/2024)

141. Ghosh, A.; Lima, C. D. Enzymology of RNA Cap Synthesis. *Wiley Interdisciplinary Reviews: RNA* 2010, 1, 152–172.

142. Ramanathan, A.; Robb, G. B.; Chan, S. H. MRNA Capping: Biological Functions and Applications. *Nucleic Acids Research* 2016, 44 (16),7511–7526.

143. Furuichi, Y. Discovery of M7G-Cap in Eukaryotic MRNAs. *Proceedings of the Japan Academy Series B: Physical and Biological Sciences* 2015, 91 (8), 394–409.

144. Kean, W. F.; Lock, C. J. L.; Howard-Lock, H. gold complex research in medical science. difficulties with experimental design. *Inflammopharmacology* 1991, 1, 103-114.

145. Di Sarra, F.; Fresch, B.; Bini, R.; Saielli, G.; Bagno, A. Reactivity of Auranofin with Selenols and Thiols- Implications for the Anticancer Activity of Gold(I) Compounds. *Eur J Inorg Chem* 2013, No. 15, 2718–2727.

146. Shen, S.; Shen, J.; Luo, Z.; Wang, F.; Min, J. Molecular Mechanisms and Clinical Implications of the Gold Drug Auranofin. *Coord Chem Rev* 2023, *493*, 215323.

147. Pratesi, A.; Gabbiani, C.; Michelucci, E.; Ginanneschi, M.; Papini, A. M.; Rubbiani, R.; Ott, I.; Messori, L. Insights on the Mechanism of Thioredoxin Reductase Inhibition by Gold N-Heterocyclic Carbene Compounds Using the Synthetic Linear Selenocysteine Containing C-Terminal Peptide HTrxR(488-499): An ESI-MS Investigation. *J Inorg Biochem* 2014, 136, 161-169.

148. Bindoli, A.; Rigobello, M. P.; Scutari, G.; Gabbiani, C.; Casini, A.; Messori, L. Thioredoxin Reductase: A Target for Gold Compounds Acting as Potential Anticancer Drugs. *Coord Chem Rev* 2009, *253* (11–12), 1692–1707.

149. Ott, I. On the Medicinal Chemistry of Gold Complexes as Anticancer Drugs. *Coordination Chemistry Reviews* 2009, 253 (11), 1670–1681.

150. Holenya, P.; Can, S.; Rubbiani, R.; Alborzinia, H.; Jünger, A.; Cheng, X.; Ott, I.; Wölfl, S. Detailed Analysis of Pro-Apoptotic Signaling and Metabolic Adaptation Triggered by a N-Heterocyclic Carbene-Gold(i) Complex. *Metallomics* 2014, *6* (9), 1591–1601.

151. Zou, T.; Lok, C. N.; Wan, P. K.; Zhang, Z. F.; Fung, S. K.; Che, C. M. Anticancer Metal-N-Heterocyclic Carbene Complexes of Gold, Platinum and Palladium. *Current Opinion in Chemical Biology* 2018, 43, 30–36.

152. Lopes-Nunes, J.; Oliveira, P. A.; Cruz, C. G-Quadruplex-Based Drug Delivery Systems for Cancer Therapy. *Pharmaceuticals* 2021, 14 (7), 671.

153. Nakanishi, C.; Seimiya, H. G-Quadruplex in Cancer Biology and Drug Discovery. *Biochem Biophys Res Commun* 2020, *531* (1), 45–50.

154. Awadasseid, A.; Ma, X.; Wu, Y.; Zhang, W. NC-ND License G-Quadruplex Stabilization via Small-Molecules as a Potential Anti-Cancer Strategy. *Biomedicine & Pharmacotherapy* 2021, 139, 111550

155. Collie, G. W.; Parkinson, G. N. The Application of DNA and RNA G-Quadruplexes to Therapeutic Medicines. *Chem Soc Rev* 2011, *40* (12), 5867–5892.

156. Bernal, A.; Tusell, L. Telomeres: Implications for Cancer Development. *International Journal of Molecular Sciences* 2018. 19 (1), 294.

157. Izumi, H.; Funa, K. Telomere Function and the G-Quadruplex Formation Are Regulated by HnRNP U. *Cells* 2019, *8* (5).

158. Siddiqui, G.; Stebani, J.; Wragg, D.; Koutsourelakis, P.-S.; Casini, A.; Gagliardi, A. Application of Machine Learning Algorithms to Metadynamics for the Elucidation of the Binding Modes and Free Energy Landscape of Drug/Target Interactions: A Case Study. *Chemistry – A European Journal* 2023, e202302375.

159. Stefan, L.; Bertrand, B.; Richard, P.; Le Gendre, P.; Denat, F.; Picquet, M.; Monchaud, D. Assessing the Differential Affinity of Small Molecules for Noncanonical DNA Structures. *ChemBioChem* 2012, *13* (13), 1905–1912.

160. Sessler, J. L.; Jayawickramarajah, J. Functionalized Base-Pairs: Versatile Scaffolds for Self-Assembly. *Chem. Commun.* 2005, 15, 1939–1949.

161. Huynh, H. V.; Guo, S.; Wu, W. Detailed Structural, Spectroscopic, and Electrochemical Trends of Halido Mono- and Bis(NHC) Complexes of Au(I) and Au(III). *Organometallics* 2013, *32* (16), 4591–4600.

162. Collado, A.; Gómez-Suárez, A.; Martin, A. R.; Slawin, A. M. Z.; Nolan, S. P. Straightforward Synthesis of [Au(NHC)X] (NHC =N-Heterocyclic Carbene, X = Cl, Br, I) Complexes. *Chemical Communications* **2013**, *49* (49), 5541–5543.

163. Visbal, R.; Laguna, A.; Concepción Gimeno, M. Simple and Efficient Synthesis of [MCl(NHC)] (M = Au, Ag) Complexes. *Chemical Communications* **2013**, *49* (50), 5642–5644.

164. Tresin, F.; Stoppa, V.; Baron, M.; Biffis, A.; Annunziata, A.; D'Elia, L.; Monti, D. M.; Ruffo, F.; Roverso, M.; Sgarbossa, P.; Bogialli, S.; Tubaro, C. Synthesis and Biological Studies on Dinuclear Gold(I) Complexes with Di-(N-Heterocyclic Carbene) Ligands Functionalized with Carbohydrates. *Molecules* **2020**, *25* (17).

165. Marchenko, A.; Koidan, G.; Hurieva, A.; Vlasenko, Y.; Kostyuk, A.; Lenarda, A.; Biffis, A.; Tubaro, C.; Baron, M.; Graiff, C.; Nestola, F. Neutral Dinuclear Gold(I) Complexes with N-Phosphanyl, N-Heterocyclic Carbenes (NHCPs). *J Organomet Chem* **2017**, *829*, 71–78.

166. Ouji, M.; Barnoin, G.; Álvarez, Á. F.; Augereau, J. M.; Hemmert, C.; Benoit-Vical, F.; Gornitzka, H. Hybrid Gold(I) NHC-Artemether Complexes to Target Falciparum Malaria Parasites. *Molecules* **2020**, *25* (12).

167. Gasperini, D.; Collado, A.; Goméz-Suárez, A.; Cordes, D. B.; Slawin, A. M. Z.; Nolan, S. P. Gold-Acetonyl Complexes: From Side-Products to Valuable Synthons. *Chemistry - A European Journal* **2015**, *21* (14), 5403–5412.

168. Collado, A.; Gómez-Suárez, A.; Martin, A. R.; Slawin, A. M. Z.; Nolan, S. P. Straightforward Synthesis of [Au(NHC)X] (NHC = N-Heterocyclic Carbene, X = Cl, Br, I) Complexes. *Chem. Commun* **2013**, *49*, 5541.

169. Collado, A.; Bohnenberger, J.; Oliva-Madrid, M. J.; Nun, P.; Cordes, D. B.; Slawin, A. M. Z.; Nolan, S. P. Synthesis of AuI- and AuIII-Bis(NHC) Complexes: Ligand Influence on Oxidative Addition to AuISpecies. *Eur J Inorg Chem* **2016**, *2016* (25), 4111–4122.

170. Jothibasu, R.; Vinh Huynh, H.; Lin Koh, L. Au(I) and Au(III) Complexes of a Sterically Bulky Benzimidazole-Derived N-Heterocyclic Carbene. *J. Organometallic Chemistry* 2007. 693, 374–380.

171. Fernández, G. A.; Picco, A. S.; Ceolín, M. R.; Chopa, A. B.; Silbestri, G. F. Synthesis and Structural Characterization of Water-Soluble Gold(I) N-Heterocyclic Carbene Complexes. An X-Ray Absorption Fine Structure Spectroscopy (XAFS) Study. *Organometallics* 2013, *32* (21), 6315–6323.

172. De Frémont, P.; Scott, N. M.; Stevens, E. D.; Ramnial, T.; Lightbody, O. C.; Macdonald, C. L. B.; Clyburne, J. A. C.; Abernethy, C. D.; Nolan, S. P. Synthesis of Well-Defined N-Heterocyclic Carbene Silver(I) Complexes. *Organometallics* 2005, *24* (26), 6301–6309.

173. Scattolin, T.; Tonon, G.; Botter, E.; Guillet, S. G.; Tzouras, N. V.; Nolan, S. P. Gold(I)-N-Heterocyclic Carbene Synthons in Organometallic Synthesis. *Chemistry - A European Journal* 2023, *29* (58).

174. Messori, L.; Marchetti, L.; Massai, L.; Scaletti, F.; Guerri, A.; Landini, I.; Nobili, S.; Perrone, G.; Mini, E.; Leoni, P.; Pasquali, M.; Gabbiani, C. Chemistry and Biology of Two Novel Gold(I) Carbene Complexes as Prospective Anticancer Agents. *Inorg Chem* 2014, *53* (5), 2396–2403.

175. Wang, D.; Astruc, D. The Golden Age of Transfer Hydrogenation. *Chemical Reviews* 2015, 115 (13), 6621–6686.

176. Vries, J. G. de.; Elsevier, C. J.; Klomp, D.; Hanefeld, U.; Peters, J. A. Transfer Hydrogenation Including the Meerwein-Ponndorf-Verley Reduction. In *The Handbook of Homogeneous Hydrogenation*; Wiley-VCH 2007, 585-588.

177. Knoevenagel, E.; Bergdolt, B. Ueber Das Verhalten Des Δ2.5-Dihydroterephtalsäuredimethylesters Bei Höheren Temperaturen Und in Gegenwart

von Palladiummohr. *Berichte der deutschen chemischen Gesellschaft* 1903, *36* (3), 2857–2860.

178. Haddad, Y. M. Y.; Henbest, H. B.; Husbands, J.; Mitchell, T. R. B. Reduction of Cyclohexanones to Axial Alcohols via Iridium-Containing Catalysts. *Proc. Chem. Soc* 1964, *361*.

179. Sasson, Y.; Blum, J. Homogenous catalytic transfer hydrogenation of α,β-unsaturated carbonyl compounds by dichlorotris (triphenylphosphine) ruthenium(II). *Tetrahedron letter* 1971, 24, 2167-2170.

180. Baráth, E. Hydrogen Transfer Reactions of Carbonyls, Alkynes, and Alkenes with Noble Metals in the Presence of Alcohols/Ethers and Amines as Hydrogen Donors. *Catalysts* 2018, 8 (12), 671.

181. Wei, Y. F.; Liang, Y.; Luo, R.; Ouyang, L. Recent Advances of Cp*Ir Complexes for Transfer Hydrogenation: Focus on Formic Acid/Formate as Hydrogen Donors. *Organic and Biomolecular Chemistry* 2023, 21, 7484.

182. Yang, Y.; Sauve, A. A. NAD + Metabolism: Bioenergetics, Signaling and Manipulation for Therapy. *Biochimica et Biophysica Acta* 2016, 1864, 1787–1800.

183. Xie, N.; Zhang, L.; Gao, W.; Huang, C.; Huber, P. E.; Zhou, X.; Li, C.; Shen, G.; Zou, B. NAD+ Metabolism: Pathophysiologic Mechanisms and Therapeutic Potential. *Signal Transduction and Targeted Therapy* 2020, 5 (1), 227.

184. Xiao, W.; Wang, R. S.; Handy, D. E.; Loscalzo, J. NAD(H) and NADP(H) Redox Couples and Cellular Energy Metabolism. *Antioxid Redox Signal* 2018, *28* (3), 251–272.

185. Soldevila-Barreda, J. J.; Romero-Canelón, I.; Habtemariam, A.; Sadler, P. J. Transfer Hydrogenation Catalysis in Cells as a New Approach to Anticancer Drug Design. *Nat Commun* 2015, *6*.

186. Tensi, L.; Macchioni, A. Extremely Fast NADH-Regeneration Using Phosphonic Acid as Hydride Source and Iridium-Pyridine-2-Sulfonamidate Catalysts. *ACS Catal* 2020, *10* (14), 7945–7949.

187. Lovison, D.; Berghausen, T.; Thomas, S. R.; Robson, J.; Drees, M.; Jandl, C.; Pöthig, A.; Mollik, P.; Halter, D. P.; Baratta, W.; Casini, A. Beyond Metal-Arenes: Monocarbonyl Ruthenium(II) Catalysts for Transfer Hydrogenation Reactions in Water and in Cells. *ACS Catal* 2023, *13* (16), 10798–10823.

188. Koutaantonis, G. A.; Selegue, J. P. Analytical Study of a Series of Substituted (2,2'-Bipyridyl) (Pentamet Hylcyclopentadienyl)Rhodium and-Iridium Complexes with Regard to Their Effectiveness as Redox Catalysts for the Indirect Electrochemical and Chemical Reduction of NAD(P)+. *Organometallics* 1991, 10, 1568-1577.

189. Lo, H. C.; Leiva, C.; Buriez, O.; Kerr, J. B.; Olmstead, M. M.; Fish, R. H. Bioorganometallic Chemistry. 13. Regioselective Reduction of NAD+ Models, 1-Benzylnicotinamde Triflate and B-Nicotinamide Ribose-5′-Methyl Phosphate, with in Situ Generated [Cp*Rh(Bpy)H]+: Structure-Activity Relationships, Kinetics, and Mechanistic Aspects in the Formation of the 1,4-NADH Derivatives. *Inorg Chem* 2001, *40* (26), 6705–6716.

190. Yan, Y. K.; Melchart, M.; Habtemariam, A.; Peacock, A. F. A.; Sadler, P. J. Catalysis of Regioselective Reduction of NAD+ by Ruthenium(II) Arene Complexes under Biologically Relevant Conditions. *Journal of Biological Inorganic Chemistry* 2006, *11* (4), 483–488.

191. Coverdale, J. P. C.; Sanchez-Cano, C.; Clarkson, G. J.; Soni, R.; Wills, M.; Sadler, P. J. Easy To Synthesize, Robust Organo-Osmium Asymmetric Transfer Hydrogenation Catalysts. *Chemistry – A European Journal* 2015, *21* (22), 8043–8046.

192. Coverdale, J. P. C.; Romero-Canelón, I.; Sanchez-Cano, C.; Clarkson, G. J.; Habtemariam, A.; Wills, M.; Sadler, P. J. Asymmetric Transfer Hydrogenation by

Synthetic Catalysts in Cancer Cells. *Nature Chemistry 2018 10:3* 2018, *10* (3), 347–354.

193. Schmidt, A.; Kinderman, M. K.; Vainiotalo, P.; Nieger, M. Charge-Separated Modified Nucleobases. On π-Interactions and Hydrogen Bonding of Self-Complementary Cationic and Betainic Uracils. *Journal of Organic Chemistry* 1999, *64* (26), 9499–9506.

194. Krüger, A. K.; Neels, A.; Albrecht, M. Rhodium-Mediated Activation of an Alkane-Type C-H Bond. *Chem Commun* 2010, 46 (2), 315-317.

195. Krüger, A.; Albrecht, M. Rhodium Carbene Complexes as Versatile Catalyst Precursors for Si-H Bond Activation. *Chemistry - A European Journal* 2012, *18* (2), 652–658.

196. Petronilho, A.; Woods, J. A.; Mueller-Bunz, H.; Bernhard, S.; Albrecht, M. Iridium Complexes Containing Mesoionic C Donors: Selective C(Sp3)-H versus C(Sp2)-H Bond Activation, Reactivity towards Acids and Bases, and Catalytic Oxidation of Silanes and Water. *Chemistry* 2014, *20* (48), 15775–15784.

197. Maji, B.; Choudhury, J. Switchable Hydrogenation with a Betaine-Derived Bifunctional Ir-NHC Catalyst. *Chemical Communications* 2019, *55* (31), 4574–4577.

198. Crabtree, R. H. Abnormal, Mesoionic and Remote N-Heterocyclic Carbene Complexes. *Coordination Chemistry Reviews* 2013, 257 (3), 755–766.

199. Song, G.; Wang, X.; Li, Y.; Li, X. Iridium Abnormal N-Heterocyclic Carbene Hydrides via Highly Selective C-H Activation. *Organometallics* 2008, *27* (6), 1187–1192.

200. Gong, X.; Zhang, H.; Li, X. Iridium Phosphine Abnormal N-Heterocyclic Carbene Complexes in Catalytic Hydrogen Transfer Reactions. *Tetrahedron Letters* 2011, 52, 5596–5600.

201. Viciano, M.; Feliz, M.; Corberán, R.; Mata, J. A.; Clot, E.; Peris, E. Aliphatic versus Aromatic C-H Activation in the Formation of Abnormal Carbenes with Iridium: A Combined Experimental and Theoretical Study. *Organometallics* **2007**, *26* (22), 5304–5314.

202. Albrecht, M. Cyclometalation Using D-Block Transition Metals: Fundamental Aspects and Recent Trends. *Chem Rev* **2010**, *110* (2), 576–623.

203. Song, G.; Li, X.; Song, Z.; Zhao, J.; Zhang, H. Methyleneimidazoline Complexes of Iridium, Rhodium, and Palladium from Selective C(Sp3)-H Bond Activation. *Chemistry - A European Journal* **2009**, *15* (22), 5535–5544.

204. Petronilho, A.; Woods, J. A.; Mueller-Bunz, H.; Bernhard, S.; Albrecht, M. Iridium Complexes Containing Mesoionic C Donors: Selective C(Sp3)-H versus C(Sp2)-H Bond Activation, Reactivity towards Acids and Bases, and Catalytic Oxidation of Silanes and Water. *Chemistry* **2014**, *20* (48), 15775–15784.

205. Chianese, A. R.; Kovacevic, A.; Zeglis, B. M.; Faller, J. W.; Crabtree, R. H. Abnormal C5-Bound N-Heterocyclic Carbenes: Extremely Strong Electron Donor Ligands and Their Iridium(I) and Iridium(III) Complexes. *Organometallics* **2004**, *23* (10), 2461–2468.

206. Bernet, L.; Lalrempuia, R.; Ghattas, W.; Mueller-Bunz, H.; Vigara, L.; Llobet, A.; Albrecht, M. Tunable Single-Site Ruthenium Catalysts for Efficient Water Oxidation. *Chemical Communications* **2011**, *47* (28), 8058–8060.